Fischer and N-heterocyclic carbene complexes of Group (VII) transition metals

by

Roan Fraser

Submitted in partial fulfilment of the requirements for the degree

Philosophiae Doctor

in the Faculty of Natural and Agricultural Sciences
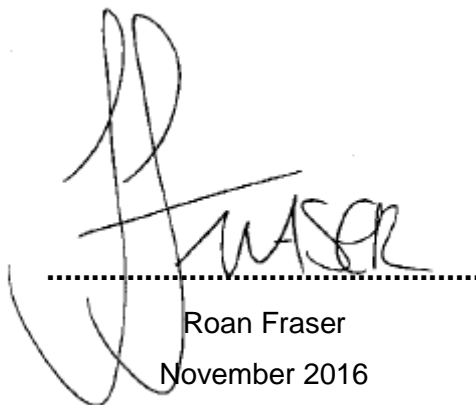
University of Pretoria

Pretoria

Supervisor:

Professor Marilé Landman

November 2016

DECLARATION

The synthesis, characterisation and molecular modelling outlined in this dissertation were carried out at the Department of Chemistry, University of Pretoria, between January 2013 and November 2016. Professor Marilé Landman served as supervisor for the entire duration of the research project and I, Roan Fraser, declare that all work published on my behalf is my own and has not previously been submitted by myself or in my authority for the degree Philosophiae Doctor at this or any other tertiary institution.

....
Roan Fraser
November 2016

ACKNOWLEDGEMENTS

I would like to thank the following individuals for their contribution to either my personal or professional life:

First and foremost, Professor Marilé Landman, for all her hard work, compassion and wisdom. Without her expert leadership neither this research nor my thesis would have been feasible. Thank you for the hugs, the tears, the wine and all the laughs through the more than 7 years of working so closely together.

My extended family – Elmari, Johan and Emile Fraser, Chantelle and Janus van Rooyen and all of the Luegers. They offer a truly diverse family model, built on pillars of loyalty, trust and love.

My inspirational lab partners and colleagues - Frikkie, Marina and Lauren. You guys made research not only bearable but created a family environment in the laboratories.

My friends – Madelize, Ruan, Shalene, Dreyer, Andries, Noël and Annindita. Different qualifications and specialities did not pose any obstacle to my loyal friends in providing innovative solutions to any problems that might have presented themselves throughout the course of my research.

Dr Cornie van Sittert of North West University, Potchefstroom and Prof Jeanette Conradie of the University of the Free state, The Free state - for assistance with the computational studies.

Prof P.H. van Rooyen and Mr Dave Liles - our crystallography experts.

Berni Leander Lueger – Austria, South Africa, Italy, Hungary, Swaziland, Croatia, the Vatican and Slovenia. Thank you for being my pillar through all my endeavours. I DID IT!

iii

TABLE OF CONTENT

Chapter 7: Bonding aspects of group VII carbene complexes

SUMMARY

Fischer and N-heterocyclic carbene complexes of Group (VII) transition metals

By

Roan Fraser

Supervisor: Professor M. Landman

Submitted in partial fulfilment of the requirements for the degree Philosophiae Doctor, Department of Chemistry, University of Pretoria, Pretoria

Fischer- and N-heterocyclic carbene (NHCs) complexes of the group VII transition metals, including the cymantrenyl moiety as either carbene metal or carbene substituent (or both) have been successfully synthesised and studied in the solid state. Fischer carbene complexes of type $[M(CO)_{y-1}\{C(OR)R'\}]$, y = 10, 6 or 3, have been afforded employing classical Fischer methodology, where the initial lithiated synthons (cymantrene, $CpRe(CO)_3$ or phenylacetylene), R', were metallated by either $Cr(CO)_6$, $Mo(CO)_6$, $W(CO)_6$, $Mn_2(CO)_{10}$, $Re_2(CO)_{10}$, $CpMn(CO)_3$ or $MeCpMn(CO)_3$ and subsequently quenched by the addition of triethyloxonium tetrafluoroborate to ultimately produce ethoxy R' carbene complexes. Ligand substitution reactions between labile carbonyl ligands of the carbene metal moiety and triphenyl phosphine ligands were achieved in high yield and the substitution exclusively favoured the formation of *cis* products to produce *cis*- $[M(CO)_4(PPh_3)\{carbene)\}]$ products where M= Cr, Mo and W or $[LM(CO)(PPh_3)\{carbene)\}]$ products where LM= CpMn or MeCpMn.

N-heterocyclic carbene (NHCs) complexes were synthesised through carbonyl substitution reactions preformed on carbonyl-carrying metal synthons. $CpMn(CO)_3$ and $MeCpMn(CO)_3$ underwent carbonyl substitutions under photochemical conditions to generate NHCs with the general formula $[M(CO)_2\{\overline{CNRCHCHNR'}\}]$ *via* the intermediates $CpMn(CO)_2THF$ or $MeCpMn(CO)_2THF$. The R-groups were methodically varied [L1: R = Me, R' = Et; L2: R = Me, R' = Isopropyl and L3: R = Me, R' = EtPh] to produce an assortment of asymmetrically functionalized complexes. The dimetallic synthons, $Mn_2(CO)_{10}$ and $Re_2(CO)_{10}$, allowed for direct carbonyl substitution with the introduction of the deprotonated imidazolium carbene ligands at low temperature to produce the corresponding NHC-dimetal carbene complexes.

This approach also afforded monometallic halogenated NHC complexes as a minor side product.

Density functional theory (DFT) calculations were performed on the range of complexes synthesised in this study. Application of the second-order perturbation theory (SOPT) of the natural bond orbitals (NBOs) method indicated stabilization interactions between the methylene C-H bond of the ethoxy substituent and a carbonyl ligand of the metalating metal moiety of the Fischer carbene complexes. Metallation of a deportonated cymantrene or CpRe(CO)$_3$ synthon through a second equivalent of a CpM(CO)$_3$ complex produced the *trans* Cp-orientated homo- or hetero-dimetallic carbene complexes. DFT calculations support the hypothesis that the *trans* conformation is lower in energy as witnessed experimentally in the solid state. Frontier orbital analysis was possible from DFT calculations. The majority of the structures provided by the computed model illustrated that the d atomic orbitals of the metal contributed considerably to the HOMO, whereas the LUMO was mainly distributed on the carbene carbon atom. Computational results also described the similarities and differences between the electronic and bonding modes of the Fischer- and NHC complexes. The theoretical results were validated by experimental parameters of characterization methods such as vibration spectroscopy, nuclear magnetic spectroscopy, mass spectrometry and X-ray crystallography.

Finally, application prospects for both the Fischer- and N-heterocyclic carbene complexes were explored. Both the dimetallic Fischer carbene complexes and NHCs containing the cymantrenyl moiety illustrated possible catalytic activity in the dimerization of thiols. Using DFT calculations, the plausible mechanism and energy cycle for the catalytic activity were postulated.

LIST OF ABBREVIATIONS

Å	Angstrom
ADF	Amsterdam density functional
AIM	atoms in molecules
BDE	bond dissociation energy
Bn	benzyl
BO	Bond order
CDA	charge decomposition analysis
Cp	cyclopentadienyl
Cy	cyclohexyl
d	doublet
DCM	dichloromethane
DFT	density functional theory
E	electrophile
Et	ethyl
EDA	energy decomposition analysis
EtPh	ethylphenyl
GC	gas chromatography
HRESI$^+$	high resolution electrospray ionization
HOMO	highest occupied molecular orbital
$h v$	Planck's constant x frequency
^{i}Pr	isopropyl
Im	imidazole
IR	Infrared
J	coupling constant
LUMO	lowest unoccupied molecular orbital
MO	molecular orbital
m	medium (IR spectroscopy)
m	multiplet (NMR spectroscopy)
Me	methyl
Mes	mesityl
MS	mass spectrometry
NBO	natural bond orbital
NHC	N-heterocyclic carbene
Nu	nucleophile
%Vbur	percentage buried volume

Ph	phenyl
q	quartet (NMR spectroscopy)
R	alkyl groups
RT	room temperature
s	strong (IR spectroscopy)
s	singlet (NMR spectroscopy)
SOPT	second-order perturbation theory
t	triplet (NMR spectroscopy)
THF	tetrahydrofuran
tlc	thin layer chromatography
vs	very strong (IR spectroscopy)
w	weak (IR spectroscopy)
WBI	Wiberg bond indices

LIST OF COMPLEXES
Only novel complexes are included in this section

CHAPTER 2

1

2

3

4

5

6

CHAPTER 5

1

2

3

4

5

6

7

8

9

10

1

2

3

4

5

6

1

2

3

4

5
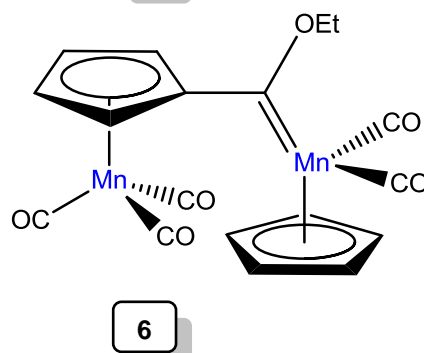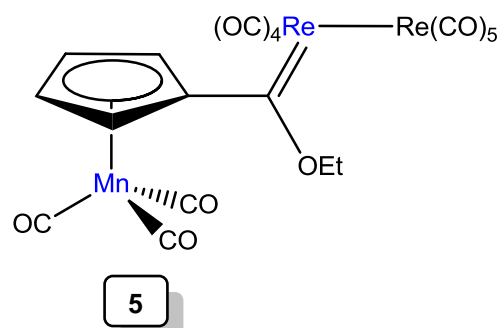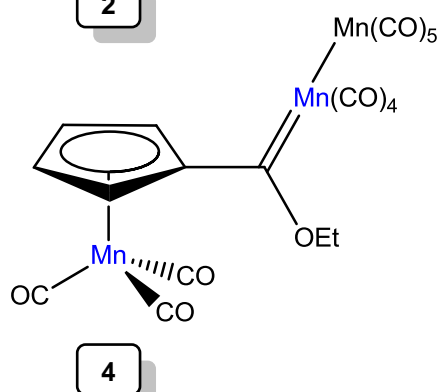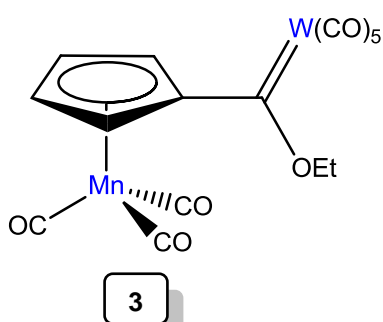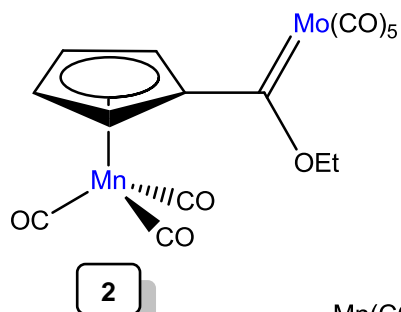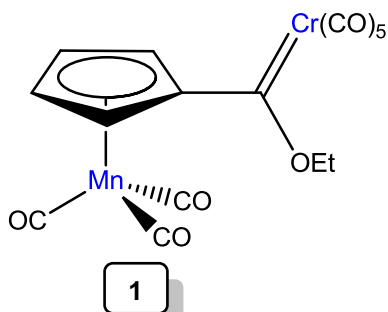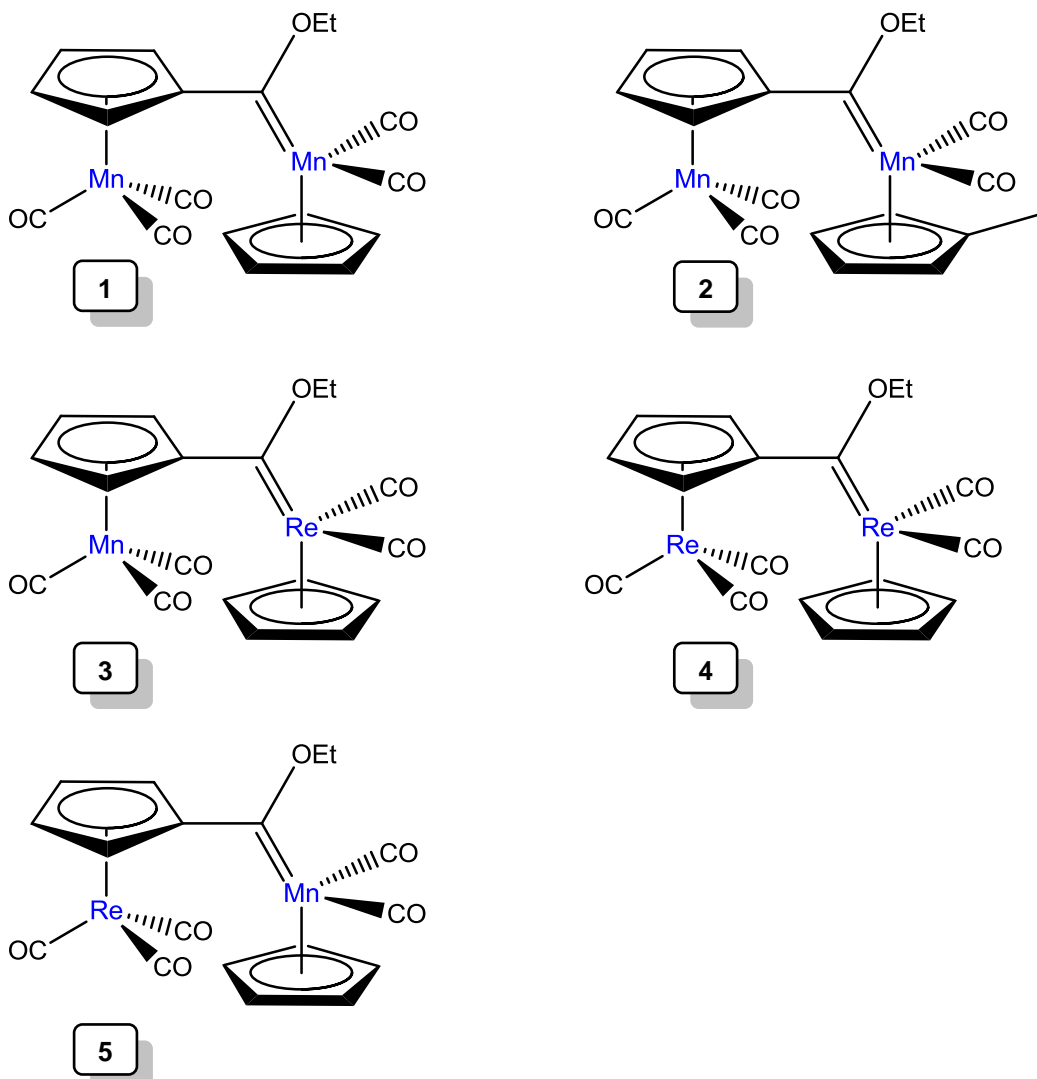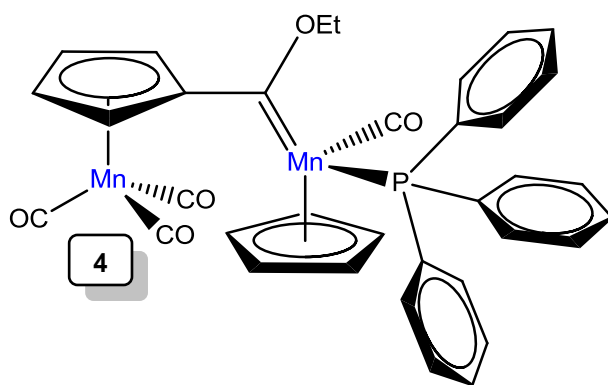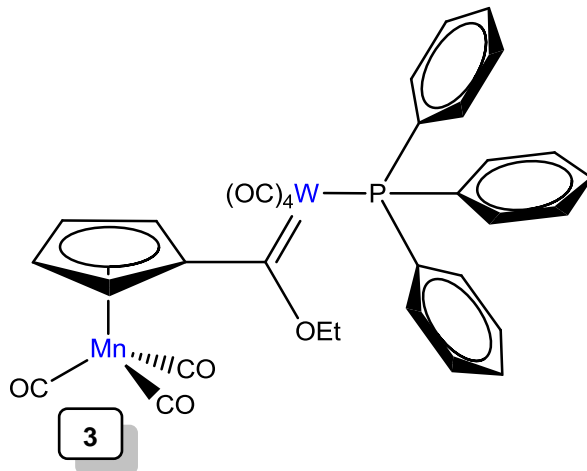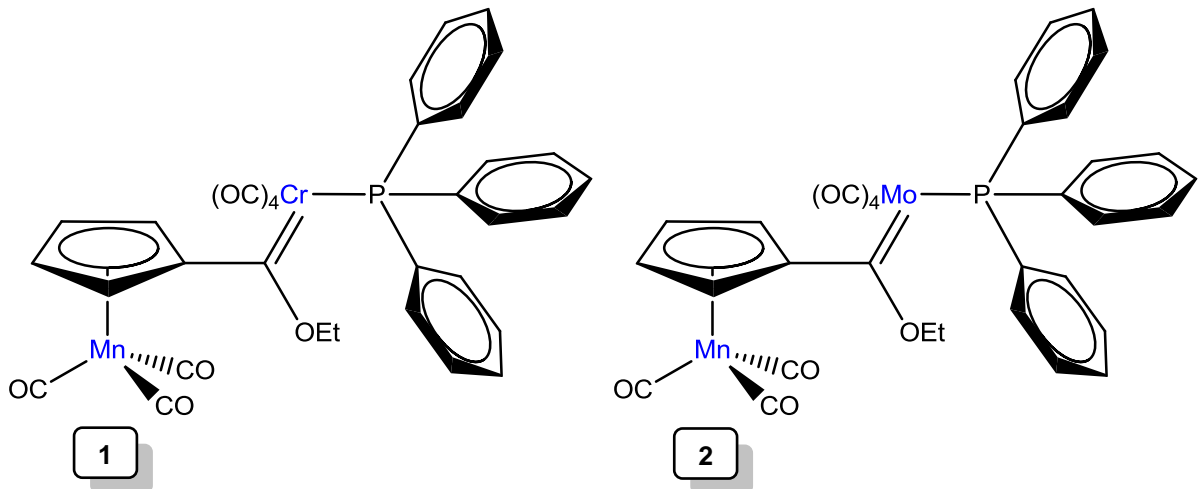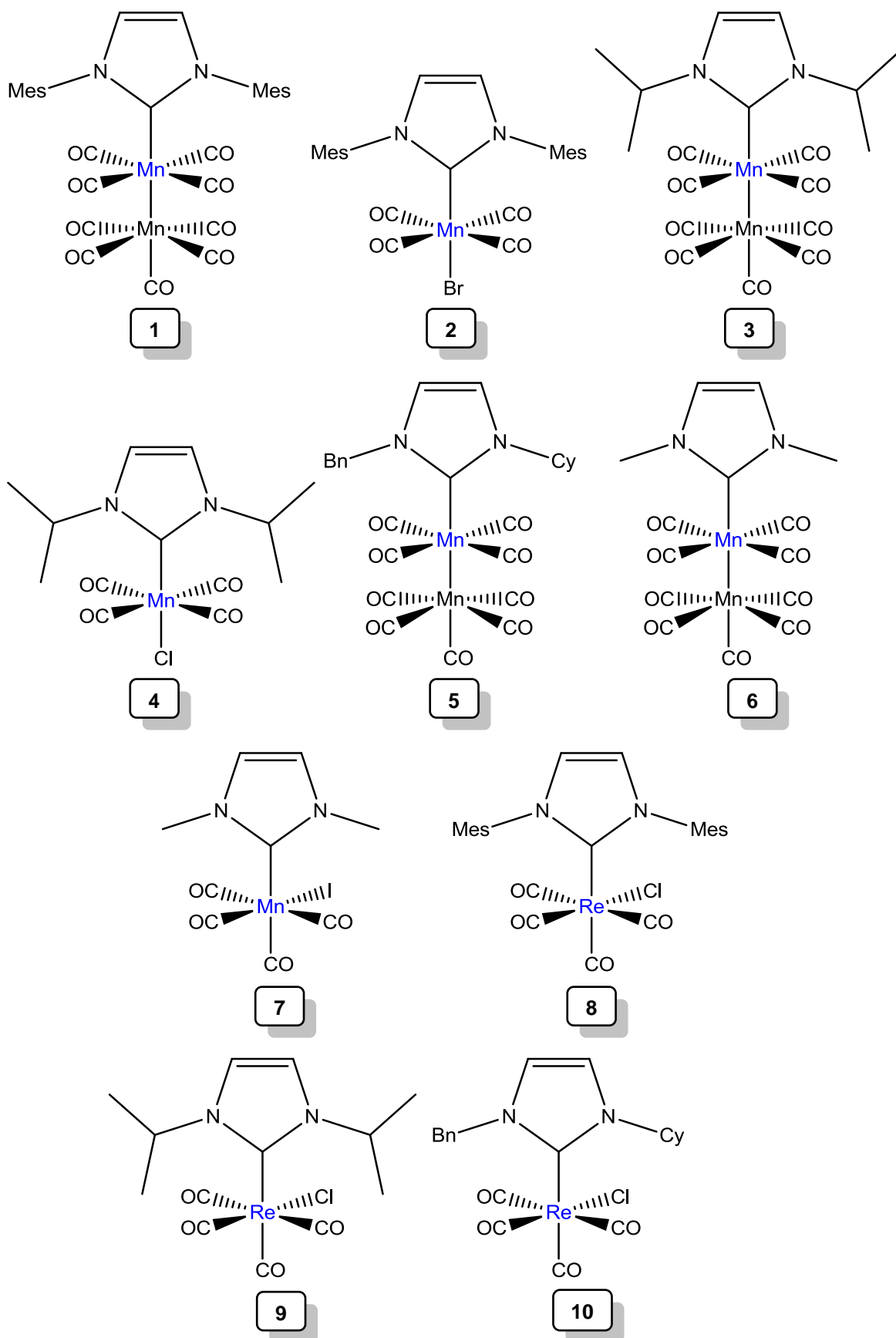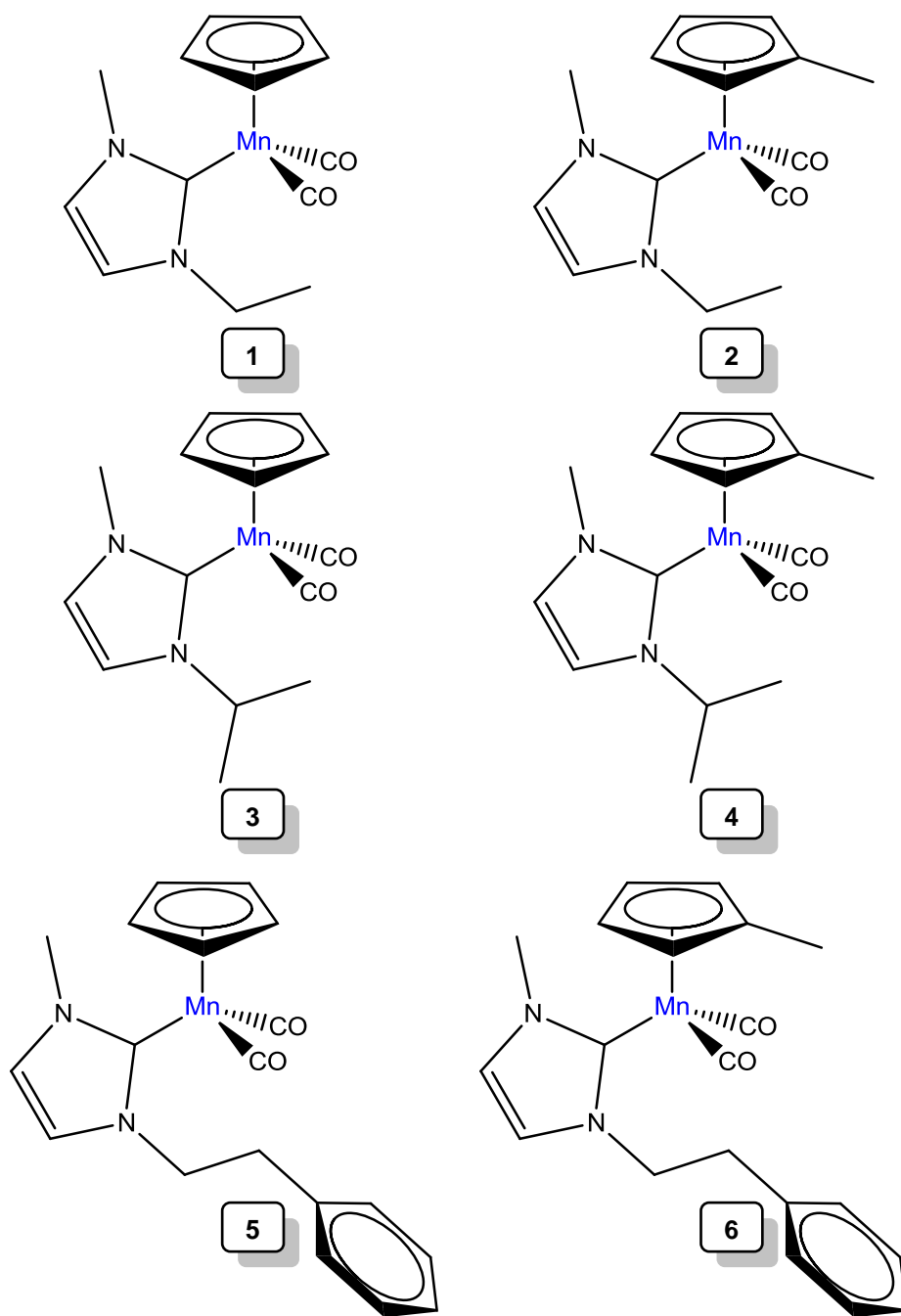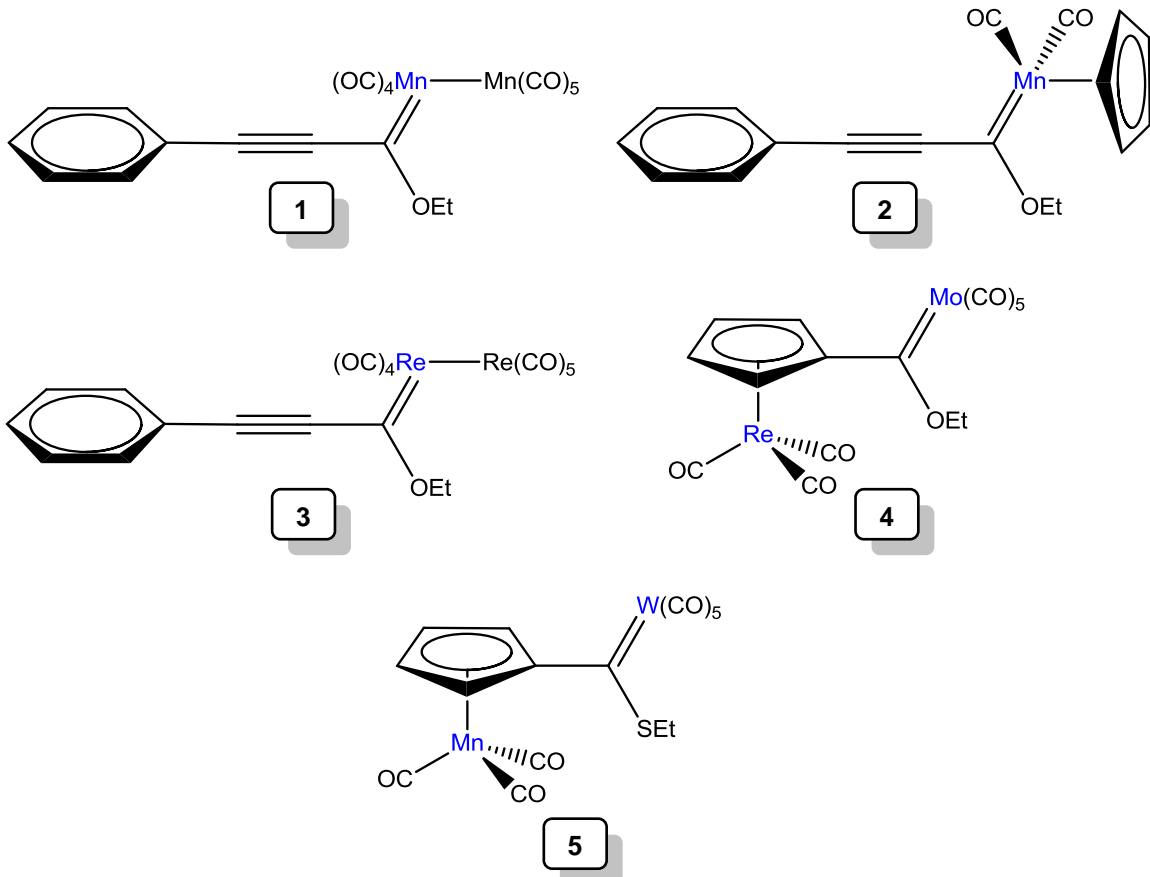
1 Introduction
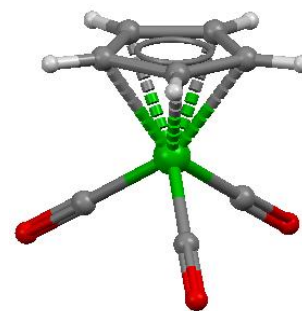
1.1 Early development of organometallic chemistry

The term 'organometallic' was coined by Sir Edward Frankland after the successful preparation of important alkylmercury compounds such as Me_2Hg [1]. The latter half of the 20th century witnessed remarkable growing interest in the field of organometallic chemistry [2]. The discoveries of ferrocene [3] and the Ziegler catalysts [4] established a new era in the development of organometallic chemistry, that had been ill-explored until these discoveries were made [2]. Organometallic compounds of non-transition elements such as lithium, magnesium and zinc, were by that stage practically useful as reagents in a variety of organic synthesis reactions but the field was still developing [2]. At best, the field was seen as a sphere of organic chemistry, apart from the Werner-type coordination chemistry. The introduction of the first sandwich structure, ferrocene, to the scientific community, was both fascinating and aroused the interest of theoretical and synthetic chemists. Although the structural aspects of ferrocene were difficult to elucidate, the final proposed double cone and antiprismatic structures proposed by Fischer (I) and Woodward and Wilkinson (II) respectively proved to be accurate and aesthetically beautiful (Figure 1) [3].
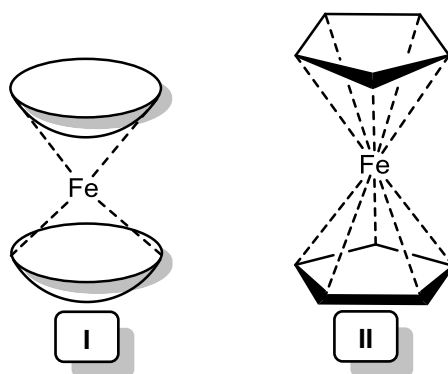
Figure 1: The structures proposed by Fischer (I) and Woodward and Wilkinson (II).

[1] (a) E. Frankland, Phil. Trans. R. Soc. 142 (1852) 417; (b) E. Frankland, Ann. Chem. Pharm. 95 (1855) 28.
[2] A. Yamamoto, J. Organomet. Chem. 600 (2000) 159.
[3] G. Wilkinson, J. Organomet. Chem. 100 (1975) 273.
[4] K. Ziegler, E. Holtzkamp, H. Breil, H. Martin, Angew. Chem. 67 (1955) 541.

The pace of growth in the field of organometallic chemistry was heightened by another unexpected discovery by Ziegler [5]. His fundamental studies on the reactions of organometal salts of lithium and aluminium in attempts to clarify the mysterious effects of nickel on the oligomerization of ethylene in the presence of triethylaluminum, led to his ground-breaking discovery of the uses for organometallic compounds as catalysts for oligomerization of ethylene. Ziegler also later found applications for zirconium acetylacetonate and titanium trichloride in oligomerization processes [5]. The first half of the 20th century marked the development of the field of catalysis [6]. The fundamental distinction between homogeneous and heterogeneous catalysis [7] was first delineated by the French chemist Paul Sabatier, who focussed on the heterogeneous hydrogenation of olefins to saturated hydrocarbons using a nickel-base catalyst [8]. This discovery led to the sharing of a Nobel Prize between Sabatier and Gringard in 1912. 10 years later, in 1922, Fischer and Tropsch reported the heterogeneous catalyzed reaction of syngas [9] to form a mixture of different linear alkanes and alkenes and limiting oxygenates as by-products, a process that was ultimately industrialized in 1925 [10]. The first σ-alkyl metal- [11], diene- [12] and metal-hydride [13] complex was discovered during this period by Pope (1909), Reihen (1930) and Hieber (1931), respectively, and increased the assortment of complexes synthetically viable (Figure 2).
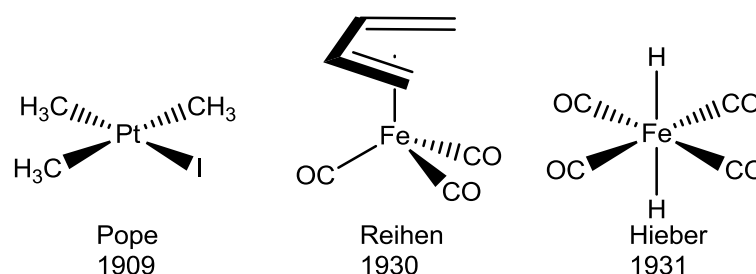
Figure 2: The first σ-alkyl metal-, diene- and metal-hydride complexes reported by Pope (1909), Reihen (1930) and Hieber (1931)

Structural bio-organometallic chemistry had its origin between 1953 and 1961, when the English chemist, Dorothy Crowfoot Hodgkin, determined the X-ray crystal structure of

[5] A. Yamamoto, J. Organomet. Chem. 600 (2000) 159.
[6] J.L. Casci, C. M. Lok, M.D. Shannon. Catal. Today 145 (2009) 38.
[7] P. Sabatier, La Catalyse en Chimie Organique, Librairie Polytechnique. Paris (1913).
[8] P. Sabatier, J. B. Senderens, C. R. Acad. Sci. Paris 134 (1902) 514.
[9] F. Fischer, H. Tropsch, Brennstoff Chem. 193 (1923) 276.
[10] F. Fischer, H. Tropsch, Brennstoff Chem. 7 (1926) 61.
[11] W.J. Pope, S. T. Peachey, J. Chem. Soc. Trans. 95 (1909) 571.
[12] W.A. Donaldson, S. Chaudhury, Eur. J. Org. Chem. (2009) 3831.
[13] W. Hieber, F. Leutert, Die Naturwissenschaften 19 (1931) 17.

vitamin B12 coenzyme using a primitive computer [14]. She was ultimately awarded the Nobel Prize in 1964 and in 1972 the legendary Harvard University chemist, R. B. Woodward [15], was able to completely synthesise the coenzyme in 70 steps. In 1962 Vaska published the famous 16-electron complex [Ir(CO)(Cl)(PPh$_3$)] that ultimately bears his name in honour [16]. The complex is recognized for the ability to reversibly ligate dioxygen along with the series of other oxidative addition reactions plausible with a large number of different substrates [17]. In 1964, the first metal-carbene complex was published by E.O Fischer and was reported as being olefin metathesis active by Banks [18].

1.2   The development of carbene chemistry

In 1964, organometallic chemistry introduced a new member to the previously extensive and expanding world of inorganic chemistry. With the synthesis of the first recognised metal-to-carbon double bond, Fischer broke new ground and produced an entirely new area of research [19]. Although, it was not the actual first metal carbene to be synthesised, the pentacarbonyl[methoxybenzylidene]tungsten(0) was the first, fully and correctly characterized carbene complex published (Figure 3).
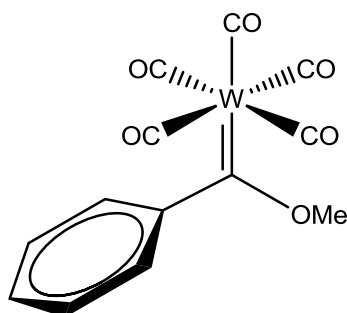
Figure 3: The first recognised metal-carbene complex prepared by Fischer *et al.* [19]

The true honours actually belong to King, who synthesised the first, true Fischer-type carbene, in 1963, through the reaction between a pentacarbonyl manganese complex and dibromopropane. He, however, wrongly assigned the structure of the complex with molecular

[14] D. Crowfoot Hodgkin, J. Kamper, J. Lindsey, M. MacKay, J. Pickworth, J. H. Robertson, Proc. R. Soc. A. 242 (1957) 1229.
[15] R.B. Woodward, Pure Appl. Chem. 2 (1961) 383.
[16] L. Vaska, J. Am. Chem. Soc. 83 (1961) 12.
[17] M. Selke, C. S. Foote, J. Am. Chem. Soc. 115 (1993) 1166.
[18] R.L. Banks, G. C. Bailey, Ind. Eng. Chem. Prod. Res. Dev. 3 (1964) 3.
[19] E.O.Fischer, A. Maasböl, Angew. Chem., Int. Ed. Engl., 3 (1964) 580.

formula $[Mn_2(CO)_{10}(CH_2)_3]$ as illustrated in Figure 4 [20]. Only after Fischer reported the correct structure of his pentacarbonyl[methoxybenzylidene]tungsten(0) carbene compound, did Casey propose the correct structure of King's complex in 1970 (Figure 4). Although the correct structure of the King's complex reflects the first metal-carbene complex synthesised, it was sadly never recognised as such at the time.
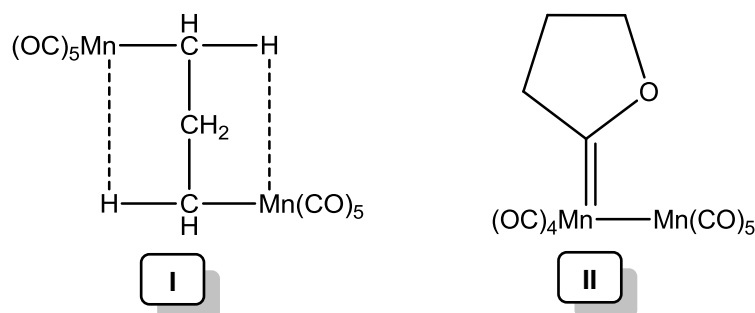
Figure 4: The manganese structure as proposed by King(I) and the correct structure by Casey (II)

About 10 years later the second distinct class of carbene complexes were realized when Richard R. Schrock proposed the synthesis of a high oxidation state (d^0) metal-alkylidene complex [21]. The synthesis of the complex was accomplished by α-hydrogen abstraction on a tris(2,2-dimethylpropyl)methyl tantalum(V) dichloride precursor to produce Schrock carbene [22]. The tantalum neopentylidene complex was the only known example of a stable M=CHR carbene complex (Scheme 1). The complex illustrated remarkable properties and displayed a metal in the highest oxidation state with the metal-carbon bond polarised, leaving the metal positively charged and the carbene carbon nucleophilic in nature [23]. Schrock carbenes are typically highly thermally stable and resistant to intermolecular decomposition reactions. These compounds are produced by using early transition metals in high oxidation states with strong donor and weak π-acceptor ligands [32]. Schrock-type carbenes have been included into the design of well-known catalysts, as in the case of the Grubbs catalyst, and various new derivatives are now in existence.

[20] R.B. King, J. Am. Chem. Soc. 85 (1963) 1922.
[21] R.R. Schrock, J. Am. Chem. Soc. 96 (1974) 6796.
[22] P. De Frémont, N. Marion, S. P. Nolan, Coord. Chem. Rev. 253 (2009) 862.
[23] R.R. Schrock, Angew. Chem. Int. Ed. Engl. 45 (2006) 3748.
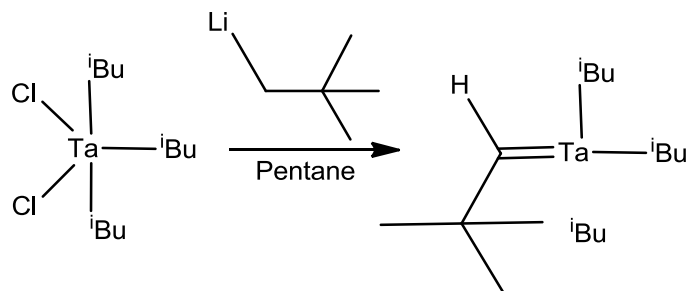
Scheme 1: The synthesis of the first Schrock carbene

In 1968 a third derivative class of carbene complexes, termed 'N-heterocyclic carbenes' (NHCs) were prepared independently by Öfele (Figure 5), and Wanzlick and Schönherr [24,25a]. The class of carbene complexes is distinct, since the carbene carbon has two adjacent heteroatoms providing competitive electronic stabilization. NHC's are strong σ-donating ligands and can be compared to classic P-, N-, O-donating auxiliary ligands in contrast with the conventional Fischer- or Schrock-type carbenes [26]. NHC complexes have developed over recent years to become an important part of organometallic chemistry. The alteration of the Grubbs first-generation catalyst through a substitution reaction of a phosphine ligand with an NHC ligand produced the corresponding second-generation catalyst with improved catalytic activity. The superior activity of this second-generation catalyst over its predecessor illustrates the usability and applicability of this class of carbene complex [27].
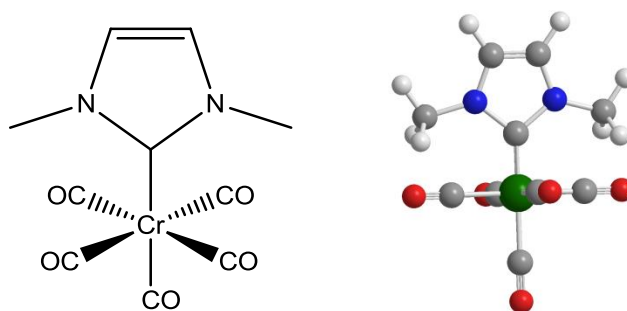
Figure 5: Chromium NHC complex synthesised by Öfele [24]

[24] K. Öfele, J. Organomet. Chem. 12 (1968) 42.
[25] (a) H.W. Wanzlick, H. Schönherr, J. Angew. Chem. 80 (1968)154; Angew. Chem. Int. Ed. Engl. 7 (1968) 141;
(b) P. Luger, G. Ruban, Acta Crystallogr. Sect. B., 27 (1971) 2276.
[26] T. Weskamp, P.W. Volker, A.H Wolfgang, J.Organomet Chem. 600 (2000) 12.
[27] J. Huang, E.D. Stevens, S.P. Nolan, J.L. Petersen, J. Am. Chem. Soc. 121 (1999) 2674.

1.2.1 Developments in Fischer-type carbene chemistry

Fischer and Maasböl published the first, recognised carbene complex containing a transition metal in 1964 [28]. Fischer carbenes are generally synthesised from lower valent transition metals between and including Group VI to VIII and typically contain σ-donor, π-acceptor ligands such as carbonyl ligands which can accommodate varying electron density on the metal sphere [28]. The carbene carbon is electrophilic in nature and is additionally stabilised through electron back-donation from the metal d-electrons. Supplementary electron support is also available through electronic contribution by the heteroatom substituents to the carbene carbon centre.
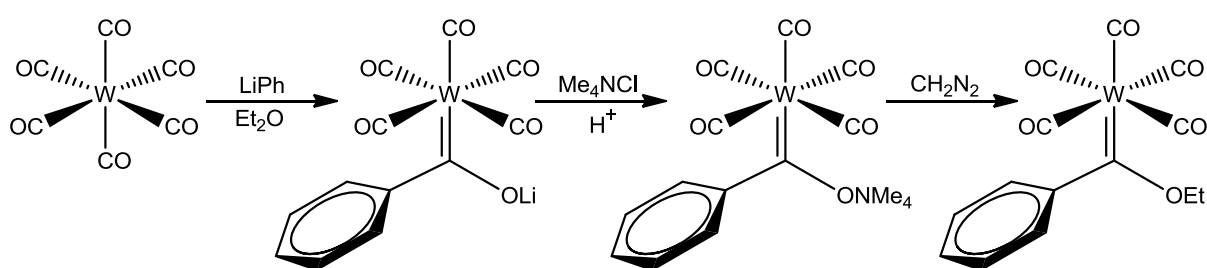
Scheme 2: The synthesis of a Fischer carbene complex as proposed by Fischer [28]
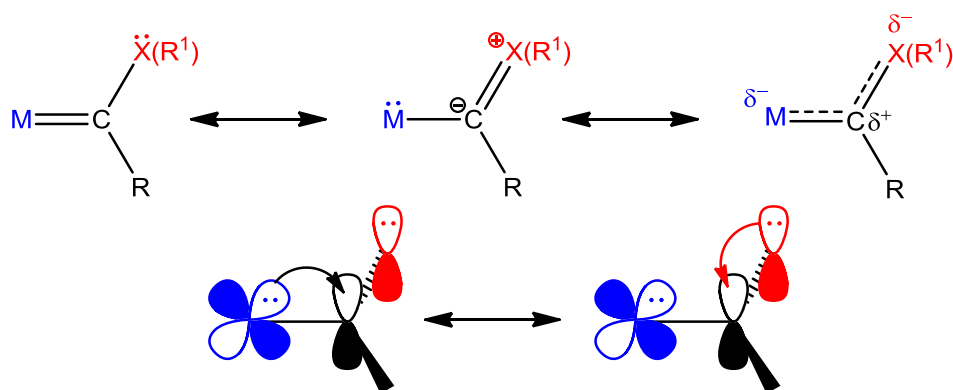
Figure 6: Stabilisation of Fischer carbene complexes through the acyl form (resonance effect)

Development in the field of Fischer-type carbene complexes has been significant with a wide range of applicability. Stable mononuclear biscarbene complexes of group VI metals have been fairly scarce in literature [29]. The handling of these complexes is troublesome mainly due to the inherent instability or heightened reactivity of these complexes in solution.

[28] E.O. Fischer, A. Maasböl, Angew, Chem., Int. Ed. Engl. 76 (1964) 645.
[29] D.I Bezuidenhout, S. Lotz, D.C. Liles, B. van der Westhuizen, Coord. Chem. Rev., 256 (2012) 479.

Heteroatom-stabilized mononuclear biscarbene complexes have been reported by Fischer [30] and Lappert [31]. More recently, Sierra and co-workers [32] studied carbene-carbene coupling reactions of monocarbene chromium complexes in the presence of a palladium catalyst. Employing two subsequent transfer reactions of the chromium monocarbene complex, the mononuclear biscarbene of palladium was formed. In 2008, Barluenga reported the isolation of a mononuclear biscarbene tungsten complex after attempting an intermolecular coupling between a hydroxy- and alkoxycarbene complex of tungsten [33].
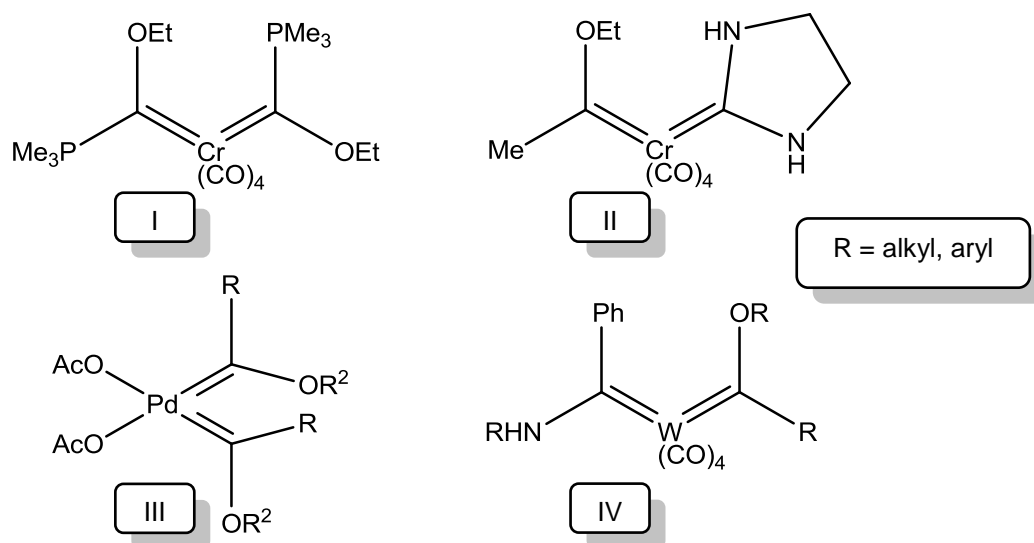
Figure 7: Biscarbene mononuclear carbene complexes proposed by Fischer (I), Lappert (II), Sierra (III) and Barluenga (IV)

Fischer mononuclear biscarbene complexes can also be stabilized by the chelate ring effect when incorporated in a metallocyclic ring. Biscarbene chelates are rare in literature mainly due to synthetic problems associated with the formation of a dianionic intermediate on adjacent carbons or heteroatoms in organic substrates [29]. A few examples of symmetrically bound biscarbene chelates are reported by Fischer and co-workers but limited progress has been made in this area of Fischer carbene complexes [29].

[30] E.O. Fischer, F.R. Kreissl, C.G. Kreiter, E.W. Meineke, Chem. Ber. 105 (1972) 2558.
[31] P.B. Hitchcock, M.F. Lappert, P.L. Pye, J. Chem. Soc., Dalton Trans.123 (2001) 5021.
[32] M.A. Sierra, J.C. del Amo, M.J. Mancheno, M. Gomez-Gallego, J. Am Chem. Soc. 23 (2004) 851 .
[33] J. Barluenga, A.A. Trabanco, I. Perez-Sanchez, R. De la Campa, J. Florez, S. Garcia-Granda, A. Aguirre, Chem. Eur. J. 14 (2008) 5401.

2016
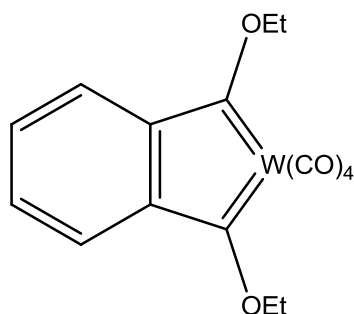
Figure 8: Mononuclear biscarbene complex as proposed by Fischer

One of the most versatile reactions accessible to Fischer carbene complexes are substitution reactions performed on the carbene metal sphere. The carbonyl ligands are typically highly labile and readily undergo substitutions with less labile counterparts to produce highly derivatized complexes [34,35]. Substitution reactions with both phosphorous-containing and nitrogen-containing ligands are abundant in literature and provide a rich selection of complexes. Examples of bidentate phosphine ligand coordination to carbene complexes (Figure 9) have been reported [36-38].There have been interesting improvements to this area as a result of the introduction of microwave reactions, in which bidentate ligands can be effortlessly coordinated to metal centres through induced substitution reactions [39].
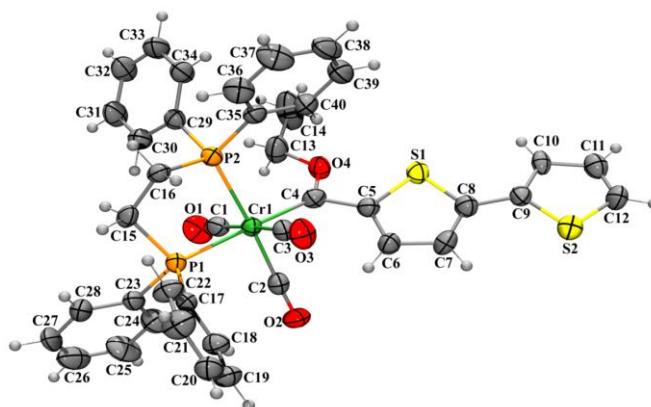
Figure 9: Structure of a phosphine bidentate substituted carbene complex [38]

[34] M. Landman, R. Pretorius, R. Fraser, B.E. Buitendach, M.M. Conradie, P.H. van Rooyen, J. Conradie. Electrochimica Acta. 130 (2014) 104.
[35] K.H. Dötz, J. Stendel Jr., Chem. Rev. 109, 2009, 3227.
[36] A. Arrieta, F.P. Cossío, I. Fernández, M. Gómez-Gallego, B. Lecea, M.J. Mancheño, M.A. Sierra, J. Am. Chem. Soc. 122 (2000)11509.
[37] J. Barluenga, K. Muñiz, M.Tomás, A. Ballesteros, S. García-Granda, Organometallics. 22 (2003) 1756.
[38] M. Landman, R. Liu, R. Fraser, P. H. van Rooyen, J. Conradie, J. Organomet. Chem. 752 (2014) 171.
[39] S.L. Van Atta, B.A. Duclos, D.B. Green, Organometallics. 19 (2000) 2397.

Interest in the synthesis of homo- and heterodimetallic carbene complexes soon followed after the discovery of the first Fischer carbene complex of ferrocene. Treatment of lithiated ferrocene with a metal carbonyl moiety and subsequent quenching with [Et$_3$O]BF$_4$ yielded the corresponding dimetallic ferrocenyl carbene complex (Figure 10) [40]. Soon, multiple structures were elucidated where a metal-containing synthon was deprotonated to produce homo- and heterodimetallic carbene complexes. η^6-Arene [41], half-sandwich moieties [42] and heteroarene metal synthons [41] have been converted to carbene complexes using classical Fischer carbene methodologies and in recent years the scope of the area has been expanded to include trinuclear, tetranuclear and even hexanuclear carbene complexes [43]. Research focussing on the use of dimetallic metal carbonyls also grew in popularity after the King complex was correctly assigned and Fischer, meanwhile, reported the structure of the first characterized group VII transition metal dinuclear carbene complex of Mn [44]. Both Re$_2$(CO)$_{10}$ and Tc$_2$(CO)$_{10}$ were also incorporated into multimetal carbene complexes when Weiss and Fischer treated the carbonyl compound with PhLi, followed by the alkylation with [Me$_3$O]BF$_4$ [45]. Interestingly, the treatment of Re$_2$(CO)$_{10}$ with an excess of LiSiPPh$_3$ yielded not only the monocarbene complex but also a biscarbene complex with each Re-fragment containing a the carbene ligand [46,47].
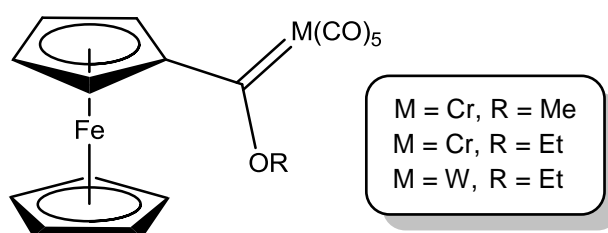
Figure 10: First ferrocene-containing Fischer carbene complexes [40]

1.2.2 Developments in N-heterocyclic carbene chemistry

Arduengo carbenes, also known as N-heterocyclic carbenes (NHCs), have dominated carbene research since the free analogue was isolated and ligated to transition metal

[40] J.A. Connor, J.P. Lloyd, J. Chem. Soc., Dalton Trans.(1972) 1470.
[41] E.O Fischer, F.J. Gammel, D. Neugebauer, Chem. Ber. 113 (1980) 1010.
[42] U. Behrendt, R.M. Pfeifer, R. Wartchow, H. Butenschön, New J. Chem. 23 (1999) 891.
[43] D.I. Bezuidenhout, E. van der Watt, D.C. Liles, M. Landman, S. Lotz, Organometallics 27 (2008) 2447.
[44] (a) E.O. Fischer, E. Offhaus, Chem. Ber. 102 (1969) 2549. (b) G. Hutter, D. Regler, Chem. Ber. 10 (1972) 3027.
[45] K. Weiss, E.O. Fischer, Chem. Ber. 109 (1976) 1120.
[46] U. Schubert, K. Ackermann, P. Rustenmeyer, J. Organomet. Chem. 231 (1982) 323.
[47] E.O. Fischer, P. Rustenmeyer, O. Orama, D. Neugebauer, U. Schubert, J. Organomet. Chem. 247 (1983) 7.

2016

complexes by Arduengo in the 1990s [48]. Prior to the conclusions of Arduengo, Öfele [24] and Wanzlick and Schönherr [25] were able to successfully coordinate NHC ligands to metal centres but failed to isolate the deprotonated carbene moiety. Literature indicates several publications relating to carbene-metal coordination, properties and catalytic ability that have surfaced over the past few decades [49] and have predominantly commented on the NHC complex's stability towards moisture, heat and oxygen [50]. Current research advances of employing silver (I) complexes as metal carbene transfer reagents have attracted much interest and application and this method is often applied as an alternative to classic deprotonation techniques employing a metal base [51]. NHC complexes of the majority of late transition metals are known, and are accessible via silver NHC transfer reactions [52] and a significant number of these silver transfer reagents show potential application in material sciences [53]. N-heterocyclic carbenes are singlet carbenes, similar to Fischer-type carbenes, and bordered by two π-donor heteroatoms. The interaction of the π-electron pairs of the heteroatoms with the p_π orbital of the carbene carbon centre elevates the relative energy of the p_π orbital but does not, however, affect the energy of the carbene carbon σ orbital; as a result, the σ-p_π energy gap expands [54], adding additional stability to the bent singlet ground state of the heterocyclic ligand (Figure 11). Carbenes such as NHCs, that receive electron density from both α-groups (R-groups), achieve the optimum bent geometry with a small valence angle for strongly and effortlessly binding to metal fragments [55,56]. Since NHC ligands bind so strongly to the metal centre, the ligands exhibit high dissociation energies, which have been quantified by theoretical calculations for several different metal complexes. The elevated dissociation energies are calculated in comparison with typical ligands such as phosphine, carbonyl and amine ligands [57,58].

[48] (a) A.J. Arduengo, R.L. Harlow, M. Kline, J. Am. Chem. Soc. 113 (1991) 361; (b) A.J. Arduengo, M. Kline, J.C. Calabrese, F. Davidson, J. Am. Chem. Soc. 113 (1991) 9704; (c) A.J. Arduengo, R. Krafczyk, R. Schmutzler, H.A. Craig, J.R. Goerlich, W.J. Marshall, M. Unverzagt, Tetrahedron. 55 (1999) 14523.
[49] W.A. Herrmann, Angew. Chem. Int. Ed. Engl. 41 *(*2002) 1290.
[50] P.L. Chiu, C.Y. Chen, J.Y. Zeng, C.Y. Lu, H.M. Lee, J. Organomet. Chem. 690 (2005) 1682.
[51] (a) H.M.J. Wang, I.J.B. Lin, Organometallics 17 *(*1998) 972; (b) B. Bildstein, M. Malaun, H. Kopacka, K. Wurst, M. Mitterböck, K.H Ongania, G. Opromolla, P. Zanello, Organometallics 18 (1999) 4325.
[52] (a) L.G. Bonnet, R.E. Douthwaite, B.M. Kariuki, Organometallics, 22 (2003) 4187; (b) A.A. Danopoulos, A.A.D. Tulloch, S. Winston, G. Eastham, M.B. Hursthouse, J. Chem Soc., Dalton Trans. (2003) 1009.
[53] (a) C.K. Lee, K.M. Lee, I.J.B. Lin, Organometallics 21 (2002) 10; (b) J.C.C. Chen, I.J.B. Lin, J. Chem. Soc., Dalton Trans. (2000) 839.
[54] F.E. Hahn, M.C. Jahnke, Angew. Chem. Int. Ed. Engl. 47 (2008) 3122.
[55] (a) J.F.Harrison, J. Am. Chem. Soc. 93 (1971) 4112. (b) J.F. Harrison, C.R. Liedtke, J.F. Liebman, J. Am. Chem. Soc. 101 (1979) 7162. (c) L. Pauling, J. Chem. Soc. Chem. Commun. (1980) 688.
[56] K.K. Irikura, W.A. Goddard III, J.L. Beauchamp, J. Am. Chem. Soc. 114 (1992) 48.
[57] T. Weskamp, F.J. Kohl, W. Hieringer, D. Gleich, W.A. Herrmann, Angew. Chem. 111 *(*1999) 2573.
[58] J. Schwarz, V.P.W. Böhm, M.G. Gardiner, M.Groscher, W.A. Herrmann, W. Hieringer, G. Raudaschl-Sieber, Chem. Eur. J. 6 (2000) 1173.
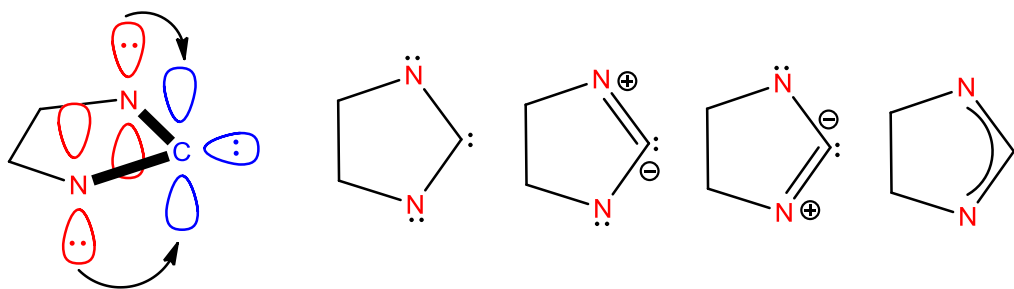
Figure 11: Internal stabilization and resonance structures of a NHC ligand

Advances in the field of NHCs have been abundant and have been expanded to include early, middle and late transition metals in the complexes. Group VII transition metal NHC complexes, however, have been mostly ignored and only a few literature reports of these complexes have been noted. Most published works on manganese NHC complexes focus on manganese (I) and the first literature reports by Lappert and Pye [59] in 1977 (Figure 12), describe the synthesis of NHC complexes of manganese tricarbonyl at elevated reaction temperatures (180ºC) in decalin as solvent and produced only low yields [59]. Aumann and Heinen improved on the synthetic methodology and were able to produce Mn-NHC complexes in higher yields via a ketenimine intermediate (Figure 12) [60]. The improvement in the reaction methodology also enabled the research group to produce a variety of different 5-membered normal and abnormal NHC metal complex derivatives. Fehlhammer [61] described multicomponent reactions of Mn(I) complexes with the aim of finding viable reaction pathways to produce new substitution patterns on NHC analogues such as oxazoles and imidazoles [62]. Building on this fundamental work, Ruiz [63] also reported multicomponent reactions but with the main focus of actually isolating the Mn(I) carbene complexes (Figure 12). Ruiz describes the applicability of using substituted cyano manganese compounds as synthons for the production manganese(I) NHC complexes. The synthetic methodology was applicable in the synthesis of N,O-heterocyclic carbene complexes of manganese(I) which, in turn, could be used as transfer reagents [64] to produce Au complexes via transmetallation. A DFT study complemented the experimental report in order to deduce the mechanistic aspects of the reaction.

[59] M. F. Lappert, P. L. Pye, J. Chem. Soc., Dalton Trans. (1977) 2172.
[60] R. Aumann, H. Heiken, Chem. Ber. 122 (1989) 77.
[61] D. Rieger, S.D Lotz, U. Kernbach, C. André, J. Biertran-Nadal, W.P. Fehlhammer. J. Organomet, Chem. 491 (1995) 135.
[62] W. P. Fehlhammer, M. Fritz, Chem. Rev. 93 (1993) 1243.
[63] J. Ruiz, B.F. Perandones, G. Garcia, M.E.G. Mosquera, Organometallics 26 (2007) 5687.
[64] J. Ruiz, A. Berros, B.F. Perandones, M. Vivanco, Dalton Trans. (2009) 6999.
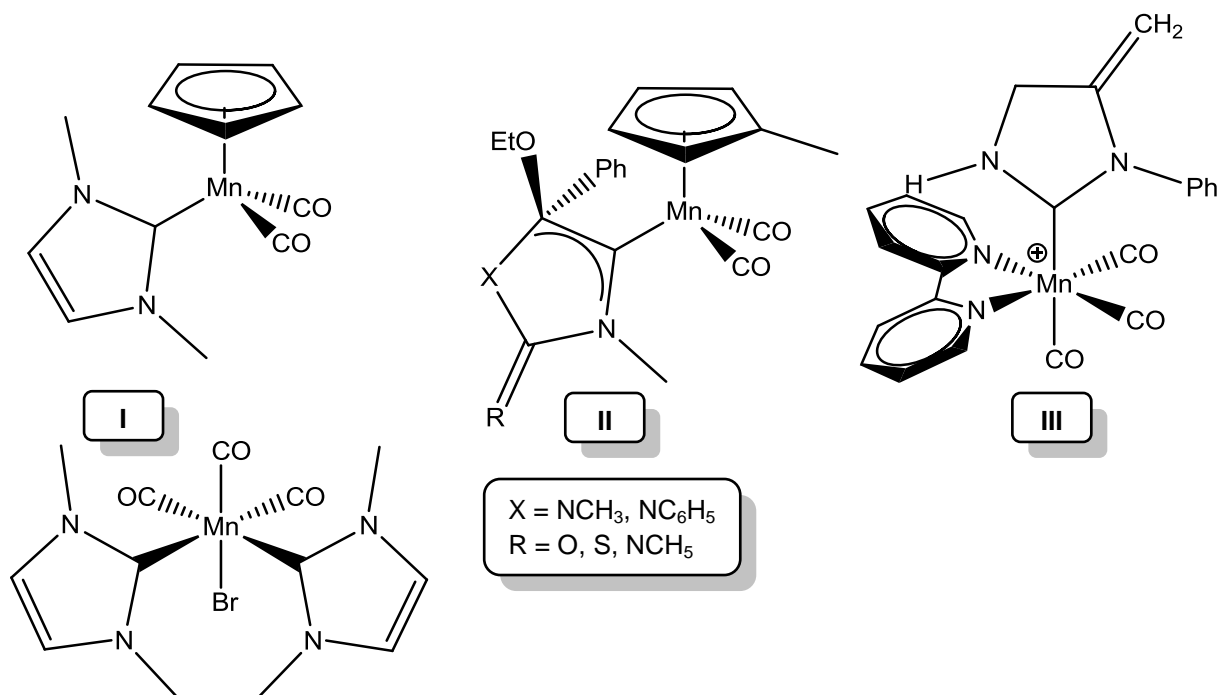
Figure 12: First NHC complexes of manganese(I) as described by Lappert and Pye (I) [59], Aumann (II) [60] and Ruiz (III) [63]

Apart from success in the synthesis of a few NHC complexes of manganese, Edwards, Hahn and co-workers managed to isolate biscarbene and triscarbene complexes of rhenium [65]. The group also later managed to isolate novel phosphine, pincer-type NHC complexes of group VII metals. Meanwhile, Whittlesey and co-workers returned to the low yielding reactions of Lappert and Pye and were able to synthesise an NHC complex of MeCpMn(CO)$_3$ by the photo irradiation of the manganese tricarbonyl complex in a fairly high yield (40%) in hexane [66]. Further irradiation of the isolated carbene complex releases a second carbonyl ligand and internal stabilization of the complex occurs via an agnostic interaction [66]. Only a few examples exist of manganese(II) NHC complexes and the first was reported about a decade ago by Cowley *et al.* [67]. Treating manganocene with a mesitylene NHC ligand afforded two different NHC complexes, a mono- and a biscarbene complex. Both complexes were electron deficient and decomposed in a matter of days even when stored under argon. Complexes of rhenium in oxidation states I and V were the main

[65] O. Kaufhold, A, Stasch, T. Pape, A. Hepp, P.G. Edwards, P.D. Newman, F.E. Hahn, J. Am. Chem. Soc. 131 (2008) 306.
[66] M. Batool, T.A. Martin, A.G. Algarra, M.W. George, S.A. Macgregor, M.F. Mahon, M.K. Whittlesey, Organometallics 30 (2011) 2200.
[67] C.D. Abernethy, A.H. Cowley, R.A. Jones, C.L.B. Macdonald, P. Shukla, L.K. Thompson, Organometallics 20 (2001) 362.

focus during the development of group VII NHC complexes and this is mainly due to the stability of these oxidation states [68]. Mono- [69], bis- [70] and even tetrakiscarbene [71] complexes of rhenium have been synthesised. Building on previously reported syntheses, Herrmann synthesised a chelate bis(NHC) carbene from the $[NEt_4]_2[ReBr_3(CO)_3]$ metal precursor and the free carbene ligand. Casson [72] and Li [73] prepared a variety of chelated monocarbene complexes of rhenium(I) with a pyridyl group, which demonstrated luminescent properties. Finally, many reports of tetrakiscarbene complexes have been reported by Abram and co-workers [74,75] and Royo and co-workers [76].

1.3 Computational studies on N-heterocyclic- and Fischer carbene complexes

Theoretical and computational chemistry simulate chemical structures and reactions numerically and provides an interface between mathematical operations, chemistry and the user [77]. It facilitates chemists to study chemical phenomena by executing calculations on computers rather than investigating reactions and complexes experimentally. Computational chemistry presents insight about molecules and reactions that would have proved impractical to achieve through inspection [77]. The advances in quantum mechanical models for calculations of electronic structures provide chemical information into the characteristics of the chemical bond in transition metal carbene complexes. Since the development and improvement of recent, well-defined quantum chemical change and energy partitioning methods, it is now feasible to study even multifaceted and complex organometallic systems [78]. Methods such as atoms in molecules (AIM) [79], charge decomposition analysis (CDA) [80], energy decomposition analysis (EDA) and natural bond orbital analysis (NBO) [81]

[68] S.J. Hock, L. Schaper, W.A. Herrmann, F.E. Kühn, Chem. Soc. Rev. 42 (2013) 5073.
[69] W.M. Xue, M.C.W. Chan, Z.M. Su, K.K. Cheung, S.T. Liu, C.M. Che, Organometallics 17 (1998) 1622.
[70] W.A. Herrmann, K. Öfele, M. Elison, F.E. Kühn, P.W. Roesky, J. Organomet. Chem. 480 (1994) c7.
[71] H. Braband, D. Przyrembel, U. Abram. Z. Anorg, Allg. Chem. 632 (2006) 779.
[72] L.A. Casson, S. Muzzioli, P. Raiteri, B.W. Skelton, S. Stagni, M. Massi, D.H. Brown, Dalton Trans. 40 (2011) 11960.
[73] X.W. Li, H.Y. Li, G.F. Wang, F. Chen, Y.Z. Li, X.T. Chen, Y.X. Zheng, Z.L. Xue, Organometallics 31 (2012) 3829.
[74] E. Oehlke, S. Kong, P. Arciszewski, S. Wiebalck, U. Abram, J. Am. Chem. Soc. 134 (2012) 9118.
[75] H. Braband, E. Oehlke, U. Abram, Z. Anorg. Allg. Chem. 632 (2006) 1051.
[76] B. Royo, E. Herdtweck, C.C. Romão, Eur. J. Inorg. Chem. (2004) 3305.
[77] J.B. Foresman, Æ Frisch, Exploring Chemistry with Electronic Structure Methods, 2nd edn., Gaussian, Inc. Pittsburgh USA, (1996).
[78] G. Frenking, N. Fröhlich. Chem. Rev. 100 (2000) 717.
[79] R.F.W. Bader, Atoms in Molecules: A Quantum Theory, Oxford University Press, (1990).
[80] S. Dapprich, G. Frenking, CDA 2.1, Marburg, (1994); (b) S. Dapprich, G. Frenking J. Phys. Chem. 99 (1995) 9352.
[81] T. Ziegler, A. Rauk, Inorg. Chem. 18 (1979) 1755; (b) F.M. Bickelhaupt, N.M.M. Nibbering, E.M. van Wezenbeek, E.J. Baerends, J. Phys. Chem. 96 (1992) 4864; (c) T. Ziegler, A. Rauk, Inorg. Chem. 18 (1979)

have proven very useful in comprehensive studies of complex molecules. In 2000 Frenking and Frölich published an in-depth summary of the methods and approaches of theoretical chemistry as applied to the bonding in transition metal complexes [78]. Reports on the linear relationship between DFT calculated E_{HOMO} and experimental oxidation potentials E_{pa} of phosphine-substituted Fischer have been published and show good correlation [82]. Similarly the calculated E_{LUMO} and experimental reduction potential E_{PC} also indicates a linear relationship. Incidences of non-covalent intramolecular interligand interactions were described by Lugan and Lavigne [83] where methylene protons of methoxycarbene complexes showed interactions with carbonyls of the metal carbene centre. These interactions were visualised using NBO's and indicated intramolecular stabilizations supporting the conformation aspects found in the solid state structure. The finding also supports seminal MO calculations by Hoffmann *et al.* [84] that have predicted that carbene ligands in piano-stool complexes preferred the so-called vertical coordination mode rather than the horizontal mode (Figure 13).
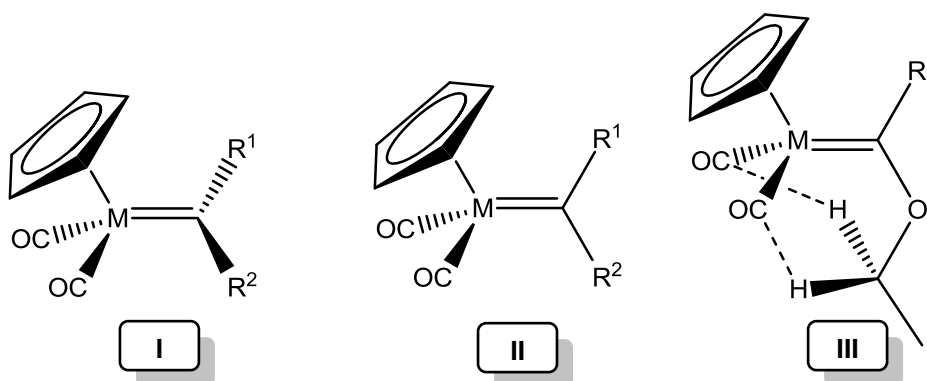
Figure 13: The horizontal coordination mode (I), the vertical coordination mode (II) and the stabilization of the vertical coordination mode (III) as described by Lugan and Lavigne [83]

Albrecht and co-workers [85] also applied principles of theoretical chemistry to CpFe NHC complexes in an attempt to probe bond characteristics between the metal and the carbene carbon. It was established that there is limited π-characteristics between the pianostool Fe complex and the NHC carbon, especially in reference to σ-donor or even σ-donor, π-

1558; (d) T. Ziegler, A. Rauk, Theor. Chim. Acta 46 (1977) 1; (e) K. Kitaura, K. Morokuma, Int. J. Quantum Chem. 10 (1976) 325.

[82] M. Landman, R. Liu, R. Fraser, P. H. van Rooyen, J. Conradie, J. Organomet. Chem. 752 (2014) 171.

[83] N. Lugan, I. Fernández, R. Brousses, D.A. Valyaev, G. Lavigne, N.A. Ustynyuk, Dalton Trans. 42 (2013) 898.

[84] B.E.R. Schilling, R. Hoffmann, D.L. Lichtenberger, J. Am. Chem. Soc. 101 (1979) 585.

[85] L. Mercs, G. Labat, A. Neels, A. Ehlers, M. Albrecht, Organometallics 25 (2006) 5648.

acceptor ligands. It was determined that the π-characteristic diminishes in the order: CO > py > NHC ligands and there was only 15.4% π-character in the Fe-NHC bond.

The chemical bonding in transition metal complexes were also probed by Frenking and co-workers [86] and they found low double-bond characteristics in Fischer-type carbene complexes. Calculated Cioslowski-Mixon bond orders of between 0.93-1.18 indicated limited double-bond properties of the metal-carbene bonds in Fischer carbene complexes compared to values of between 1.48-1.87 for Schrock-type carbene complexes. The study indicated the carbene-metal σ-donation (d) compared to π-back-donation (b) via the metal electrons is significantly lower or even negligible in NHC complexes and low in Fischer carbene complexes (Figure 14). Back-donation from the metal to the carbene centre becomes more significant in Fischer-type carbene complexes when the heteroatom (X-group) provides less stabilizing π-donation. Aminocarbene complexes are thus greatly stabilized via the heteroatom and requires less back donation from the metal centre as indicated by the donation/back-donation ratio (d/b) (Figure 14).
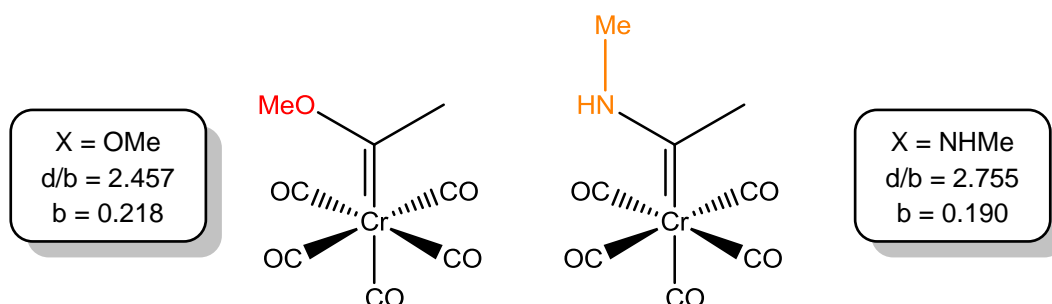
Figure 14: σ and π-back donation in chromium carbene complexes

[86] G. Frenking, M. Solà, S.F. Vyboishchikov, J. Organomet. Chem. 690 (2005) 6178.

1.4 Aim of the study

The aim of this study was the complete synthesis, characterization, structural and application investigation of group VI and VII transition metal Fischer and N-heterocyclic carbene complexes to identify chemical similarities and differences between the two carbene types.

The following aspects were studied:

- The synthesis of cymantrenyl and cyclopentadienyl rhenium tricarbonyl Fischer carbene complexes of group VI and VII transition metals.
- The synthesis of phosphine-substituted cymantrenyl Fischer carbene complexes.
- The synthesis of NHC complexes of cymantrene.
- The synthesis of NHC complexes of group VII transition metals.
- The full characterization of all the complexes synthesised in this study by use of ^{1}H, ^{13}C and ^{31}P nuclear magnetic resonance spectroscopy, infrared spectroscopy and electrospray-ionization mass spectrometry.
- Single-crystal X-ray diffraction studies to obtain experimental data to compare with theoretical DFT results.
- Theoretical DFT studies to highlight fundamental similarities and differences between the bonding models of Fischer carbenes and NHC complexes.
- Theoretical DFT studies to predict electronic changes in complexes after the coordination of phosphines or carbene ligands.
- Investigation of appropriate application possibilities for the novel carbene complexes, with focus on catalytic dimerization of thiols.

Carbene complexes of Group VII transition metals have been underrepresented in literature and very few new publications focus on complexes of this type. Group VII transition metal carbene complexes have found application in catalytic conversions [87], designing organometallic multi-tags [88] and recognised for their contribution in the synthesis of organic building blocks [89]. Mono-, di- and trimetallic Fischer and N-heterocyclic carbene complexes of group VII metals including the cymantrene moiety as either carbene metal or carbene substituent (or both) have been successfully synthesised and characterized. Using DFT calculations, a detailed structural investigation, natural bonding orbital analysis and well as and isomeric feature analysis were attempted.

[87] K.Y.D. Tan, J.W. Kee, W.Y. Fan, Organometallics 29 (2010) 4459.
[88] D.I. Bezuidenhout, B. van der Westhuizen, P.J. Swarts, T. Chatturgoon, O.Q. Munro, I. Fernández, J.C. Swarts, Chem. Eur. J. 20 (2014) 4974.
[89] K.H. Dötz, J. Stendel Jr. Chem. Rev.109 (2009) 3227.

Mixed metal systems, all in electronic contact, have also been investigated by the employment of the cymantrenyl moiety as deprotonated synthon and subsequent metalation by a group VI or VII metal carbonyl group. The DFT study was also extended to propose energy plot diagrams for the synthesis of the above mentioned Fischer carbene complexes. To compare reactivity, a series of NHC complexes were also synthesised from the cymentrene synthon and both the Fischer and NHC complexes exploited in the dimerization catalysis of alkyl, aryl and biological thiols and isothiocyanates (Scheme 3).

$$2\ RSH \xrightarrow[hv]{Catalyst} RS\text{-}SR + H_2$$

R = Fischer carbene, L= CO
R = H, L= NHC ligand
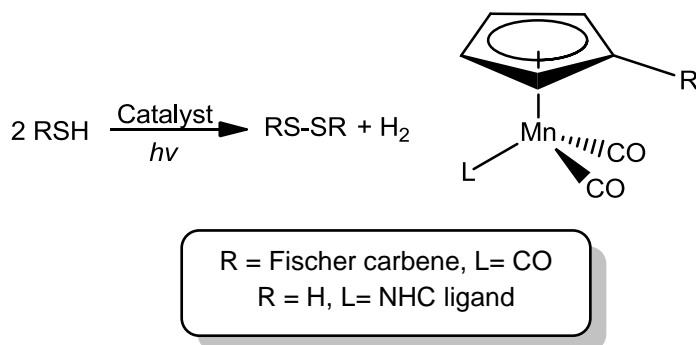
Scheme 3: The dimerization of thiol substrates

Literature presidents already exist for the dimerization of thiol- and isocyanate substrates by cyclopentadienyl manganesetricarbonyl. Apart from proposing a stepwise mechanism for the dimerizations of thiols and isothiocyanates, energy profiles were also determined for the mechanism. The syntheses of both Fischer- and N-heterocyclic carbene complexes allowed for the comparison of the metal-carbene properties of the two different types of carbenes. Literature indicates that the π- back-donation from the metal centre to the Fischer-type carbene empty p-orbital is less significant that originally established and may even be irrelevant in NHC complexes M-carbene bond [90]. A study was also attempted to extend this literature finding to group VII carbene complexes.

1.5   Organization of this thesis

The thesis is based on a compilation of different published articles by the student. The articles might be composed in different formats as required by the publication and results might also be presented in more than one article, since different aspects are considered in each.

---

[90] W.A. Herrmann, C. Köcher, Angew. Chem. 109 (1997) 2257; (b) Angew. Chem. Int. Ed. Engl. 36 (1997) 2162.

CHAPTER 2

Synthesis, structure and DFT study of cymantrenyl Fischer carbene complexes of group VI and VII transition metals

Chapter 2 was adapted from an article published in Journal of Molecular Structure. The format reflects the requirements of the journal.

Graphical Abstract:
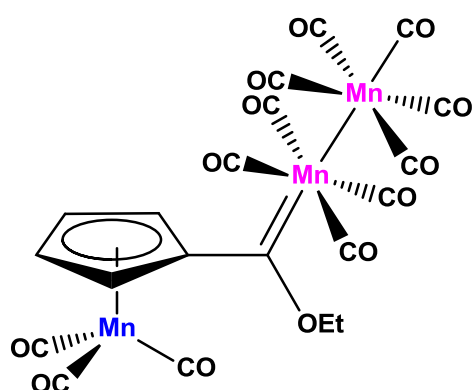
Contributions:

Roan Fraser: Author, synthesis, DFT studies

Petrus H. van Rooyen: Co-author, crystallography

Marilé Landman: Corresponding author, supervisor

2

Synthesis, structure and DFT study of cymantrenyl Fischer carbene complexes of group VI and VII transition metals

Roan Fraser, Petrus H. van Rooyen and Marilé Landman*

Department of Chemistry, University of Pretoria, Private Bag X20, Hatfield, 0028, South Africa. Tel: +27-12-4202527, Fax: +27-12-4204687

Contact author details:

Name: Marilé Landman Tel: +27-12-4202527, Fax: +27-12-4204687, e-mail: marile.landman@up.ac.za

Keywords

Graphical abstract

TOC abstract

Synthesis, X-ray study and NBO analysis of Fischer ethoxy carbene complexes with cymantrenyl substituents

Research highlights

- DFT calculations on configurations of trimetallic complexes

- Crystal structure of first carbene complex with cymantrenyl substituent

- Crystal structures of axial and equatorial trimetallic carbene complexes

- Calculated NBO donor-acceptor interactions show intramolecular stabilization

Abstract

Bi- and trimetallic carbene complexes of group VI and VII transition metals (Cr, Mo, W, Mn and Re), with $CpMn(CO)_3$ as the initial synthon, have been synthesised according to the classical Fischer methodology. Crystal structures of the novel carbene complexes with general formula $[M_x(CO)_{y-1}\{C(OEt)(MnCp(CO)_3)\}]$, where x = 1 then y = 3 or 6; x = 2 then y = 0, of the complexes are reported. A density functional theory (DFT) study was undertaken to determine natural bonding orbitals (NBOs) and conformational as well as isomeric aspects of the polymetallic complexes. Application of the second-order perturbation theory (SOPT) of the natural bond orbital (NBO) method revealed stabilizing interactions between the methylene C-H bonds and the carbonyl ligands of the carbene metal moiety. These stabilization interactions show a linear decrease for the group VI metal carbene complexes down the group.

1   Introduction

The number of classical Fischer carbene complexes containing group VI and group VII transition metals have grown significantly in number since the initial synthesis by Fischer and Maasböl in 1964 [1]. Highly functionalized carbene complexes [2], polymetallic systems [3] and polynuclear biscarbene complexes [4] have all been reported in literature. In particular, complexes where the pianostool complexes, cymantrene ($CpMn(CO)_3$) [5, 6] and $CpRe(CO)_3$ [7], are applied as metallating agent have been studied comprehensively. The electronic nature of

[1] E.O. Fischer, A. Maasböl, Angew. Chem. Int. Ed. Engl. 3 (1964) 580.
[2] C.A. Toledano, J. Levisalles, M. Rudler, H. Rudler, J. Daran, Y. Jeannin, J. Organomet. Chem. 1 (1982) C7.
[3](a) J.M. Garner, A. Irving , J.R. Moss, Organometallics, 9 (1989) 2836. (b) D.I. Bezuidenhout, B. van der Westhuizen, P.J. Swarts, T. Chatturgoon, O.Q. Munro, I. Fernández, J.C. Swarts, Chem. Eur. J. 20 (2014) 2974.
[4] G.M. Chu, I. Fernández, M.A. Sierra, Chem. Eur. J. 19 (2013) 5899.
[5] N. Maoz, A. Mandelbaum, M.A. Cais, Tetrahedron Lett. 25 (1965) 2087.
[6] E.O. Fischer, W. Kleine, W. Schambeck, U. Schubert, Z. Naturforsch, B: Anorg.Chem. All. Chem. 36B (1981) 1575.
[7] C.P. Casey, C.J. Czerwinski, D.R. Powell, R.K. Hayashi, J. Am. Chem. Soc. 119 (1997) 5750.

the carbene ligand's substituents has a direct effect on the bond order of the metal-carbon double bond whilst the steric bulk of these substituents influences the observed bond angles. There is competition for the π-bonding between the three moieties bonded to the carbene carbon centre [8,9]. Intermetallic interactions in complexes containing more than one metal centre are interesting with respect to the potential communication pathways between the metal centres. Communication between metal centres may facilitate electron transfer chemistry, catalysis, molecular electronics and nonlinear optics applications [10]. Carbene complexes containing transition metals other than Mn or Re, bonded to Cp ligands, have also been reported in literature. Complexes employing $CpFe(CO)_2Me$ or $CpFe(CO)_2Bz$ as the initial deprotonated synthon have been reported by Butenschön [10] in an attempt to study the influence of a second metal centre, incorporated into the carbene substituent, on the electrochemical nature of the system. Heterometallic carbene complexes of ferrocenyl are numerous in literature [11,12] and often undergo lithiation on both Cp rings to produce trinuclear biscarbene complexes. Bimetallic complexes where $CpMn(CO)_3$ and $CpRe(CO)_3$ are used as the initial building synthons, have been limited to studies published by Fischer [13,14] and Casey [15] on the homonuclear bimetallic monocarbene complexes (Figure 1) and Sierra [16], who reported heteronuclear monocarbene complexes of group VI metals. To our knowledge, these studies constitute the only examples where deprotonated cymantrenyl moieties served as the nucleophile in carbene synthesis.
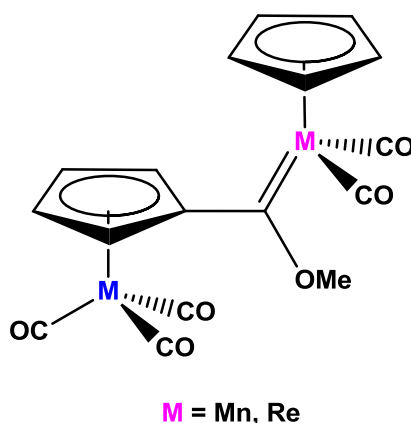
M = Mn, Re

Figure 1: Homonuclear bimetallic monocarbene complexes containing $CpM(CO)_3$ (M = Mn, Re) as initial building blocks synthesised by Fischer and Casey [32]

[8] M. Landman, W. Barnard, P.H. van Rooyen, D.C. Liles. J. Mol. Struct. 1021 (2012) 76.
[9] U. Schubert, Organometallics 1 (1982) 1085.
[10] U. Behrendt, R. M. Pfeifer, R. Wartchow, H. Butenschön, New J. Chem. 23 (1999) 891.
[11] J.G. López-Cortés, L.F.C. de la Cruz, M.C. Ortega-Alfaro, R.A. Toscano, C. Alvarez-Toledano, H. Rudler, J. Organomet. Chem. 690 (2005) 2229.
[12] Cambridge Structural Database (CSD), Version 5.35, May 2014 update, CSD reference code: BAVBIK, Private communication of M. B. Hursthouse, D. E. Hibbs and I. R. Butler to CCDC (2003).
[13] E.O. Fischer, V.N. Postnov, F.R Kreissl, J. Organomet. Chem. 231 (1982) C73.
[14] E.O. Fischer, V.N. Postnov, F.R Kreissl, J. Organomet. Chem. 127 (1977) C19.
[15] C.P. Casey, C.J. Czerwinski, R.K. Hayashi, Organometallics 15 (1996) 4362.
[16] M.L. Lage, I. Fernández, M.J. Mancheño, M. Gómez-Gallego, M.A. Sierra, Chem. Eur. J. 16 (2010) 6616.

21

Multiple computational studies have been performed on the rate of ligand substitution and stabilities of $CpMn(CO)_3$ derivatives compared to $TpMn(CO)_3$. Tp is the scorpionate ligand, hydridotris(1-pyrazolyl)borate and is considered to be an equivalent of the cyclopentadienyl (Cp) ligand. It was observed that the relative displacement rate of a carbonyl ligands from $TpMn(CO)_3$ was significantly higher than for the $CpMn(CO)_3$ analogue. It was concluded that the $TpMn(CO)_2$-L interaction was significantly weaker than that of $CpMn(CO)_2$-L and the bonding enthalpies was found to be 50% lower for the TpMn complex [17]. DFT calculations proved useful in the assignment of a metal-to-ligand charge-transfer transition during a photo slippage process observed by Sierra [16].

Literature ascribes the isomeric differences of group VII complexes, at the point of substitution, to both steric and electronic factors. [18,19]. Nucleophilic attack on either manganese or rhenium carbonyls is expected to be regioselective and occurs on the more electron-poor, equatorial carbonyl position. With bulkier ligands, and in manganese systems with shorter metal-metal bond lengths, axial nucleophilic attack becomes more favourable. Substitution of the carbonyl groups follow a similar reactivity pattern and the equatorial positions are typically favoured for smaller ligands while the axial position becomes favourable with bulkier groups [18,19]. Additional substitution can give rise to at least eight possible isomers [20]. Equatorially substituted $Mn_2(CO)_9$-carbene complexes with bulky ligands are, however, also found in literature. In these cases, the alkoxy carbene substituent may be found in the uncommon *syn* conformation relative to the other carbene substituent. Steric hindrance does not allow for the *trans* conformation [21].

In recent studies by Lugan *et al.* [22] as well as Landman *et al.* [23] the influence of NBO donor-acceptor interactions in stabilizing a specific carbene conformation was illustrated. These studies involved monometallic carbene complexes where the NBO interactions were observed between carbene substituents (alkoxy or heteroaryl substituent) and a carbonyl ligand of the carbene metal moiety. Based on these reports, a DFT study was initiated to determine whether any of these interactions were present in the novel complexes of this study, which contain an additional metal carbonyl moiety as carbene sustituent, *i.e.* $CpMn(CO)_3$. This study reports the

[17] B.H. G. Swennenhuis, R. Poland, N.J. DeYonker, C.E. Webster, D.J. Darensbourg, A.A. Bengali, Organometallics 30 (2011) 3054.
[18] E. Luncenti, G. D'Alfonso, C. Dragonetti, D. Roberto, A. Sironi, R. Ugo, Organometallics 28 (2009) 3040.
[19] P.J. Fraser, W.R. Roper, F.G.A. Stone, J. Chem. Soc. Dalton Trans. (1974) 760.
[20] C.C. Grimm, R.J. Clark, Organometallics 9 (1990) 1123.
[21] G. Huttner and D. Regler, Chem. Ber. 105 (1972) 1230.
[22] N. Lugan, I. Fernández, R. Brousses, D. A. Valyaev, G. Lavigne, N. A. Ustynyuk, Dalton Trans. 42 (2013) 898.
[23] S. Thompson, H.R. Wessels, R. Fraser, P.H. van Rooyen, D.C. Liles, M. Landman, J. Mol. Struct. 1060 (2014) 111.

synthesis of the five novel heteroatomic bimetallic and polynuclear complexes of group VI and VII transition metals (Figure 2-3), X-ray crystal structures of four of the complexes and a DFT study.
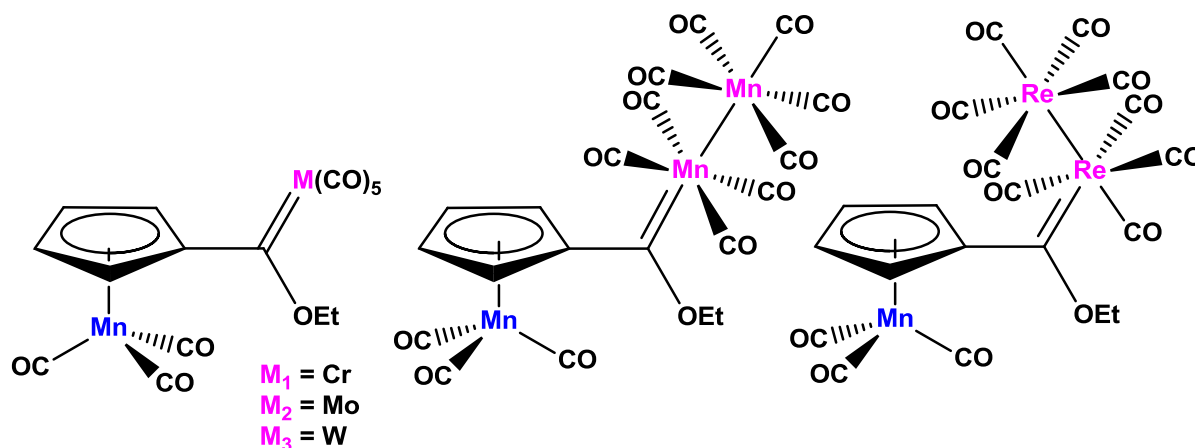
Figure 2: Heteronuclear bimetallic **1-3** and trimetallic monocarbene complexes **4** and **5**
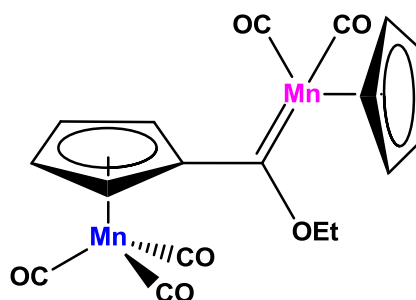
Figure 3: Homonuclear bimetallic monocarbene complex **6**

2 Experimental

2.1 General

All reactions, unless otherwise noted, were performed under inert nitrogen or argon atmospheres using standard Schlenk techniques [24]. All solvents were freshly distilled, dried and collected under inert conditions, with the exception of toluene. Toluene was not dried, but used after bubbling nitrogen gas through the solvent for 5 to 10 minutes. Column chromatography was carried out under inert nitrogen and argon atmospheres using silica gel (particle size 0.063-0.200 mm) as the stationary phase. Percentage yields were calculated

---

[24] D.F. Schriver, M.A. Drezdzon, The manipulation of Air-Sensitive Compounds, 2nd ed., Wiley, New York, USA, 1986.

23

relative to the limiting reactant. Crystallization was done using hexane:DCM or hexane:ether diffusion methods. Triethyloxonium tetrafluoroborate [25] was prepared according to a reported literature procedure. The reagents $CpMn(CO)_3$, $Cr(CO)_6$, $W(CO)_6$, $Mo(CO)_6$, $Mn_2(CO)_{10}$, $Re_2(CO)_{10}$, n-butyl lithium (1.6 M solution in hexane) and other commercial reagents were used as purchased. Complex **3** was synthesized according to a literature method [14]. NMR spectra were recorded on a Bruker ARX-300. NMR spectra were recorded in $CDCl_3$ using the deuterated solvent peak as internal reference. ^{1}H and ^{13}C NMR spectra were measured at 300.1 and 75.5 MHz, respectively. The numbering of atoms in the NMR assignment is according to the numbers used in Figure 4-7. IR spectra were recorded on a Perkin Elmer Spectrum RXI FT-IR spectrophotometer as KBr pellets and only the vibration bands in the carbonyl-stretching region (*ca.* 1500-2200 cm^{-1}) are reported.

2.2 Synthesis of complexes 1-6

2.2.1 Synthesis of 1

$CpMn(CO)_3$ (0.612 g, 3.0 mmole) was dissolved in 40 ml of dry THF. n-Butyl lithium (2.00 ml, 3.0 mmole) was added at -30 ˚C and stirred at this temperature for 30 min. The colour of the reaction mixture changed from yellow to a dark brown colour. $Cr(CO)_6$ (0.660 g, 3.0 mmole) were added to the reaction mixture at -79˚C and allowed to react at this temperature for 1 hour and warmed to room temperature. After completion of the reaction, the solvent was removed *in vacuo* and the residue redissolved in dichloromethane. Triethyl oxonium tetrafluoroborate (0.55 g, 3.0 mmole) was dissolved in 20 ml of dichloromethane and this was added to the cooled reaction mixture (-20 ˚C). An immediate colour change was observed, from brown to a deep red solution, and the reaction mixture was dry loaded onto a silica gel column for purification. The product was isolated using a 10:1 hexane: DCM eluent ratio. Two products were isolated: the first was a deep red monocarbene complex **1** (yield: 0.622g; 46%) and a second brownish product, complex **6** (yield: 0.195 g; 15%).

^{1}H NMR (δ(ppm), J(Hz)): H11 and H14 5.51 (s); H12 and H13 4.93 (s); O**CH$_2$**CH$_3$ 5.12 (q) 7.1; OCH$_2$**CH$_3$** 1.65 (t) 6.7. ^{13}C{^{1}H} NMR (δ(ppm)): C6 331.0; Mn(**CO**)$_3$ 222.8; Cr(**CO**-*trans*) 222.6; Cr(**CO**-*cis*) 216.4; C10 106.6; C11 and C14 87.6; C12 and C13 83.8; O**CH$_2$**CH$_3$ 77.2; OCH$_2$**CH$_3$** 15.1**.** IR (cm^{-1}): 2064 (s), 2031 (s), 1946 (s), 1922 (m).

2.2.2 Synthesis of 2

The syntheses of **2-6** were done using a similar procedure as for the synthesis of **1**. $CpMn(CO)_3$ (0.612 g, 3.0 mmole) was dissolved in THF and lithiated at -30 ˚C. The lithiated

[25] H. Meerwein, Org. Synth. 46 (1966) 113.

Cp metal moiety was then metallated with 0.792 g (3.00 mmole) of $Mo(CO)_6$ and quenched with the oxonium salt. Two products were isolated: a dark red monocarbene complex **2** (yield: 0.564 g; 38%) and a second brownish product **6** (yield: 0.130 g; 10%).

^{1}H NMR (δ(ppm), J(Hz)): H11 and H14 5.51 (s, br); H12 and H13 4.98 (s, br); O**CH₂**CH₃ 4.98 (s, br); OCH₂**CH₃** 1.62 (s, br). ^{13}C{^{1}H} NMR (δ(ppm)): C6 321.0; Mn(**CO**)₃ 222.7; Mo(**CO**-*trans*) 212.2; Mo(**CO**-*cis*) 205.6; C10 106.4; C11 and C14 88.4; C12 and C13 84.0; O**CH₂**CH₃ 77.2; OCH₂**CH₃** 15.0. IR (cm^{-1}): 2071 (s), 2032 (s), 1951 (s), 1925 (m).

2.2.3 Synthesis of *3* [14]

CpMn(CO)₃ (0.612 g, 3.0 mmole) was dissolved in THF and lithiated at -30 °C. The lithiated Cp metal moiety was then metallated with 1.056 g (3.00 mmole) of $W(CO)_6$ and quenched with the oxonium salt. Two products were isolated: a dark red monocarbene **3** (yield: 0.770 g; 44%) and a second brownish product **6** (yield: 0.234 g; 18%).

^{1}H NMR (δ(ppm), J(Hz)): H11 and H14 5.52 (s); H12 and H13 4.96 (s); O**CH₂**CH₃ 4.91 (q) 7.1; OCH₂**CH₃** 1.63 (t) 7.1. ^{13}C{^{1}H} NMR (δ(ppm)): C6 303.9; Mn(**CO**)₃ 222.7; W(**CO**-*trans*) 202.0; W(**CO**-*cis*) 197.0; C10 108.8; C11 and C14 88.8; C12 and C13 84.02; O**CH₂**CH₃ 77.2; OCH₂**CH₃** 14.8. IR (cm^{-1}): 2072 (m), 2031 (s), 1958 (s), 1944 (s).

2.2.4 Synthesis of *4*

CpMn(CO)₃ (0.612 g, 3.0 mmole) was dissolved in THF and lithiated at -30 °C. The lithiated Cp metal moiety was then metallated with 1.170 g (3.00 mmole) of $Mn_2(CO)_{10}$ and quenched with the oxonium salt. Two products were isolated: an orange-brown monocarbene complex **4** (yield: 0.652 g; 35%) and a second brownish product **6** (yield: 0.130 g; 10%).

^{1}H NMR (δ(ppm), J(Hz)): H11 and H12 5.78 (s, br); O**CH₂**CH₃ 5.31 (s, br); H12 and H13 5.03 (s, br); OCH₂**CH₃** 1.79 (s, br). ^{13}C{^{1}H} NMR (δ(ppm)): C6 305.8; Mn(**CO**)₃ 226.6; Mn₂(**CO**)₉ 224.6, 223.6, 209.5; C10 107.9; C11 and C14 87.9; C12 and C13 84.6; O**CH₂**CH₃ 75.9; OCH₂**CH₃** 14.2. IR (cm^{-1}): 2093 (w), 2034 (s), 2007 (s), 1998 (s), 1978 (s), 1941 (s), 1930 (s).

2.2.5 Synthesis of *5*

CpMn(CO)₃ (0.612 g, 3.0 mmole) was dissolved in THF and lithiated at -30 °C. The lithiated Cp metal moiety was then metallated with 1.958 g (3.0 mmole) of $Re_2(CO)_{10}$ and quenched with the oxonium salt. One product was isolated: a yellow-brown monocarbene complex **5** (yield: 0.795 g; 30%).

^{1}H NMR (δ(ppm), J(Hz)): H11 and H14 5.38 (s, br); H12 and H13 4.81 (s, br); O**CH₂**CH₃ 4.47 (q) 7.0; OCH₂**CH₃** 1.65 (t) 7.0. ^{13}C{^{1}H} NMR (δ(ppm)): C6 302.1; Mn(**CO**)₃ 223.3; Re₂(**CO**)₉

198.2, 194.2, 191.8; C10 115.4; C11 and C14 87.2; C12 and C13 82.2; O**CH₂**CH₃ 77.2; OCH₂**CH₃** 14.1. IR (cm⁻¹): 2071 (w), 2045 (w), 2030 (w), 2015 (s), 2003 (w), 1995 (w), 1977 (w), 1955 (w), 1953 (w), 1944 (w).

2.2.6   Synthesis of **6**

CpMn(CO)₃ (0.612 g, 3.0 mmole) was dissolved in THF and lithiated at -30 ˚C. The lithiated Cp metal moiety was then metallated with a second equivalent of CpMn(CO)₃ and quenched with the oxonium salt One product was isolated: a dark brown monocarbene complex **6** (yield: 0.520 g; 52%). This product was also formed during the synthesis of **1-5** as a minor side product.

¹H NMR (δ(ppm), J(Hz)): H11 and H14 5.49 (s, br); H12 and H13 5.25 (s, br); Cp 4.70 (s, br); O**CH₂**CH₃ 4.94 (s, br); OCH₂**CH₃** 1.55 (s, br). ¹³C{¹H} NMR (δ(ppm)): C6 329.3; Mn(**CO**)₂ 230.7; Mn(CO)₃ 224.6; C10 110.0; C11 and C14 87.4; C12 and C13 84.3; Cp 83.0; O**CH₂**CH₃ 74.3; OCH₂**CH₃** 14.3. IR (cm⁻¹): 2026 (s), 1953 (s), 1944 (s), 1896 (s).

2.3   X-ray crystallography

Data for complexes **1** and **4-6** were collected at 150 K on a Bruker D8 Venture kappa geometry diffractometer, with duo Iμs sources, a Photon 100 CMOS detector and APEX II control software using Quazar multi-layer optics, monochromated Mo-Kα radiation and by means of a combination of ϕ and ω scans. Data reduction was performed using SAINT+ and the intensities were corrected for absorption using SADABS [26]. The structures were solved by intrinsic phasing using SHELXTS and refined by full-matrix least squares using SHELXTL and SHELXL-2013 [27]. In the structure refinement, all hydrogen atoms were added in calculated positions and treated as riding on the atom to which they are attached. All nonhydrogen atoms were refined with anisotropic displacement parameters, all isotropic displacement parameters for hydrogen atoms were calculated as X × Ueq of the atom to which they are attached, X = 1.5 for the methyl hydrogens and 1.2 for all other hydrogens. Crystallographic data and refinement parameters are given in Table 1. Ortep drawings [28] of the three structures are included in Figure 4-7. The crystal structures (cif) have been deposited at the Cambridge Crystallographic Data Centre and allocated the deposition numbers: CCDC 1417538-1417541. Data collection, structure solution and refinement details are available in each cif.

[26] APEX2 (including SAINT and SADABS); Bruker AXS Inc., Madison, WI (2012).

[27] G.M. Sheldrick, Acta Crystallogr. A64 (2008) 112.

[28] L.J.J. Farrugia, Appl. Crystallogr. 30 (1997) 565.

2.4 Molecular modelling

The calculations reported in this paper were obtained using the Gaussian 09 [29] suite of programs. Calculations were carried out in the singlet spin state using the hybrid functional B3LYP [30,31]. Geometries of the neutral complexes were optimized in gas phase with the triple-ζ basis set 6-311G* on all atoms except for the metal atoms. Stuttgart/Dresden (SDD) pseudopotential was used to describe the metal electronic core, while the valence electrons were described def2-TZVPP [32]. No symmetry constraints were applied and only the default convergence criteria were used during the geometric optimizations. Vibrational frequencies [33] were calculated at the optimized geometries and no imaginary frequencies were observed, to confirm true minima. Donor-acceptor interactions have been computed using the natural bond order (NBO) method [34].

3 Results and discussion

3.1 Synthesis and characterization

M = Cr, Mo, W, Mn, Re
x = 1, y = 6
x = 2, y = 10

Scheme 1: Synthetic procedure followed for the synthesis of complexes **1**-**6**

[29] M.J. Frisch, G.W. Trucks, H.B. Schlegel, G.E. Scuseria, M.A. Robb, J.R. Cheeseman, G. Scalmani, V. Barone, B. Mennucci, G.A. Petersson, H. Nakatsuji, M. Caricato, X. Li, H.P. Hratchian, A.F. Izmaylov, J. Bloino, G. Zheng, J.L. Sonnenberg, M. Hada, M. Ehara, K. Toyota, R. Fukuda, J. Hasegawa, M. Ishida, T. Nakajima, Y. Honda, O. Kitao, H. Nakai, T. Vreven, J.A. Montgomery (Jr), J.E. Peralta, F. Ogliaro, M. Bearpark, J.J. Heyd, E. Brothers, K.N. Kudin, V.N. Staroverov, T. Keith, R. Kobayashi, J. Normand, K. Raghavachari, A. Rendell, J.C. Burant, S.S. Iyengar, J. Tomasi, M. Cossi, N. Rega, J.M. Millam, M. Klene, J.E. Knox, J.B. Cross, V. Bakken, C. Adamo, J. Jaramillo, R. Gomperts, R.E. Stratmann, O. Yazyev, A.J. Austin, R. Cammi, C. Pomelli, J.W. Ochterski, R.L. Martin, K. Morokuma, V.G. Zakrzewski, G.A. Voth, P. Salvador, J.J. Dannenberg, S. Dapprich, A.D. Daniels, O. Farkas, J.B. Foresman, J.V. Ortiz, J. Cioslowski, D.J. Fox, Gaussian 09, Revision D.01, Gaussian Inc., Wallingford CT, 2010.
[30] A.D. Becke, J. Chem. Phys. 98 (1993) 5648.
[31] C. Lee, W. Yang, R.G. Parr, Phys. Rev. B 37 (1988) 785.
[32] F. Weigend, R. Ahlrichs, Phys. Chem. Chem. Phys. 7, (2005) 3297.
[33] J.W. McIver, A.K. Komornicki, J. Am. Chem. Soc. 94 (1972) 2625.
[34] (a) J.P. Foster, F. Weinhold, J. Am. Chem. Soc. 102 (1980) 7211. (b) A.E. Reed, F. Weinhold, J. Chem. Phys. 83 (1985) 1736. (c) A.E. Reed, R.B. Weinstock, F. Weinhold, J. Chem. Phys. 83 (1985) 735. (d) A.E. Reed, L.A. Curtiss, F. Weinhold, Chem. Rev. 88 (1988) 899.

Complexes **1**-**5** were synthesised as major products in the reactions based on typical Fischer methodology (Scheme 1) [35]. During the synthesis of the proposed complexes, the formation of a homonuclear bimetallic-CpMn monocarbene complex, **6**, (Figure 3) was observed as a minor side product and isolated in low yields [13]. The infrared (IR) spectra of complexes **1**-**3**, using hexane as the solvent, showed two bands corresponding to the stretching frequency of the $CpMn(CO)_3$ tricarbonyl fragment [13] and four bands corresponding to the vibrational modes of the pentacarbonyl metal moiety, corresponding to literature reports [10,36]. Depending on the position of substitution, axial *vs.* equatorial, different patterns are expected in the IR spectra of the trimetallic complexes. Eleven bands should indicate equatorially substituted trimetallic complexes while seven bands are expected for the axially substituted trimetallic complexes [37]. These bands include two stretching frequency for the tricarbonyl metal moiety while the rest are ascribed to carbonyl stretching frequencies of the $M_2(CO)_9$-fragment. Seven IR active bands were observed for **4**, predicting an axial carbene ligand for the $Mn_2(CO)_9$ moiety while the ten bands observed on the IR spectrum of **5** led to the conclusion of an equatorially substituted carbene ligand for the $Re_2(CO)_9$ moiety. These structural predictions were confirmed with X-ray diffraction studies of the two complexes and will be presented in the next section.

3.2   X-ray Crystallography

In this section, X-ray structures of complex **1** (as representative example of the structure of bimetallic monocarbene complexes **1**-**3**), complexes **4** and **5** (to illustrate the axial and equatorial bonding mode in polynuclear monocarbene complexes) and complex **6**, a homonuclear bimetallic monocarbene complex, are presented. Complexes **1** and **4**-**6** were crystallized from hexane:DCM (1:1) solutions. Complex **1** formed red crystals while **4**, **5** and **6** crystallized as light brown-yellow (**4** and **5**), and dark brown-black crystals (**6**), respectively. The crystal structures are shown in Figure 4-7 and selected bond lengths and angles are reported in Table 1.

---

[35] See Ref. [5] and references therein.
[36] M.L. Ziegler, H. Haas, R.K. Sheline, Chem. Ber. 98 (1965) 2454.
[37] E. W. Post, K. L. Watters, Inorg. Chim. Acta 26 (1978) 29.
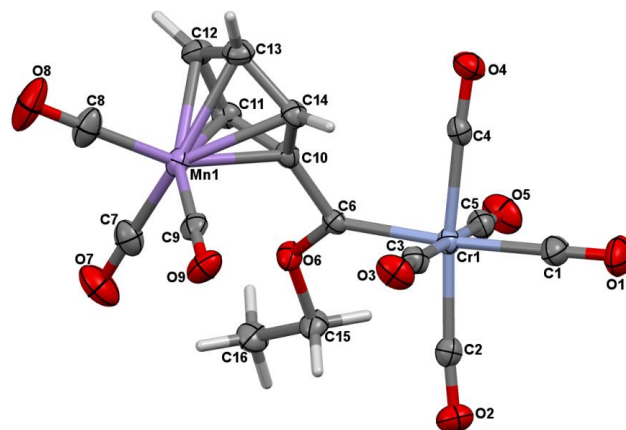
Figure 4: Perspective view of **1** with thermal ellipsoids drawn at the 50% probability level
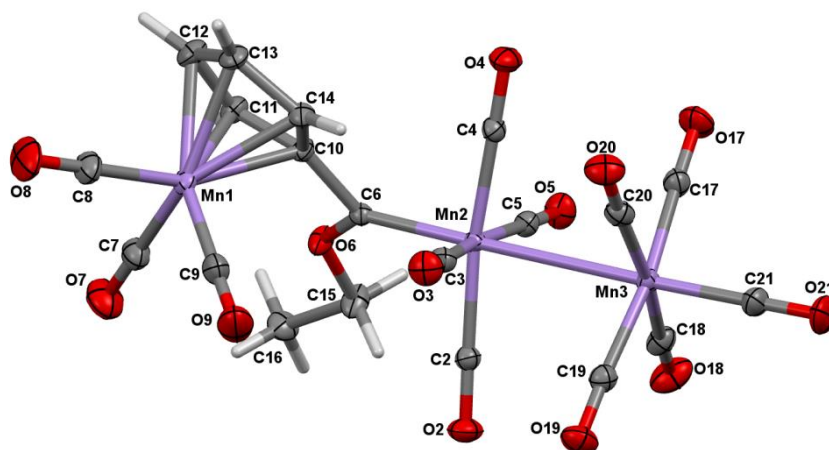
Figure 5: Perspective view of **4** with thermal ellipsoids drawn at the 50% probability level
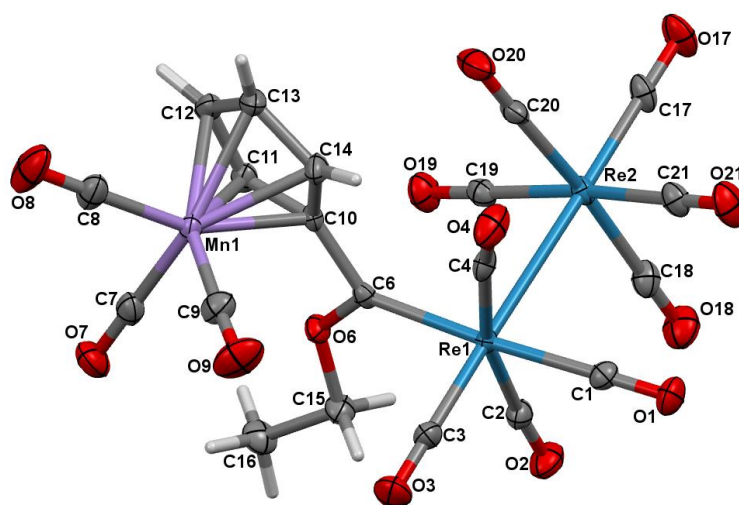
Figure 6: Perspective view of **5** with thermal ellipsoids drawn at the 50% probability level
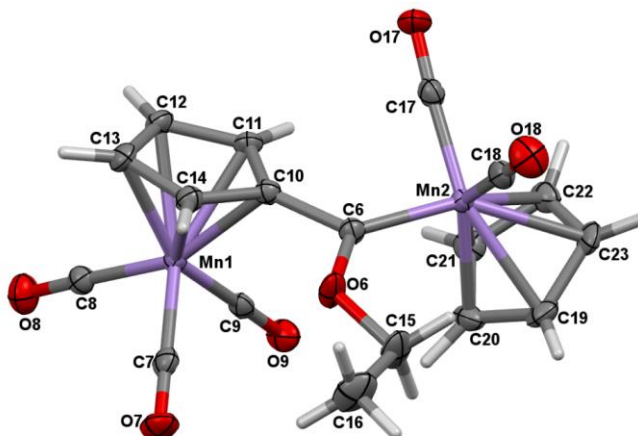
Figure 7: Perspective view of **6** with thermal ellipsoids drawn at the 50% probability level

Selected structural parameters of importance are summarized in Table 1. The carbene moiety, as represented by the M-C6-O6-C15 dihedral angles, deviate from planarity by less than 7° in all complexes. The M-C(carbene) distances increase in the order 1.905(4) Å (Mn-C6 in **6**) < 1.934(1) Å (Mn-C6 in **4**) < 2.037(2) Å (Cr-C6 in **1**) < 2.115(3) Å (Re-C6 in **5**), reflecting the double bond character of M=C6. These values are similar or in general shorter than M=C bond for analogous complexes with heteroarene substituents instead of a cymantrenyl substituent [8],[23],[38]-[41]. The angles between the carbene plane (M-C6-O6-C10) and the plane of the Cp ring (C10 - C14) are very similar for complexes **4** - **6** (*ca*. 18°) while it increase to 28° for **1**. Of significance is the bending of the C2=M=C4 bonds *cis* and nearest to the carbene ligand as indicated by non-linear bond angles of 173.93(8), 172.08(6) and 166.13(14)° for **1**, **4** and **5** respectively. The bending may indicate that an interaction between the groups on the carbene ligand and the carbonyl groups exists. This interaction will further be described in the DFT study section.The X-ray structures of **4** and **5** show that the carbene ligand is bonded in an axial position in the Mn-complex **4**, while it is in the equatorial position in the Re-complex **5**. In both structures the CO groups of the M(CO)$_5$ moiety in the equatorial positions are staggered with respect to the CO groups of the M(CO)$_4$ moiety, the preferred conformation in this kind of complexes [39]-[44]. The preference for axial *versus* equatorial substitution is further investigated by a DFT study; see section 3.3. Complex **6** exhibits the more uncommon 'horizontal' coordination mode (Figure 9) of the carbene ligand in pianostool complexes [22],

[38] D.I. Bezuidenhout, E. van der Watt, D.C. Liles, M. Landman, S. Lotz, Organometallics 27 (2008) 2447.

[39] S. Lotz, M. Landman, D.I. Bezuidenhout, A.J. Olivier, D.C. Liles, P.H. van Rooyen, J. Organomet. Chem. 690 (2005) 5929.

[40] D.I. Bezuidenhout, D.C. Liles, P.H. van Rooyen, S. Lotz, J. Organomet. Chem. 692 (2007) 774.

[41] S. Lotz, M. Landman, A.J. Olivier, D.I. Bezuidenhout , D.C. Liles, E.R. Palmer, Dalton Trans. 40 (2014) 9394.

[42] G.Huttner, D.Regler, Chem.Ber. 105 (1972) 1230.

[43] C. Alvarez-Toledano, A. Parlier, H. Rudler, M. Rudler, J Organomet. Chem. 328 (1987) 357.

[44] K. Osowska, K. Mierzwicki, S. Szafert, Organometallics 25 (2006) 3544.

where the carbene plane lies perpendicular to the pseudo-mirror plane of the $[CpMn(CO)_2]$ moiety; the angle between the two planes 73.2° in this case. This should limit the often-observed stabilizing interaction between the methyl or methylene hydrogen atoms and carbonyl ligands on the metal in this conformation.

Table 1: Selected bond lengths and angles

	1	**4**	**5**	**6**
Bond length (Å)				
Mn1-COx (x = 7-9)	1.800(2)	1.800(2)	1.805(4)	1.793(4)
M-C6	2.037(2)	1.934(1)	2.115(3)	1.905(4)
C6-C10	1.478(3)	1.480(2)	1.488(4)	1.487(5)
M-COx (x = 2-5)[a]	1.907(2)	1.849(2)	1.979(4)	-
M-COx (x = 17-20)[a]	-	1.853(2)	1.994(4)	1.779(4)
M-CO$_{trans}$	1.893(2)	1.809(2)	1.985(3)	-
Re1-CO3	-	-	1.924(4)	-
Re2-CO21	-	-	1.932(4)	-
C6-O6	1.322(2)	1.324(2)	1.324(4)	1.333(4)
M-M	-	2.9243(3)	3.0817(2)	-
Bond angle (°)				
C1-M-C6	175.2(1)	-	176.1(1)	-
M-C6-O6	131.1(1)	130.1(1)	127.9(2)	128.7(3)
M-C6-C10	123.4(1)	125.3(1)	127.9(2)	126.8(2)
O6-C6-C10	105.1(2)	104.4(1)	104.2(3)	104.5(3)
C6-M-M	-	177.60(4)	90.28(8)	-
M-M-C21	-	178.06(5)	177.5(1)	-
C2-M-C4	173.93(8)	172.08(6)	166.1(1)	-
Torsion angle (°)				
Mn1-C10-C6-M	-122.9(1)	-114.2(1)	-110.7(3)	108.5(3)
C2-M-M-C18	-	49.85	-18.64	-
M-C6-O6-C15	6.4(3)	2.4(2)	4.5(4)	-6.7(6)
Plane angle (°)				
Carbene/Cp	28.2	19.4	18.0	18.1
Cp/Cp	-	-	-	48.3

[a] Average value for *cis*-carbonyls; For **5** x = 2 and 4 only; For **6** x = 17 and 18 only

3.3   DFT study

A DFT study was performed to investigate the following two different aspects: firstly, hydrogen bond interactions between the carbene ligand and the carbene metal carbonyl groups, and secondly, axial and equatorial carbene bond formation in the case of **4** and **5**. The incidence of non-covalent intramolecular interligand interactions between a methoxy carbene substituent and carbonyl ligands, has recently been confirmed [22] in a case study of the carbene complex [(CO)$_2$CpMnC(OMe)Me], a pianostool complex with a 'vertical' orientation (Figure 9) of the carbene substituent relative to the pseudo-mirror plane of the CpMn(CO)$_2$ moiety. This literature study confirmed the existence of stabilizing two-electron delocalizations from both σ-(C-H$_{OMe}$) molecular orbitals of the methoxy moiety into the π*-(C≡O) molecular orbital of the closer carbonyl ligand (3.98 and 3.43 kJ/mol respectively) of the carbene metal moiety CpMn(CO)$_2$. In conjunction with this, back-donation from the π-(C≡O) to the unoccupied σ*-(C-H$_{OMe}$) orbital (2.85 kJ/mol) was observed. These interactions are put forward as one of the reasons for the *anti* conformational preference of the ethoxy group relative to the second carbene substituent (Me [22], heteroarene furan [23] or CpMn(CO)$_3$ in this study). The X-ray structures of this study confirm the *anti* conformational preference of the ethoxy group relative to the CpMn(CO)$_3$ substituent.
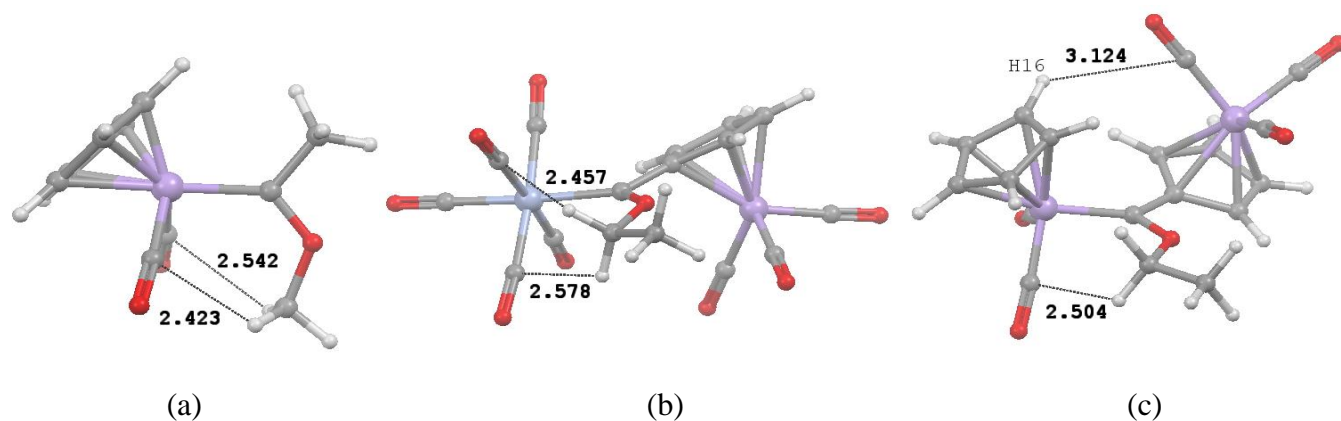
Figure 8: NBO interaction distances (in Å) observed by (a) Lugan *et al.* [22] in [(CO)$_2$CpMnC(OMe)Me] and (b) in **1** (to **5**) and (c) **6** of this study

In contrast with the reported values of Lugan *et al.* [22], computational results for the complexes of this study indicate no stabilization from the π-(C≡O) orbital of a carbonyl ligand on the carbene metal moiety ([Cr], [Mo], [W], [Mn] or [Re]) to the unoccupied σ*-(C-H$_{OEt}$) orbital in **1**-**6**. Only σ-(C-H$_{OEt}$) → π*-(C≡O) interactions were observed between OEt and CO ligands of the carbene metal moiety these values are smaller than the values reported by Lugan *et al.* [22], see Figure **8** and interactions labelled **B** and **C** in Table 2. An additional NBO interaction was

observed between an aromatic C-H bond on the Cp ring of the cymantrenyl substituent $CpMn(CO)_3$ and a carbonyl ligand on the carbene metal moiety ($Re_2(CO)_9$) for **5** (**A** in Table 2). This stabilization energy was calculated as 2.55 kJ/mol.

Table 2: Stabilization energies associated with NBO interactions

Interaction	Energy (kJ/mol)/(d in Å)[a]					
	1	**2**	**3**	**4**	**5**	**6**
A: σ-(C-H$_{Cp}$) → π*-(C≡O)	-	-	-	-	2.55 (2.349, 2.514)	
B: σ-(C-H$_{OEt}$) → π*-(C≡O)	3.26 (2.612, 2.457)	2.51 (2.509)	2.13 (2.512)	3.01 (2.386, 2.468)	2.85 (2.498, 2.456)	2.97 (2.497, 2.504)
C: σ-(C-H$_{OEt}$) → π*-(C≡O)	2.34 (2.619, 2.578)	2.22 (2.598)	-	2.60 (2.647, 2.533)	2.76 (2.547, 2.615)	-
TOTAL (kJ/mol)	**5.60**	**4.73**	**2.13**	**5.61**	**8.12**	**2.97**

[a] Distance between H and C atoms from experimental and *theoretical* data

Due to the horizontal orientation of the carbene ligand relative to the carbene metal moiety $CpMn(CO)_2$ in **6** (Figure 9), the SOPT energy calculated is only 2.97 kJ/mol and only one interaction between the methylene C-H bond and a carbonyl ligand of the carbene metal moiety is observed. This is much weaker than the two interactions reported for the vertical conformation of the carbene ligand relative to the carbene metal moiety $CpMn(CO)_2$ in [(CO)$_2$CpMnC(OMe)Me] [22], see Figure 9. The only interactions between a carbonyl ligand of the second metal moiety in the complex, the cymantrenyl substituent ($CpMn(CO)_3$), and a methyl C16-H16 bond of the ethoxy group, were observed for **5** (Figure **8**). The SOPT energy associated with these interactions, from cymantrenyl carbonyl π orbitals to a σ*(C-H) orbital, was only 0.63 kJ/mol (d_{C-H} = 3.124 Å).
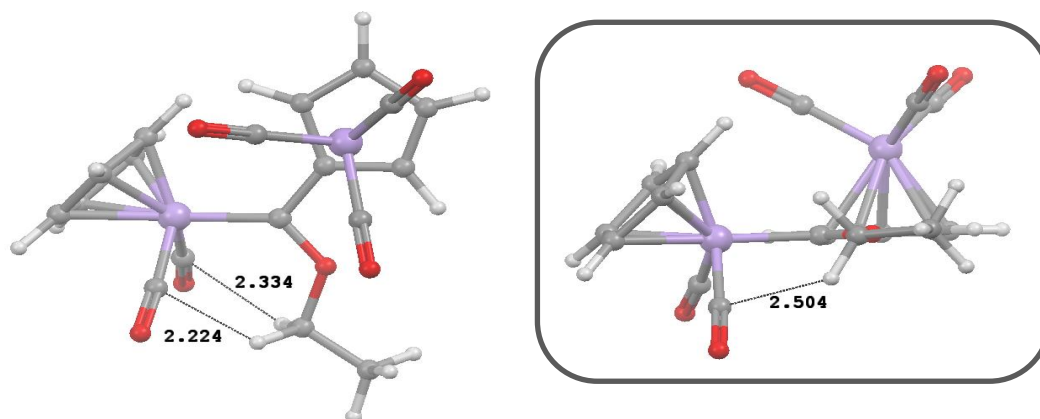
Figure 9: Possible vertical (left) or horizontal (right) orientations of the carbene ligand relative to the carbene metal moiety CpMn(CO)$_2$ for **6**, contacts in Å

A   **B**   **C**
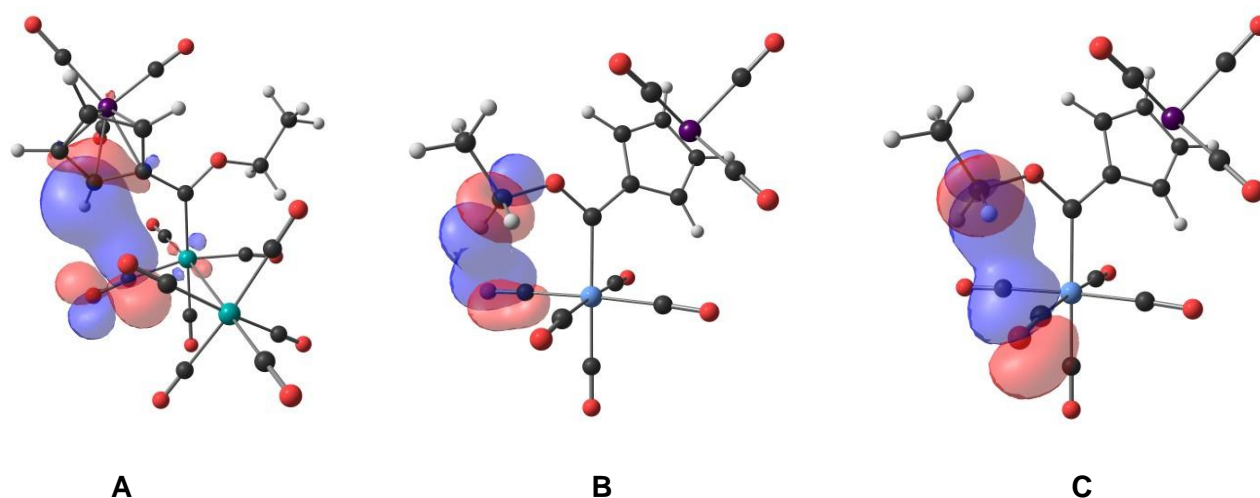
Figure 10: Calculated NBO stabilization interaction **A** (Table 2) between a cyclopentadienyl C-H bond and carbonyl ligand for **5** and between methylene C-H bonds and carbonyl ligands for **1** (**B** and **C**). Colour code for atoms (online version): Re (turquoise), Mn (mauve), Cr (powder blue), C (grey), O (red), H (white).

A linear relationship between the group VI metals' combined SOPT energy for the σ-(C-H$_{OEt}$) → π*-(C≡O) NBO interactions in complexes **1-3** was found when plotted against atomic mass of the metal (Figure 11). As one moves down the group, the NBO interaction decreases with increasing atomic mass of the metal. Neither the M=C6 theoretical bond lengths (Cr < W < Mo) nor the average CO to CH$_{methylene}$ NBO interaction distances (Cr < W < Mo) followed this same trend and could therefore not be proposed as explanation for this observation.
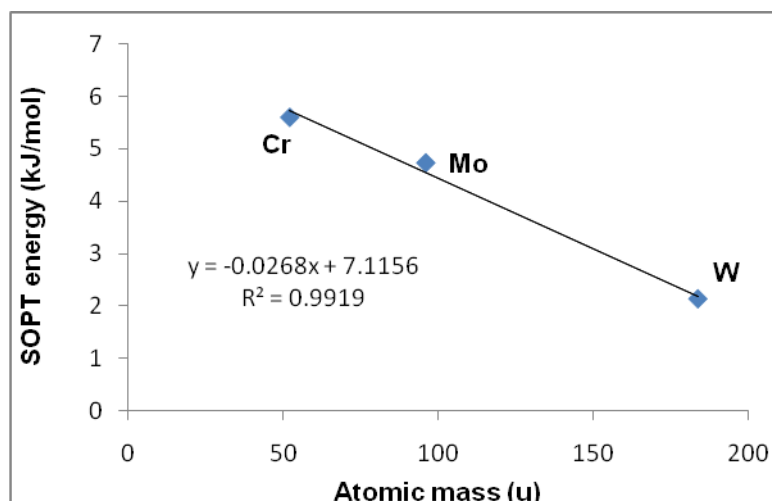
Figure 11: Linear decrease in SOPT energy (kJ/mol) of NBO stabilizing interaction down the group for group VI metals in complexes of the type $[(CO)_5MC(OEt)CpMn(CO)_3]$; M = Cr, Mo, W.

DFT calculations show that both manganese and rhenium complexes **4** and **5** prefer the axial configuration of the carbene ligand by approximately 16.1 kJ/mol for **4** and only 3.2 kJ/mol for **5**. The preference of **5** to form the equatorial coordinated complex is supported by literature [40]. DFT calculations support the molecular structure obtained experimentally for **4** (Figure 5). Although equatorial substitution is more favourable from an electronic perspective, the bulkiness of the cymantrenyl carbene substituent plays a significant role in directing nucleophilic attack. Complex **6** also has two possible conformations in the solid state, namely the *cis* or *trans* conformations of the cyclopentadienyl ring of the cymantrenyl substituent relative to that of the carbene metal moiety (Figure 12). Gas-phase computational results indicate that the energies of *cis* and *trans* conformations of the Cp rings relative to one another are very similar, with the *trans* conformation lower in energy by only 1.2 kJ/mol, supporting the conformation found in the solid-state structure (Figure 7). The small difference in energy between the two conformations allows both conformations to be experimentally feasible.
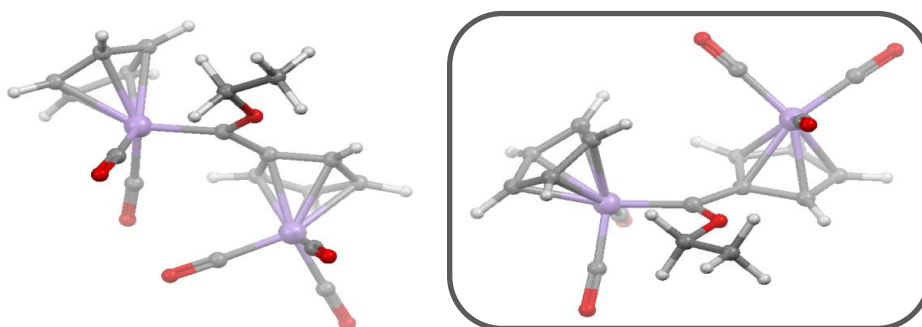
Figure 12: Optimized *cis* (left) and *trans* (right) conformations for **6**

The crystal structure of a CpRe analogue of **6**, [(CO)$_2$CpReC(OMe)ReCp(CO)$_3$] exhibits the *cis*-conformation [7]. One of the reasons for **6** found as the *trans*-conformation in the solid state may be ascribed to crystal packing forces. Several intermolecular close contact interactions are observed in the packing of this molecule in favour of the *trans*-conformation for **6**. A few of these interactions are shown in Figure 13.
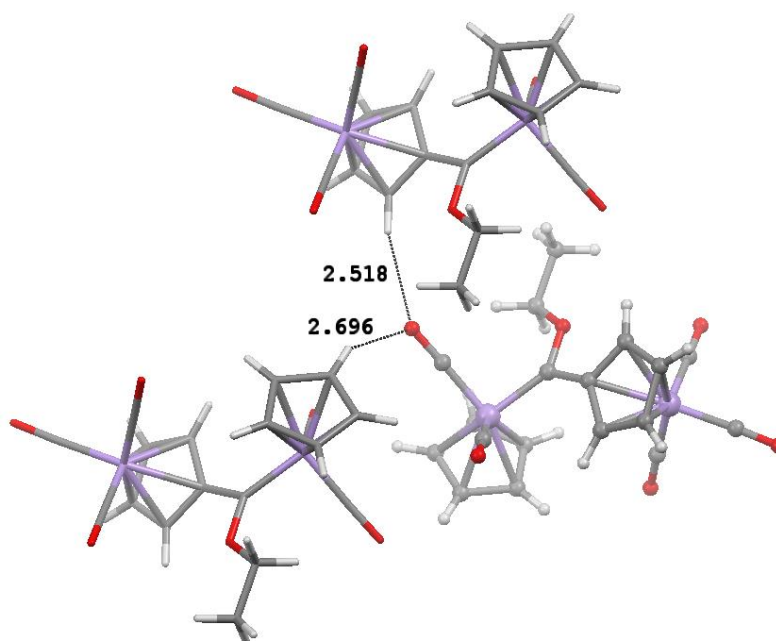
Figure 13: Intermolecular close contact interactions (in Å) in the crystal packing of **6**

4   Conclusion

Bimetallic and trimetallic complexes **1-5** were synthesized in satisfactory yield (Scheme 1). Complex 6 was isolated as a minor product and formed as a side product during the initial lithiation of CpMn(CO)$_3$. The molecular structures of these complexes were confirmed with NMR and IR spectroscopy, and single crystal X-ray diffraction studies of **1** and **4-6**. Applying DFT calculations, it was possible to determine and visualise the intramolecular NBO interactions as well as to determine relative energies associated with axial- and equatorial-substituted polymetallic complexes. The results provide an indication as to the steric and electronic parameters governing the regioselectivity of the polymetallic carbonyl complexes. The theoretical infrared spectra of the carbene complexes show good agreement with the experimental spectra obtained. Both steric and electronic reasons for isomer preference have been proposed to explain the bonding differences in the manganese and rhenium complexes.

Acknowledgements

Supporting Information

The electronic supporting information includes Table S1, lists of bond distances and angles for crystal structures reported and the optimized coordinates of the DFT calculations. CCDC 1417538-1417541 contains the supplementary crystallographic data for this paper. This data can be obtained free of charge *via* http://www.ccdc.cam.ac.uk/conts/retrieving.html (or from the Cambridge Crystallographic Data Centre, 12, Union Road, Cambridge CB2 1EZ, UK; fax: +44 1223 336033).

CHAPTER 3

Conformational preferences of heteronuclear Fischer carbene complexes of cymantrene and cyclopentadienyl rhenium tricarbonyl

Chapter 3 was adapted from an article published in Journal of Coordination Chemistry. The format reflects the requirements of the journal.

Date: 2016

Volume: 69

Pages: 2972-2987

Authors: Roan Fraser, Petrus H. van Rooyen and Marilé Landman

Status: Submitted, accepted and published

Graphical Abstract:
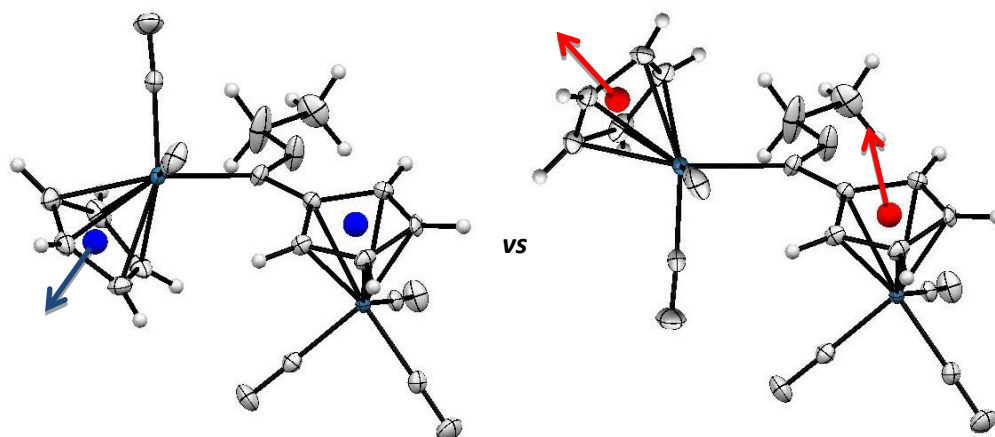
Contributions:

Roan Fraser: Author, synthesis, DFT studies

Petrus H. van Rooyen: Co-author, crystallography

Marilé Landman: Corresponding Author, supervisor

3
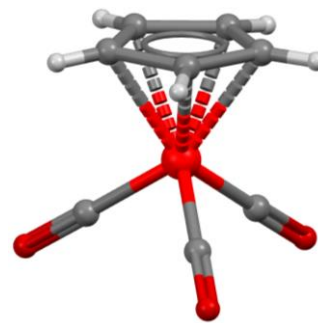
Conformational preferences of heteronuclear Fischer carbene complexes of cymantrene and cyclopentadienyl rhenium tricarbonyl

Roan Fraser, Petrus H. van Rooyen and Marilé Landman*

Department of Chemistry, University of Pretoria, Private Bag X20, Hatfield, 0028, South Africa. Tel: +27-12-4202527, Fax: +27-12-4204687

Contact author details:

Name: Marilé Landman Tel: +27-12-4202527, Fax: +27-12-4204687, email: marile.landman@up.ac.za

Keywords

Fischer carbene; cymantrenyl; cyclopentadienyl rhenium tricarbonyl; DFT; NBO analysis

Graphical abstract
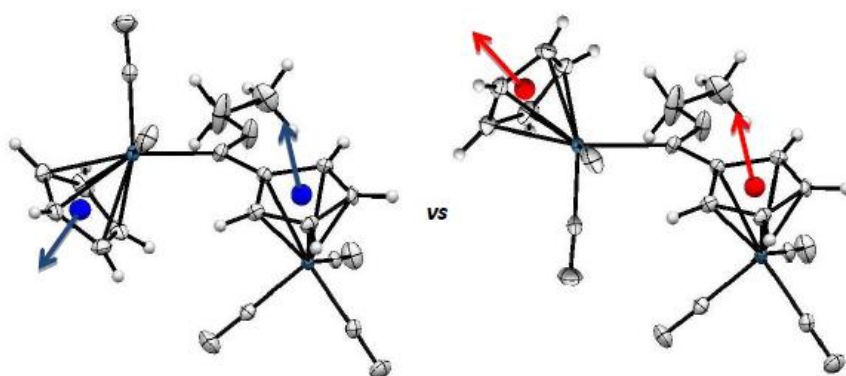
TOC abstract

Synthesis, single crystal X-ray study and NBO analysis of Fischer ethoxy carbene complexes with cymantrenyl and cyclopentadienyl rhenium tricarbonyl substituents

Research highlights

- DFT calculations on configurations of homo- and heteronuclear complexes
- Crystal structure of first carbene complex containing a mixed cyclopentadienyl rhenium tricarbonyl and cymantrene system
- Calculated energy diagram for the synthetic methodology of the *trans* carbene complexes
- Calculated energy values, comparing the *cis* and *trans* carbene formation

Abstract

Homo- and heteronuclear bimetallic carbene complexes of group VII transition metals (Mn and Re), with cymantrene or cyclopentadienyl rhenium tricarbonyl as the starting synthon, have been synthesised according to classic Fischer methodology. Crystal structures of the novel carbene complexes with general formula $[RC_5H_4M'(CO)_2\{C(OEt)(C_5H_4M(CO)_3)\}]$, where M = M' = Mn, R = H (**1**), R = Me (**2**); M = Mn, M' = Re, R = H (**3**); M = M' = Re, R = H (**4**) and M = Re, M' = Mn, R = H (**5**) are reported. A density functional theory (DFT) study was undertaken to determine natural bonding orbitals (NBOs) and conformational as well as isomeric aspects of the binuclear complexes. Application of the second-order perturbation theory (SOPT) of the NBO method revealed stabilizing interactions between the methylene C-H bonds and the carbonyl ligands of the carbene metal moiety. Energy calculations in the gas phase of the *cis* and *trans* conformations of the Cp rings relative to one another are comparable, with the *trans* conformation slightly lower in energy. The theoretical findings have also been confirmed with single crystal X-ray diffraction and all solid state structures are found in the *trans* geometry.

1   Introduction

Metal carbene complexes as discovered by E.O Fischer in the 1960's, have since been established as irreplaceable building blocks for the synthesis of organic molecules [1,2]. Fischer carbene complexes have found application in cycloaddition reactions [3], heterocyclization [4], catalytic carbene transfer reactions [5] and in the so-called Dötz benzannulation reactions [6]. The synthesis of Fischer carbene complexes from metal-containing carbene substituents are well described in literature. Carbene complexes of ruthenocene [7], ferrocene [8] and

[1] E.O. Fischer, A. Maasböl. Angew. Chem. Int. Ed. Engl. 580 (1964) 3.
[2] A. de Meijer, H. Schirmer, M. Duetsch. Angew. Chem. Int. Ed. 39 (2000) 3964.
[3] J. Barluenga. J. Pure Appl. Chem., 68 (1996) 543.
[4] J. Barluenga, J. Santamaría, M. Tomás. Chem. Rev. 104 (2004) 2259.
[5] M. A. Sierra. J. Am. Chem. Soc. 123 (2001) 851.
[6] K. H. Dötz. Angew. Chem. 87 (1975) 672.
[7] E. O. Fische, F. J. Gamel, J. O. Besenhard, A. Frank, D. Neugebauer. J. Organomet. Chem. 191 (1980) 261.
[8] J. G. López-Cortés, L. F. C. de la Cruz, M. C. Ortega-Alfaro, R. A. Toscano, C. Alvarez-Toledano, H. Rudler. J. Organomet. Chem., 690 (2005) 2229.

cyclopentadienyl metal half sandwich moieties [9] are known and the electrochemical properties of these complexes examined [9] (Figure 1).
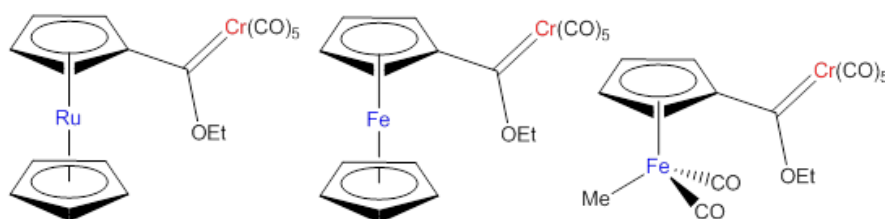
Figure 1: Multi-metal carbene complexes containing a Cp metal bearing moiety

A study on the synthesis and structural aspects of multi-metal carbene complexes, bearing cymantrene as the carbene substituent, was recently published by our research group [10]. This study found NBO stabilizing interactions between the C-H atoms of the cyclopentadienyl of the cymantrenyl substituent and the carbene metal carbonyl ligands (Figure 2).
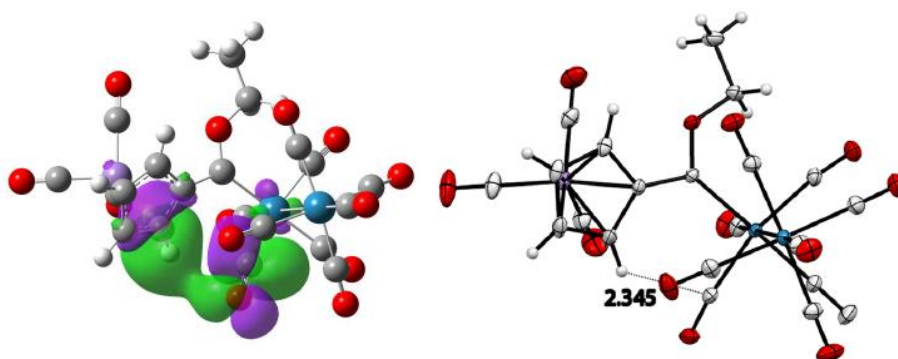
Figure 2: NBO interaction between the cyclopentadienyl C-H atoms and the carbene metal carbonyl ligands of the cymantrenyl dirhenium carbene complex

The study also indicated additional NBO stabilization interactions between the methylene protons and the carbonyl ligands situated on the carbene metal moiety. A linear decrease in NBO stabilizing interactions was observed down the group, for the group VI metal carbene complexes (Cr > Mo > W). The total second-order perturbation theory (SOPT) energy thus decreases in the order Cr > Mo > W [10]. Incidences of non-covalent intramolecular interligand interactions were also described by Lugan and Lavigne [11] when methylene protons of methoxycarbene complexes interacted with carbonyls associated with the carbene moiety. These interactions were determined using NBO calculations and indicated

[9] U. Behrendt, R. M. Pfeifer, R. Wartchow, H. Butenschön. New J. Chem. 23 (1982) C73.
[10] R. Fraser, P.H van Rooyen, M. Landman. J. Mol. Struct. 1105 (2016) 178.
[11] N. Lugan, I. Fernández, R. Brousses, D. A. Valyaev, G. Lavigne, N. A. Ustynyuk. Dalton Trans. 42 (2013) 898.

additional intramolecular stabilizations supporting the conformational aspects found in the solid state structure. The finding also supports seminal MO calculations by Hoffmann *et al.* [12] that predicted that carbene ligands in piano-stool complexes preferred the so-called vertical coordination mode rather than the horizontal mode (Figure 3).
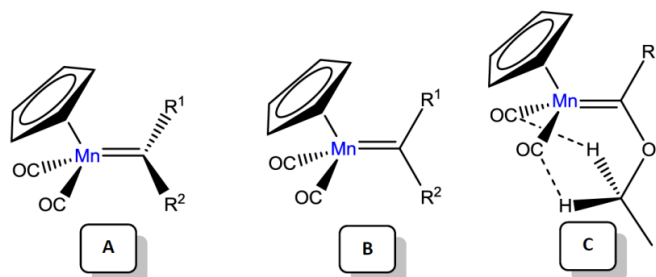
Figure 3: The horizontal coordination mode (A), the vertical coordination mode (B) and the stabilization of the vertical coordination mode (C) as described by Lugan and Lavigne [11]

Complexes where $MnCp(CO)_3$ and $ReCp(CO)_3$ constitute both the initial building synthons as well as the metallating agent have been studied and published by Fischer [13] and Casey [14] (Figure 4). Their studies are restricted to either homonuclear carbene complexes or carbene complexes of group VI and according to our knowledge constitute the only other examples where the cymantrene and cyclopentadienyl rhenium substituents serve as both the initial deprotonated moiety and metallating agent.
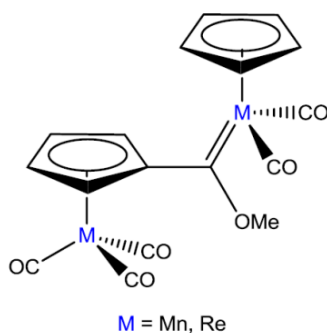
M = Mn, Re

Figure 4: Homonuclear carbene complexes containing $MCp(CO)_3$ (M = Mn, Re) as initial building blocks synthesised by Fischer [13] and Casey [14]

The abovementioned carbene complexes may present either a *cis* or *trans* conformation of the cyclopentadienyl ring of the cymantrenyl substituent relative to the carbene metal moiety (Figure

[12] B. E. R. Schilling, R. Hoffmann, D. L. Lichtenberger. J. Am. Chem. Soc. 101 (1979) 585.
[13] E.O. Fischer, V.N. Postnov, F.R Kreissl. J. Organomet. Chem. 231, C73 (1982).
[14] C.P. Casey, C.J. Czerwinski, R.K. Hayashi. Organometallics15 (1996) 4362.

5). Theoretical calculations on the homonuclear carbene complexes indicate similar energies between the two conformers with the *trans* conformation lower in energy by only 1.2 kJ/mol. Several intermolecular close contact interactions in the packing of this molecule are observed supporting the formation of the *trans*-conformation [10].
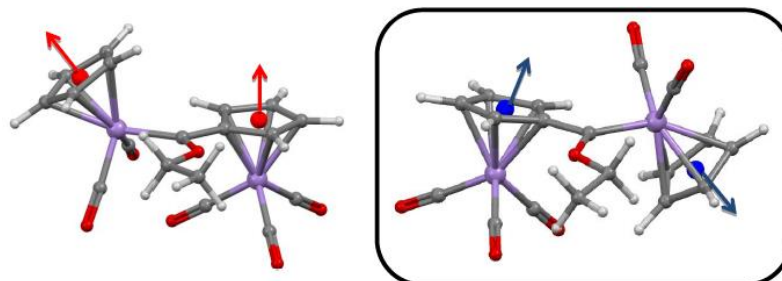
Figure 5: Optimized *cis* (left) and *trans* (right) conformations for the homonuclear cymantrenyl carbene complex

Based on these existing studies, a DFT study was initiated to extend the scope and understanding of multi-metallic systems focussing on homo- and heteronuclear carbene complexes bearing cymantrenyl and cyclopentadienyl rhenium tricarbonyl substituents. This study reports the synthesis of the four novel homo- and heteronuclear bimetallic complexes of group VII transition metals (Figure 6), crystal structures of three of the complexes and a DFT study.

1 M = Mn, M' = Mn, R = H
2 M = Mn, M' = Mn, R = Me
3 M = Mn, M' = Re, R = H
4 M = Re, M' = Re, R = H
5 M = Re, M' = Mn, R = H
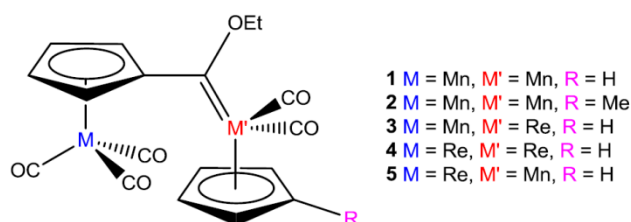
Figure 6: Bimetallic monocarbene complex **1**-**5**

2 Experimental

2.1 Materials and instrumentation

All reactions, unless otherwise noted, were performed under inert nitrogen or argon atmospheres using standard Schlenk techniques [15]. All solvents were freshly distilled, dried and collected under inert conditions. Column chromatography was carried out under inert nitrogen and argon atmospheres using silica gel (particle size 0.063-0.200 mm) as the

---

[15] D.F. Schriver, M.A. Drezdzon. *The manipulation of Air-Sensitive Compounds, 2nd ed.,* Wiley, New York, USA*,* (1986).

stationary phase. Percentage yields were calculated relative to the limiting reactant. Crystallization was done using hexane:DCM or hexane:ether diffusion methods. Triethyloxonium tetrafluoroborate [16] was prepared according to a reported literature procedure. The reagents $CpMn(CO)_3$, $MeCpMn(CO)_3$, $CpRe(CO)_3$, n-butyl lithium (1.6 M solution in hexane) and other commercial reagents were used as purchased. NMR spectra were recorded on a Bruker ARX-300. NMR spectra were recorded in CDCl3 using the deuterated solvent peak as internal reference. ^1H and ^{13}C NMR spectra were measured at 300.1 and 75.5 MHz, respectively. The numbering of atoms in the NMR assignment is according to the numbers used Figure 7 - Figure 9. IR spectra were recorded on a Perkin Elmer Spectrum RXI FT-IR spectrophotometer as KBr pellets and only the vibration bands in the carbonyl-stretching region (ca. 1500-2200 cm^{-1}) are reported.

2.2 X-ray crystallography

Data for complexes **2** and **4** and **5** were collected at 150 K on a Bruker D8 Venture kappa geometry diffractometer, with duo Iμs sources, a Photon 100 CMOS detector and APEX II control software using Quazar multi-layer optics, monochromated Mo-Kα radiation and by means of a combination of ϕ and ω scans. Data reduction was performed using SAINT+ and the intensities were corrected for absorption using SADABS [17]. The structures were solved by intrinsic phasing using SHELXTS and refined by full-matrix least squares using SHELXTL and SHELXL-2013 [18]. In the structure refinement, all hydrogen atoms were added in calculated positions and treated as riding on the atom to which they are attached. All nonhydrogen atoms were refined with anisotropic displacement parameters, all isotropic displacement parameters for hydrogen atoms were calculated as X ⨯ Ueq of the atom to which they are attached, X = 1.5 for the methyl hydrogens and 1.2 for all other hydrogens. Crystallographic data and refinement parameters are given in Table 1. Ortep drawings [19] of the three structures are included in Figure 7, Figure 8 and Figure 9. In the structure of **5**, some metal mixing occurs, where both metals Mn and Re are present at both metal positions (6% mixing). However, the major component of this structure is the complex where the substituent metal atom is Re and the carbene metal atom is Mn, *i.e.* **5** (94%). The crystal structures (cif) have been deposited at the Cambridge Crystallographic Data Centre and allocated the deposition numbers: CCDC 1482771-1482773. Data collection, structure solution and refinement details are available in each cif.

[16] H. Meerwein. Org. Synth. 46 (1966) 113.
[17] APEX2 (including SAINT and SADABS); Bruker AXS Inc., Madison, WI (2012).
[18] G.M. Sheldrick. Acta Crystallogr. A64 (2008) 112.
[19] L.J. Farrugia. J. Appl. Crystallogr. 30 (1997) 565.

44

2.3 Synthesis of complexes 1-5

2.3.1 Synthesis of 1

Complex **1** has been synthesised and reported previously [10].

2.3.2 Synthesis of 2

CpMn(CO)$_3$ (0.612 g, 3.0 mmole) was dissolved in 40 ml of dry THF. n-Butyl lithium (2.00 ml, 3.0 mmole) was added at -30 °C and stirred at this temperature for 30 min. The colour of the reaction mixture changed from yellow to a dark brown colour. MeCpMn(CO)$_3$ (0.654 g, 3.0 mmole) were added to the reaction mixture at -79°C and allowed to react at this temperature for 1 hour and warmed to room temperature. After completion of the reaction, the solvent was removed *in vacuo* and the residue redissolved in dichloromethane. Triethyl oxonium tetrafluoroborate (0.55 g, 3.0 mmole) was dissolved in 20 ml of dichloromethane and this was added to the cooled reaction mixture (-20°C). An immediate colour change was observed, from brown to a deep red solution, and the reaction mixture was dry loaded onto a silica gel column for purification. The product was isolated using a 10:1 hexane: DCM eluent ratio. A single brown product was isolated of complex **2** (yield: 0.720 g; 50%)^{1}H NMR (300 MHz, CDCl$_3$): δ = 5.51 (s, 2H, H$_{17}$ and H$_{14}$); 4.93 (s, 2H, H$_{15}$ and H$_{16}$); 5.12 (q, 2H, J_{HH} = 7.1, O**CH$_2$**CH$_3$); 1.65 (t, 3H, J_{HH} = 6.7, OCH$_2$**CH$_3$**). ^{13}C{^{1}H} NMR (75.5 MHz, CDCl$_3$): C$_{(Carbene)}$ 331.0; Mn(**CO**)$_3$ 222.8; MeMn(**CO**) 222.6; C$_5$H$_4$ 106.6; C$_5$H$_4$ 87.6; C$_5$H$_4$ 83.8; O**CH$_2$**CH$_3$ 77.2; OCH$_2$**CH$_3$** 15.1. IR (cm^{-1}): 2064 (s), 2031 (s), 1946 (s), 1922 (m). HRESI$^+$-MS, m/z: 450.9779 (calcd 450.9786).

2.3.3 Synthesis of 3

The syntheses of **3-5** were done using a similar procedure as for the synthesis of **2**. CpMn(CO)$_3$ (0.612 g, 3.0 mmole) was dissolved in THF and lithiated at -30 °C. The lithiated Cp metal moiety was then metallated with 1.062 g (3.00 mmole) of CpRe(CO)$_3$ and quenched with the oxonium salt. A single brown product was isolated: a dark brown monocarbene complex **3** (yield: 0.766 g; 45%). ^{1}H NMR (300 MHz, CDCl$_3$): δ = 5.58 (s br, 5H, C$_5$H$_5$), 5.50 (s br, 2H, C$_5$H$_4$); 5.00 (s br, 2H, C$_5$H$_4$); 4.68 (s br, 2H, O**CH$_2$**CH$_3$); 1.51 (s br, 3H, OCH$_2$**CH$_3$**). ^{13}C{^{1}H} NMR (75.5 MHz, CDCl$_3$): C$_{(Carbene)}$ 273.8; CpMn(CO) 223.5; CpRe(CO) 206.5; C$_5$H$_4$ (ipso) 113.9; C$_5$H$_4$ 89.4; C$_5$H$_4$ 88.8; C$_5$H$_5$ 85.0; O**CH$_2$**CH$_3$ 74.3; OCH$_2$**CH$_3$** 14.3. IR (cm^{-1}): 2028 (m), 1952 (m), 1940 (s), 1896 (m). HRESI$^+$-MS, m/z: 568.9846 (calcd 568.9806).

2.3.4 Synthesis of 4

A 0.671 g (2.0 mmole) of $CpRe(CO)_3$ was dissolved in THF and lithiated at -30 °C. The lithiated Cp moiety was then metallated with a second equivalent of $CpRe(CO)_3$ (0.671 g, 2.0 mmole) and quenched with the oxonium salt. One product was isolated: a red monocarbene complex 4 (yield: 0.699 g; 50%).^{1}H NMR (300 MHz, CDCl_3): δ = 5.82 (s, 2H, C_5H_4); 5.37 (s, 5H, C_5H_5); 5.29 (s, 2H, C_5H_4); 4.51 (q, 2H, J_{HH} = 7.1, O**CH_2**CH_3); 1.55 (t, 3H, J_{HH} = 7.0, OCH_2**CH_3**). ^{13}C{^{1}H} NMR (75.5 MHz, CDCl_3): $C_{(Carbene)}$ 269.1; Re(CO) 202.3; Re(CO) 193.8; C_5H_4 (ipso) 87.4; C_5H_5 86.2; C_5H_4 84.5; C_5H_4 82.8; O**CH_2**CH_3 74.9; OCH_2**CH_3** 14.4. IR (cm^{-1}): 2030 (m), 1969 (m), 1941 (s), 1889 (m). HRESI^+-MS, m/z: 700.9908 (calcd 700.9983).

2.3.4   *Synthesis of 5*

A 0.671 g (2.0 mmole) of $CpRe(CO)_3$ was dissolved in THF and lithiated at -30 °C. The lithiated Cp moiety was then metallated with a second equivalent of $CpMn(CO)_3$ (0.436 g, 2.0 mmole) and quenched with the oxonium salt. One product was isolated: a brown monocarbene complex **5** (yield: 0.522 g; 46%) ^{1}H NMR (300 MHz, CDCl_3): 5.31(s, 2H, C_5H_4); 5.08(s, 2H, C_5H_4); 4.65 (s, 5H, C_5H_5); 4.54(q, 2H, J_{HH} = 7.4, O**CH_2**CH_3); 1.31(t, 3H, J_{HH} = 7.0, OCH_2**CH_3**). ^{13}C{^{1}H} NMR (75.5 MHz, CDCl_3): $C_{(Carbene)}$ 331.3; Mn(CO) 230.8; Re(CO) 193.5; C_5H_4 (ipso) 94.2; C_5H_4 86.8; C_5H_5 83.8; C_5H_4 83.4; O**CH_2**CH_3 73.1; OCH_2**CH_3** 14.5. IR (cm^{-1}): 2028 (m), 1952 (s), 1939 (s), 1896 (m). HRESI^+-MS, m/z: 568.9846 (calcd 568.9806).

2.4   **Molecular modelling**

The calculations reported in this paper were obtained using the Gaussian 09 [20] suite of programs. Calculations were carried out in the singlet spin state using the hybrid functional B3LYP [21,22]. Geometries of the neutral complexes were optimized in gas phase with the triple-ζ basis set 6-311G* on all atoms except for the metal atoms. Stuttgart/Dresden (SDD) pseudopotential was used to describe the metal electronic core, while the valence electrons were described using def2-TZVPP [23]. No symmetry constraints were applied and only the

[20] M.J. Frisch, G.W. Trucks, H.B. Schlegel, G.E. Scuseria, M.A. Robb, J.R. Cheeseman, G. Scalmani, V. Barone, B. Mennucci, G.A. Petersson, H. Nakatsuji, M. Caricato, X. Li, H.P. Hratchian, A.F. Izmaylov, J. Bloino, G. Zheng, J.L. Sonnenberg, M. Hada, M. Ehara, K. Toyota, R. Fukuda, J. Hasegawa, M. Ishida, T. Nakajima, Y. Honda, O. Kitao, H. Nakai, T. Vreven, J.A. Montgomery (Jr), J.E. Peralta, F. Ogliaro, M. Bearpark, J.J. Heyd, E. Brothers, K.N. Kudin, V.N. Staroverov, T. Keith, R. Kobayashi, J. Normand, K. Raghavachari, A. Rendell, J.C. Burant, S.S. Iyengar, J. Tomasi, M. Cossi, N. Rega, J.M. Millam, M. Klene, J.E. Knox, J.B. Cross, V. Bakken, C. Adamo, J. Jaramillo, R. Gomperts, R.E. Stratmann, O. Yazyev, A.J. Austin, R. Cammi, C. Pomelli, J.W. Ochterski, R.L. Martin, K. Morokuma, V.G. Zakrzewski, G.A. Voth, P. Salvador, J.J. Dannenberg, S. Dapprich, A.D. Daniels, O. Farkas, J.B. Foresman, J.V. Ortiz, J. Cioslowski, D.J. Fox, Gaussian 09, Revision D.01, Gaussian Inc., Wallingford CT, (2010).
[21] A.D. Becke. J. Chem. Phys. 98 (1993) 5648.
[22] C. Lee, W. Yang, R.G. Parr. Phys. Rev. B 37 (1998) 785.
[23] F. Weigend, R. Ahlrichs. Chem. Phys. 7 (2005) 3297.

default convergence criteria were used during the geometric optimizations. Vibrational frequencies [24] were calculated at the optimized geometries and no imaginary frequencies were observed, to confirm true minima. Donor-acceptor interactions have been computed using the natural bonding orbital (NBO) method [25].

3   Results and discussion

3.1   Synthesis and characterisation

1 M = Mn, M' = Mn, R = H
2 M = Mn, M' = Mn, R = Me
3 M = Mn, M' = Re, R = H
4 M = Re, M' = Re, R = H
5 M = Re, M' = Mn, R = H
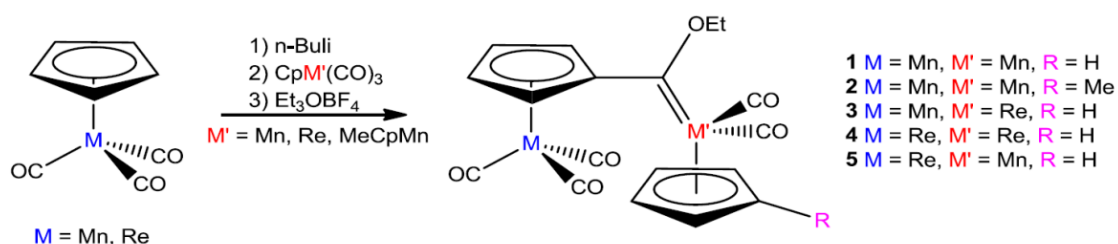
Scheme 1: Synthetic procedure followed for the synthesis of complexes **1-5**

Complexes **1-5** were synthesised as major products in the reactions based on classic Fischer methodology (Scheme 1) [26]. During the synthesis of complexes **2** and **3**, the formation of the homonuclear bimetallic monocarbene complex **1** [10] was observed as a minor side product and isolated in low yields [10]. The bimetallic-CpRe monocarbene complex, **4**, was also isolated as a side product in the synthesis of **5**. The infrared (IR) spectrum of **1** has been reported [10] and the spectra of **2-5**, using hexane as the solvent, showed the presence of four stretching frequencies. The IR spectra of **1-5** indicate two stretching frequencies attributed to the tricarbonyl moieties and two observed frequencies attributed to the carbene metal carbonyl stretching frequencies. Two stretching frequencies for both the $Re(CO)_2$ and the $Mn(CO)_2$ moiety were observed between 1889 and 1952 cm^{-1} and stretchings were seen in the same region regardless of the identity of the metal centre. The observation of these stretching frequencies are supported by literature [13,14]. NMR spectroscopy indicates downfield-shifted carbene carbon peaks between δ = 269.1 and 331.3 ppm. The carbene peaks were also significantly more deshielded for the complexes where the carbene carbon were coordinated to a $Mn(CO)_2$ moiety compared to the rhenium analogue. These structural characterisations were also confirmed with X-ray diffraction studies of the three complexes and will be presented in the next section.

[24] J.W. McIver, A.K. Komornicki. J. Am. Chem. Soc. 94 (1972) 2625.
[25] (a) J.P. Foster, F. Weinhold. J. Am. Chem. Soc. 102 (1980) 7211; (b) A.E. Reed, F. Weinhold. J. Chem. Phys. 83 (1985) 1736; (c) A.E. Reed, R.B. Weinstock, F. Weinhold. J. Chem. Phys. 83 (1985) 735; (d) A.E. Reed, L.A. Curtiss, F. Weinhold. Chem. Rev. 88 (1988) 899.
[26] See Ref. [5] and references therein.
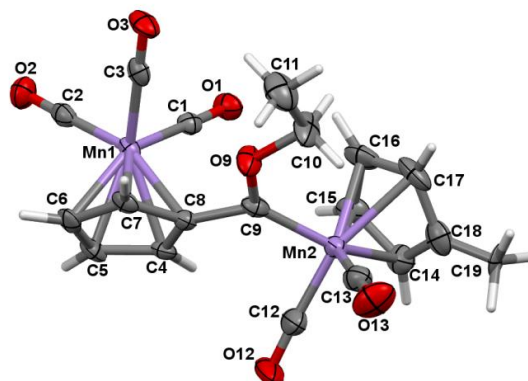
Figure 7: Perspective view of **2** with thermal ellipsoids drawn at the 50% probability level
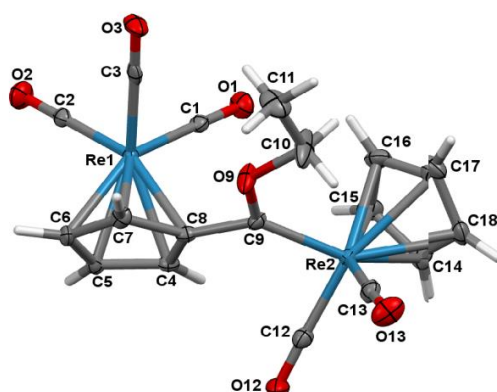
Figure 8: Perspective view of **4** with thermal ellipsoids drawn at the 50% probability level
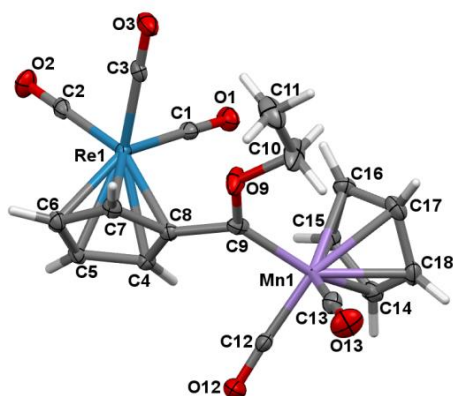
Figure 9: Perspective view of **5** with thermal ellipsoids drawn at the 50% probability level

The three molecular structures, complex **2**, **4** and **5** were isostructural. In addition, complex **2** could not be separated successfully from the mixture of complexes **1** and **2**, and this resulted in the co-crystallisation of complex **1** and **2** in a 0.69465 : 0.30535 ratio. Selected structural parameters of importance are summarized in Table 1. The carbene ligand, as defined by the C10-O9-C9-M'dihedral angle, deviates from planarity by less than 9° in all three complexes.

48

The carbene-metal bond distance was found to be 1.919(6), 2.022(5) and 1.918(6) for **2**, **4** and **5** respectively and indicated limited deviation between the manganese and rhenium carbene complex when cyclopentadienyl rhenium tricarbonyl serves as starting synthon. The bond distances reflect the double bond character of M'=C9. These values are similar to the M=C bond for analogous complexes with heteroarene substituents instead of a cyclopentadienyl metal substituent. The angles between the carbene plane (M'-C9-O9 and C8) and the plane of the Cp ring (C14 - C18) are very similar for complexes **2**, **4** and **5** (*ca.* 37°). Of significance is the orientation of the cyclopentadienyl metal moieties towards one another (preference of the *trans*-orientation) indicating possible interactions between the groups on the carbene ligand and the carbonyl groups of the metal associated with the carbene moiety. These interactions will further be described in the DFT study section. The angle between the planes defined by the Cp ligands were determined to be similar for complexes **2**, **4** and **5** (*ca.* 47°).

Table 1: Selected bond lengths and angles

	2	**4**	**5**
Bond length (Å)			
M-COx (x = 1-3)	1.796(6)	1.912(5)	1.916(5)
M'-C9	1.919(6)	2.022(5)	1.918(6)
C8-C9	1.485(7)	1.483(6)	1.489(7)
O9-C9	1.336(6)	1.333(5)	1.336(7)
M'-COx (x = 12, 13)[a]	1.767(7)	1.893(5)	1.775(6)
Bond angle (°)			
O9-C9- M'	129.1(4)	126.8(3)	129.0(4)
C8-C9- M'	121.2(3)	126.8(3)	126.6(4)
O9-C9-C8	103.9(7)	104.4(4)	104.4(4)
Torsion angle (°)			
C10-O9-C9-M'	6.0(8)	4.1(8)	8.6(9)
C7-C8-C9-M'	164.5(4)	168.6(4)	165.2(4)
C4-C8-C9-M'	-19.7(8)	-13.8(7)	-17.5(8)
Plane angle (°)			
Carbene/Cp	37.59	36.58	36.60
Cp/Cp	47.59	4.88	46.74

[a] Average value for metal-carbonyls
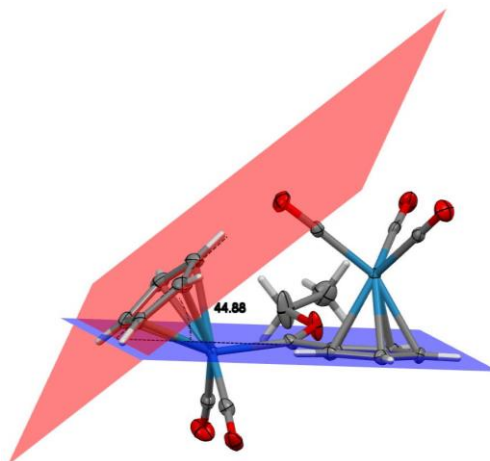
Figure 10: The angle (°) between the planes calculated for the two Cp ligands of the dirhenium complex **4**

The plane angles between the two Cp ligands in reference to one another have been determined for the *cis-* and vertical coordination mode conformers and were established to be 21.67⁰ and 44.86⁰ respectively (Figure 10). The angle between the carbene ligand and the metallating metal Cp was found to be 47.33⁰ for the *cis* conformer and 79.23⁰ for the vertical coordination mode.

3.3   DFT study

A DFT study was undertaken to investigate certain aspects of the dinuclear carbene species. Firstly, the rotational conformation preferred by the carbene metal cyclopentadienyl moiety in reference to the metal cyclopentadienyl starting synthon will be calculated and secondly, an investigation into which synthetic step determines the resulting *cis* or *trans* conformation of the final product will be determined. Finally experimental carbene bond lengths were compared to theoretically generated carbene bond lengths as a simple indication as to the validity of the applied model. In this study, Wiberg bond indices were calculated to provide theoretical support for the determination of rotation barriers within the molecule. The dinuclear carbene complexes have two possible conformations in the solid state, namely the *cis* or *trans* conformations of the cyclopentadienyl ring of the cymantrenyl substituent relative to that of the carbene metal moiety (Figure 5). Gas-phase theoretical calculation results show that the energies of *cis* and *trans* conformations of the Cp rings relative to one another are comparable (Table 2); however, the *trans* conformation remains lower in energy for complexes **1**-**5** (Figure 11), supporting the conformation determined in the solid-state structure (Figures 7-9). The energy of the horizontal coordination mode has been

50

determined to be lower for all the complexes in this study compared to the vertical mode as described by Lugan [11] and Hoffman [12].

Table 2: Calculated energy values of the *cis* and *trans* conformation for the complexes.

Complex	*Cis* (kJ/mol)	*Trans* (kJ/mol)	Vertical mode(kJ/mol)	Horizontal mode(kJ/mol)
1	+1.2	0	+7.3	0
2	+1.2	0	+7.7	0
3	+1.3	0	+2.0	0
4	+4.3	0	+1.2	0
5	+3.3	0	+9.4	0

Minor energy difference between the two conformations permits both conformations to be experimentally feasible. The incidence of the methoxy analogue of **4** provides an example of a solid state structure of a *cis*-orientated carbene complex $[C_5H_5Re(CO)_2\{C(OMe)C_5H_4Re(CO)_3\}]$ [14]. However, the solid state structures of the ethoxy complexes (**1**, **2**, **4**, **5**) all exhibit the *trans* orientation.
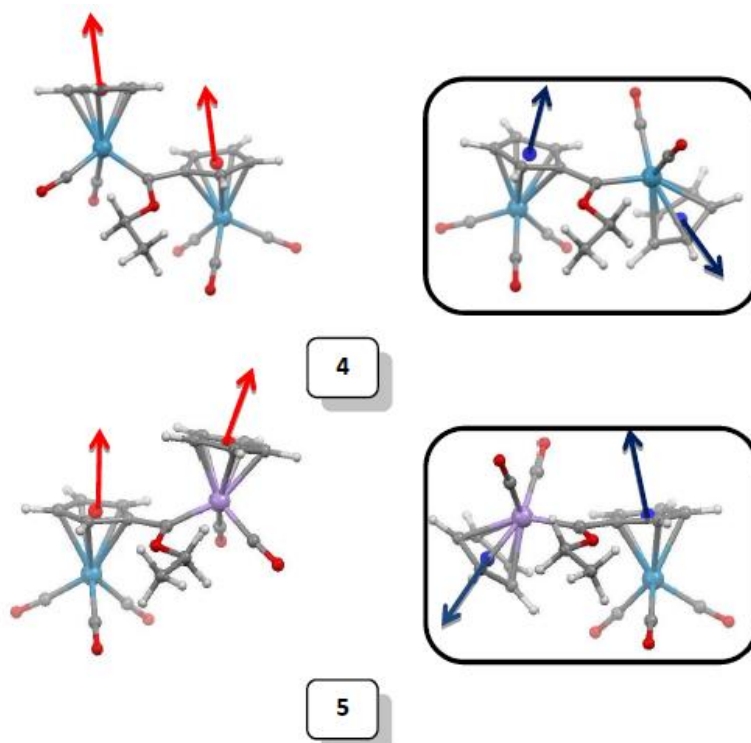
Figure 11: Optimized *cis* (left) and *trans* (right) conformations for **4** and **5**

Numerous intermolecular close contact interactions observed in the packing of the carbene complexes in favour of the *trans*-conformation, can be witnessed. A few of these interactions are shown in Figure 12 and these interactions range from 2.499 to 2.694Å.
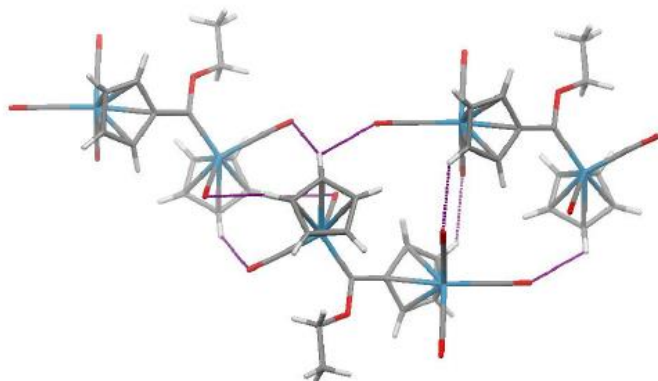
Figure 12: Intermolecular close contact interactions in the crystal packing of **4**

The formation of the metal acylate should establish delocalization of electron density from the acylate to the carbene metal moiety (Figure 13) [27]. The delocalized system provides extra electron density to the highly electrophilic carbene centre. Donation from the other alkyl or aryl substituent is only feasible in situations where the substituent contains additional donating groups such as hydroxyl or alkoxy groups. Rotation around the metal-carbene bond and metal-oxygen acylate bond should thus be restricted (Figure 13). Taking the theoretical bond orders into consideration, significant π-contribution from the ethoxy to the carbene carbon is witnessed with the greatest double bond character seen between the carbene carbon and alkoxy substituent (Table 3). Wiberg bond indices have found application in determining the bond order in carbene complexes [28] and seem to indicate that the bond between the carbene carbon and the carbene metal displays almost exclusively σ-bond character, or that in the case where π-contribution is present, that this contribution was found to be almost negligible.
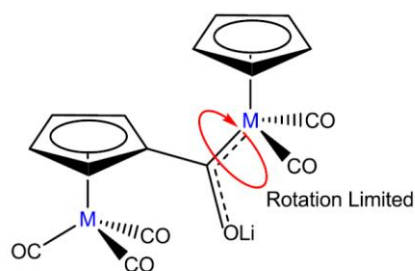
Figure 13: The delocalized electronic system after the formation of the metal acylate

[27] J. A. Connor, E. M. Jones. J. Chem. Soc. 1974 (1971).
[28] G. Occhipinti, H. R. Bjørsvik, K. W. Törnroos, A. Fürstner, V. R. Jensen. Organometallics 26 (2007) 4383.

Although literature provides sound precedence defining the carbene moiety as an σ-donating π-accepting ligand, our calculations indicate that the π-donation from the ethoxy substituent to the carbene centre takes preference above the π-donation from the metal species. This finding also correlates with literature reports by Fischer *et al.* [29]. The bond order between the carbene and oxygen acylate substituent also diminishes after alkylation, with limited variation between the metal-carbene bond and between the carbene and the cyclopentadienyl metal substituent. The bond order slightly increases between the carbene metal and the carbene carbon upon alkylation of the acylate. The formation of a six-membered metal acylate ring affords ridged stability within the molecule (Figure 14) and also restricts rotation around the metal-carbon double bond.

Slightly higher bond orders are calculated when the CpRe(CO)$_3$ acts as the metallating agent, which is expected since the carbene metal, possessing of a greater electon density, would be able to contribute this density towards the electrophillic carbene carbon. This electronic aspect is also mirrored by the slightly lowered bond order between the carbene carbon and the ethoxy carbene. Total bond indices are calculated for the carbene carbon atom and indicate non-ideal values of below 3.5 (ideal BO = 4) and indicate the limitation of this method for accurately calculate bond orders.

Table 3: Wiberg bond indices for the carbene complexes **1-5** and acylates

Complex	Wiberg bond indices			
	C$_{carb}$-M	C$_{carb}$-O	C$_{carb}$-C$_{Cp}$	Total
1	0.99	1.17	1.09	3.25
2	0.97	1.17	1.10	3.24
3	1.09	1.11	1.09	3.29
4	1.10	1.12	1.08	3.30
5	0.98	1.18	1.09	3.25
Cis Li-acylate	0.92	1.48	1.02	3.42
Trans Li-acylate	0.92	1.46	1.02	3.40

Based on bond orders of above **1**, rotation around the carbene carbon and the cyclopentadienyl metal substituent should still be possible. As supported by literature [29], the calculated bond orders indicate limited or no π-contribution from this substituent. The

[29] E. O. Fischer. Pure Appl. Chem. 30 (1972) 353.

formation and prevalence of the *trans* carbene complex could thus only be attributed to either the energetics of the formed product or additional stabilization within the molecule after formation. An NBO analysis of the carbene complexes found internal stabilization between the ethoxy substituent and the carbene metal carbonyl moieties and favours the formation of the *trans* conformer.

Cis lithium acylate   *Trans* lithium acylate
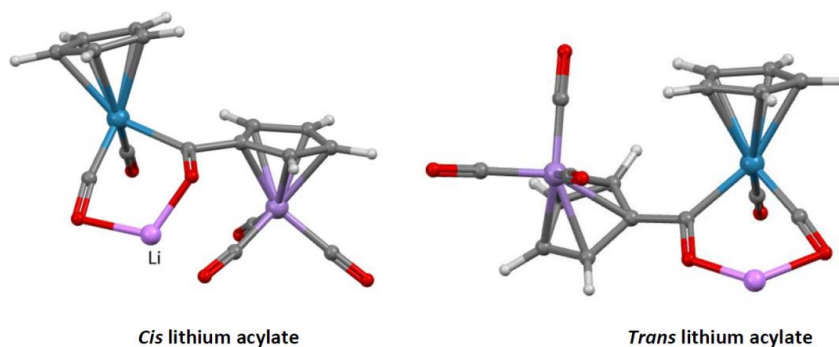
Figure 14: Stabilization through a six-membered acylate ring for complex **3**

Incidences of non-covalent intramolecular ligand interactions are witnessed between the methylene protons of the carbene substituent and the metal carbonyl ligands associated with the carbene moiety. Interaction energies determined between 2.1 and 2.9 kJ/mol were observed for **1**-**5**. The interactions, although weak, were completely absent in the *cis* conformations and could contribute to the stability and preferential formation of the *trans* conformer (Figure 15).

Complex 1: 2.93 kJ/mol   Complex 2: 2.34 kJ/mol

Complex 3: 2.64 kJ/mol   Complex 5: 2.13 kJ/mol
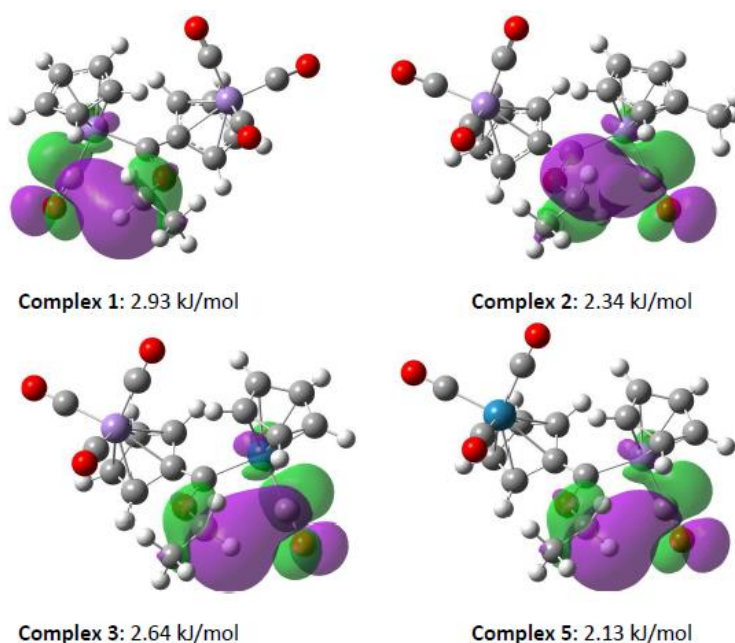
Figure 15: NBO interactions in the *trans* conformation

In contrast with the published values of Lugan *et al.* [11], theoretical results for the complexes of this study show no stabilization from the π-(C≡O) orbital of a carbonyl ligand on the carbene metal moiety [Mn] or [Re] to the unoccupied σ^*-(C-H$_{OEt}$) orbital in **1-5**. Only σ-(C-H$_{OEt}$) $\rightarrow$ π^*-(C≡O) interactions were observed between OEt and CO ligands of the carbene metal moiety and these interaction values are less significant than the values reported by Lugan *et al.* [11]. This may be due to the difference in horizontal (our complexes) and vertical (Lugan *et al.*) orientations of the carbene substituents. To provide insight into the energetics of the carbene formation, and in regards to the prevalence of the *trans* conformation, a full energy profile of the carbene synthesis has been calculated (Scheme 2). Lithiation of the cyclopentadienyl metal synthon leads to the formation of the lithiated cyclopentadienyl metal species, with a sharp decrease in the energy of the molecule. The energy release is accompanied by the formation of the very stable butane and the lithium entity, now stabilized by the larger CpMn(CO)$_3$ moiety. The formation of the LiCpMn(CO)$_3$ is achieved by the irreversible deprotonation through the employment of a strong base such as n-butyl lithium. The formation of the metal acylate is accompanied by the release of energy to produce a more stable intermediate and the *cis* conformation, surprisingly, exhibits higher stability compared to the *trans* conformer. The final carbene complex favours the formation of the *trans* conformer, regardless of the identity of the starting metal synthon or the metalating agent. The *trans* complex is more favourable when CpRe(CO)$_3$ acts as the deprotonated moiety compared to CpMn(CO)$_3$ and in addition, the *trans* complex is also favoured when CpRe(CO)$_3$ acts as the metalating agent. From Table 2, the *trans* complex of **4** would thus be the most preferential, consisting only out of CpRe(CO)$_x$ fragments and will be followed in stability by **5**, which is a *trans* carbene complexes where CpRe(CO)$_3$ served only as the initial deprotonated synthon. Since we are interested in the nature of the conformation around the carbene-metal moiety, the correlation between experimental results and theoretical findings plays a crucial role in the validation of the computation results. An analysis was undertaken to correlate the structural properties of the M-carbene fragment to that of theoretical findings and a plot of calculated verses experimental M-carbene bond lengths is displayed in supplementary data. The data displays a satisfying linear relationship, with the regression line having a R^2 value of 0.99. The theoretical carbene-metal bond length is also 0.011 pm longer on average compared to the experimentally determined structural parameter.
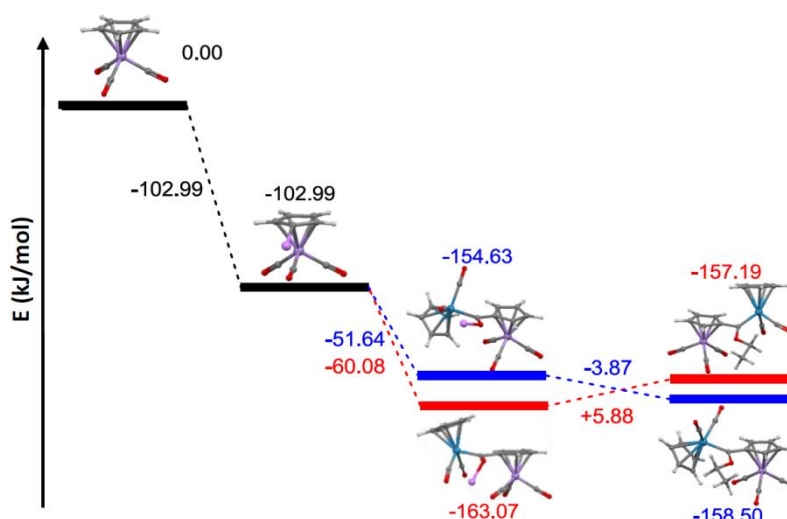
Scheme 2: Energy plot for the synthetic methodology that was followed in the formation of the *cis* (red) and *trans* (blue) product.

As mentioned previously, the theoretical lithium acylate intermediate shows an interaction between the lithium counter ion and one of the carbonyl ligands of the carbene metal. The formation of the six-membered ring influences the binding structure of the lithium acylate considerably and stabilization of the positive ion with the carbonyl ligands occurs preferentially towards the carbene centre carbonyls compared to that of the substituent half-sandwich metal synthon. The interaction can easily be explained when the electrostatic potential maps of the acylates are taken into consideration (Figure 16). The ESP map indicates, in red, the presence of highly negative carbonyl groups of the carbene centre especially in comparison to the substituent $CpM(CO)_3$ carbonyl groups. The carbene carbonyl group, stabilized by the lithium ion, has more equally shared electron density over the entire ligand group compared to the non-stabilized carbonyl ligand. Future explorations will focus on including THF solvent effects to energy profile calculations to identify if a THF-lithium coordination in the acylate has any meaningful repercussions to outcome of the proposed energy profile. Re-C and C-O bond orders were determined as 1.59 and 1.74 respectively for the stabilized-ligand compared to 1.37 and 1.99 for the non-stabilized carbonyl group in the *cis* conformer. The *trans* conformer indicated an even greater sharing of electron densities and the bond orders of the Re-C and C-O bonds, of the stabilized carbonyl ligand, were calculated as 1.66 and 1.71 respectively. The bond orders of the non-stabilized carbonyl ligand were determined as 1.32 and 2.02 for the Re-C and C-O bonds respectively.
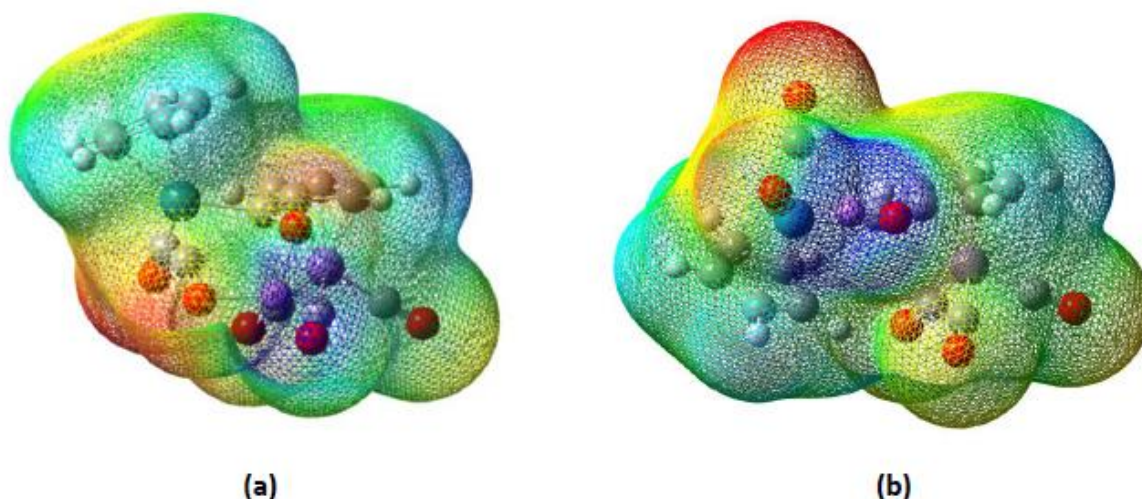
Figure 16: Electron potential map of the *cis*-acylate (a) and the *trans*-acylate (b) of **3**

4   Conclusion

Bimetallic complexes **2-5** were synthesized in satisfactory yield. The molecular structures of the novel complexes were confirmed with NMR and IR spectroscopy, and single crystal X-ray diffraction studies of **2**, **4** and **5**. Applying DFT calculations, it was possible to explain and visualise conformational stabilities of the *cis* and *trans* conformers as well as to determine the origin of the preferential conformation by means of an energy plot. Complexes **1-6** were found to be more stable in the *trans* conformation compared to this *cis* conformer. The preference of the *trans* conformers above the *cis* analogues are also witnessed in the solid state structure. Theoretical calculations indicated the origin of stabilization of the electrophilic carbene centre through greater π-donation from the ethoxy substituent and less back donation from the carbene metal moiety towards the carbene carbon atom. NBO stabilization interactions were visualized and illustrated the ability of the *trans* conformer to produce intramolecular stabilization between the methylene protons of the ethoxy substituent and the carbonyl ligands associated with the carbene metal moiety. These interactions were absent in the *cis* conformation. The calculated results of the lithium acylate intermediate suggest internal stabilization via the formation of a six-membered ring. Theoretical calculations were validated by a comparison between experimental and calculated carbene-metal bonds. The results provide an indication as to the steric and electronic parameters governing the conformations of the dimetallic carbonyl complexes.

Acknowledgements

Supporting Information

The electronic supporting information includes Table S1, lists of bond distances and angles for crystal structures reported and the optimized coordinates of the DFT calculations. CCDC 1482771-1482773 contains the supplementary crystallographic data for this paper. This data can be obtained free of charge *via* http://www.ccdc.cam.ac.uk/conts/retrieving.html (or from the Cambridge Crystallographic Data Centre, 12, Union Road, Cambridge CB2 1EZ, UK; fax: +44 1223 336033).

CHAPTER 4

Synthesis, structure and substitution pattern study of phosphine-substituted dimetallic Fischer carbene complexes of cymantrene

Chapter 4 was adapted from an article published in Polyhedron. The format reflects the requirements of the journal.

Graphical Abstract:

Contributions:

Roan Fraser: Author, synthesis, DFT studies

Petrus H. van Rooyen: Co-author, crystallography

Marilé Landman: Corresponding author, supervisor

4

Synthesis, structure and substitution pattern study of phosphine-substituted dimetallic Fischer carbene complexes of cymantrene

Roan Fraser, Petrus H. van Rooyen and Marilé Landman*

Department of Chemistry, University of Pretoria, Private Bag X20, Hatfield, 0028, South Africa. Tel: +27-12-4202527, Fax: +27-12-4204687

Contact author details:
Name: Marilé Landman Tel: +27-12-4202527, Fax: +27-12-4204687, email: marile.landman@up.ac.za

Keywords

Fischer carbene; cymantrenyl; DFT; Wiberg bond orders; phosphine

Graphical abstract
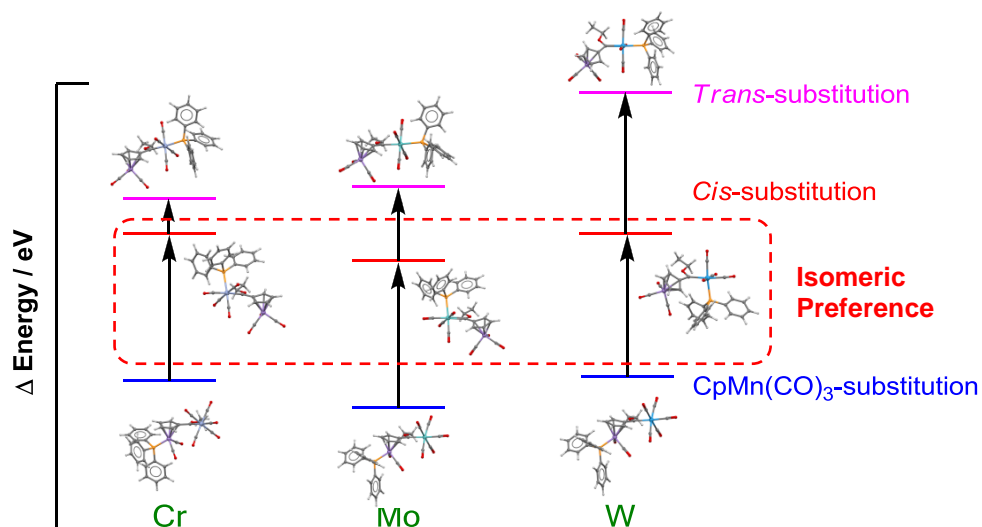
TOC abstract

Synthesis, X-ray study and NBO analysis of phosphine-substituted dimetallic Fischer ethoxy carbene complexes of cymantrene

Research highlights

- DFT calculations on configurations of homo- and heteronuclear phosphine-substituted Fischer carbene complexes
- Crystal structure of three carbene complexes constituting of phosphinated, mixed metallic systems
- Comparing the substitution patterns of the carbene systems using calculated energy values
- Calculated bond dissociation energies and solid angle sterical parameters

Abstract

Phosphine-substituted Fischer carbene complexes of cymantrene [M'(CO)$_x$PPh$_3${C(OEt)(C$_5$H$_4$M(CO)$_3$)}] where M = Mn, M' = Cr, x = 4 (**1**); M = Mn, M' = Mo, x = 4 (**2**); M = Mn, M' = W, x = 4 (**3**) and M = Mn, M' = CpMn, x = 1 (**4**) have been synthesized through thermal substitution of carbonyl ligands in the presence of triphenylphosphine. Through the variation of the carbene metal group, subtle structural differences were witnessed. DFT calculations indicated that three plausible substituted structures were possible namely substitution of a carbonyl ligand on the tricarbonyl cymantrene synthon or the substitution of either a *cis* or *trans* carbonyl group on the carbene metal coordination sphere. The solid state crystal structures of three of the complexes provided insight into the bonding preference of the ligand towards the two available metal centres. Substitution of a *cis* carbonyl ligand was favoured in all four complexes. A DFT study provided rationalization into electronical and sterical aspects of the phosphinated dimetallic carbene complexes. Bonding and electronic insights into ligand-metal interactions in the complexes were discussed using calculated Wiberg bond indices, bond dissociation enthalpies and solid angle analysis. Theoretical aspects were confirmed with solid state structural data.

1 Introduction

The electronic aspects of the carbene-metal bond in carbene complexes determine the reactivity of the complex [1]. Typical Fischer-type carbene complexes feature strong π-acceptor ligands (such as CO) coordinated to the metal sphere and have electrophilic character at the carbene carbon atom [2]. Ligand substitution of carbonyl carbene complexes for phosphine analogues have also emerged in literature not long after the discovery of the first Fischer carbene complex [3]. The phosphine complexes display higher stability, especially inertness to decomposition pathways in oxygen [4]. Recently, electrochemical studies by our laboratories were extended to examine the effects of ligand sphere variation on the electrochemical behaviour of chromium, molybdenum and tungsten Fischer carbene complexes [5]. The studies indicated a linear relationship between the oxidation potential of the metal sphere and the energy of the highest occupied molecular orbital (HOMO) and between the reduction potential of the carbene carbon and the energy of the lowest unoccupied molecular orbital (LUMO) [5]. The application of computational chemistry in the determination of HOMO and LUMO energies provided important predictions on the location of oxidation and reduction of metal carbene complexes [5]. Comparative studies also indicate similarities in the location and distribution of frontier orbitals irrespective of the type of pnicotogen ligand coordinated to the metal sphere [5]. Metal atoms characteristically contribute towards the HOMO and the carbene carbon towards the LUMO. The typical Fischer carbene HOMO and LUMO distributions are presented in Figure 1. Apart from the establishment of the relationship between the frontier orbitals and the oxidative and reduction properties of Fischer carbene complexes, incidences of intramolecular stabilization in these carbene complexes have also been witnessed [6]. Natural bonding orbital (NBO) interactions have been calculated for a variety of Fischer carbene complexes and the application of the second-order perturbation theory (SOPT) to these natural bond orbitals (NBOs) revealed stabilizing interactions between the methylene C-H bonds of the ethoxy substituent, and the carbonyl ligands of the carbene metal moiety [7].

[1] (a) W. Jiang, M.J. Fuertes, W.D. Wulff, Tetrahedron 56 (2000) 2183; (b) G. Frenking, N. Frohlich, Chem. Rev. 100 (2000) 717.
[2] K.H. Dotz, Angew. Chem. Int. Ed. 23 (1984) 587.
[3] H. Werner, H. Rascher, Inorg. Chim. Acta 2 (1968) 181.
[4] E.O. Fischer, R. Aumann, Chem. Ber. 102 (1969) 1495.
[5] (a) A. Jansen van Rensburg, M. Landman, D. Van der Westhuizen, M.M. Conradie, J. Conradie, Electrochimica Acta 186 (2015) 321; (b) M. Landman, R. Liu, R. Fraser, P. H. van Rooyen, J. Conradie, J. Organomet. Chem. 752 (2014) 171.
[6] A. Jansen van Rensburg, M. Landman, P. H. van Rooyen, M.M. Conradie, J. Conradie, J. Mol. Struct. 1105 (2016) 205.
[7] R. Fraser, P.H van Rooyen, M. Landman, J. Mol. Struct. 1105 (2016) 178.
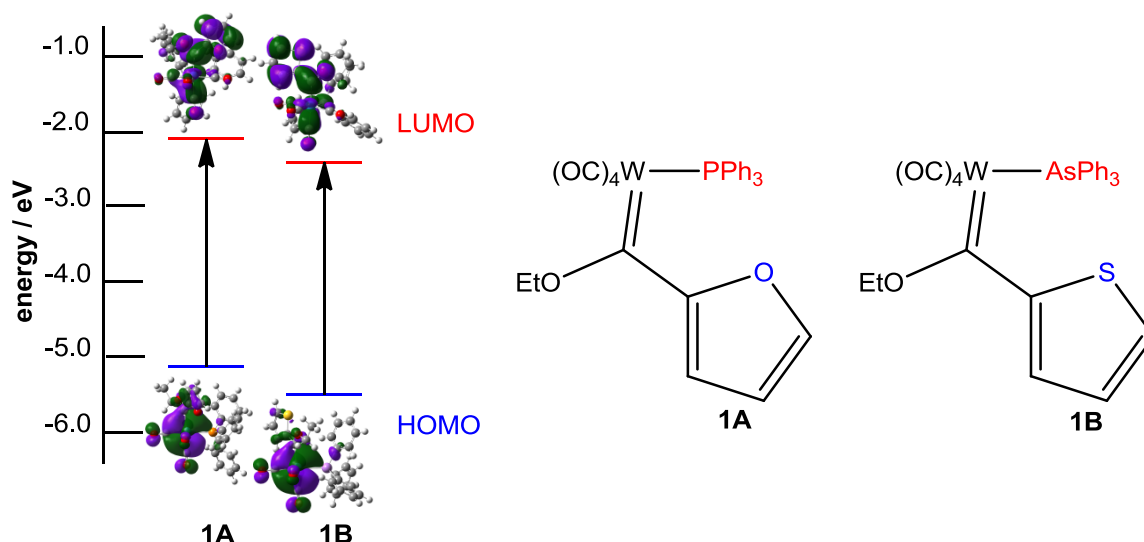
Figure 1: The HOMO and LUMO of pnictogen-substituted carbene complexes **1A** and **1B**

Additional NBO interactions can also be witnessed between heteroatomic carbene substituents and carbonyl groups of the metal associated with the carbene moiety [6]. These NBO interactions are well documented in literature [8]. Although the substitution of carbonyl groups for an assortment of ligands in Fischer carbene complexes is known, the scope of theoretical studies have been limited to frontier orbital distribution and simple intramolecular interactions [5].
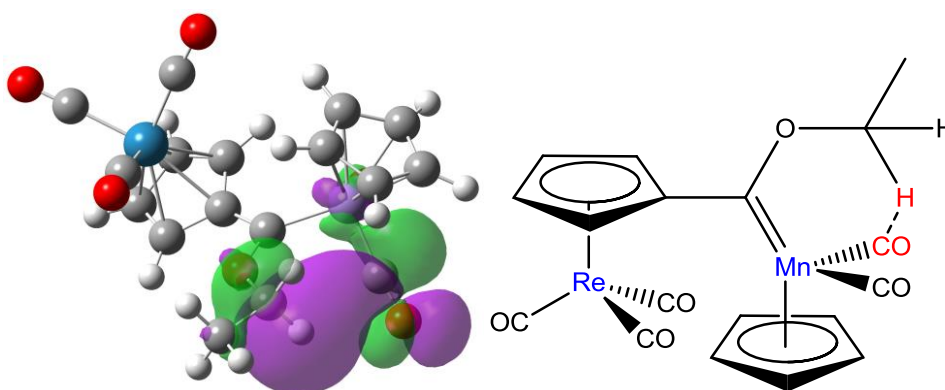
Figure 2: Intramolecular interaction between the carbene substituent and the metal carbonyl groups associated with the carbene moiety

---

[8] N. Lugan, I. Fernández, R. Brousses, D. A. Valyaev, G. Lavigne, N. A. Ustynyuk, Dalton Trans. 42 (2013)898.

Carbonyl ligands have the exceptional ability to stabilize metal complexes based on their good σ-donating, π-accepting ability [9]. Phosphine ligands have similar σ-donating abilities but diminished π-accepting ability and are often more compared to N-heterocyclic carbene complexes (NHCs) [10]. Theoretical studies [10] indicate similar bond orders between metal-NHCs and M-PPh$_3$ groups but elevated bond dissociation energies indicate the superior ligand-metal interaction NHC's offer (54 kJ/mol higher) [10]. In light of the limited theoretical insights that literature provides, especially on multimetallic phosphine-substituted Fischer carbene complexes, on the coordination and complexation effects of phosphine ligands to metal centres, an in-depth computational study was envisaged. Aspects of isomeric preferences, bond indices, bond dissociation energies and structural properties have been investigated for all the phosphine-substituted complexes of this study. This study therefore reports the synthesis of the four novel phosphine-substituted complexes of cymantrene, X-ray crystal structures of three of the complexes and a DFT study.

M = Cr, Mo, W and x = 3, L = CO
M = Mn and x = 1, L = Cp
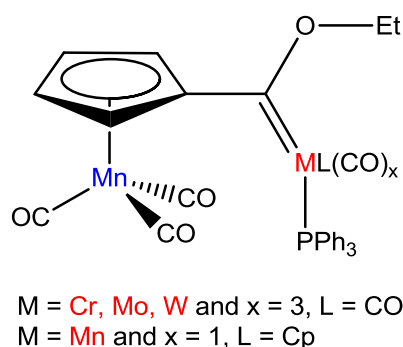
Figure 3: Bimetallic phosphine-substituted monocarbene complexes **1-4**

2 Experimental

2.1 Materials and instrumentation

All reactions, unless otherwise noted, were performed under inert nitrogen or argon atmospheres using standard Schlenk techniques [11]. All solvents were freshly distilled, dried and collected under inert conditions. Column chromatography was carried out under inert nitrogen and argon atmospheres using silica gel (particle size 0.063-0.200 mm) as the

[9] M. Landman, R. Pretorius, R. Fraser, B.E. Buitendach, M.M., Conradie, P.H. van Rooyen, J. Conradie, Electrochimica Acta.130 (2014) 104.
[10] R. Fraser, P.H. van Rooyen, C.G.C.E van Sittert, M. Landman, J. Organomet. Chem. *Submitted* .
[11] D.F. Schriver, M.A. Drezdzon. *The* manipulation of Air-Sensitive Compounds, 2nd ed., Wiley, New York, USA*,* (1986).

stationary phase. Percentage yields were calculated relative to the limiting reactant. Crystallization was done using hexane:DCM or hexane:ether diffusion methods. Triethyloxonium tetrafluoroborate [12] was prepared according to a reported literature procedure. The reagents $CpMn(CO)_3$, $MeCpMn(CO)_3$, $Cr(CO)_6$, $Mo(CO)_6$, $W(CO)_6$, n-butyl lithium (1.6 M solution in hexane) and other commercial reagents were used as purchased. NMR spectra were recorded on a Bruker ARX-300. NMR spectra were recorded in CDCl3 using the deuterated solvent peak as internal reference. ^1H and ^{13}C NMR spectra were measured at 300.1 and 75.5 MHz, respectively. The numbering of atoms in the NMR assignment is according to the numbering in Figure 5, Figure 7 and Figure 8. IR spectra were recorded on a Perkin Elmer Spectrum RXI FT-IR spectrophotometer in hexane and only the vibration bands in the carbonyl-stretching region (ca. 1500-2200 cm^{-1}) are reported.

2.2 X-ray crystallography

Data for complexes **1**, **3** and **4** were collected at 150 K on a Bruker D8 Venture kappa geometry diffractometer, with duo Iμs sources, a Photon 100 CMOS detector and APEX II control software using Quazar multi-layer optics, monochromated Mo-Kα radiation and by means of a combination of φ and ω scans. Data reduction was performed using SAINT+ and the intensities were corrected for absorption using SADABS [13]. The structures were solved by intrinsic phasing using SHELXTS and refined by full-matrix least squares using SHELXTL and SHELXL-2013 [14]. In the structure refinement, all hydrogen atoms were added in calculated positions and treated as riding on the atom to which they are attached. All nonhydrogen atoms were refined with anisotropic displacement parameters, all isotropic displacement parameters for hydrogen atoms were calculated as X × Ueq of the atom to which they are attached, X = 1.5 for the methyl hydrogens and 1.2 for all other hydrogens. Crystallographic data and refinement parameters are given in Table 1. Ortep drawings [15] of the three structures are included in Figure 5, Figure 7 and Figure 8. The crystal structures (cifs) have been deposited at the Cambridge Crystallographic Data Centre and allocated the deposition numbers: CCDC 1488006-1488008. Data collection, structure solution and refinement details are available in each cif.

[12] H. Meerwein, Org. Synth. 46 (1966)113.
[13] APEX2 (including SAINT and SADABS); Bruker AXS Inc., Madison, WI (2012).
[14] G.M. Sheldrick, Acta Crystallogr. A64 (2008)112.
[15] L.J.J. Farrugia, Appl. Crystallogr. 30 (1997) 565.

2.3 Synthesis of complexes 1-4

2.3.1   Synthesis of dimetallic carbene complexes A-D

The dimetallic carbene starting materials (**A**-**D**) have been synthesised according to literature procedures [7].

2.3.2   Synthesis of complexes 1

$Cr(CO)_5\{C(OEt)(MnCp(CO)_3)\}$ (0.452 g, 1.0 mmole) was dissolved in 40 ml of dry hexane. Triphenylphosphine (0.328 g, 1.25 mmole) was added at room temperature and the reaction mixture heated to reflux until TLC indicated satisfactory conversion. The complex was purified using column chromatography with aluminium oxide as stationary phase and a hexane:DCM 4:1 solvent ratio to yield **1** as a peach-brown complex (yield: 0.345 g; 50%).
^1H NMR (CDCl$_3$, ppm): δ 7.28-7.71 (m, PPh$_3$), 5.53 (s, H10 and H13), 4.95 (s, H11 and H12), 4.30 (q, H14, 7.3 Hz), 1.36 (t, H15, 7.1 Hz). $^{13}C\{^1H\}$ NMR (CDCl$_3$, ppm): δ 309.7 (C5), 236.3 (CO1), 224.0 (CO3), 222.8 (CpMn-CO), 216.4 (CO2), 128.1-130.9 (PPh$_3$), 110.1 (C9), 87.6 (C10 and C13), 83.8 (C11 and C12), 77.2 (C14), 15.0 (C15). ^{31}P NMR (CDCl$_3$, ppm): δ 57.12. IR (Hexane, cm^{-1}): vCO 2031 (m), 2010 (m), 1955 (s), 1946 (s), 1907 (s). HRESI$^+$-MS, m/z: 715.0036 (calcd 715.0022).

2.3.3   Synthesis of complexes 2

Complexes **2**-**4** were synthesised using a similar procedure as for the synthesis of **1**. $Mo(CO)_5\{C(OEt)(MnCp(CO)_3)\}$(0.497 g, 1.0 mmole) and triphenylphosphine (0.328 g, 1.25 mmole) was dissolved in hexane and refluxed. After purification, **2** was yielded as a brown complex (yield: 0.389 g; 53%). ^1H NMR (CDCl$_3$, ppm): δ 7.31-7.71 (m, PPh$_3$), 5.48 (s, H10 and H13), 4.96 (s, H11 and H12), 4.81 (s br, H14), 1.35 (t, H15, 7.2 Hz). $^{13}C\{^1H\}$ NMR (CDCl$_3$, ppm): δ 304.4 (C5), 222.8 (CpMn-CO), 221.2 (CO1), 216.0 (CO3), 212.9 (CO2), 127.9-130.1 (PPh$_3$), 106.6 (C9), 88.0 (C10 and C13), 84.9 (C11 and C12), 77.3 (C14), 14.3 (C15). ^{31}P NMR (CDCl$_3$, ppm): δ 39.41. IR (Hexane, cm^{-1}): vCO 2035 (s), 1982 (w), 1955 (s), 1940 (m), 1897 (m). HRESI$^+$-MS, m/z: 764.9962 (calcd 764.9984).

2.3.4   Synthesis of complexes 3

Complex **3** was synthesised using a similar procedure as for the synthesis of **1**. $W(CO)_5\{C(OEt)(MnCp(CO)_3)\}$(0.584 g, 1.0 mmole) and triphenylphosphine (0.328 g, 1.25 mmole) was dissolved in hexane and refluxed. After purification, **3** was yielded as a peach-brown complex (yield: 0.419 g; 51%). ^1H NMR (CDCl$_3$, ppm): δ 7.27-7.59 (m, PPh$_3$), 5.50 (m, H10 and H13), 5.08 (t, H11 and H12, 2.3 Hz), 4.48 (q, H14, 6.7 Hz), 1.62 (t, H15, 7.0 Hz).

$^{13}C\{^1H\}$ NMR (CDCl$_3$, ppm): δ 305.6 (d, C5, J$_{P-C}$ = 7.2 Hz), 224.2 (CpMn-CO), 210.7 (d, CO1, J$_{P-C}$ = 6.6 Hz), 205.9 (d, CO3, J$_{P-C}$ = 22.7 Hz), 202.7 (d, CO2, J$_{P-C}$ = 6.9 Hz), 135.3 (d, PhC, J$_{P-C}$ = 39.1 Hz), 133.1 (d, PhC, J$_{P-C}$ = 11.8 Hz), 130.5 (d, PhC, J$_{P-C}$ = 1.6 Hz), 128.7 (d, PhC, J$_{P-C}$ = 9.7 Hz), 112.3 (C9), 88.2 (C10 and C13), 83.3 (C11 and C12), 77.7 (C14), 13.8 (C15). ^{31}P NMR (CDCl$_3$, ppm): δ 24.12. IR (Hexane, cm^{-1}): vCO 2035 (s), 1979 (w), 1955 (s), 1947 (s), 1855 (m). HRESI$^+$-MS, m/z: 851.0461 (calcd 851.0439).

2.3.5 Synthesis of complexes 4

Complex **4** was synthesised using a similar procedure as for the synthesis of **1**. CpMn(CO)$_2${C(OEt)(MnCp(CO)$_3$)} (0.436 g, 1.0 mmole) and triphenylphosphine (0.328 g, 1.25 mmole) was dissolved in hexane and refluxed. After purification, **4** was yielded as a brown-black complex (yield: 0.282 g; 42%). ^1H NMR (CDCl$_3$, ppm): δ 7.32-7.68 (s br, PPh$_3$), 5.46 (s br, H10 and H13), 5.00 (s br, H11 and H12), 4.81 (s br, H14), 1.30 (s br, H15). $^{13}C\{^1H\}$ NMR (CDCl$_3$, ppm): δ 324.5 (C5), 225.9 (CO1) 223.5 (CpMn-CO), 221.2 (CO1), 125.5-130.6 (PPh$_3$), 107.4 (C9), 86.0 (C10 and C13), 84.2 (C11 and C12), 82.9 (C34-C38), 77.7 (C14), 14.3 (C15). ^{31}P NMR (CDCl$_3$, ppm): δ 85.11. IR (Hexane, cm^{-1}): vCO 2035 (s), 1958 (s), 1955 (s), 1939 (s). HRESI$^+$-MS, m/z: 675.0912 (calcd 675.0905).

2.4 Molecular modelling

The computational data reported in this paper were obtained using the Gaussian 09 suite of programs [16]. Calculations were carried out in the singlet spin state using the hybrid functional B3LYP [17,18]. Geometries of the neutral complexes were optimized in the gas phase with the triple-ζ basis set 6-311G* on all atoms except for the metal atoms. Stuttgart/Dresden (SDD) pseudopotential was used to describe the metal electronic core, while the valence electrons were described def2-TZVPP [19]. No symmetry constraints were applied and only the default convergence criteria were used during the geometric optimizations. Vibrational frequencies [20]

[16] M.J. Frisch, G.W. Trucks, H.B. Schlegel, G.E. Scuseria, M.A. Robb, J.R. Cheeseman, G. Scalmani, V. Barone, B. Mennucci, G.A. Petersson, H. Nakatsuji, M. Caricato, X. Li, H.P. Hratchian, A.F. Izmaylov, J. Bloino, G. Zheng, J.L. Sonnenberg, M. Hada, M. Ehara, K. Toyota, R. Fukuda, J. Hasegawa, M. Ishida, T. Nakajima, Y. Honda, O. Kitao, H. Nakai, T. Vreven, J.A. Montgomery (Jr), J.E. Peralta, F. Ogliaro, M. Bearpark, J.J. Heyd, E. Brothers, K.N. Kudin, V.N. Staroverov, T. Keith, R. Kobayashi, J. Normand, K. Raghavachari, A. Rendell, J.C. Burant, S.S. Iyengar, J. Tomasi, M. Cossi, N. Rega, J.M. Millam, M. Klene, J.E. Knox, J.B. Cross, V. Bakken, C. Adamo, J. Jaramillo, R. Gomperts, R.E. Stratmann, O. Yazyev, A.J. Austin, R. Cammi, C. Pomelli, J.W. Ochterski, R.L. Martin, K. Morokuma, V.G. Zakrzewski, G.A. Voth, P. Salvador, J.J. Dannenberg, S. Dapprich, A.D. Daniels, O. Farkas, J.B. Foresman, J.V. Ortiz, J. Cioslowski, D.J. Fox, Gaussian 09, Revision D.01, Gaussian Inc., Wallingford CT, (2010).
[17] A.D. Becke, J. Chem. Phys. 98 (1993) 5648.
[18] C. Lee, W. Yang, R.G. Parr, Phys. Rev. B37 (1988) 785.
[19] F. Weigend, R. Ahlrichs, Chem. Phys. **7** (2005) 3297.
[20] J.W. McIver, A.K. Komornicki, J. Am. Chem. Soc. 94 (1972) 2625.

were calculated at the optimized geometries and no imaginary frequencies were observed, to confirm true minima. Donor-acceptor interactions have been computed using the natural bond order (NBO) method [21].

3   Results and discussion

3.1   Synthesis and characterization

Complexes **1-4** were synthesised as major products in the reactions based on classic Fischer methodology (Figure 4) [22]. Carbonyl ligand substitution reactions have been reported by our laboratories recently [6]. During the synthesis of the proposed complexes **1-3**, the formation of three possible isomer complexes seemed plausible. The substitution of a carbonyl ligand is possible from: (i) the tricarbonyl metal synthon or the substitution of a (ii) *cis* or (iii) *trans* carbonyl ligand from the metal carbonyl groups associated with the carbene fragment. Complex **4** could undergo either carbonyl substitution at the Cp(CO)$_3$ moiety or, alternatively, a carbonyl group from the carbene metal ligands. For **1-4** carbonyl substitution occurred exclusively on the carbene metal carbonyl ligands and for **1-3**, substitution of the *cis* carbonyl ligands occurred exclusively.
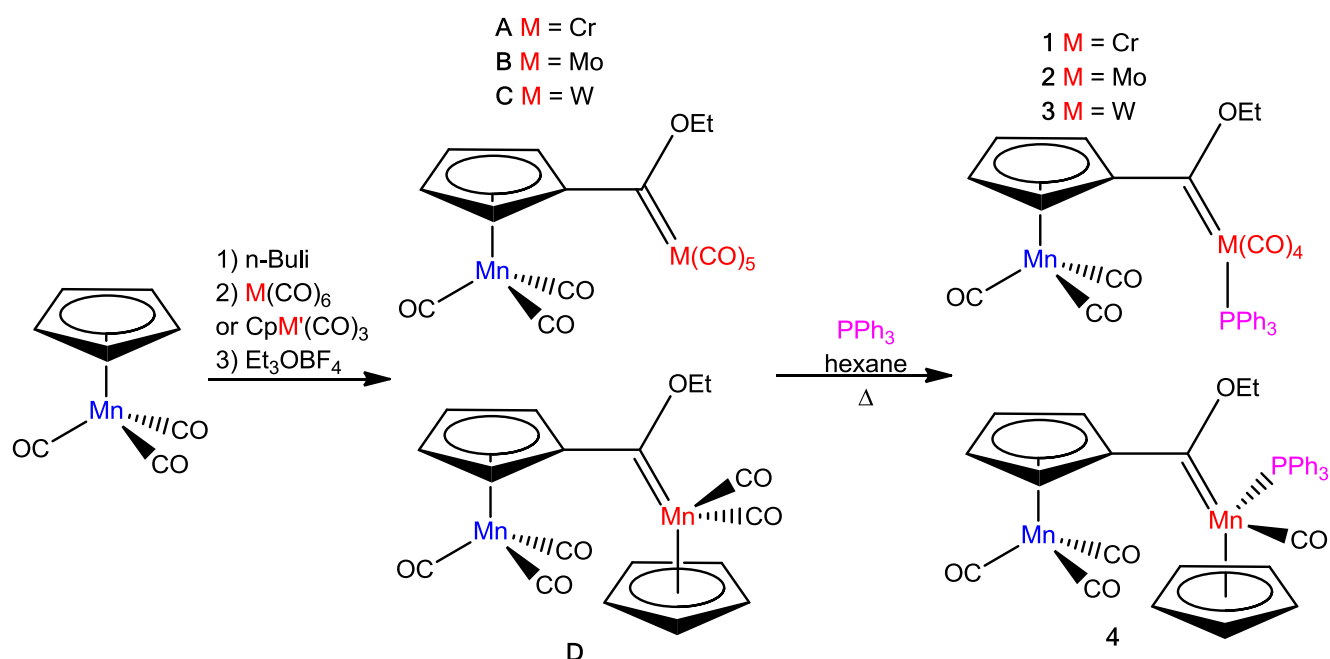
Figure 4: Synthetic methodology followed in the synthesis of **1-4**

[21] (a) J.P. Foster, F. Weinhold, J. Am. Chem. Soc. 102 (1980) 7211; (b) A.E. Reed, F. Weinhold, J. Chem. Phys. 83 (1985) 1736; (c) A.E. Reed, R.B. Weinstock, F. Weinhold, *J.* Chem. Phys. 83 (1985) 735. (d) A.E. Reed, L.A. Curtiss, F. Weinhold, Chem. Rev. 88 (1988) 899.
[22] See Ref. [5] and references therein.

3.2 Spectroscopic characterization

The IR spectra of **1**-**4** were measured in hexane and indicate four stretching frequencies attributed to the *cis* substituted metal carbonyl moiety. In addition, one distinguishable observed frequency could be unambiguously assigned to the cymantrenyl metal carbonyl stretching frequencies (A_1 band at 2031). The second expected band (E) can be observed as a shoulder overlapping peak of the tetracarbonyl moiety in the range 1955-1960 cm^{-1}. The stretching frequencies for the substituted metal carbonyls were observed between 1855 and 2035 cm^{-1} and the observation of these frequencies is supported by literature [23]. ^{13}C NMR spectroscopy indicates downfield-shifted carbene carbon peaks between δ = 304.4 and 324.5 ppm. The addition carbonyl peak of the cymantrenyl carbonyl ligands was visible at *ca* δ = 224 ppm whilst the ^{31}P phosphorus peak was witnessed between δ = 24.12 and 85.11 ppm. The structural characterizations were also confirmed with solid state X-ray diffraction studies.

3.3 Single crystal X-ray diffraction studies

Selected structural parameters are summarized in Table 1. The carbene moiety deviates from planarity by less than 10° for complexes **1** (Figure 5), **3** (Figure 7) and **4**, as shown by the C14-O5-C5-M' dihedral angles. The carbene-metal bond lengths were determined to be 2.039 Å, 2.172 Å and 1.869 Å respectively for **1**, **3** and **4** while the M'-P bond was 2.4162 Å, 2.5386 Å and 2.2386 Å. Complex **1** crystallized in a tetragonal system and a P-42$_1$-c space group and the crystal structure was refined as a two-component inversion twin. There were some ill-defined peaks present in the final difference electron density maps that may resulted from two diffuse water molecules, as the compound was hygroscopic. The Platon Squeeze method was used to treat its contribution to the structure factors, yielding an improved final solution (R=0.439 vs R=0.0487) [24]. The solid state crystal structures confirmed the NMR and IR spectroscopy indications that *cis* substitution is preferred over the formation of the *trans* isomer.

[23] M. Landman, T.J. Levell, M.M. Conradie, P.H. van Rooyen, J. Conradie, J. Mol. Struct. 1086 (2015) 190.

[24] A.L. Spek, Acta Cryst. C71 (2015) 9.
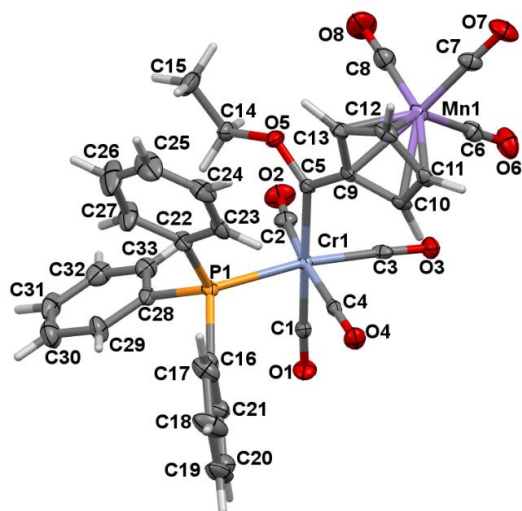
Figure 5: Perspective view of **1** with thermal ellipsoids drawn at the 50% probability level
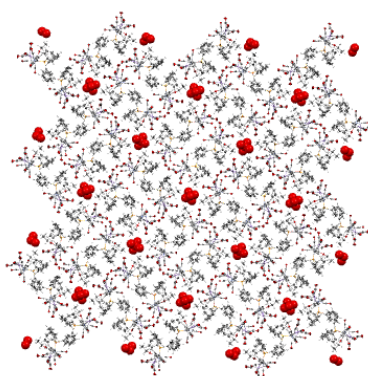
Figure 6: Packing diagram of in **1**
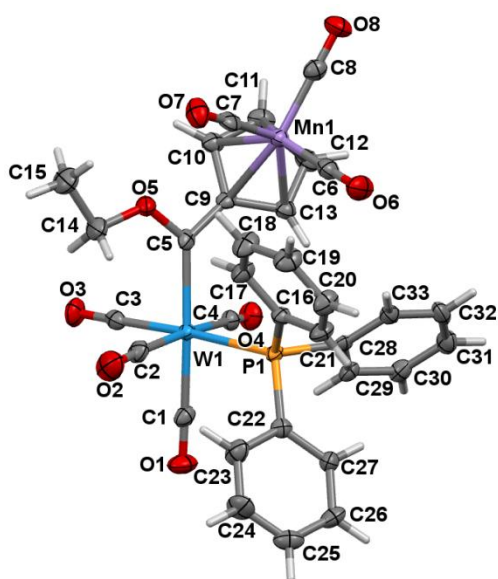
Figure 7: Perspective view of **3** with thermal ellipsoids drawn at the 50% probability level
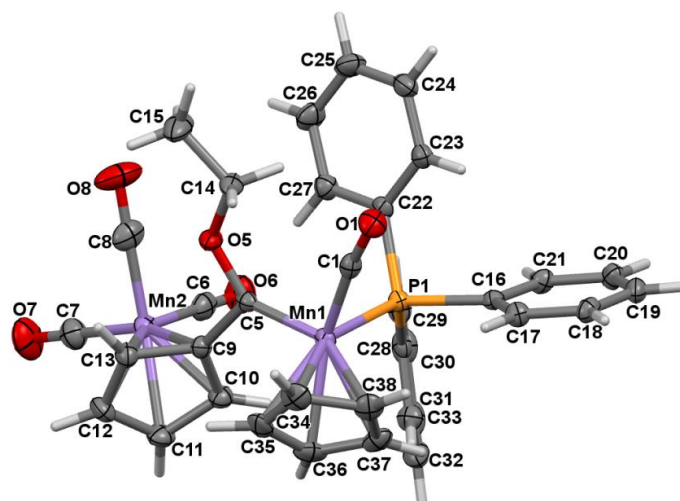
Figure 8: Perspective view of **4** with thermal ellipsoids drawn at the 50% probability level

Table 1: Selected bond lengths and angles of **1**, **3** and **4**

	1	3	4
Bond length (Å)			
M-CO$_x$ (x = 6-8)	1.799(6)	1.799(5)	1.790(3)
M'-CO$_x$ (x = 1)	1.874(5)	2.029(5)	1.753(3)
M'-CO$_x$ (x = 2 and 4)	1.899(5)	2.036(5)	-
M'-CO$_x$ (x = 3)	1.857(5)	1.998(5)	-
M'-C5	2.039(4)	2.172(4)	1.869(3)
M'-P1	2.4162(13)	2.5386(11)	2.2386(7)
C5-C9	1.476(7)	1.474(7)	1.496(3)
O5-C5	1.320(5)	1.341(5)	1.354(3)
Bond angle (°)			
O5-C5-M'	130.9(3)	129.1(3)	134.84(18)
C9-C5-M'	124.7(3)	124.5(3)	120.22(19)
O5-C5-C9	104.4(3)	105.2(4)	104.1(2)
Torsion angle (°)			
C14-O5-C5-M'	2.0(7)	9.5(6)	0.4(4)

The phenyl rings of the PPh$_3$ ligand can adopt one of two propeller-type conformations, that can be orientated in clockwise or anti-clockwise rotation [25]. The solid state structures of **1**,

[25] M. Landman, T.J. Levell, P.H. van Rooyen, J. Conradie, J. Mol. Struct. 1065 (2014) 29.

3 and **4** display a preference for the clockwise rotation conformer. Optimized DFT coordinates of **1-4** also indicated the preference of the clock-wise rotation, as described later. The preferred orientation of the phenyl rings of the phosphine ligand correlates with findings reported in literature [25].

Clockwise   *Anti-clockwise*

Figure 9: Clock- and anti-clockwise conformations of the triphenylphosphine ligands

Incidences of intermolecular hydrogen bond interactions can be witnessed between neighbouring molecules of **4**. The interactions originate between hydrogen atoms on the phenyl rings of the phospine ligand and carbonyl groups of the cymantrenyl moieties on adjacent molecules.
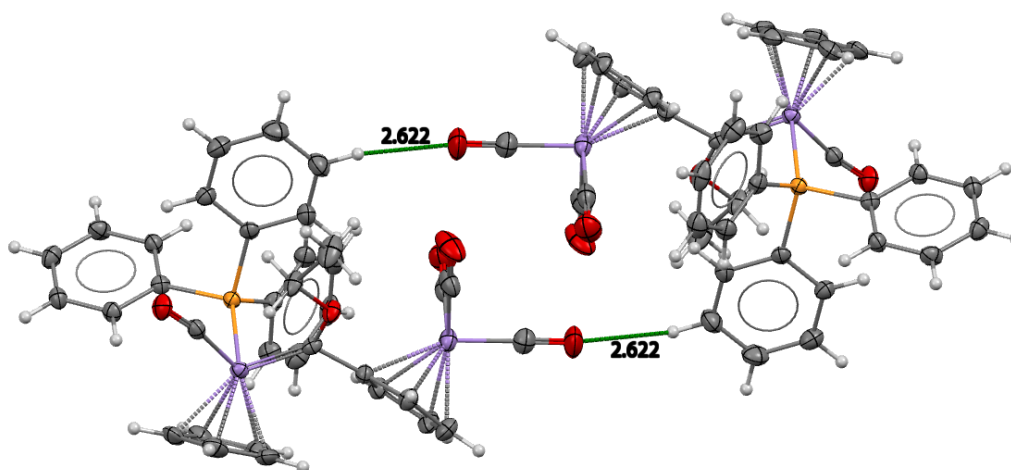
Figure 10: Intermolecular hydrogen bond interactions (Å) in **4**

3.4   DFT study

Theoretical studies on Fischer-type carbene complexes are well described in literature [7,23,25]. Computational studies typically focus on the interactions of the frontier orbitals and the predictions that can be made from these interactions on the oxidation and reduction potential trends witnessed for metal centres. Linear relationships exist between the oxidation of the metal sphere and the HOMO and between the reduction of the carbene carbon and the LUMO [5]. These studies have, however, been restricted to mostly electronic parameters and limited insights have been provided on the sterical aspects of phosphine-substituted carbene complexes. A DFT study has thus been considered to describe not only the electronic influences that phosphine substitution poses to the coordination sphere of carbene metal complexes but also structural and steric influences imparted by these ligands on the metal moiety.

3.4.1 Phosphine substitution pattern

Literature indicates substitution of carbonyl ligands for pnictogen analogues occurs preferentially *cis* to the carbene moiety [6]. Solid state structures and gas phase computational studies support this finding. In this study, however, substitution of carbonyl ligands can occur at three different sites, namely either the (i) *cis* (CS) or (ii) *trans* (TS) positions of the carbene-$M(CO)_5$ centre or (iii) at the $CpMn(CO)_3$ moiety (MnS) (Figure 11). Energy calculations indicate the preference of substituting carbonyl ligands at the $CpMn(CO)_3$ moiety first, followed by the substitution of a *cis* carbonyl group of the carbene-$M(CO)_5$ centre and lastly the *trans* carbonyl ligands. Since *cis* carbonyl substitution was theoretically determined to be more energetically favourable than *trans* carbonyl substitution (Figure 11), it comes as little surprise that only the *cis* substituted complexes of **1**-**3** were experimentally obtained and no *trans* complexes. Complex **4** contains two CpMn carbonyl moieties and one can only distinguish between two conformers for this complex based on the relative orientations of the two Cp rings, either the *cis* conformer (CC) or the *trans* conformer (TC) [7]. During the synthesis of the phosphine-substituted carbene complexes, no formation of the isomer bearing the phosphine on the $CpMn(CO)_3$ was witnessed even though theoretical results indicate this product as the most energetically favoured isomer. It could be suggested that the formation of this isomer is due to the thermal synthetic route followed for substitution, while substitution of $CpMn(CO)_3$ carbonyl ligands are known to be promoted only photochemically. The energy profiles of the possible isomers obtainable through carbonyl substitution of complexes **A-D** are presented in Figure 11.
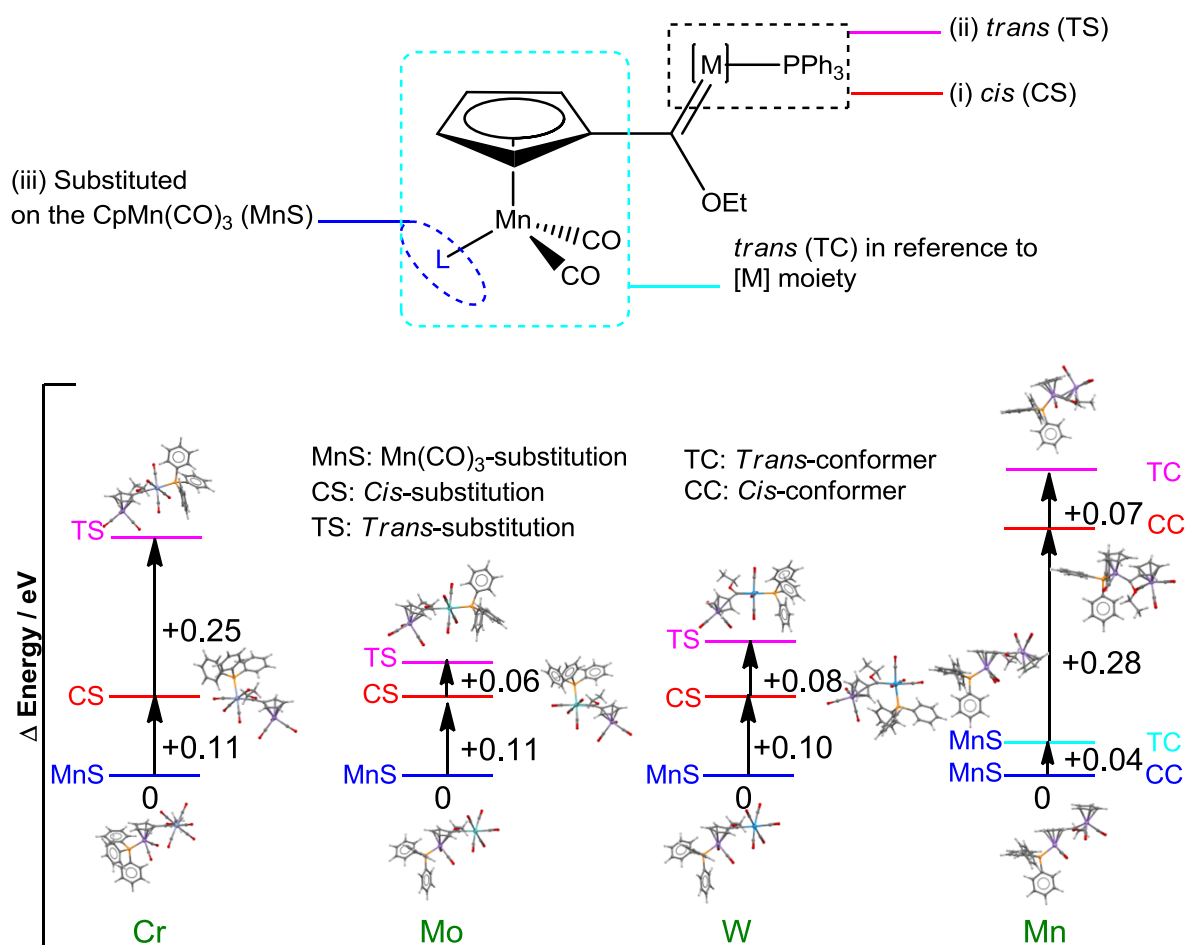
Figure 11: Energy profiles of the possible isomers of **1-4** obtainable through carbonyl substitution of complexes **A-D**

DFT optimized structures indicated the preference of a clockwise rotated PPh$_3$ ligand, as witnessed in the solid state crystal structures. Correlated tilting of the phenyl rings stems from the relative size of the ligands and counteracts possible inter ring-ring and inter ring-ligand interaction. The conformations of **1** and **3** are presented in Figure 12. The preferred clockwise orientation of the phenyl rings of the phosphine ligand correlates with findings reported in literature [25].
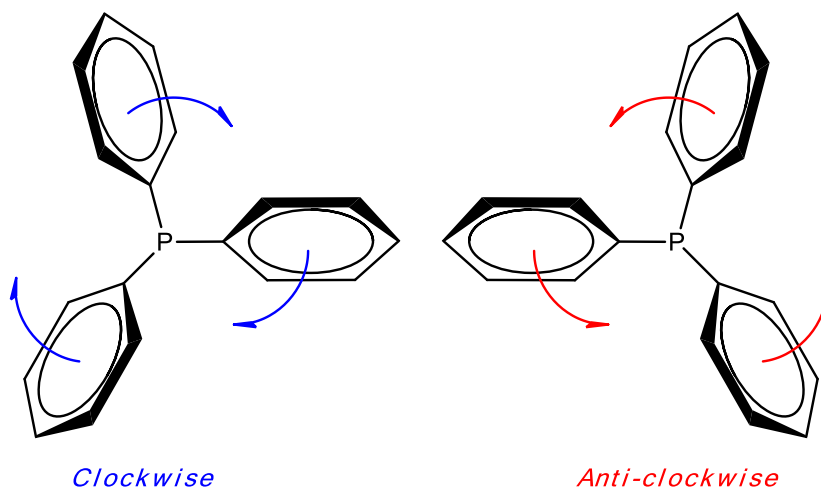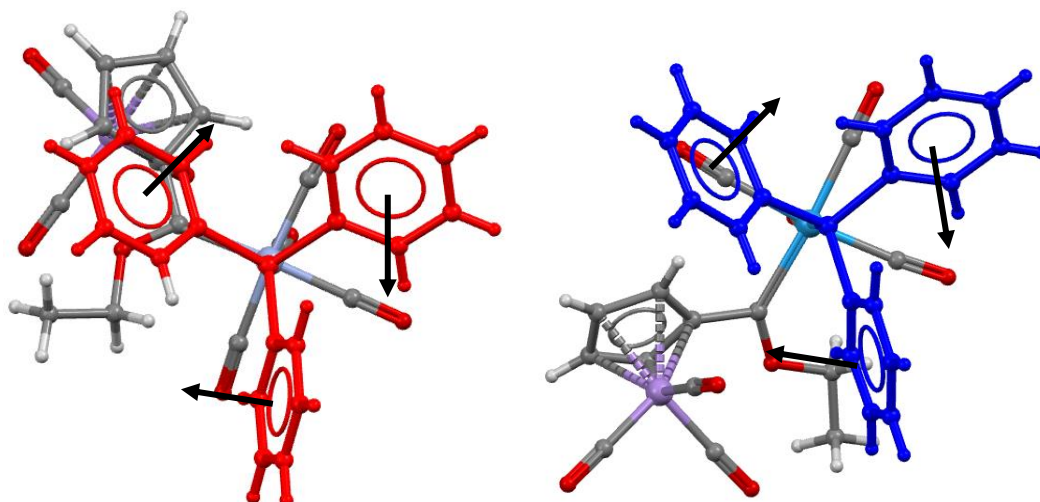
Figure 12: The clockwise conformations of **1** and **3**

3.4.2 Solid angle parameters

Numerous measurements of ligand steric parameters [26] have been investigated to establish a relationship between the steric bulk of a ligands with the reaction rates and equilibrium constants and chemical or physical characteristics of organometallic systems [27]. The steric influences enforced by ligands surrounding the coordination sphere have typically been described by the $\%V_{bur}$ or Tolman cone angles [27] but visualization of the total accessibility or shielding of the metal sphere has been elusive. The use of solid angle (Ω) [28], where each ligand can be described by the percentage of the coordination sphere of the central atom shielded by the ligand, has found application in defining the steric influences of ligands [28]. In this approach, each ligand is described by a $G_M(L)$ value which is the percentage of the metal coordination sphere shielded by the particular ligand. The G_M(Complex) value describes the total shielding of the metal centre and is predominantly indicative of the total crowding and available ligation space surrounding the metal centre (Figure 13). The solid angle parameters are available in Table 2. The equivalent cone angle (as defined by the solid angle definition) between the three aromatic rings and the phosphine atom is also presented.

[26] G.K. Fukin, I.A. Guzei, E.V. Baranov, J. Coord. Chem. **9** (2007) 937.
[27] I.A. Guzei, M.E. Sánchez-Castro, A. Ramirez-Monroy, M. Cervantes-Vásquez, I. R.A. Figueroa, M.A. Paz-Sand, Inorg. Chim. Acta. 359 (2006) 701.
[28] I.A. Guzei, M. Wendt, Dalton Trans. (2006) 3991.
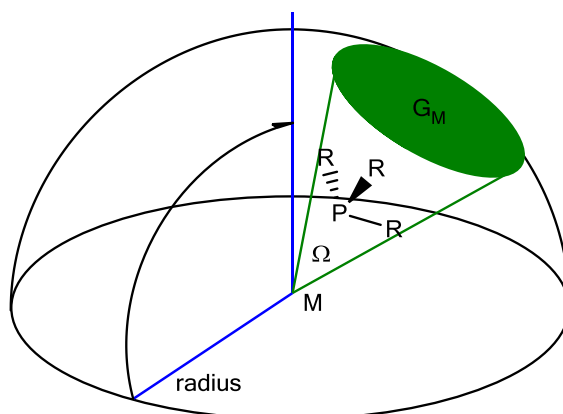
Figure 13: Representation of the solid angle (Ω) and G_M of a complex

Table 2: Solid angle parameters of **1-4**

Complex	Solid Angle (PPh$_3$) (Steradians)	Equivalent Cone angle (⁰)	G_M(Complex) %
1	2.87	114.15	99.61
2	2.70	110.56	97.51
3	2.77	112.04	97.97
4	3.17	120.55	97.06

The steric impact of the ligand sphere can be visualized as a set of overlapping ligand 'shadows' creating occupied and vacant regions. For **3** the total occupied space in the complex is calculated at 97.97 % with only small unoccupied regions, as indicated in Figure 14.
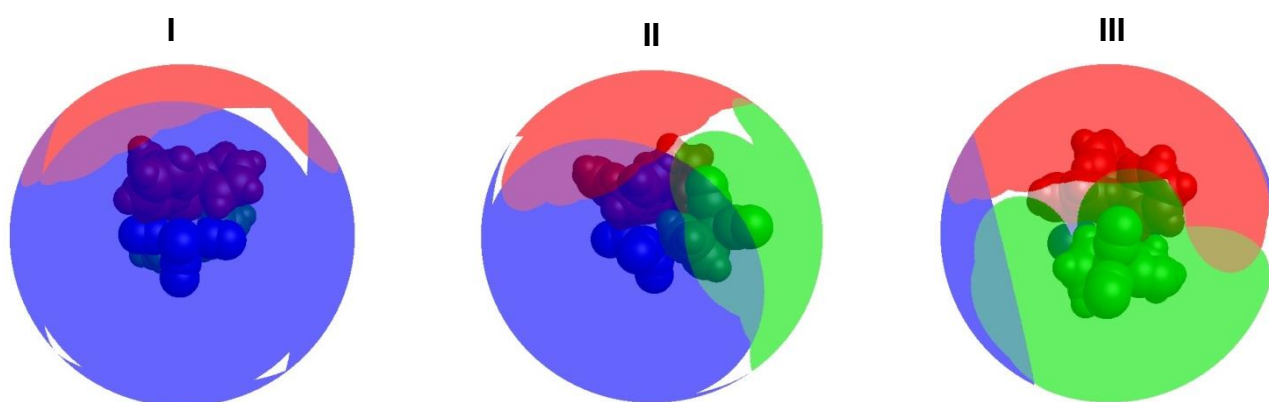
Figure 14: The G_M of **3** from the front (I), side (II) and top (III) view

76

Limited variation in the G_M is witnessed upon the substitution of a carbonyl group for a phosphine ligand. Although this notion seems counter intuitive, and one expects the steric influence to change significantly, the biggest change can be witnessed in the $G_{(Y)}$ value. $G_{(Y)}$ indicates the percentage of the metal sphere shielded by more than one ligand and creates overlapping regions of sterical bulk. These regions would severely limit metal-ligand interactions with uncoordinated ligands approaching coordination sites near highly dense regions. Substituting a carbonyl ligand of **A** to form complex **1** indicates no significant change in G_M but an increase of 3.03 % of overlapping steric regions (Figure 15).

A
G_M = 99.65 %
G_Y = 28.13 %

+ PPh$_3$
Δ

1
G_M = 99.61 %
G_Y = 31.16 %
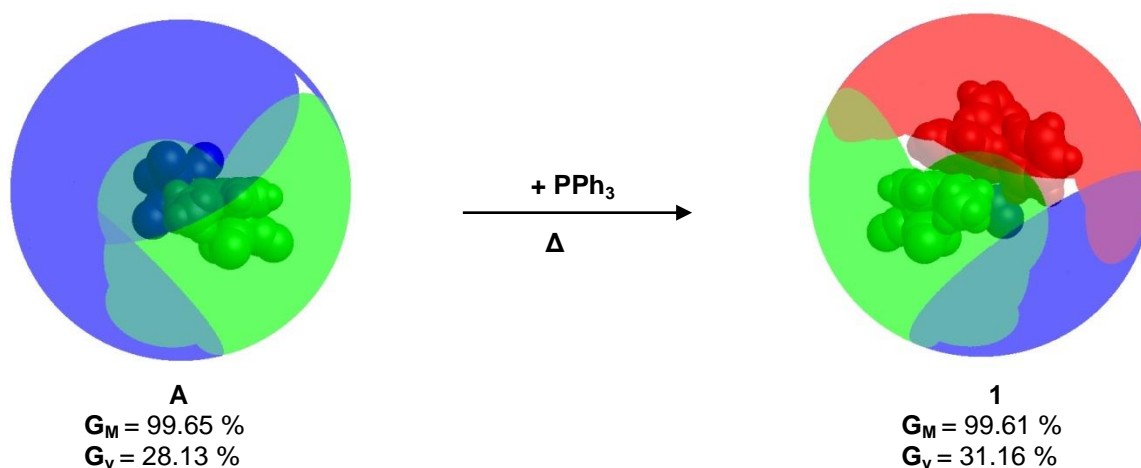
Figure 15: The G_M and G_Y of A before and after carbonyl substitution

Complex **1** displays the greatest values of G_M and G_Y. The phosphine ligand thus not only shields the metal moiety the most but also has a greater sterical impact on the other coordinating ligands. It may thus be suggested that through the modification of the Fischer carbene starting material complex to form a more bulky phosphine-substituted analogue, the resulting complex may display increased catalytic activity due to the ability of the phosphine to act as a better leaving group. This hypothesis is also supported by the decrease in the HOMO and LUMO energy gap when the phosphine-substituted carbene complexes are formed, as discussed later. Low bond orders and bond dissociation energies of the metal-phosphine bonds also support this finding, as discussed later.

3.4.3 NBO analysis

The solid state crystal structure of complex **D** has been reported and indicated greater stability when the two Cp moieties are orientated away from one another (TC). The preference of this orientation in the solid state has also been confirmed by gas state

calculations. It was thus interesting to note that the orientation of the *cis* conformer (CC) was preferred to the *trans* isomer in the solid state structure of the phospine-substituted carbene complex (**4**). Incidences of internal interactions were determined to contribute significantly to the preference of the *trans* conformation to the *cis* isomer for **D** and thus a parallel study was performed to determine if NBO analysis could potentially explain the change in isomeric preference of **4**. The overall NBO internal stabilization interactions of the *cis* isomer of **4** (Figure 16) was determined to be 7.3 kJ·mol^{-1} while 6.1 kJ·mol^{-1} was calculated for the *trans* isomer of **4**, explaining why the CC conformer was obtained.
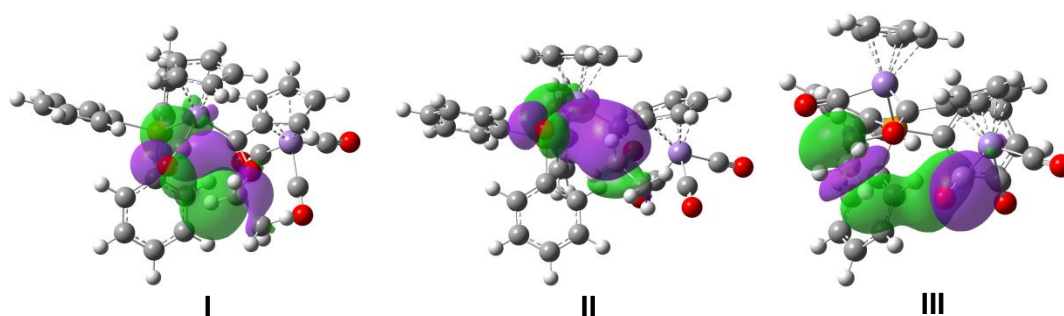
Figure 16: NBO stabilization witnessed in **4** (CC). I and II display the NBO interaction between the methylene proton of the ethoxy substituent and a carbonyl group on the carbene metal moiety, III displays the interaction of the methyl proton of the ethoxy substituent and a carbonyl ligand on the CpMn(CO)$_3$ moiety.

3.4.4 Bond order analysis

Fischer carbene complexes are well described in literature and typically defined by the double bond characteristics between the carbene carbon atom and the metallating metal centre [29]. Although literature provides precedence defining the carbene moiety as a σ-donating π-accepting ligand, studies conducted by our laboratories indicate that the π-donation from the alkoxy substituent to the carbene centre takes preference above the π-donation from the metal moiety [29]. This theoretical finding also correlates with literature reports by Fischer *et al.* [30]. Wiberg bond orders have found application in determining the bond indices in carbene complexes [31] and signify that the bonding interaction between the carbene carbon and the carbene metal displays almost exclusively σ-bond character, or that in the case where π-contribution is present, that this contribution was determined to be negligible. The application of these indices towards substituted Fischer carbene complexes have, however, been neglected to date. Substitution reactions of the carbonyl ligands of the metal moiety are possible for Fischer carbene complexes and the electronic characteristics
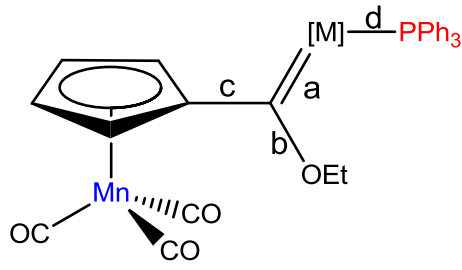
[29] J.S. Griffith, L.E. Orgel, Q. Rev. Chem. Soc. 11 (1957) 381.
[30] E.O. Fischer. Pure Appl. Chem. 30 (1972) 353.
[31] G. Occhipinti, H.R. Bjørsvik, K.W. Törnroos, A. Fürstner, V.R. Jensen Organometallics 26 (2007) 4383.

of these complexes are influenced greatly by the electron donation and withdrawal of the coordinating ligands. This study attempted to investigate the effects of phosphine substitution of carbonyl ligands towards the bond orders of the novel complexes. The Wiberg bond indices are presented in Table 3.

Table 3: Wiberg bond orders of **1-4**

Complex	Bond order			
	a	b	c	d
1	0.89	1.19	1.10	0.66
2	0.90	1.18	1.10	0.67
3	0.96	1.14	1.08	0.68
4	1.12	1.11	1.05	0.74

Wiberg bond indices indicate orders of between 0.89 and 1.12 for the $C_{carbene}$=M bond in **1-4**. Complex **4** displays a bond order of above 1, indicating the presence of possible π-back-bonding from the metal centre and thus exhibit some double bond characteristics. The BO of 1.12 is an increase of 0.13 from the reported literature value of 0.99 for the unsubstituted monocarbene starting material [10]. The bond order calculations of **4** show an equal donation situation between the metal-carbene and the ethoxy-carbene moieties compared to complexes **1-3**. Donation to the electrophilic carbene carbon occurs preferentially from the ethoxy substituent, leading to low donation from the carbene metal atom. The bond order of the metal-phosphine bond is independent of the identity of the carbene metal moiety and only displays a slight increase in the case where $CpMn(CO)_2$ is introduced as the carbene metal moiety. Complex **1** displays the lowest BO for the phosphine-metal bond and thus supports the findings of the solid angle analysis that this complex will have the most labile M-P bond. The phosphine ligand can thus act as a potential leaving group in a catalytic cycle.

3.4.5 Frontier orbital analysis

The theoretical energy levels and energy gaps for the frontier orbitals of the studied complexes are presented in Figure 17. The band gap between the two frontier orbitals is

indicative of the stability and reactivity of transition metal complexes [32]. In this study, band gaps of between 3.23 and 3.40 eV were determined for the complexes, with the greatest differences witnessed for **1**. Upon the substitution of a carbonyl ligand for the phosphine ligand, a decrease in the band gap was witnessed. The HOMO and LUMO energies also increased in energy value after substitution occurred.
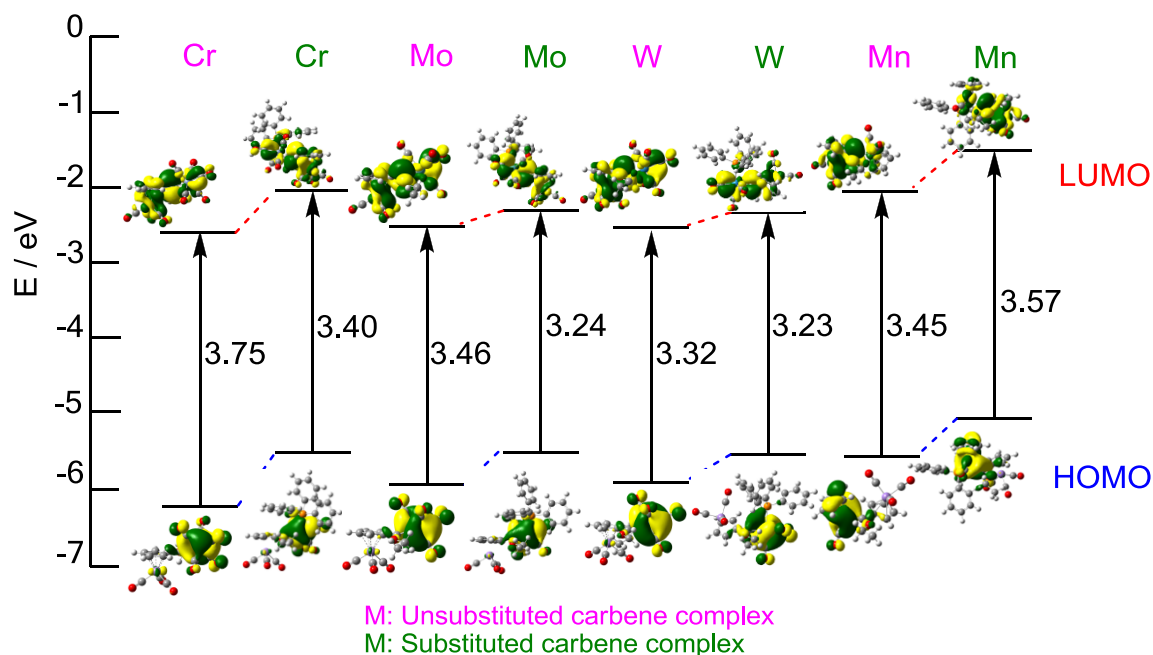
Figure 17: Frontier orbitals of the unsubstituted (pink) and phosphine-substituted (green) carbene complexes

Since the HOMO-LUMO energy cap diminishes in size upon coordination of the phosphine ligands, the resulting substituted complexes might display increases in reactivity and possible application in catalysis as suggested by the solid angle predictions [33] .

3.4.6 Bond Dissociation energy analysis

Bond dissociation energy (BDE) of a chemical bond is defined as the change in enthalpy at 298 K and 101.3 kPa for the gas-phase reaction as defined by A-B → A•(g) + B•(g) [34]. Although DFT approaches tend to systematically underestimate absolute bond dissociations, evaluations based on these models are still relevant in the assessment of molecules and ligand systems. Applicable bond dissociation energies for **1-4** are listed in Table 4. From the

[32] J.S. Griffith, L.E. Orgel. Q. Rev. Chem. Soc. 11(1957) 381.
[33] (a) A.E. Allen, D.W.C. MacMillan. Chem. Sci. 3 (2012) 633; (b) A. Arrieta, F.P. Cossío, I. Fernández, M. Gomez-Gallego, B. Lecea, M.J. Mancheno, M.A. Sierra, J. Am. Chem. Soc. 122 (2000) 11509.
[34] X. Qi, Y. Feng, L. Liu, Q. Guo, Chin. J. Chem. 23 (2005) 194.

data presented in Table 4, it can be deduced that the BDE of the M-PPh$_3$ bond increases in the order Cr < Mo < W. The trend can be explained by the increase of electron density found on heavier metal atoms, which becomes more readily available for back donation towards the phosphine ligand. A similar argument explains the linear increase in BDE for the M-C$_{carbene}$ bond for both the substituted and unsubstituted complexes. The BDE trend for the M-C$_{carbene}$ bond also increases in the order Cr < Mo < W.

Table 4: Bond dissociation energies of applicable bonds and carbene starting material (A-D)

Complex	BDE (kJ.mol^{-1})		
	Metal-C$_{carbene}$	M-PPh$_3$	Metal-C$_{carbene}$[a]
1	174.48	96.66	188.76
2	198.35	113.36	208.07
3	240.31	142.71	236.98
4	232.27	133.43	220.35

[a] Bond dissociation energies of the corresponding carbene starting material

The linear relationship trends in the BDE of the M-PPh$_3$ and M-Carbene bonds are displayed in Figure 18.
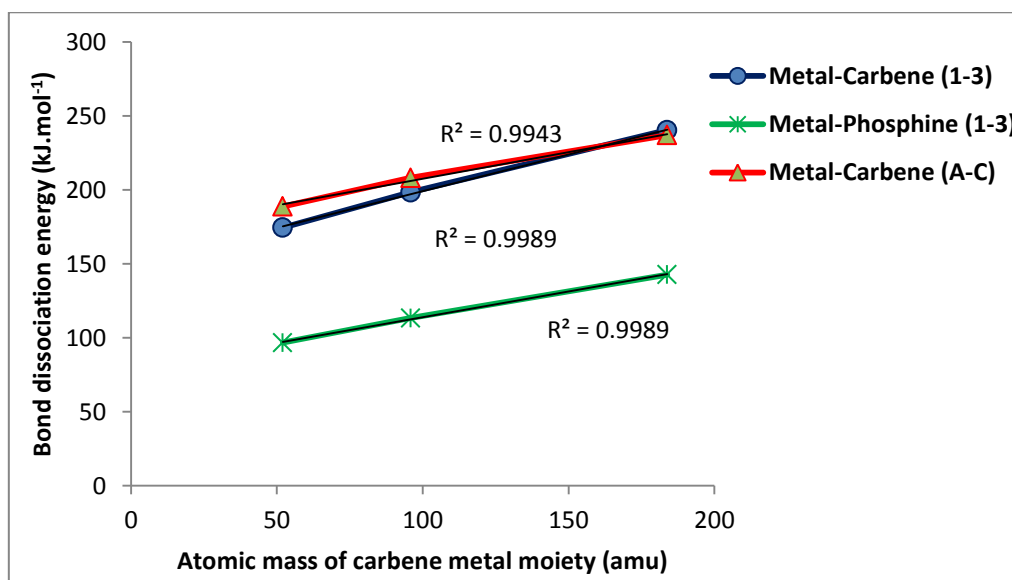
Figure 18: Linear relationships between the BDE and the molar mass of the carbene metal moiety for **1-3** and **A-C**

4   Conclusion

Bimetallic phosphine-substituted complexes **1-4** were synthesized in satisfactory yield. The molecular structures of the novel complexes were confirmed with NMR and IR spectroscopy, and single crystal X-ray diffraction studies of **1**, **3** and **4**. Applying DFT calculations, it was possible to explain the substitution pattern witnessed for the complexes as well as describe the sterical influences the triphenylphosphine ligand imposes on **1-4**. NBO stabilization interactions were visualized and illustrated the ability of the *cis* conformer of **4** to produce intramolecular stabilization between the methylene protons of the ethoxy substituent and the carbonyl ligands associated with the carbene metal moiety. These interactions were present in a lesser extent in the *trans* conformation for **4**. Wiberg bond indices indicated orders of between 0.89 and 1.12 for the C=M bond in **1-4**. Only **4** displays a bond order of above 1 and the possibility of π-back-bonding from the metal centre and thus exhibit some double bond characteristics. The frontier orbital analysis indicated that upon substitution of a carbonyl ligand for a phosphine ligand, a decrease in the HOMO-LUMO band gap was witnessed. The decrease in the band gap may indicate higher reactivity of the phosphine-substituted complexes. Finally, BDE energies showed a linear relationship between the associated energies and the molar mass of the carbene metal moiety. The BDE of the substituted carbene complexes were also on average higher than the unsubstituted monocarbene starting material.

Acknowledgements

Supporting Information

The electronic supporting information includes Table S1, lists of bond distances and angles for crystal structures reported and the optimized coordinates of the DFT calculations. CCDC 1488006-1488008 contains the supplementary crystallographic data for this paper. This data can be obtained free of charge *via* http://www.ccdc.cam.ac.uk/conts/retrieving.html (or from the Cambridge Crystallographic Data Centre, 12, Union Road, Cambridge CB2 1EZ, UK; fax: +44 1223 336033).

82

CHAPTER 5

Synthesis and Structural Investigation of mono- and dimetallic N-heterocyclic Carbene Complexes of Group VII Transition metals

Chapter 5 was adapted from an article published in Journal of Organometallic Chemistry. The format reflects the requirements of the journal.

Authors: Roan Fraser, Petrus H. van Rooyen, Cornelia G.C.E. van Sittert and Marilé Landman
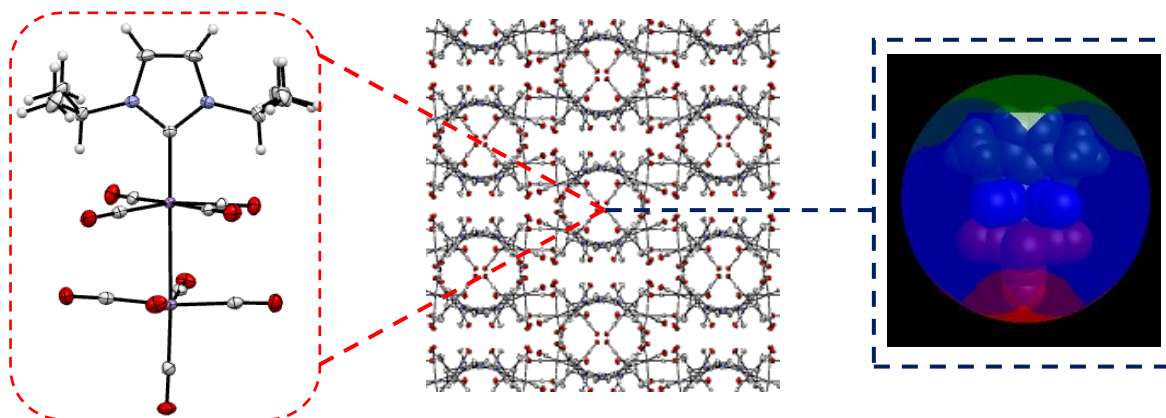
Graphical Abstract:

Contributions:

Roan Fraser: Author, synthesis, DFT studies

Petrus H. van Rooyen: Co-author, crystallography

Cornelia G.C.E. van Sittert: Co-author, DFT studies ($Mn_2(CO)_{10}$ and $Re_2(CO)_{10}$)

Marilé Landman: Corresponding author, supervisor

5
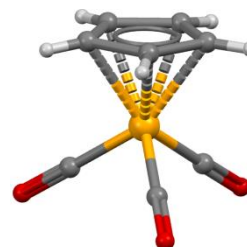
Synthesis and Structural Investigation of mono- and dimetallic N-heterocyclic Carbene Complexes of Group VII Transition metals

Roan Fraser[a], Marilé Landman[a], Cornelia G.C.E. van Sittert[b] and Petrus H. van Rooyen[a]*

[a] Department of Chemistry, University of Pretoria, Private Bag X20, Hatfield, 0028, South Africa. Tel: +27-12-4202527, Fax: +27-12-4204687

[b] Catalysis and Synthesis research group: Chemical Resource Beneficiation, North-West University, Potchefstroom Campus, South Africa

Contact author details:

Name: Marilé Landman Tel: +27-12-4202527, Fax: +27-12-4204687, email: marile.landman@up.ac.za

Keywords

N-heterocyclic carbene; Manganese; Rhenium; Solid angle; DFT; NBO analysis

Graphical abstract
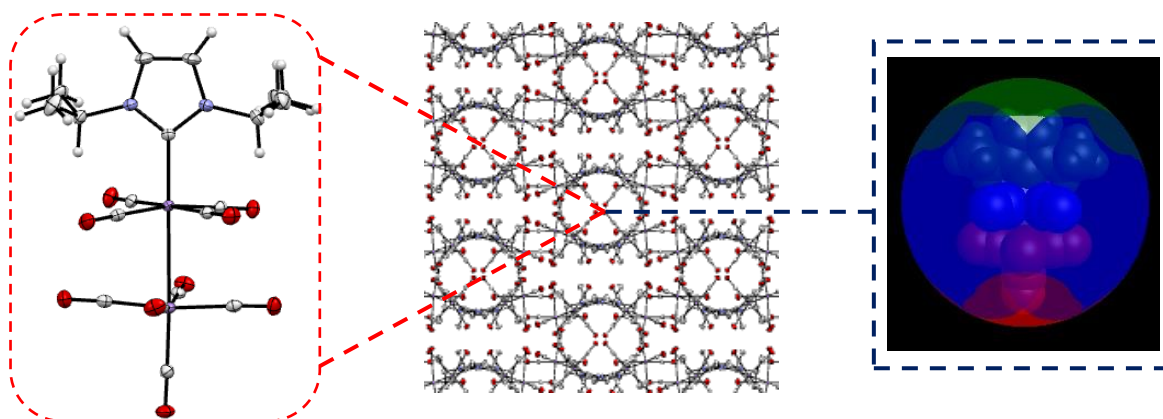
TOC abstract

Synthesis, single crystal X-ray structures and DFT study of N-heterocylic carbene complexes of dimanganese- and rhenium carbonyls.

Research highlights

- DFT calculations on mono- and dimetallic NHC complexes
- Crystal structure of the first NHC complex of dimanganese nonacarbonyl
- Calculated Wiberg bond indices, solid angle and bond dissociation energies of group VII transition metal NHC complexes

Abstract

N-heterocyclic carbene complexes of group VII transition metals (Mn and Re) were synthesised and the electronic and structural aspects theoretically investigated. The synthesis yielded carbene complexes of type $[M_x(CO)_yL(NHC)]$ where M represents Mn or Re, x = 1 , y = 4 and L = Cl, Br, I or M = Mn, x = 2, y = 9, L = CO. The synthesis of the mono- and dimetallic NHC complexes involved the substitution of labile carbonyl ligands for symmetrical and asymmetrical 1,3-disubstituted NHC ligands. Both aliphatic and aromatic N-substituent groups were incorporated into the heteroatomic, aromatic backbone of the imidazolylidene ligands. Coordination of the carbene ligand to the metal centre generated different results when comparing manganese NHC complexes to the rhenium NHC analogues. Analysis of the results indicated that only monometallic, halogenated NHC complex of Re could be synthesised and isolated, whereas the coordination of the imidazolium salts to $Mn_2(CO)_{10}$ produced axially substituted dimetallic carbene complexes. Spectroscopic [IR, NMR (^{1}H and ^{13}C) and structural (X-ray)] properties are reported and compared to those of other N-heterocyclic carbene derivatives. The structural features, coordination patterns and reactivity centres were examined to provide insight into the electronic and bonding environments of the metal-metal bond and the metal-NHC moiety.

 Introduction

Arduengo-type [1], nucleophilic N-heterocyclic carbene complexes (NHCs) have attracted extensive attention since their first discovery and isolation in the 1990s [2,3]. The vast application of NHC complexes in industry is mainly due to the positive attributes that these rigid ligands hold for homogeneous catalysis [2]. More recently NHC-type complexes have

[1] A.J. Arduengo, R.L. Harlow, M. Kline, J. Am. Chem. Soc.113 (1991) 361.
[2] (a) T. Weskamp, V.P.W. Böhm, W.A. Herrmann, J. Organomet. Chem. 600 (2000) 12; (b) L. Jafapour, S.P. Nolan, Adv. Organomet. Chem. 46 (2001) 181.
[3] (a) W.A. Hermann, T. Weskamp, V.P.W. Böhm, Adv. Organomet. Chem. 48 (2002) 1; (b) D. Bourissou, O. Guerret, F.P. Gabbaï, G. Bertrand, Chem. Rev. 100 (2000) 39.

also found application in chemotherapy [4], dye-sensitized solar cells [5], storage modes of H$_2$ and other gas molecules [6] and are particularly useful as catalysts for organic transformations and polymerization reactions [7]. The superior σ-donating interactions between the carbene ligand and the metal moiety together with the ease of incorporating different N-substituents of varying steric bulk in the imidazolium ring, are typically seen as advantageous as compared to the typical phosphine analogues [2]. While general synthetic approaches have been developed for the production of monometal carbonyl NHC complexes, coordination to dimetal centres has remained relatively unexplored [8-10]. Studies by Gibson and co-workers reported NHC complexes of dicobalt octacarbonyl through *in situ* deprotonation of imidazolium salts (Figure 1) [11]. Dimetallic NHC complexes were also more recently reported by Sigman [12], Mankad [13], Chang and co-workers [14] either via deprotonation pathways or with the application of a transfer reagent intermediate [15] (Figure 2).
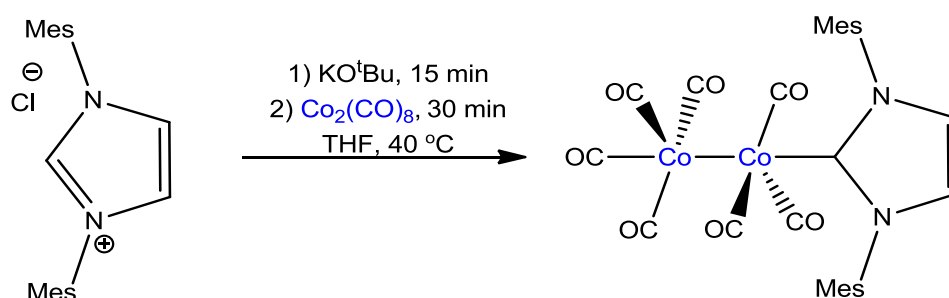
Figure 1: Synthesis of a dicobalt NHC complex as reported by Gibson *et al.* [11]

NHC complexes of group VII transition metals are well known in literature [16]. The first isolated NHC complex of manganese was prepared by Lappert through the thermal substitution of a carbonyl ligand of cymantrene in the presence of the free NHC (Figure 2)

[4] (a) W. Liu, R. Gust, Chem. Soc. Rev. 42 (2013) 755; (b) M.L. Teyssot, A.S. Jarrousse, M. Manin, A. Chevry, S. Roche, F. Norre, C. Beaudoin, L. Morel, D. Boyer, R. Mahiou, A. Gautier, Dalton Trans. (2009) 6894.
[5] (a) H.J. Park, K.H. Kim, S.Y. Choi, H.M. Kim, W.I. Lee, Y.K. Kang, Y.K.Chung, Inorg. Chem. 49 (2010) 7340; (b) W.C. Chang, H.S Chen, T.Y. Li, N.M. Hsu, Y.S. Tingare, C.Y. Li, Y.C. Liu, C. Su, W.R. Li, Angew. Chem. Int. Ed. 49 (2010) 8161.
[6] (a) O. Songis, C.S.J. Cazin, Synlett. 24 (2013) 1844; (b) O.R. Luca, D.L Huang, M.K. Takase, R.H. Crabtree, New J. Chem. 37 (2013) 3402.
[7] (a) Y. Kayaki, M. Yamamoto, T. Ikariya, Angew. Chem., Int. Ed. 48 (2009) 4194; (b) H. Zhou, W.Z. Zhang, C.H. Liu, J.P. Qu, X.B. Lu, J. Org. Chem. 73 (2008) 8039; (c) N.P. Mankad, T.G. Gray, D.S. Laitar, J.P. Sadighi, Organometallics 23 (2004) 1191.
[8] C. Liu, D. Chen, G. Lee, S. Peng, S. Liu, Organometallics 15 (1995) 1055-1061.
[9] N. Meier, F.E. Hahn, T. Pape, C. Siering, S.R. Waldvogel, Eur. J. Inorg. Chem. (2007) 1210.
[10] F. E. Hahn, M.C. Jahnke, Angew. Chem. Int. Ed. Engl., 47 (2008) 3122.
[11] S. E. Gibson, G. Johnstone, J.A. Loch, J.W. Steed, A. Stevenazzi, Organometallics 22 (2003) 5374.
[12] R.D. Benjamin, M.S. Sigman, A.M. Arif, Inorg. Chem. 44 (2005) 3774.
[13] U. Jayarathne, S.R. Parmelee, N.P. Mankad, Inorg. Chem. 53 (2014) 7730.
[14] J. Kwak, M. Kim, S. Chang, J. Am. Chem. Soc. 133 (2011) 3780.
[15] H.M.J. Wang, I.J.B Lin, Organometallics 17 (1998) 972.
[16] S. J. Hock, L. Schaper, W. A. Herrmann, F. E. Kühn. Chem. Soc. Rev. 42 (2013) 5073.

[17]. Although, examples of group VII metal multicarbene complexes are scarce in comparison to monocarbene analogues, a few examples of bis- and triscarbene complexes are known. Rhenium NHC analogues have been recognized for their luminescent properties and found particular application as biological markers and organic light-emitting diodes, while technetium complexes are interesting candidates for radiochemical applications [16].
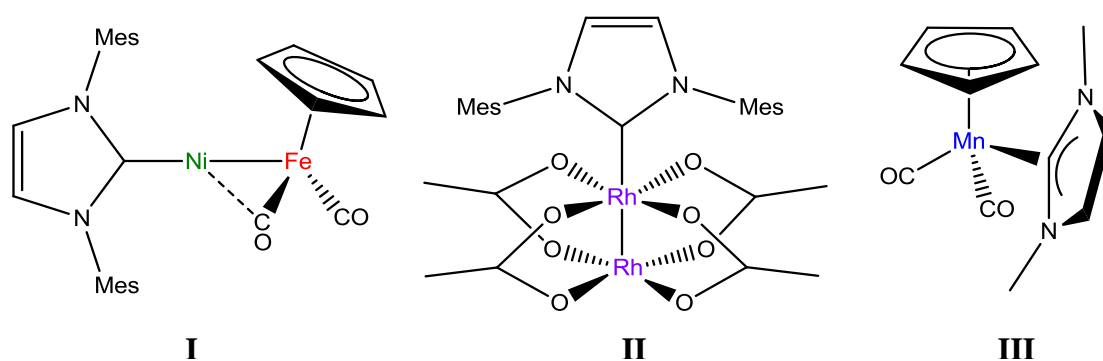
Figure 2: NHC complexes as reported by Mankad (I) [13], Chang (II) [14] and Lappert (III) [17]

Mono- and dimetallic NHC complexes of dirhenium carbonyls have been synthesised and indicated the substitution of an equatorial carbonyl ligand for the NHC moiety [18,19]. Literature attributes the isomeric differences of group VII carbene complexes, at the point of substitution, to both steric and electronic aspects [20]. Nucleophilic attack on group VII transition metal carbonyl complexes is expected to be regioselective and occurs on the more electron-deficient, equatorial carbonyl positions. With sterically bulky ligands, and in manganese systems, with characteristically shorter metal-metal bond lengths, axial nucleophilic attack becomes increasingly favourable. The substitution of the carbonyl ligands follow a similar reactivity pattern and the equatorial positions are generally favoured for less builky ligands while the axial position becomes favourable with steric ligands [21,22]. Dimetallic rhenium complexes were only formed when less bulky carbene substituents were incorporated into the NHC ligand or when only a single nitrogen atom was functionalized. Substitution of carbonyl groups for bulky NHC ligands produced cleavage at the metal-metal bond and formed monometallic rhenium complexes. Although theoretical studies have been attempted on group VII transition metal carbene complexes, no study has specifically

[17] M.F.Lappert, J. Organomet. Chem. 358 (1988) 185.
[18] C. Chen, Y. Liu, S. Peng, J. Chen. S. Liu, Dalton Trans. 41 (2012) 2747.
[19] C. Hille, F.E. Kühn, Dalton Trans. 45 (2016) 15.
[20] E. Luncenti, G. D'Alfonso, C. Dragonetti, D. Roberto, A. Sironi, R. Ugo, Organometallics 28 (2009) 3040.
[21] P.J. Fraser, W.R. Roper, F.G.A. Stone, J. Chem. Soc. Dalton Trans. (1974) 760.
[22] S. Lotz, M. Landman, D.I. Bezuidenhout, A.J. Olivier, D.C. Liles, P.H. van Rooyen, J. Organomet. Chem. 690 (2005) 5929.

focused on NHC complexes of dimetallic group VII transition metals [23]. This study aims to add valuable perspectives into the bonding and electronic characteristics of dimetallic group VII transition metal carbene complexes. Utilizing a similar methodology as Gibson *et al.* [11], this study endeavoured to produce novel dimetallic carbene complexes of group VII transition metals in conjunction with a theoretical study to determine electronic and structural aspects of the complexes. Generating free carbenes *in situ* from imidazolium salts (**L1-L4**, Figure 3), followed by the addition of either $Mn_2(CO)_{10}$ or $Re_2(CO)_{10}$ to the reaction mixture successfully produced multi-metal NHC complexes of Mn (**1**, **2**, **3** and **4**) and halogenated monometallic complexes of Re (**8**, **9** and **10**). The formation of the NHC-metal bond often increases the stability of the metal complex by donating additional electron density to the metal centre [10-17].

L1: R = R^1 = Mes
L2: R = R^1 = ^{i}Pr
L3: R = Bn, R^1 = Cy
L4: R = R^1 = Me
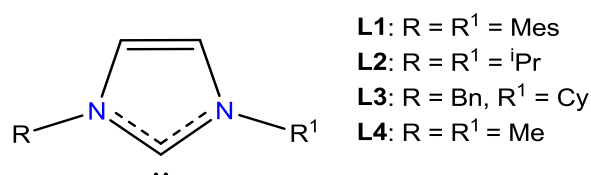
Figure 3: Deprotonated NHC ligands, **L1-4**

2 Experimental

2.1 General considerations

All reactions, unless otherwise noted, were performed under inert nitrogen or argon atmospheres using standard Schlenk techniques [24]. All solvents were freshly distilled, dried and collected under inert conditions. Column chromatography was carried out under inert nitrogen and argon atmospheres using silica gel (particle size 0.063-0.200 mm) as the stationary phase. Percentage yields were calculated relative to the limiting reactant. Crystallization was done using hexane:DCM or hexane:ether diffusion methods. The reagents $Mn_2(CO)_{10}$, $Re_2(CO)_{10}$, n-butyl lithium (1.6 M solution in hexane) and other commercial reagents were used as purchased. NMR spectra were recorded on a Bruker ARX-300 in $CDCl_3$ using the deuterated solvent peak as internal reference. ^{1}H and ^{13}C NMR spectra were measured at 300.1 and 75.5 MHz, respectively. IR spectra were recorded on a Perkin Elmer Spectrum RXI FT-IR spectrophotometer in hexane and only the vibration bands in the carbonyl-stretching region (ca. 1500-2200 cm^{-1}) are reported. The imidazolium halide ligands (**L1**-**L4**) were synthesied and purified according to literature procedures [25].

[23] R. Fraser, P. H. van Rooyen, M. Landman. J. Mol. Struct. 1105 (2016) 178.
[24] D.F. Schriver, M.A. Drezdzon. *The manipulation of Air-Sensitive Compounds*, 2nd ed., Wiley, New York, USA, (1986).
[25] F. P. Malan, E. Singleton, P. H. van Rooyen, M. Landman. J. Organomet. Chem. 813 (2016) 7.

2.2 Synthesis of metal NHC complexes (1-10)

2.2.1 Preparation of 1 (Mn$_2$(CO)$_9$-L1) and 2 (Mn(CO)$_4$Br-L1)

0.340 g (1.00 mmol) of 1,3-bis(2,4,6-trimethylphenyl)imidazolium chloride was deprotonated by the addition of n-BuLi (1.00 mmol) in THF at -40°C. The reaction mixture was allowed to stir for 30 min after which 0.390 g dimanganese decacarbonyl (1.00 mmol) was added. The reaction mixture turned a deep orange colour after the introduction of the metal complex and the reaction mixture was allowed to slowly warm up to room temperature. The solvent was removed in vacuo and purified via silica gel chromatography by eluting first with hexane and secondly with a hexane-DCM 1:1 mixture. The product was recovered as a deep orange solid. Yield: 30% (0.200 g). ^{1}H NMR (CDCl$_3$, ppm): δ 7.59 (s br, 2H, **H**C=C**H**), 6.72 (s br, 4H, CH$_m$), 2.13 (s br, 12H, Ar**CH$_3$**), 2.07 (s br, 6H, Ar**CH$_3$**). ^{13}C{^{1}H} NMR (δ$_{ppm}$): δ 192.2 NCN, 212.1, 208.9, 202.4 Mn(CO), 155.3 Ph$_{ipso}$, 130.3 Ph$_{meta}$, 128.8 Ph$_{ortho}$, 123.1 H**C=C**H; 122.0 Ph$_{para}$, 15.2 Ar**CH$_3$**,14.7 Ar**CH$_3$**. IR (cm^{-1}): 2077 (s), 2028 (s), 2000 (s), 1961 (s), 1938 (s). HRESI$^+$-MS, m/z: 667.0356 (calcd. 667.0321).

Complex 2 was isolated as a second yellow solid product. Yield: 21% (0.116 g): ^{1}H NMR (CDCl$_3$, ppm): δ 7.18 (s, 2H, C**H=CH**), 7.12 (br, 4H,CH$_m$), 2.38 (br, 12H, Ar**CH$_3$**), 2.14 (br, 6H, Ar**CH$_3$**).^{13}C{^{1}H} NMR (δ$_{ppm}$): δ 195.1 NCN, 191.9 Mn(CO), 140.7 Ph$_{ipso}$, 137.6 Ph$_{meta}$, 136.8 Ph$_{ortho}$, 129.3 Ph$_{para}$, 125.3 N**C=C**N, Ar**CH$_3$** 21.9, Ar**CH$_3$** 18.0. IR (cm^{-1}): 2075 (m), 1993 (s), 1916 (s). HRESI$^+$-MS, m/z: 551.0343 (calcd. 551.0379).

2.2.2 Preparation of 3 (Mn$_2$(CO)$_9$-L2) and 4 (Mn(CO)$_4$Cl-L2)

A similar synthetic methodology was followed as for **1**. 0.189 g (1.00 mmol) of 1,3-bis(isopropyl)imidazolium chloride was deprotonated by addition of n-BuLi (1.00 mmol) in THF at -40°C. The product was recovered as a deep orange solid. Yield: 33% (0.170 g). ^{1}H NMR (CDCl$_3$, ppm): δ 7.13 (s, 2H, C**H=CH**); 4.27 (m, 2H, **CH**(CH$_3$)$_2$), 1.47 (s br,12H,CH(**CH$_3$**)$_2$).^{13}C{^{1}H} NMR (δ$_{ppm}$): δ 209.7, 206.9, 202.2 Mn(CO), 189.1 N**C**N, 119.0 N**C=C**N, 51.9 N-**C**H, 13.3 CH(**CH$_3$**)$_2$. IR (cm^{-1}): 2085 (s), 1995 (s), 1979 (s), 1965 (s), 1950(s). HRESI$^+$-MS, m/z: 514.9647 (calcd. 514.9695).

Complex 4 was isolated as a second yellow product. Yield: 26% (0.92 g). ^{1}H NMR (CDCl$_3$, ppm): δ 7.31 **H**C=C**H** (br, s); H2 4.67 (s br, 2H, **CH**(CH$_3$)$_2$); 1.54 (s br,12H,CH(**CH$_3$**)$_2$).^{13}C{^{1}H} NMR (δ$_{ppm}$): δ 196.4 N**C**N, 187.7 Mn(CO), 120.6 H**C=C**H, 53.2 N-**C**H; 22.1 CH(**CH$_3$**)$_2$. IR (cm^{-1}): 2077(m), 1979 (s), 1910 (s). HRESI$^+$-MS, m/z: 355.0112 (calcd. 355.0179).

2.2.3 Preparation of 5 (Mn$_2$(CO)$_9$-L3)

A similar synthetic methodology was followed as for **1**. 0.277 g (1.00 mmol) of 1-benzyl-3-cyclohexylimidazolium chloride was deprotonated by addition of n-BuLi (1.00 mmol) in THF

at -40°C. The product was recovered as a yellow solid and only the dimetallic NHC complex was isolated. Yield: 16% (0.096g). ^{1}H NMR (CDCl$_3$, ppm): δ 7.44-7.55 (m, 5H, PhH), C**H=CH** 7.24 (br, s) 5.09 (s, 2H, PhC**H$_2$**), 3.76 (m, 1H, Cy-C**H**), 2.47 (m, 2H, Cy-C**H$_2$**), 1.94 (m, 2H, Cy-C**H$_2$**), 1.47 (m, 2H, Cy-C**H$_2$**), 1.03 (m, 2H, Cy-C**H$_2$**). ^{13}C{^{1}H} NMR (δ$_{ppm}$): δ 212.7, 209.7, 206.9 Mn(CO), 191.5 N**C**N, 139.6 Ph$_{ipso}$, 130.6 Ph$_{meta}$, 128.8 Ph$_{ortho}$, 128.3 Ph$_{para}$, 124.7 N**C=C**N, 67.4 Cy, 57.5 N-**CH$_2$**, 33.7 Cy, 25.0 Cy, 24.8 Cy. IR (cm^{-1}): 2086 (w), 2025 (s), 1987 (m), 1913 (s). HRESI$^+$-MS, m/z: 603.0018 (calcd. 603.0008).

2.2.4 Preparation of 6 (Mn$_2$(CO)$_9$-L4) and 7 (Mn(CO)$_4$I-L4)

A similar synthetic methodology was followed as for **1**. 0.224 g (1.00 mmol) of 1,3-bis(methyl)imidazolium iodide was deprotonated by addition of n-BuLi (1.00 mmol) in THF at -40°C. The product was recovered as a yellow solid. Yield: 15% (0.069 g). ^{1}H NMR (CDCl$_3$, ppm): δ 7.23 (s, 2H, C**H=CH**), 3.81 (s, 6H, N-C**H$_3$**). ^{13}C{^{1}H} NMR (δ$_{ppm}$): δ 221.1, 212.7, 207.7 Mn(CO), 194.3 N**C**N, 128.1 N**C=C**N, 39.8 N-**C**H$_3$. IR (cm^{-1}): 2089 (m), 2075 (s), 2035 (s), 2005 (m), 1991 (s), 1978 (s), 1969 (m), 1943 (s). HRESI$^+$-MS, m/z: 458.9000 (calcd. 458.9069).

Complex 7 was isolated as a second yellow product. Yield: 15% (0.059 g). ^{1}H NMR (CDCl$_3$, ppm): δ 7.17 (s, 2H, **H**C=C**H**), 3.80 (s, 6H, NCH$_3$). ^{13}C{^{1}H} NMR (δ$_{ppm}$): δ 195.6, 194.6 Mn(CO), 194.2 N**C**N, 192.7 Mn(CO), 126.7 H**C=C**H, 40.3 N-**CH$_3$**. IR (cm^{-1}): 2077(m), 1979 (s), 1910 (s). HRESI$^+$-MS, m/z: 390.8964 (calcd. 390.8987).

2.2.5 Preparation of 8 (Re(CO)$_4$Cl-L1)

A similar synthetic methodology was followed as in **1**. 0.340 g (1.00 mmol) of 1,3-bis(2,4,6-trimethylphenyl)imidazolium chloride was deprotonated by addition of n-BuLi (1.00 mmol) in THF at -40°C. The product was recovered as a beige-white solid and only the cleaved monometallic NHC complex was isolated. Yield: 27% (0.172 g) ^{1}H NMR (CDCl$_3$, ppm): δ 7.12 (s, 4H, C**H$_m$**), 7.05 (s br, 2H, **H**C=C**H**), 2.34 (s, 12H, ArC**H$_3$**), 2.16 (s, 6H, ArC**H$_3$**). ^{13}C{^{1}H} NMR (δ$_{ppm}$): δ 191.3 N**C**N, 185.7, 183.5, 178.9 Re(**C**O), 141.1 Ph$_{ipso}$, 137.6 Ph$_{meta}$, 136.8 Ph$_{ortho}$, 129.9 Ph$_{para}$, 123.6 H**C=C**H, 21.4 ArC**H$_3$**; 18.2 ArC**H$_3$**. IR (cm^{-1}): 2094 (m), 1982 (s), 1919 (s). HRESI$^+$-MS, m/z: 555.0137 (calcd. 555.0120).

2.2.6 Preparation of 9 (Re(CO)$_4$Cl-L2)

A similar synthetic methodology was followed as in **1**. 0.189 g (1.00 mmol) of 1,3-bis(isopropyl)imidazolium chloride was deprotonated by addition of n-BuLi (1.00 mmol) in THF at -40°C. The product was recovered as an off-white solid and only the cleaved monometallic NHC complex was isolated. Yield: 22% (0.107 g). ^{1}H NMR (CDCl$_3$, ppm): δ

7.09 (s br, 2H, **H**C=C**H**), 5.32 (m, 2H, **CH**(CH$_3$)$_2$), CH$_3$ 1.29 (m, 12H, CH(**CH$_3$**)$_2$).^{13}C{^{1}H} NMR (δ_{ppm}): δ 192.8 N**C**N, 186.5, 185.2, 179.8 Re(**C**O), H**C**=**C**H 125.0, N-**C**H 48.7, 23.2 CH(**CH$_3$**)$_2$. IR (cm^{-1}): 2100 (m), 1982 (s), 1917 (s). HRESI$^+$-MS, m/z: 487.0414 (calcd. 487.0434).

2.2.7 Preparation of 10 (Re(CO)$_4$Cl-L3)

A similar synthetic methodology was followed as in **1**. 0.277 g (1.00 mmol) of 1-benzyl-3-cyclohexylimidazolium chloride was deprotonated by addition of n-BuLi (1.00 mmol) in THF at -40°C.The product was recovered as a white solid and only the cleaved monometallic NHC complex was isolated. Yield: 18% (0.103 mg). ^{1}H NMR (CDCl$_3$, ppm): δ 7.36-7.53 (m, 5H, PhH), 7.09 (s br, 2H, **H**C=C**H**), 5.63 (s, 2H, PhC**H$_2$**), 4.4 (m, 1H, Cy-**CH**), 2.3 (m, 2H, Cy-**CH$_2$**), 1.8 (m, 2H, Cy-**CH$_2$**), 1.50 (m, 2H, Cy-**CH$_2$**), 1.20 (m, 2H, Cy-**CH$_2$**). ^{13}C{^{1}H} NMR (δ_{ppm}): δ 194.2 N**C**N, 184.9, 183.6, 182.2 Re(CO), 137.8 Ph$_{ipso}$, 130.5 Ph$_{meta}$, 128.9 Ph$_{ortho}$, 128.5 Ph$_{para}$, 125.0 H**C**=**C**H, 64.8 Cy, 48.7 N-**CH$_2$**, 31.7 Cy, 22.7 Cy, 22.6 Cy. IR (cm^{-1}): 2096 (m), 1976 (s), 1920 (s). HRESI$^+$-MS, m/z: 575.0766 (calcd. 575.07474).

2.3 X-ray crystallography

Data for complexes **1**, **3**, **7** and **8** were collected at 150 K on a Bruker D8 Venture kappa geometry diffractometer, with duo Iμs sources, a Photon 100 CMOS detector and APEX II control software using Quazar multi-layer optics, monochromated Mo-Kα radiation and by means of a combination of ϕ and ω scans. Data reduction was performed using SAINT+ and the intensities were corrected for absorption using SADABS [26]. The structures were solved by intrinsic phasing using SHELXTS and refined by full-matrix least squares using SHELXTL and SHELXL-2013 [27]. In the structure refinement, all hydrogen atoms were added in calculated positions and treated as riding on the atom to which they are attached. All nonhydrogen atoms were refined with anisotropic displacement parameters, all isotropic displacement parameters for hydrogen atoms were calculated as X × Ueq of the atom to which they are attached, X = 1.5 for the methyl hydrogens and 1.2 for all other hydrogens. Crystallographic data and refinement parameters are given in Table 1. Ortep drawings [28] of the four structures are included in Figure 5, Figure 6, Figure 10 and Figure 11. The crystal structures (cif) have been deposited at the Cambridge Crystallographic Data Centre and allocated the deposition numbers: CCDC 1517170-1517173. Data collection, structure solution and refinement details are available in each cif.

[26] APEX2 (including SAINT and SADABS); Bruker AXS Inc., Madison, WI (2012).
[27] G.M. Sheldrick. Acta Crystallogr., A64, 112 (2008).
[28] L.J.J. Farrugia. Appl. Crystallogr. 30 (1997) 565.

2.4 Theoretical study

The calculations reported in this paper were obtained using the Gaussian 09 [29] suite of programs. Calculations were carried out in the singlet spin state using the hybrid functional B3LYP [30,31]. Geometries of the neutral complexes were optimized in gas phase with the triple-ζ basis set 6-311G* on all atoms except for the metal atoms. Stuttgart/Dresden (SDD) pseudopotential was used to describe the metal electronic core, while the valence electrons were described def2-TZVPP [32]. No symmetry constraints were applied and only the default convergence criteria were used during the geometric optimizations. Vibrational frequencies [33] were calculated at the optimized geometries and no imaginary frequencies were observed, to confirm true minima. Donor-acceptor interactions have been computed using the natural bond orbital (NBO) method [34].

3 Results and Discussion

In order to study the electronic, reactivity and structural aspects of group VII transition metal carbene complexes, a variety of mono and dimetallic NHC complexes were synthesised and fully characterized. The characterization included theoretical studies specifically focussing on the application of theoretical insight into the bonding patterns and electronic environments of the metal complex. The theoretical and experimental results are comparable. Both spectroscopy and microanalysis are in concord with the obtained solid state structures in this study.

3.1 Synthesis of group VII metal NHC complexes

Direct carbonyl substitution can be employed to successfully produce the dimetallic NHC complexes. The above mentioned substitution methodology has previously been reported by Chen *et al.* [8] in attempts to produced multi-metal complexes of Re(0). Treatment of $M_2(CO)_{10}$ systems with deprotonated imidazolium salts readily yielded the corresponding

[29] M.J. Frisch, G.W. Trucks, H.B. Schlegel, G.E. Scuseria, M.A. Robb, J.R. Cheeseman, G. Scalmani, V. Barone, B. Mennucci, G.A. Petersson, H. Nakatsuji, M. Caricato, X. Li, H.P. Hratchian, A.F. Izmaylov, J. Bloino, G. Zheng, J.L. Sonnenberg, M. Hada, M. Ehara, K. Toyota, R. Fukuda, J. Hasegawa, M. Ishida, T. Nakajima, Y. Honda, O. Kitao, H. Nakai, T. Vreven, J.A. Montgomery (Jr), J.E. Peralta, F. Ogliaro, M. Bearpark, J.J. Heyd, E. Brothers, K.N. Kudin, V.N. Staroverov, T. Keith, R. Kobayashi, J. Normand, K. Raghavachari, A. Rendell, J.C. Burant, S.S. Iyengar, J. Tomasi, M. Cossi, N. Rega, J.M. Millam, M. Klene, J.E. Knox, J.B. Cross, V. Bakken, C. Adamo, J. Jaramillo, R. Gomperts, R.E. Stratmann, O. Yazyev, A.J. Austin, R. Cammi, C. Pomelli, J.W. Ochterski, R.L. Martin, K. Morokuma, V.G. Zakrzewski, G.A. Voth, P. Salvador, J.J. Dannenberg, S. Dapprich, A.D. Daniels, O. Farkas, J.B. Foresman, J.V. Ortiz, J. Cioslowski, D.J. Fox, Gaussian 09, Revision D.01, Gaussian Inc., Wallingford CT, 2010.
[30] A.D. Becke, J. Chem. Phys. 98 (1993) 5648.
[31] C. Lee, W. Yang, R.G. Parr, Phys. Rev. B37 (1988) 785.
[32] F. Weigend, R. Ahlrichs, Phys. Chem. Chem. Phys. 7 (2005) 3297.
[33] J.W. McIver, A.K. Komornicki, J. Am. Chem. Soc. 94 (1972) 2625.
[34](a) J.P. Foster, F. Weinhold, J. Am. Chem. Soc. 102 (1980) 7211; (b) A.E. Reed, F. Weinhold, J. Chem. Phys. 83 (1985) 1736; (c) A.E. Reed, R.B. Weinstock, F. Weinhold, J. Chem. Phys. 83 (1985) 735; (d) A.E. Reed, L.A. Curtiss, F. Weinhold, Chem. Rev. 88 (1988) 899.

metal carbonyl NHC complex in appreciative yields. In this study, however, it was found that reacting dirhenium decarbonyl complexes with the 1,3-disubstituted imidazolylidene salts, afforded only a beige or white monometallic halogenated NHC complexes. The reaction initiate with the cleavage of the metal-metal bond and the subsequent carbonyl substitution, in the *syn* position, to produce the monometallic rhenium carbene complex. In contrast reacting $Mn_2(CO)_{10}$, however, the reaction successfully produced both dimetallic- and the corresponding monometallic carbene complexes as a product mixture (Scheme 1). The complexes were synthesised in yield between 16-33%, mainly due to the production of multiple metallic complexes.
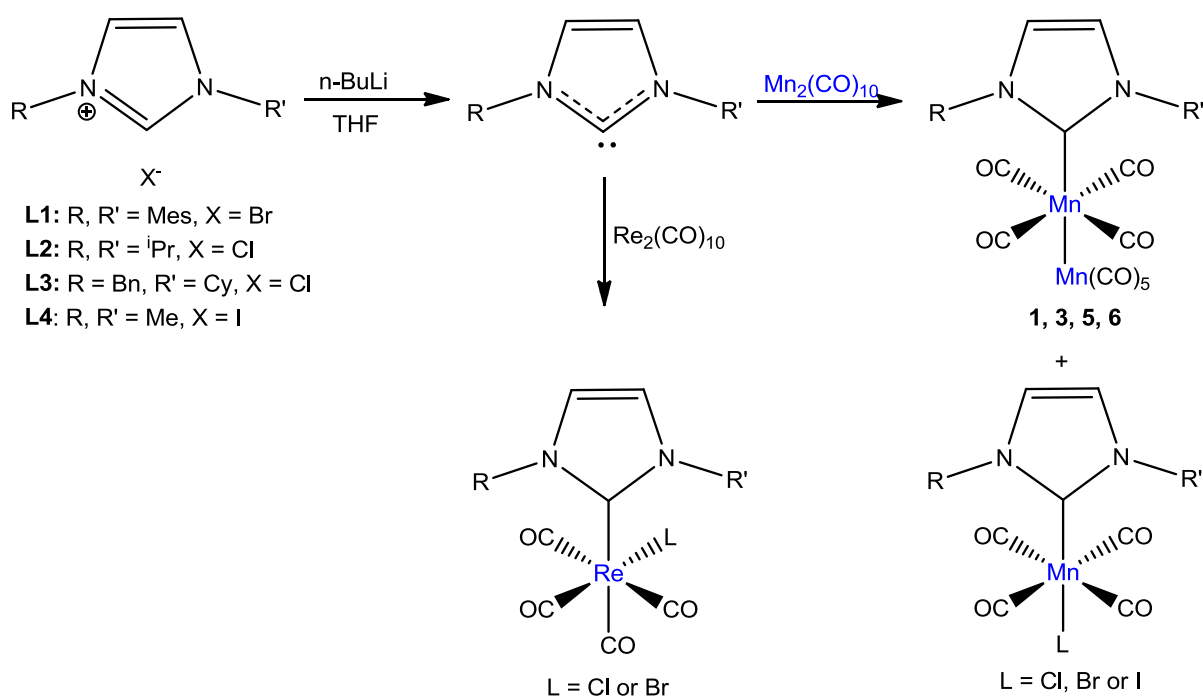
Scheme 1: Synthesis of group VII metal carbene complexes

Any attempts to synthesise the dimetallic rhenium carbene complex only yielded the monometallic analogue. Since carbene complex formation of dirhenium decacarbonyl are regiospecific and forms selectively in the equatorial position, the hypothesis was made that before the coordination of the free NHC can occur, the rhenium-rhenium bond has to be cleaved. The steric bulk of the NHC ligand would hinder equatorial coordination to an already bulky metal-metal system and thus only after cleavage would enough space remain for coordination of the carbene ligand to ensue. The merit in the hypothesis becomes evident when considering the space-fill model of the NHC complexes and the steric effects the

93

ligand would exert if the coordination occurred in the axial position without metal-metal bond cleavage (Figure 4).
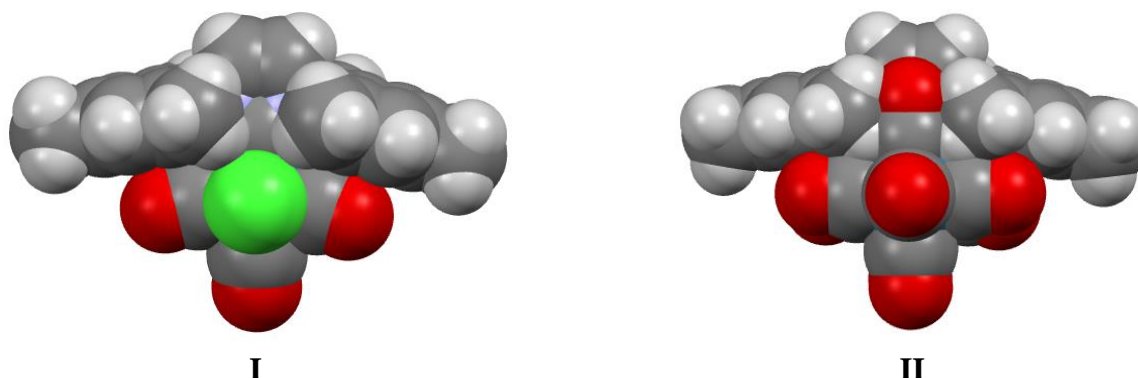
Figure 4: Space filling models of the (I) cleaved and the (II) inaccessible dimetallic rhenium carbene complex

3.2 Spectroscopic characterization

With the aid of NMR spectroscopy, with deuterated chloroform as solvent, the structural aspects of the NHC complexes were investigated. The ^{1}H NMR spectroscopic data of both the imidazolium salts and the coordinated ligands had similar peak patterns and chemical shifts. The carbene ligand salts had a characteristic carbene carbon proton peak, which presented as a singlet, around δ= 9.6 ppm. Upon coordination to the metal moiety, this peak disappeared immediately, indicating the formation of the desired group VII transition metal carbene complexes. The characteristic doublet of the aromatic C-H proton peaks associated with the ring imidazolylidene were also clearly visible between δ = 7.05 and δ = 7.59 ppm. The ^{13}C NMR of complexes **1**, **3**, **5** and **6** indicated the presence of three distinct CO peaks for the NHC complexes of manganese indicative of the dimatallic complex with the NHC ligand coordinated in the axial position. The monoatomic manganese NHC complexes only displayed a single carbonyl peak after the M-M bond has been cleaved and 4 equivalent carbonyl ligands remain. Interestingly, three distinct peaks are also visible for the rhenium tetracarbonyl carbene complexes, supporting the formation of the monometallic carbene complex with the NHC and halide ligand in the *cis* orientation to one another. The formation of an axial dirhenium nonacarbonyl complex would have shown five distinct carbonyl ligand peaks. The spectroscopic data is supported by solid state crystal structure evidence. Four distinct IR bands were observed for the dimanganese carbene complexes while only three bands were observed on the spectra of all the monometallic manganese and rhenium NHC complexes. Although five frequencies for axial carbene complexes of dimanganese nonacarbonyl are expected, only in complex **1** was this experimentally witnessed. Overlap of bands often occurs in complexes with higher carbonyl ligand numbers and in this study there was still adequate theoretical and experimental IR correlation. Carbonyl stretching frequencies between 1913 and 2086 cm^{-1} were witnessed for

nonacarbonyl complexes of manganese, between 1910 and 2077 cm^{-1} for monometallic manganese tetracarbonyl complexes and between 1910 and 2100 cm^{-1} for the rhenium tetracarbonyl carbene analogues.

3.3 Single crystal X-ray diffraction studies

The molecular structure of **1**, **3**, **7** and **8** were unambiguously confirmed by single crystal X-ray diffraction. Selected crystallographic data of **1**, **3**, **7** and **8** are tabulated in Table 1 and Table 2. Crystals suitable for X-ray diffraction were obtained from slow diffusion of hexane into a saturated solution of the complexes in diethyl ether at cooled temperatures. Complexes **1 (**Figure 5**)** and **3 (**Figure 6) crystallized in a triclinic space group P-1 and the monoclinic C2/c space group, respectively, and refined to a well-ordered structure without any co-crystallization of solvent molecules. The carbene-metal bond lengths were determined to be 2.0339(18) Å for **1** and 2.0299(12) Å for **3** and the metallic Mn-Mn bond length of 2.9576(4) Å and 2.9064(3) Å respectively. The carbonyl *trans* to the M-M bond displayed the shortest M-CO bond length and the carbonyl ligands distort to form a staggered conformation to alleviate steric strain (Figure 7).
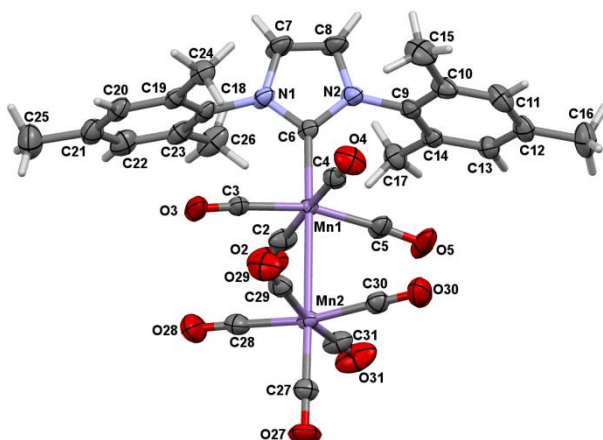
Figure 5: Perspective view of **1** with thermal ellipsoids drawn at the 50% probability level
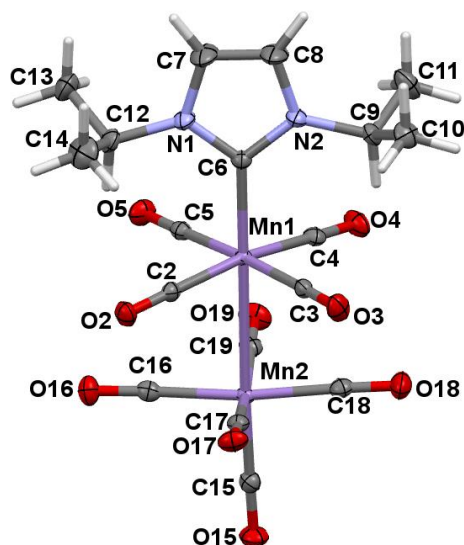
Figure 6: Perspective view of **3** with thermal ellipsoids drawn at the 50% probability level.
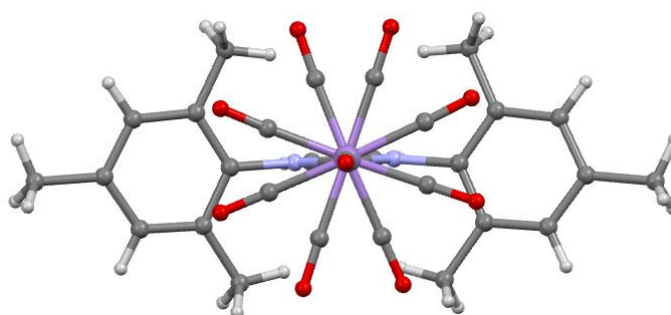
Figure 7: Staggered conformation of carbonyls witnessed in the crystal structure of **1**

The steric bulkiness of the mesityl NHC substituents enforces a repulsion of the carbonyl ligands of Mn1. This interaction results in the distorted octahedral geometry around the Mn1 centre with a bond angle of 163.18⁰ between the C3-Mn1-C5 ligands. Complex **7** also indicates the presence of this steric repulsion and the distortion in the octahedral geometry is witnessed by the *trans* C2-Re-C4 carbonyl angles of 167.64°. Complex **3** packed in circular tunnels, which was present throughout the entire packing pattern (Figure 8). The packing is unique to complex **3** and not witnessed for any other complex. Interestingly, complexes **1**, **3**, **7** and **8** all crystallize with incidences of hydrogen bonding to a CO ligand between neighbouring molecules. Complexes **7** and **8** crystallized in the triclinic P-1 and monoclinic P21/c space groups respectively.
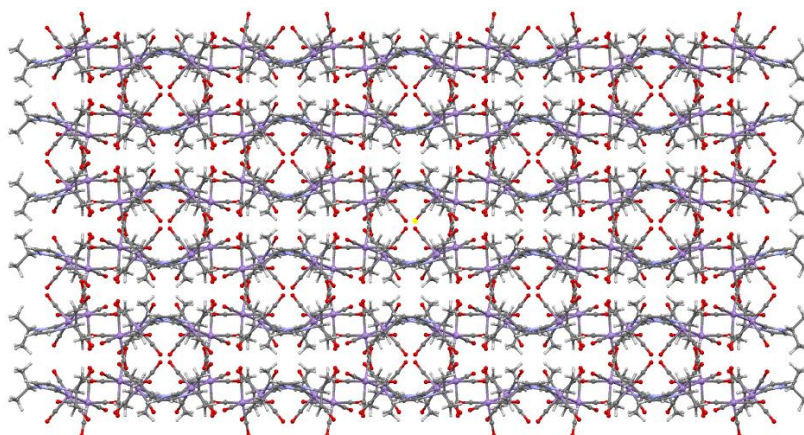
Figure 8: The packing pattern of **3**

| **1** | **3** |
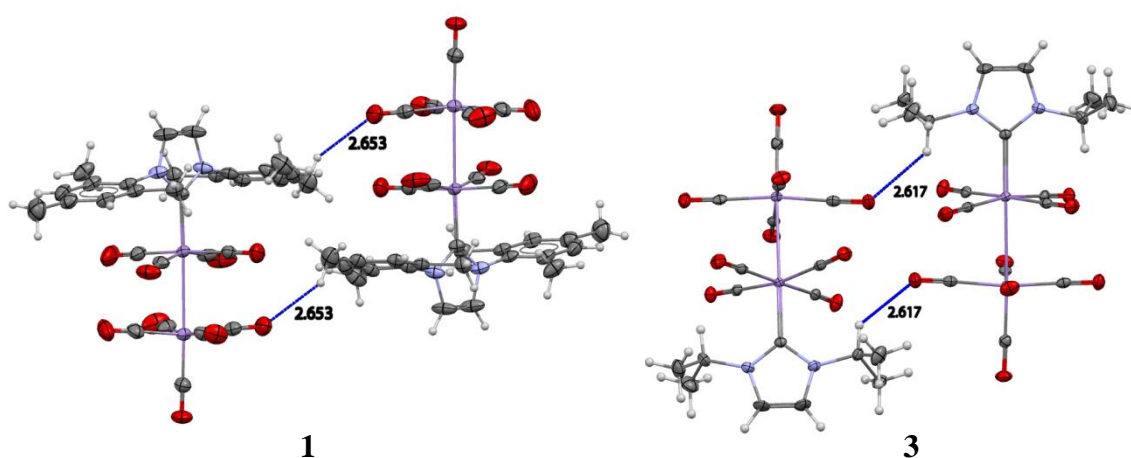
Figure 9: Hydrogen interactions (in Å) witnessed in **1** and **3**

For the monometallic complexes **7** (Figure 10) and **8** (Figure 11) the metal-carbene bond was found to be 2.077(3) Å (**7)** and 2.191(5) Å(**8),** respectively. The carbonyl ligand *trans* to the halide ligand was determined to have the shortest M-CO bond followed by the carbonyl ligand *trans* to the carbene ligand. Complexes **7** and **8** illustrate the occurrences of intramolecular H-X interactions between the substituent groups on the N atom of the NHC moiety and the halide ligated to the metal sphere. These interactions were further investigated with NBO calculations, which follow shortly and the H-I distance was found to be 2.881 Å for **7** and the H-Cl interactions 2.736 Å and 2.737 Å in 8 (Figure 12).

Table 1: Selected bond lengths and angles for **1** and **3**

|	**1**	**3**
Bond length (Å)		
Mn1-C6	2.0339(18)	2.0299(12)
N1-C6	1.372(2)	1.3661(17)
N2-N6	1.372(2)	1.3671(16)
Mn1-CO$_y$ (y= 2-5)^a	1.837(2)	1.8423(13)
Mn2-CO$_y$ (y = 16-19. 28-31)^a	1.8465(2)	1.8493(14)
Mn1-CO$_y$ (y = 15 or 27)	1.805(2)	1.8081(13)
Mn-Mn	2.9576(4)	2.9064(3)
Bond angle (°)		
N1-C6-Mn1	128.63(13)	128.11(9)
N2-C6-Mn1	129.22(13)	128.27(9)
N1-C6-N2	102.12(15)	103.59(10)
C6-Mn1-Mn2	178.17(5)	179.00(4)
C5-Mn1-C3	163.19(8)	176.92(5)
Torsion angle (°)		
C(9)-N(2)-C(8)-C(7)	172.50(19)	174.11(14)
N1-C7-C8-N2	0.7(3)	-0.06(19)

^{a} Average value for carbonyls
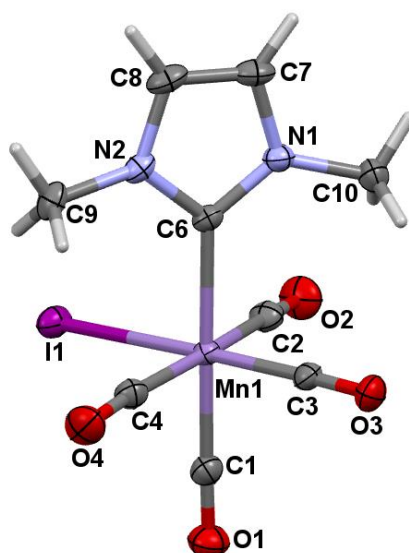
Figure 10: Perspective view of **7** with thermal ellipsoids drawn at the 50% probability level.
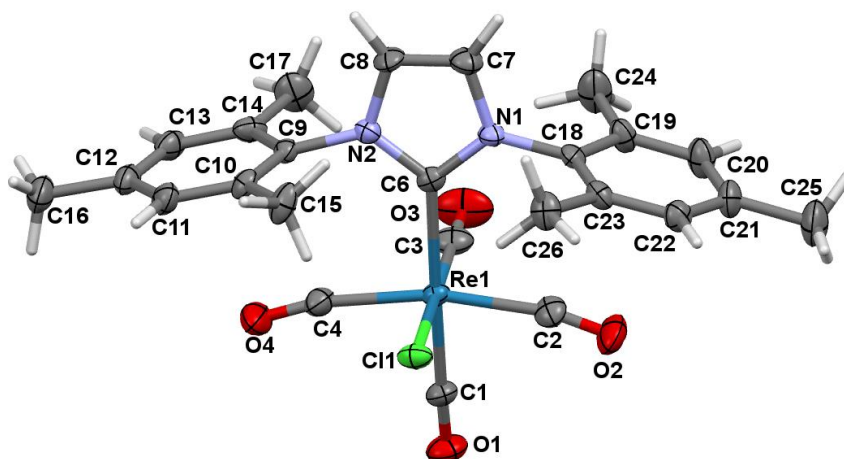
Figure 11: Perspective view of **8** with thermal ellipsoids drawn at the 50% probability level.

Table 2: Selected bond lengths and angles for **7** and **8**

	7	**8**
Bond length (Å)		
M-C6	2.077(3)	2.191(5)
N1-C6	1.360(4)	1.359(7)
N2-C6	1.364(4)	1.373(7)
Mn-COy (y = 2, 4)[a]	1.859(4)	2.005(6)
M-C1	1.850(4)	2.191(5)
M-C3	1.804(4)	1.914(7)
Halide-M	2.7205(5)	2.4843(14)
Bond angle (°)		
N1-C6-M	127.2(2)	128.7(4)
N2-C6-M	129.5(3)	128.1(4)
N1-C6-N2	103.2(3)	102.8(4)
C1-M-C6	177.40(14)	176.7(2)
C4-M-C2	171.24(16)	167.6(2)
Torsion angle (°)		
C9-N2-C6-Mn1	11.9(5)	12.3(8)
C6-N2-C8-C7	0.3(4)	0.6(7)

[a] Average value for *cis*-carbonyls (carbonyl 3 and 4)

The metal carbene bond lengths of the monometallic- and dimetallic complexes are comparable. The metal-halogen bond lengths are measured at 2.7205(5) Å and 2.4843(14) Å respectively. Finally, no significant angle deviation is found within the imidazolylidene

backbone between complexes **1**, **3**, **7** and **8** and all bond lengths between the carbene carbon atom and the nitrogen atoms are comparable. Equal back-donation from the nitrogen heteroatoms to the carbene carbon centre is thus plausible.
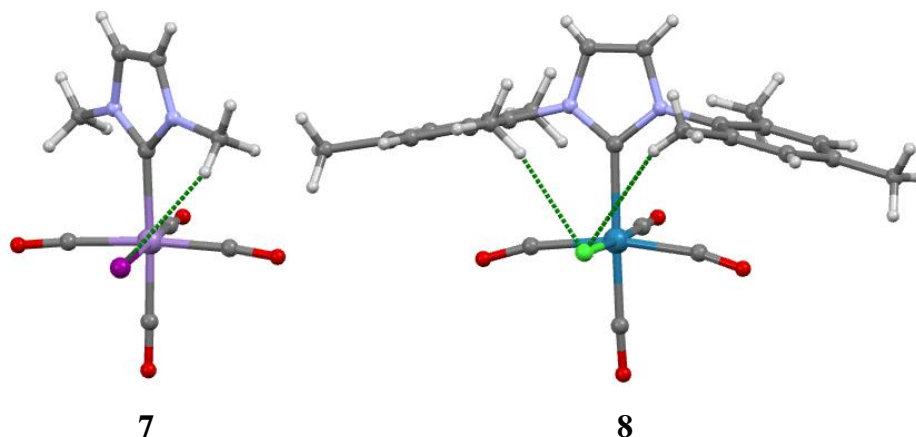
Figure 12: Hydrogen-halogen interaction in **7** and **8**

3.4 Theoretical study

A DFT study has been conducted to describe the electronic and steric influences that the carbene moiety poses to the coordination sphere of metal centres of **1-10**. The study will focus on theoretical parameters such as percentage buried volume ($\%V_{bur}$) and solid angle to describe the steric influences of the carbene ligand on the metal sphere while NBO interactions will quantify the hydrogen-halogen interactions witnessed in **7-10**. Electronic influences will be investigated using Wiberg bond indices and bond dissociation energy analysis with special focus on influences of the M-M bond aspects.

3.4.1 NBO analysis

The solid state crystal structures of **7** and **8** displayed incidences of non-covalent intramolecular hydrogen-halogen interactions (Figure 13). These interactions have been investigated using natural bond orbital interactions (NBOs) and indicate stabilization energies of between 3.56 and 4.06 kJ·mol^{-1}. Only complex **8** illustrated the presence of two H-Cl interactions and an internal stabilization of 3.56 kJ·mol^{-1} per interaction. Complex **7** presents a slightly stronger interaction between a methyl proton and the iodo ligand, which may be explained by the larger halide ligand compared to Cl (**8**). Complex **9** displays the strongest interaction (15.4 kJ·mol^{-1}).

Complex 7: 4.06 kJ·mol^{-1} **Complex 8**: 3.56 kJ·mol^{-1}

Complex 9: 15.04 kJ·mol^{-1} **Complex 10:** 4.02 kJ·mol^{-1}
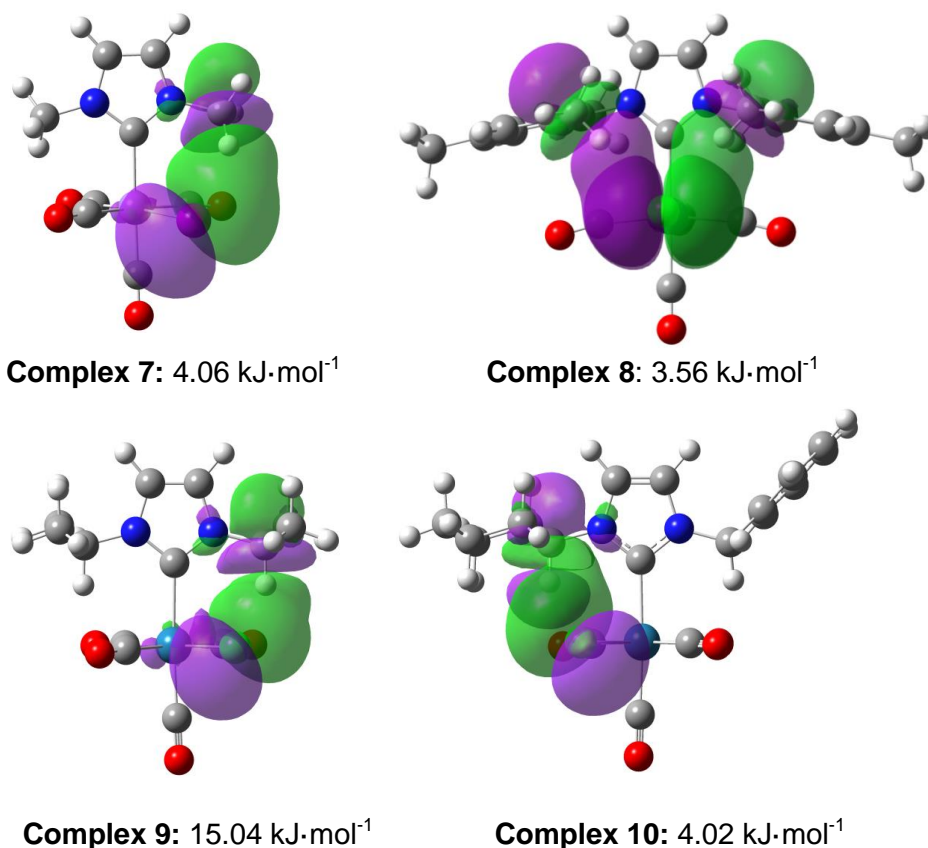
Figure 13: NBO H-X interaction of the monometallic carbene complexes

3.4.2 Ligand steric parameters

In this study the steric characteristics of the NHC ligands have been determined using two different methods namely the percentage buried volume (%V_{bur}) and the solid angle measurement of the ligands. Steric characteristics of NHC ligands can be measured by defining the volume of a sphere, centred around the metal atom, and incorporates the NHC ligand (Figure 14). This quantitative measurement is defined as the percentage buried volume (%V_{bur}) and is applicable to NHC and phosphine-containing complexes, in particular [35]. The %V_{bur} thus measures the space occupied by a ligand in the first coordination sphere of the metal centre [36]. Consequently, the more bulky the substituents on the carbene ligand, the greater the %V_{bur} would be.

[35] H. Clavier, A. Correa, L. Cavallo, E.C. Escudero-Adán, J. Benet-Buchholz, A.M.Z. Slawin, S.P. Nolan, Eur. J. Inorg. Chem. (2009) 1767.
[36] A. Poater, B. Cosenza, A. Correa, S. Giudice, F. Ragone, V. Scarano, L. Cavallo, Eur. J. Inorg. Chem. (2009) 1759.

2016
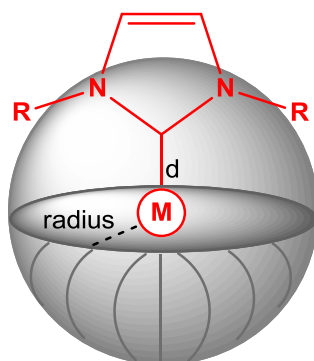
Figure 14: Graphical representation of the sphere defining %V$_{bur}$

DFT-optimized geometries of a variety of free ligands were studied by using the software developed and made freely available by Cavallo and co-workers [36]. %V$_{bur}$ was calculated by taking the optimized metal-ligand bond distance, a sphere radius of 3.5 Å and a mesh spacing of $s = 0.05$ Å. The %V$_{bur}$ values are presented in Table 3.

Table 3: The steric buried volume (%V$_{bur}$) calculated for selected complexes

Ligand	Complex	%V$_{Bur}$	Bond Length (d, Å)
L1	1	33.4	2.08
L2	3	46.5	2.08
L3	5	56.9	2.08
L4	6	30.2	2.16
L1	8	33.6	2.25
L2	9	45.1	2.26
L3	10	44.0	2.25

The buried volume of the complexes with NHC ligands (**L1** - **L4**) varied between 30.2% and 56.9 %. Ligand **L3** was found to be the bulkiest (complexes **5** and **10**), as expected, and occupied a significantly greater space of the manganese complex, especially considering the short metal-ligand bond. The percentage buried volume is inversely proportional to the metal-ligand bond length and thus the percentage buried volume is slightly less when considering the rhenium analogues. The mesitylene-containing NHC ligand (**L1**) shows basically no variation in the %V$_{bur}$ between the rhenium (**1**) and manganese complexes (**8**). The arene rings are able to rotate and occupy positions parallel to the equatorial metal

carbonyl ligands and thus limit the steric influences of this ligand. **L2** displays a high $\%V_{bur}$ with the nitrogen substituent groups found close to the metal centre and therefore occupying a significant volume of the coordination space associated with the metal moiety. For the manganese complexes $\%V_{bur}$ follows the trend **L4 < L1 < L2 < L3** and for the rhenium complexes **L1 < L3 ≤ L2**. A dominant factor seems to be the $M-C_{carbene}$ bond length. Numerous other measurements of ligand's steric influences [37] have been investigated to establish a correlation between the steric bulkiness of a ligand or group and the chemical and physical characteristics of inorganic systems [38]. The solid angle, where each ligand can be defined by the percentage of the coordination sphere of the central atom shielded by the ligand, has found relevance in depicting the steric influences of ligands [39] (Figure 15). Using this methodology, each ligand is expressed by a $G_M(L)$ value, which is the percentage of the metal coordination sphere 'protected' by the particular ligand. The $G_M(Complex)$ value defines the total shielding of the metal centre and is primarily indicative of the total crowding around the metal centre. The $G_{(Y)}$ value defines the percentage of the metal sphere shielded by more than one ligand and generates overlapping spaces of steric seclusion. The $G_M(L)$ value (the shielding of the associated NHC ligand) G_M and $G_{(Y)}$ data are presented in Table 4.

The solid angles of **1-10** indicate the size of the ligands increases in the order of **L4 < L2 < L3 < L1**. The $G_{(Y)}$ for **1**, **3**, **5** and **6** follow a similar trend as found in the $\%V_{bur}$ values and indicates that **L3** is the most bulky of the ligands when considering both the solid angle and $G_{(Y)}$ parameters. Since the formation of the dirhenium NHC complexes were not witnessed experimentally, the solid angle and $G_{(Y)}$ of the mono- and dimetallic analogue complexes were probed. The $G_M(Complex)$ and $G_{(Y)}$ were determined to be 99.32 % and 33.41% for the hypothetical dirhenium NHC complex and 97.77% and 20.06 % for complex **8**, respectively (Figure 17). This finding suggests a steric unfavourable coordination situation in the dirhenium complexes and therefore leads to the cleavage of the Re-Re bond to finally alleviate the steric strain.

[37] G.K. Fukin, I.A. Guzei, E.V. Baranov, J. Coord. Chem. 9 (2007) 937.
[38] I. Guzei, M.E. Sánchez-Castro, A. Ramirez-Monroy, M. Cervantes-Vásquez, I.R.A. Figueroa, M.A. Paz-Sand. Inorg. Chim. Acta. 359 (2006) 701.
[39] I.A. Guzei, M. Wendt. Dalton Trans. (2006) 3991.
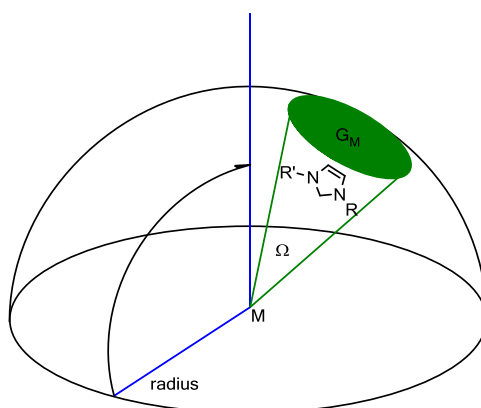
Figure 15: Representation of the Solid angle and G_M of a complex

Table 4: Solid angle parameters of **1-10**

Complex	Solid Angle[a]	G_L %	G_M(Complex) %	$G_{(Y)}$ %
1	4.36	43.13	100.00	34.68
2	4.38	33.89	99.99	33.14
3	3.27	25.99	99.67	35.67
4	3.23	25.73	98.97	22.28
5	3.35	26.65	99.69	36.33
6	2.73	21.71	99.63	33.00
7	2.75	21.90	99.05	23.41
8	4.14	32.92	97.77	20.06
9	2.98	23.70	95.72	12.98
10	3.06	24.34	95.74	13.54

[a] Solid angle of the NHC ligand measured in steradians

The G_M shielding of **1** and **2** have been visualized and is presented in Figure 16.

$G_M = 100\%$
$G_{(Y)} = 34.68$ %

$G_M = 99.99\%$
$G_{(Y)} = 33.14$ %
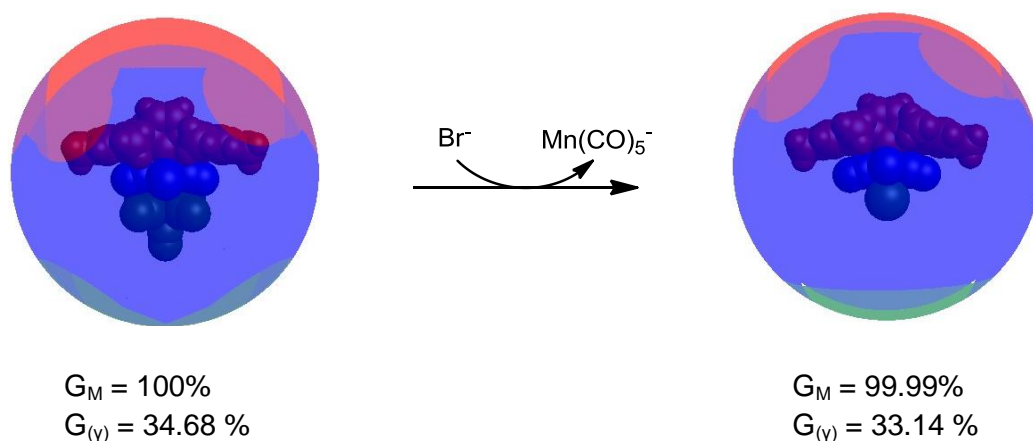
Figure 16: The G_M(Complex) of **1** (left) and **2** (right)

$G_M = 99.32\%$
$G_{(Y)} = 33.41\%$

$G_M = 97.77\%$
$G_{(Y)} = 20.06\%$
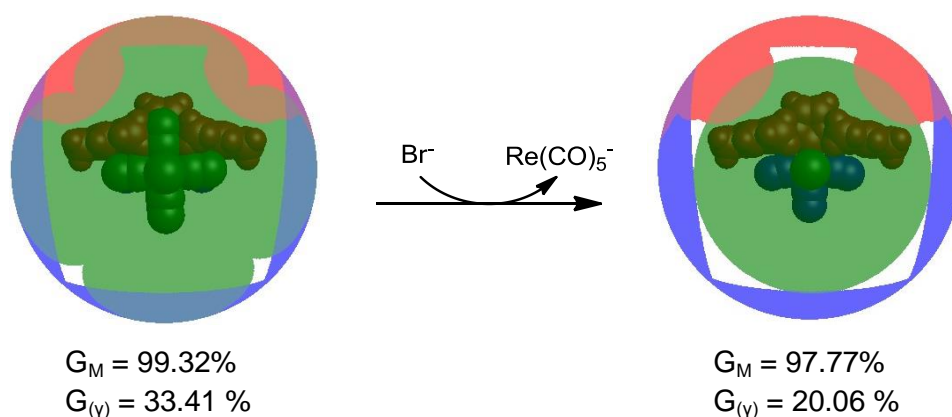
Figure 17: G_M(Complex) and $G_{(Y)}$ values of the theoretical dirhenium carbene complex (left) and **8** (right)

3.4.3 Wiberg bond indices

Literature precedence exists for the calculation and applicability of Wiberg bond orders in the aim to study NHC ligands [40] and their coordination to metal centres [41]. From our calculated results, the Wiberg bond indices (WBI) indicate a relatively strong donation from the NHC ligand towards the metal centre. A bond order of 0.7 (Table 5) displays a relative close relation to a formal single bond, although the values are lower than our recently reported bond orders for Fischer carbene complexes [42]. These values are, however, in line with reported literature values [41].

Table 5: Wiberg bond indices for **1-10**

Complex	M-C_{Carb} BO	C_{Carb}-N_1 BO	C_{Carb}-N_2 BO	M-M BO
1	0.77	1.25	1.09	0.30
2	0.79	1.25	1.25	-
3	0.77	1.26	1.26	0.30
4	0.77	1.27	1.27	-
5	0.77	1.26	1.27	0.30
6	0.70	1.26	1.26	0.30
7	0.72	1.26	1.28	-
8	0.68	1.26	1.26	-
9	0.69	1.28	1.26	-
10	0.69	1.28	1.26	-

[40] D.M. Andrada, N. Holzmann, T. Hamadi, G. Frenking, Beilstein J. Org. Chem. 11 (2015) 2727.
[41] G. Occhipinti, H. Bjørsvik, K.W. Törnroos, A. Fürstner, V. R. Jensen, Organometallics 26 (2007) 4383.
[42] R. Fraser, P.H. van Rooyen, M. Landman, J. Coord. Chem. 69 (2016) 2972.

The bond orders displayed no perceptible difference with the variation of the carbene substituents. Lower indices were witnessed for the rhenium-carbene bonds compared to the manganese analogues. As expected, both carbene carbon-nitrogen bonds of the NHC ligand have higher than 1.25 bond orders, indicating the π-donating ability of the nitrogen lone pairs toward the electronically poor carbene centre. The calculated bond order of the Mn-Mn bond of the decacarbonyl starting material and Mn-Mn carbene complex were determined to be 0.32 and 0.30 respectively, which seems to indicate that substitution of a carbonyl ligand for an NHC ligand had no substantial electronic effect on the Mn-Mn bond. The WBIs of the $Mn_2(CO)_{10}$ and $Re_2(CO)_{10}$ starting material complexes (Figure 18) show that the $C_{carbonyl}$-M value (0.66) for all equatorially bound carbonyl groups (blue) were similar. However, the green CO groups, bonded in the axial position, have a WBI of 0.79 (Figure 18). Therefore the axially bonded CO groups are more strongly bonded to the metal. This is also confirmed by the percentage contribution of the carbon and the metal atom. In the case of the equatorially bound carbonyls, carbon contributes 70% and Mn 29%. On the other hand, for the axial bonds, carbon contributes only 67% and 32%. A similar bonding situation is witnessed in the $Re_2(CO)_{10}$ complex, with the equatorial carbonyls (WBI = 0.74) bound less tightly than the axial carbonyls (WBI = 0.88) (Figure 18). The percentage contribution of the carbon and the metal atom in the equatorial blue bonds were found to be 71% and 29% for carbon and rhenium respectively. In contrast the axial carbon contributes only 63% while Re contributes 36%.
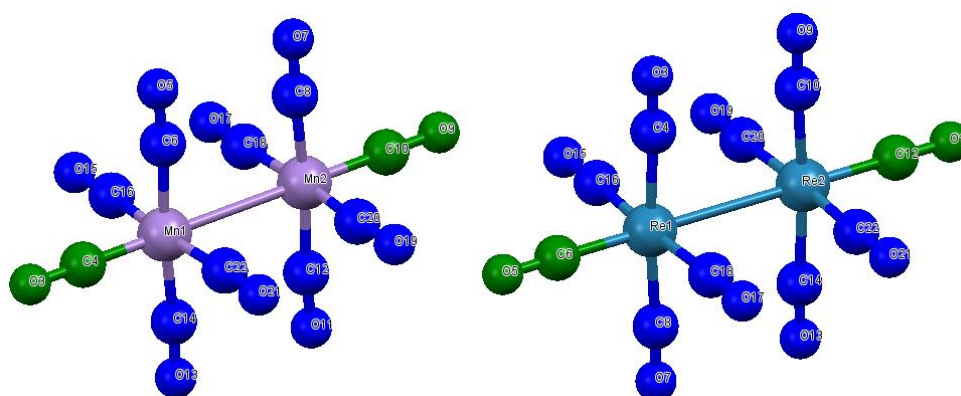
Figure 18: Wiberg bond indices of $Mn_2(CO)_{10}$ (left) and $Re_2(CO)_{10}$ (right)

The WBI confirms literature precedence [20] that carbonyl substitution for the NHC ligand should occur on the equatorially bound carbonyl groups; however, for the $Mn_2(CO)_{10}$ complex the shortened Mn-Mn bond and steric considerations favour formation of axially bound NHC complexes.

3.4.4 Bond dissociation energies (BDEs)

Bond dissociation energy (BDE) is the change in enthalpy at 298 K and 101.3 kPa for the gas-phase reaction as defined by the equation: A-B(g) → A•(g) + B•(g) [43]. Although DFT methods are inclined to systematically undervalue the absolute bond dissociations [43] estimations based on these models are still applicable in the evaluation of molecules and ligand systems. The bond dissociation energies of the M-M bond of dimetallic NHC complexes were determined and presented in Figure 19. Although Wiberg bond indices indicated no significant additional electron density between the dimetallic fragments, the BDE energy values increases upon substitution of a carbonyl ligand for an NHC ligand.
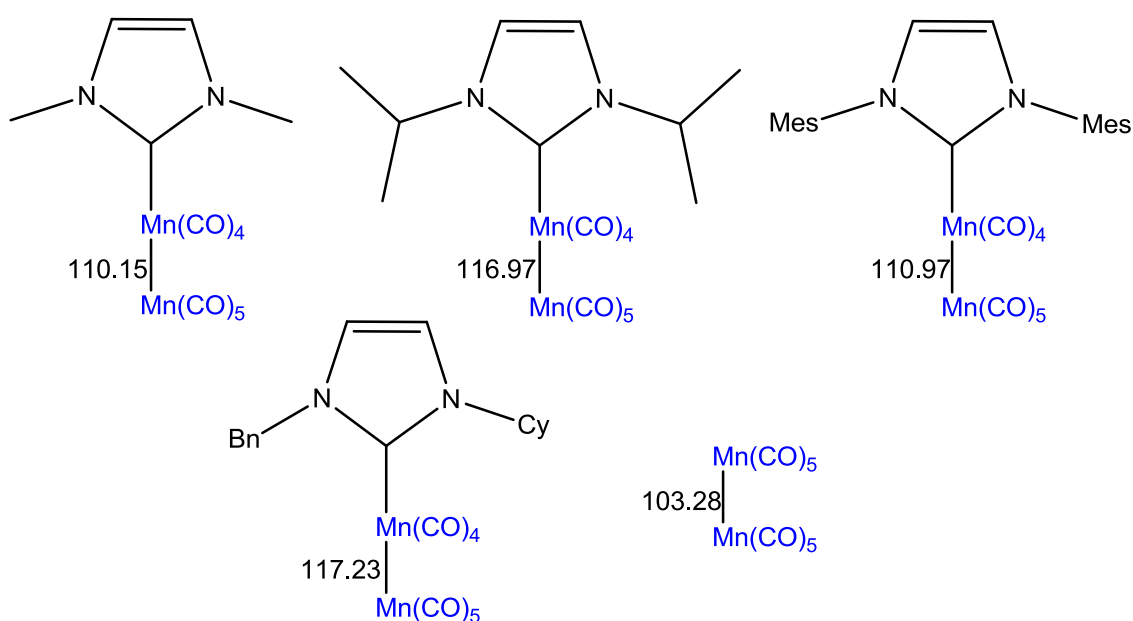
Figure 19: Bond dissociation energies in kJ·mol^{-1} of dimetallic carbene systems

The average BDE for an NHC coordinated complex was determined as 113.83 kJ·mol^{-1}, which is on average 10.55 kJ·mol^{-1} greater in comparison to the decacarbonyl manganese starting material. A linear relationship exists between both the $\%V_{bur}$ and $G_{(Y)}$ and the bond dissociation energies witnessed for the metal-metal bond. Although the relationship cannot be defined as perfectly linear, the suggestion can be made that increases in the steric properties as defined by $\%V_{bur}$ and $G_{(Y)}$, will lead to an increase in the BDE between the metal moieties (Figure 20). $\%V_{bur}$ showed the better correlation.

[43] X. Qi, Y. Feng, L. Liu, Q. Guo, Chin. J. Chem. 23 (2005) 194.
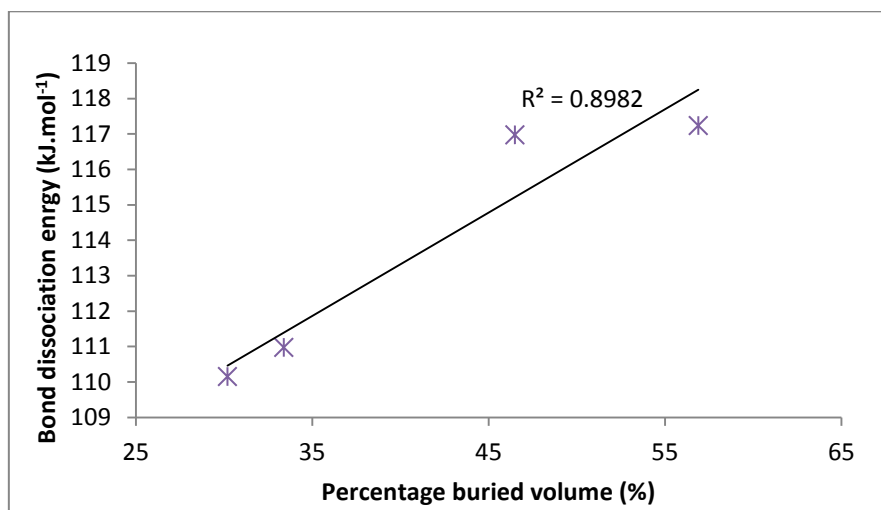
I
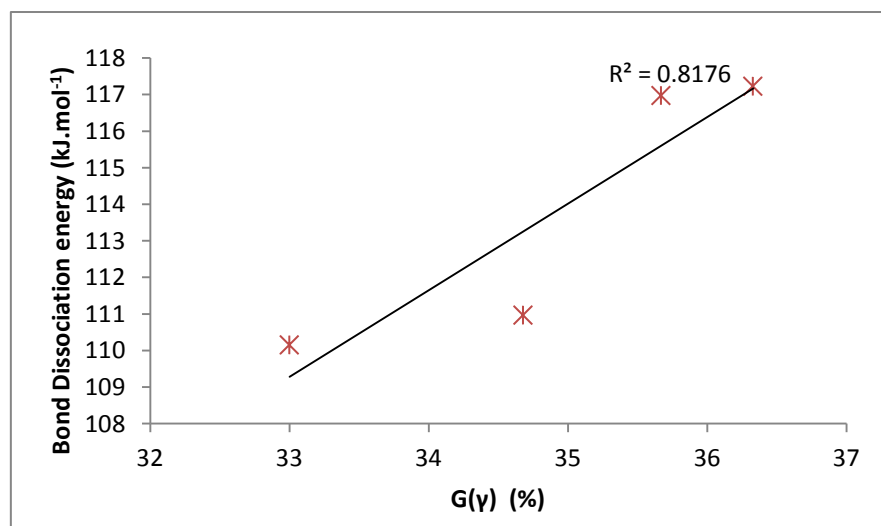
II

Figure 20: Correlation between the %Vbur (I) and G(γ) (II) and the M-M BDE of **1-4**

3.4.5 Frontier orbital analysis

The calculated energy levels and energy gaps for the frontier orbitals of dimetallic complexes **1-4** are presented in Figure 21. Band gap changes are significant since gap variation in the complexes after the NHC has been coordinated may impact the reactivity and stability [44]. In this study, band gaps of between 3.62 and 3.90 eV were determined for the complexes, with the smallest gap witnessed for **5**. Band gap analysis also indicates greater stability and lower reactivity for **2** and **3** and higher reactivity of less bulky NHC complexes. The larger band gaps witnessed for **2** and **3** correlate with higher BDE determined for these complexes as well as larger $G_{(\gamma)}$ values.

---

[44] J.S. Griffith, L.E. Orgel. Q. Rev. Chem. Soc. 11 (1957) 381.
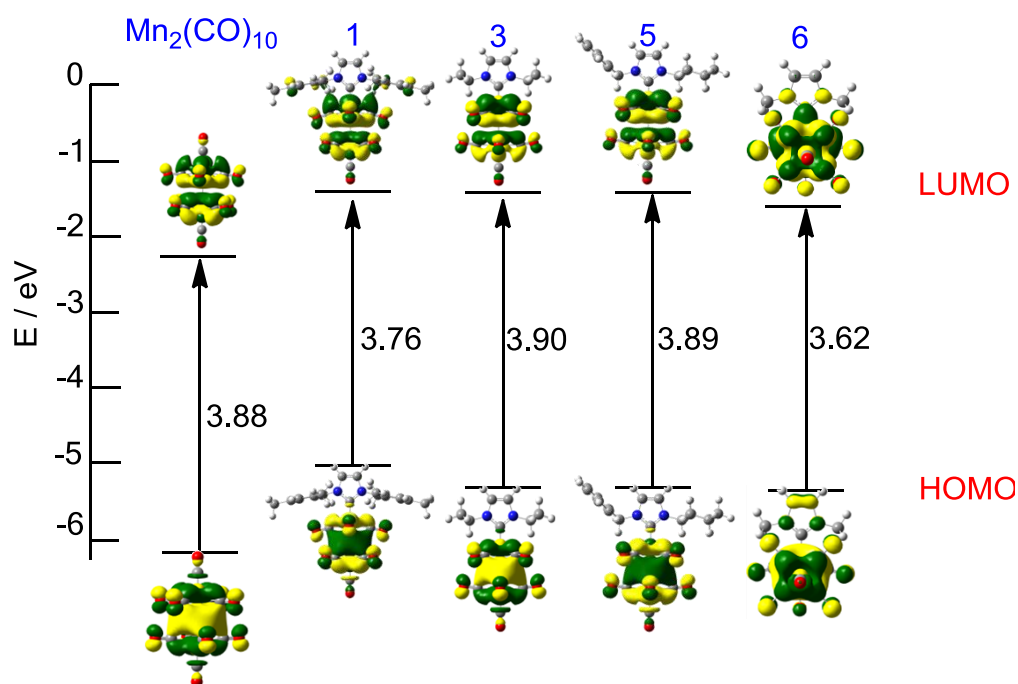
Figure 21: The frontier orbitals of $Mn_2(CO)_{10}$ and **1-4**

4 Conclusions

In this work, we reported the synthesis of mono- and dimetallic group VII NHC complexes of manganese and rhenium carbonyl metallic synthons. X-ray structures of complexes **1** and **3** featured dimetallic manganese complexes with the NHC ligand *trans* to the metal-metal bond and **7** and **8** monometallic NHC complexes with halides in the *cis* position. Intramolecular hydrogen-halide interactions were witnessed in the solid structures of **7** and **8,** which were further quantified with a DFT NBO study. The DFT study was extended to include the determination of Wiberg bond indices, the percentage buried volume (%V_{bur}) and the solid angle parameters of the complexes. Results indicate that the NHC ligands are strong sigma donor ligands, with lower donor interactions seen for the rhenium complexes compared to the manganese complexes. %V_{bur} calculations indicated that **L2** and **L3** are sterically the bulkiest of the NHC ligands and this finding is confirmed by larger $G_{(Y)}$ values for these two ligands. The frontier orbital analysis also indicated the largest band gap values for multimetallic complexes of **L2** and **L3** indicative of the superior stability of complexes featuring these ligands. The structural and electronic properties of the bulky **L2** and **L3** ligands could thus be incorporated into the group VII transition metal carbene complexes to stabilize the M-M bond during further chemical transformations or catalytic applications.

CHAPTER 6

Synthesis, structure and DFT study of asymmetrical NHC complexes of cymantrene and methylcymantrene and their application in sulfide dimerization

Chapter 6 was adapted from an article to be published in Journal of Organometallic Chemistry. The format reflects the requirements of the journal.

Authors: Roan Fraser, Petrus H. van Rooyen, Jurgens de Lange, Ignacy Cukrowski   and Marilé Landman

Graphical Abstract:
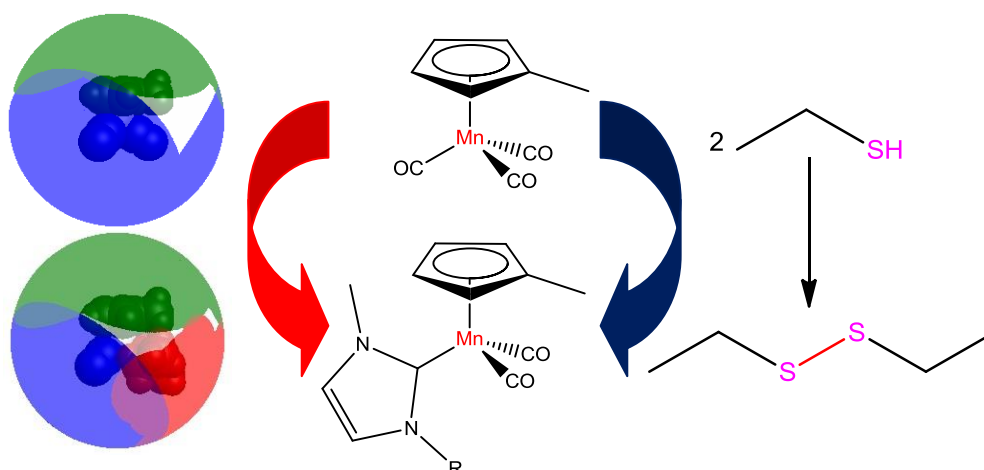
Contributions:

Roan Fraser: Author, synthesis, DFT studies

Petrus H. van Rooyen: Co-author, crystallography

Jurgens de Lange: Co-author, DFT studies

Ignacy Cukrowski : Co-author, supervisor of Jurgens de Lange

Marilé Landman: Corresponding Author, supervisor

6

Synthesis, structure and DFT study of asymmetrical NHC complexes of cymantrene and methylcymantrene and their application in sulfide dimerization

Roan Fraser, Petrus H. van Rooyen, Jurgens de Lange, Ignacy Cukrowski and Marilé Landman*

Department of Chemistry, University of Pretoria, Private Bag X20, Hatfield, 0028, South Africa. Tel: +27-12-4202527, Fax: +27-12-4204687

Contact author details:

Name: Marilé Landman Tel: +27-12-4202527, Fax: +27-12-4204687, email: *marile.landman@up.ac.za*

Keywords

N-heterocyclic carbene; cymantrenyl; Manganese; DFT; NBO analysis; percentage buried volume; bond order

Graphical abstract
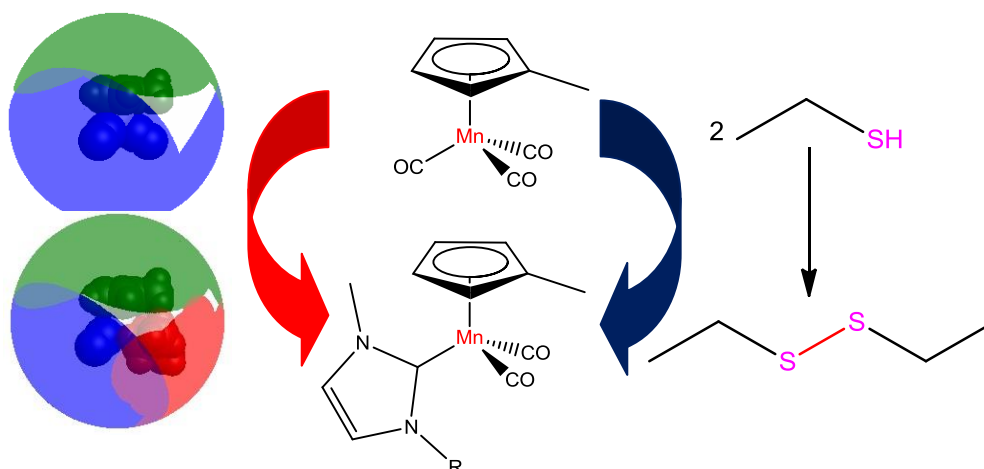
TOC abstract

Synthesis, X-ray study, structural analysis and catalytic study of cymantrenyl and methylcymantrenyl N-heterocyclic carbene complexes.

Research highlights

- DFT calculations on configurations of NHC complexes
- Crystal structure of the first cymantrenyl NHC complex
- Calculated bond orders, percentage buried volume and bond dissociation energies of $CpMn(CO)_2$-NHC and $MeCpMn(CO)_2$-NHC
- Calculated sigma and pi contributions of steric increasing NHC ligands

Abstract

Asymmetrical NHC complexes of cymantrene and methylcymantrene have been synthesised through the photochemical substitution of carbonyl ligands in the presence of the deprotonated imidazolium salts. The carbene substituents have been varied between compact (**L1**) and bulky (**L2** and **L3**) substituents to produce an array of differently sized carbene ligands. The solid state crystal structures of three of the complexes confirmed the bonding pattern of the ligand towards available metal centres and an in-depth DFT study provided insight into electronic and steric aspects. Application of the Extended Transition State coupled with Natural Orbitals for Chemical Valence (ETS-NOCV) energy decomposition technique indicated various NOCV channels for each Mn–L bond (L = 3-ethyl-1-methylimidazolylidene carbene, triphenylphosphine or acetonitrile), describing the density and energy changes of specific (σ and π) attributes of each bond. N-heterocyclic carbenes of cymantrenyl and their triphenylphosphine-substituted analogue are equivalent σ-donors, with 53% and 56% of the total binding energy originating from σ-donation, respectively. However, NHC complexes show considerably less π character in the metal-carbene bond. Hydrogen interactions in the NHC complexes were also identified in the ETS-NOCV calculations and provided quantification of the hydrogen interactions witnessed in the solid state structures. Calculated Wiberg bond indices, bond dissociation enthalpies, percentage buried volumes and percentage sigma and pi-bonding characteristics quantified the bonding and electronic aspects of the ligand-metal interactions within the complex.

1   Introduction

Since the isolation of the first stable, free N-heterocyclic carbene (NHC) by Arduengo in 1991, NHC's have transformed the field of organometallic chemistry [1]. The adjustability of the steric and electronic properties of these ligands has resulted in their persistent use for the synthesis and stabilization of metal complexes capable of cleaving very inert bonds [2]. The majority of synthetic pathways in the synthesis of transition metal (TM) NHC complexes have been thermally initiated [3] whereas photochemical induced pathways have, however, been mostly ignored [3]. This aspect is surprising, especially if taken into consideration the similarities between tertiary phosphines and NHC ligands and the applicability of photochemical reactions in producing highly reactive, coordinatively unsaturated TM-PR3 species [3]. The photolysis and the subsequent isomerisation of ruthenium NHC complexes have been reported and indicate the ability of photochemical processes to produce isomeric variations of target complexes (Figure 1) [3].
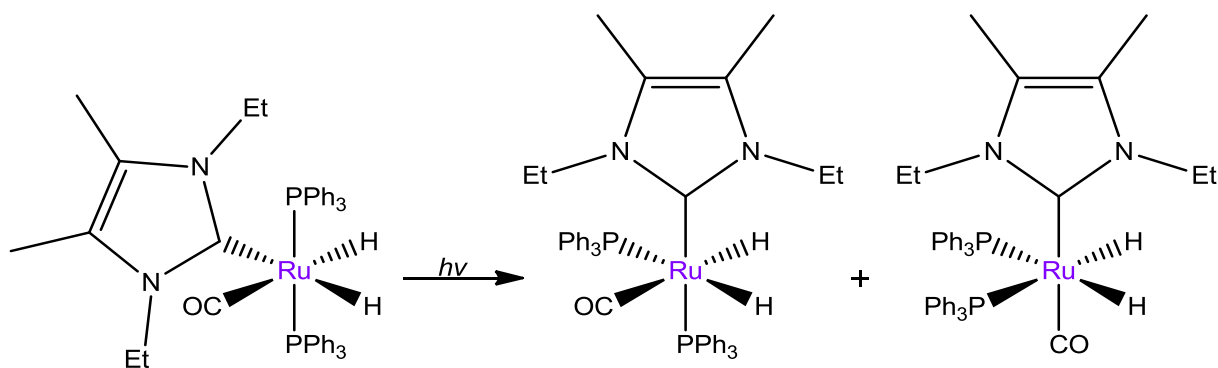
Figure 1: Isomerisation of Ru-NHC complexes afforded through photochemical processes [**3**]

Methylcyclopentadienyl manganese tricarbonyl (MMT), and to a far lesser extent, cymantrene have been successfully applied in the fuel industry as supplements in unleaded gasoline [4]. MMT not only increases octane ratings but are particularly useful as anti-knocking agents, improving combustion of fuels [5]. Studies on carbene complexes of MMT and cymantrene complexes are limited in literature and only focus on the synthesis of novel, symmetrical N-heterocyclic carbene (NHC's) complexes of MMT and cymantrene (Figure 2) [5,6].

[1] A.J. Arduengo, R.L. Harlow, M. Kline, J. Am. Chem. Soc. 113 (1991) 361.
[2] L. Cavallo, A. Correa, C. Costabile, H. Jacobsen, J. Organomet. Chem. 690 (2005) 5407.
[3] K.A.M. Ampt , S. Burling , S.M.A. Donald , S. Douglas , S.B. Duckett , S.A. Macgregor , R.N. Perutz , M. K. Whittlesey, J. Am. Chem. Soc. 128 (2006) 7452.
[4] M.Batool, T.A.Martin, A.G.Algarra, M.W.George, S.A.Macgregor, M.F.Mahon, M.K.Whittlesey, Organometallics 31 (2012) 4971.
[5] (a) J. Zheng, S. Elangovan, D.A. Valyaev, R. Brousses, V. César, J. Sortais, C. Darcel, N. Lugan, G. Lavigne, Adv. Synth. Catal. 356 (2014) 1093; (b) D.A. Valyaev, M.A. Uvarova, A.A. Grineva, V. César, S.N. Nefedov, N. Lugan, Dalton Trans. 45 (2016) 11953.
[6] M.Batool, T.A.Martin, N.A.Naser, M.W.George, S.A.Macgregor, M.F.Mahon, M.K.Whittlesey, Chem. Commun. 47 (2011) 11225.

The synthesis of symmetrical NHC complexes of MMT has been reported as early as 1977 when Lappert [7] prepared complexes of manganese from the Wanzlick dimeric NHC ligand under high thermal conditions. The complexes were stable above 180°C and displayed exceptional inertness against thermal decomposition. A small variety of symmetrical NHC cymantrenyl carbene complexes have been synthesised by means of photochemical processes and have even found application in the hydrosilylation of aldehydes and ketones [4]. The study found that the incorporation of at least one mesityl group leads to the most selective and active systems. DFT calculations also indicated the presence of an agostic stabilization when a second carbonyl ligand is removed by photolytic irradiation [4].
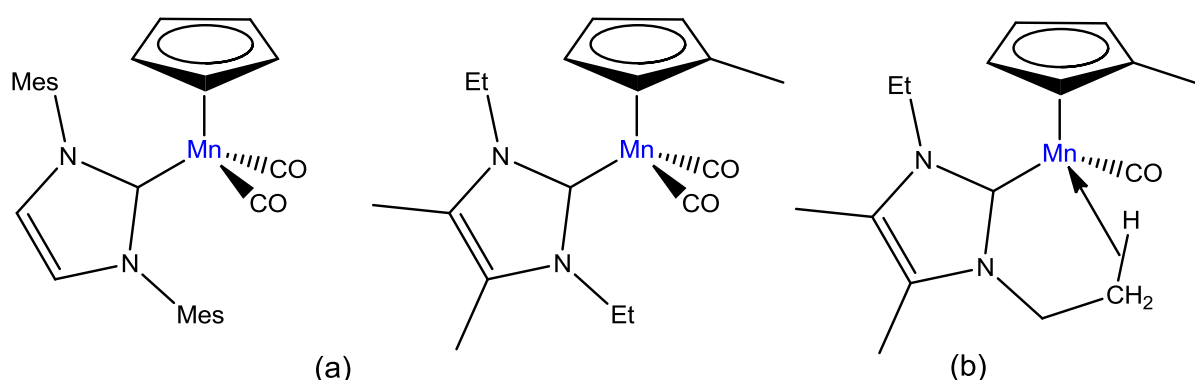
Figure 2: NHC complexes of cymantrene and MMT (a) and agostic interaction of the cymantrene NHC complex (b)

Since agostic interactions are also witnessed in the triphenylphosphine analogue [4] combined with the fact that both Cp'Mn(CO)PPh$_3$ and Cp'Mn(CO)NHC stabilize carbonyl expulsion through agnostic interactions rather than with solvent ligation, both analogues can be seen as quite similar in chemical nature. Although the synthetic methodology and catalytic potential of symmetric NHC complexes of cymantrene and MMT have been determined for a variety of different reactions and conditions, very limited understanding exists for the structural and electronic effects of different unsymmetrical NHC ligands towards the metal centre. For this purpose, asymmetrical NHC complexes with increasing steric bulk have been synthesised (Figure 3) and studied with theoretical calculations. This study reports the synthesis of the six novel asymmetrical NHC complexes of cymantrene and MMT, the synthesis of the acetonitrile and triphenylphosphine analogues of the NHC complexes, X-ray crystal structures of three of the complexes and a DFT study. The triphenylphosphine and acetonitrile analogues were synthesised to form a baseline to which

[7] M. F. Lappert, P. L. Pye. J. Chem. Soc. Dalton Trans. (1977) 2172.

the percentage sigma and pi-bonding characteristics of the NHC complexes could be compared.

1) R = Et, R' = H
2) R = Et, R' = Me
3) R = ^{i}Pr, R' = H
4) R = ^{i}Pr, R' = Me
5) R = EtPh, R' = H
6) R = EtPh, R' = Me

B1) L = PPh$_3$
C1) L = NCCH$_3$
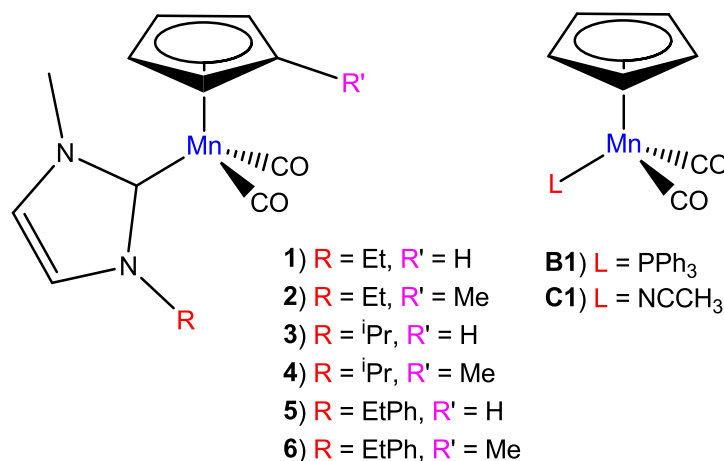
Figure 3: Cymantrenyl and MMT NHC complexes

2 Experimental

2.1 General

All reactions, unless noted otherwise, were performed under inert nitrogen or argon atmospheres using typical Schlenk techniques [8]. All solvents used, were freshly distilled, dried and collected under inert conditions. Column chromatography was carried out under inert nitrogen and argon atmospheres using silica gel (particle size 0.063-0.200 mm) as the stationary phase. Percentage yields were calculated relative to the limiting reactant. Crystallization was done using hexane:DCM or hexane:ether diffusion methods. The reagents CpMn(CO)$_3$, MeCpMn(CO)$_3$, n-butyl lithium (1.6 M solution in hexane) and other commercial reagents were used as purchased. Complexes **B1** [9] and **C1** [10] were synthesised according to literature procedures. NMR spectra were recorded on a Bruker ARX-300. NMR spectra were recorded in CD$_3$CN using the deuterated solvent peak as internal reference. The ^{1}H and ^{13}C NMR spectra were measured at 300.1 and 75.5 MHz, respectively. IR spectra were recorded on a Perkin Elmer Spectrum RXI FT-IR spectrophotometer as KBr pellets or in hexane and only the vibration bands in the carbonyl-stretching region (ca. 1500-2200 cm^{-1}) are reported.

[8] D.F. Schriver, M.A. Drezdzon, The manipulation of Air-Sensitive Compounds, 2nd ed., Wiley, New York, USA, 1986.
[9] M.D. Raush, B.H. Edwards, R.D. Rogers, J.L. Atwood, J. Am. Chem. Soc. 105 (1983) 3882.
[10] J.W. Hershberger, C. Amatore, J.K. Kochi, J. Organomet. Chem. 250 (1983) 345.

115

2.2 Synthesis of complexes 1-6

2.2.1 Synthesis of 1, CpMn(CO)$_2$L1

All complexes were synthesised according to an adapted method from the reported methodology by Lugan [5]. CpMn(CO)$_3$ (0.612 g, 3.0 mmole) was dissolved in 40 ml of dry THF and irradiated for 60 mins. at room temperature. The method as reported by Lugan has recently been improved by substituting the THF solvent for toluene [5]. Deprotonated **L1** (0.714 g, 3.0 mmole) was added to the reaction mixture via candela and the reaction allowed to stir for 90 mins. The reaction colour turned a deep brownish colour and subsequently filtered through a small aluminium oxide column. The solvent was evaporated, the product redissolved and purified with column chromatography with hexane:ether eluent to recover **1** as an orange oil. Yield 0.267 g (31%) % ^{1}H NMR(CD$_3$CN): δ 7.33 (s, 1H, NC**H**=CHN), 7.30 (s, 1H, NHC=C**H**N), 4.44 (s, 5H, Cp), 4.27 (q, 2H, J_{HH}=7.3, NC**H$_2$**CH$_3$), 3.75 (s, 3H, NC**H$_3$**), 1.30 (t, 3H, , J_{HH}=7.3, NCH$_2$C**H$_3$**) ^{13}C{^{1}H} NMR: δ 235.22 Mn(CO)$_2$, 195.7 NCN, 124.6 N**C**=CN, 121.5 NC=**C**N, 82.6 Cp, 65.4 NCH$_3$, 45.5 N**C**H$_2$CH$_3$, 16.7 NCH$_2$**C**H$_3$. IR (cm^{-1}): 1922 v(CO), 1856 v(CO). HRESI$^+$-MS, m/z: 287.0513 (calcd. 287.0592).

2.2.2 Synthesis of 2, MeCpMn(CO)$_2$L1

A similar methodology as for **1** was followed. Deprotonated **L1** (0.714 g, 3.0 mmole) was added to photo-irradiated MeCpMn(CO)$_3$ (0.654 g, 3.0 mmole). A single brown-orange oily product of complex **2** was isolated. Yield: 0.271 g (30%) ^{1}H NMR, ppm (CD$_3$CN): δ 7.20 (s, 1H, NHC=CHN), 7.15 (s, 1H, NHC=C**H**N, 4.34 (s br, 2H, NC**H$_2$**CH$_3$), 4.09 (s, 2H, Cp), 4.02 (s, 2H, Cp);), 3.36 (s, 3H, NCH$_3$), 2.86 (s, 3H, Cp-CH$_3$), 1.48 (s br 3H, NCH$_2$C**H$_3$**). ^{13}C{^{1}H} NMR, ppm: δ 234.7 Mn(**CO**)$_2$, 200.7 NCN, 129.0N**C**=CN, 128.6 NC=**C**N, Cp 101.4, Cp 81.5, Cp 79.8, 65.0 NCH$_3$; N**C**H$_2$CH$_3$ 52.27, Cp-**C**H$_3$ 37.5, NCH$_2$**C**H$_3$ 13.7. IR (cm^{-1}): 1918 v(CO), 1852 v(CO). HRESI$^+$-MS, m/z: 303.0939 (calcd. 303.0905).

2.2.3 Synthesis of 3, CpMn(CO)$_2$L2

A similar methodology as for **1** was followed. Deprotonated **L2** (0.0481 g, 3.0 mmole) was added to photo-irradiated MeCpMn(CO)$_3$ (0.612 g, 3.0 mmole). A single yellow solid product of complex **3** was isolated (yield: 0.271 g; 30%).^{1}H NMR, ppm (CD$_3$CN,): δ 7.42 (s, 1H, NHC=CHN), 7.32 (s, 1H, NCH=C**H**N), 4.45 (s, 5H, Cp), 3.76 (s, 3H, NC**H$_3$**), 3.60 (m, 2H, NC**H**(CH$_3$)$_2$), 1.32 (s, 6H, NCH(C**H$_3$**)$_2$). ^{13}C{^{1}H} NMR, ppm: δ 235.1 Mn(**CO**)$_2$, 193.5 NCN, 124.90 N**C**=CN, 118.7 NC=**C**N, Cp 82.5, 67.5 NCH$_3$, 51.9 N**C**H(CH$_3$)$_2$, 25.6 NCH(**C**H$_3$)$_2$. IR (cm^{-1}): 1922 v(CO), 1856 v(CO). HRESI$^+$-MS, m/z: 301.0789 (calcd. 301.0748).

2.2.4   Synthesis of **4, MeCpMn(CO)₂L2**

A similar methodology as for **1** was followed. Deprotonated **L2** (0.481 g, 3.0 mmole) was added to photo-irradiated MeCpMn(CO)$_3$ (0.654 g, 3.0 mmole). A single yellow solid product of complex **4** was isolated (yield: 0.255 g; 27%).^{1}H NMR, ppm (CD$_3$CN): δ 6.85 (s, 1H, NC**H**=CHN), 6.83 (s, 1H, NCH=C**H**N), 3.96 (s, 2H, Cp), 3.86 (s, 3H, NC**H₃**), 3.85 (s, 2H, Cp), 3.76 (s br, 2H, NC**H**(CH$_3$)$_2$, 2.89 (s, 3H, Cp-C**H₃**), 1.33 (d, 6H, J_{HH}=6.3, NCH(C**H₃**)$_2$). ^{13}C{^{1}H} NMR, ppm: δ 235.1 Mn(**CO**)$_2$, 195.0 NCN, 124.9 N**C**=CN, 124.1 NC=**C**N, 34.7 Cp-**C**H$_3$, 102.8 Cp, 81.9 Cp, 80.4 Cp, 60.5 NC**H₃**, 52.4 N**C**H(CH$_3$)$_2$, 13.7 NCH(**C**H$_3$)$_2$. IR (cm^{-1}): 1943 v(CO), 1852 v(CO). HRESI$^+$-MS, m/z: 317.1081 (calcd. 317.1062).

2.2.5   Synthesis of **5, CpMn(CO)₂L3**

A similar methodology as for **1** was followed. Deprotonated **L1** (0.801 g, 3.0 mmole) was added to photo-irradiated MeCpMn(CO)$_3$ (0.612 g, 3.0 mmole). A single yellow solid product of complex **3** was isolated (yield: 0.381 g; 35%). ^{1}H NMR, ppm (CD$_3$CN): δ 7.45 (s, 1H, N**H**C=CHN), 7.34 (s br, 5H, Ph), 7.26 (s, 1H, NHC=C**H**N), 4.44 (m, 2H, NC**H₂**Bn); 4.38 (s, 5H, Cp), 3.75 (s, 3H, NC**H₃**), 3.03 (m, 2H, NCH$_2$C**H₂**Ph). ^{13}C{^{1}H} NMR, ppm: δ 235.2 Mn(**CO**)$_2$, 195.1 NCN, 138.9 Ph$_{(ipso)}$, 129.3 Ph$_{(meta)}$, 129.0 Ph$_{(ortho)}$, 127.0 Ph$_{(para)}$, 124.5 N**C**=CN, 122.1 NC=**C**N, 82.7Cp, 64.4 NC**H₃**, 52.0 N**C**H$_2$Bn, 40.8 NCH$_2$**C**H$_2$Ph,. IR (cm^{-1}): 1921 v(CO), 1855 v(CO). HRESI$^+$-MS, m/z: 365.1033 (calcd. 365.1062).

2.2.6   Synthesis of **6, MeCpMn(CO)₂L3**

A similar methodology as for **1** was followed. Deprotonated **L1** (0.801 g, 3.0 mmole) was added to photo-irradiated MeCpMn(CO)$_3$ (0.654 g, 3.0 mmole). A single yellow solid product of complex **6** was isolated (yield: 0.374 g; 33%). ^{1}H NMR, ppm (CD$_3$CN): δ 7.37 (s br, 4H, Ph), 7.46 (s, 1H N**H**C=CHN, 7.25 (s, 1H NCH=C**H**N), 4.46 (m, 2H, NC**H₂**Bn), 4.26 (s br, 5H, Cp), 3.75 (s, 3H, NC**H₃**) 3.05 (m, 2H, NCH$_2$C**H₂**Ph), 2.51 (s, 3H, Cp-C**H₃**). ^{13}C{^{1}H} NMR, ppm: δ Mn(**CO**) 235.3, 196.5 NCN, 124.6 N**C**=CN, 122.2 NC=**C**N, 138.9 Ph$_{(ipso)}$, 129.3 Ph$_{(meta)}$, 129.0 Ph$_{(ortho)}$, 127.0 Ph$_{(para)}$, 103.2 Cp, 82.1 Cp, 80.4 Cp, 64.4 NC**H₃**, 52.1 N**C**H$_2$Bn, 40.8 NCH$_2$**C**H$_2$Ph,.35.6 Cp-**C**H$_3$. IR (cm^{-1}): 1917 v(CO), 1852 v(CO). HRESI$^+$-MS, m/z: 379.1248 (calcd. 379.1218).

2.3   X-ray crystallography

Data for complexes **3** and **6** and **C1** were collected at 150 K on a Bruker D8 Venture kappa geometry diffractometer, with duo Iμs sources, a Photon 100 CMOS detector and APEX II control software using Quazar multi-layer optics, monochromated Mo-Kα radiation and by means of a combination of φ and ω scans. Data reduction was performed using SAINT+ and

the intensities were corrected for absorption using SADABS [11]. The structures were solved by intrinsic phasing using SHELXTS and refined by full-matrix least squares using SHELXTL and SHELXL-2013 [12]. In the structure refinement, all hydrogen atoms were added in calculated positions and treated as riding on the atom to which they are attached. All nonhydrogen atoms were refined with anisotropic displacement parameters, all isotropic displacement parameters for hydrogen atoms were calculated as X × Ueq of the atom to which they are attached, X = 1.5 for the methyl hydrogens and 1.2 for all other hydrogens. Crystallographic data and refinement parameters are given in Table 1. Ortep drawings [13] of the three structures are included in Figure 5, Figure 6 and

Figure 9. The crystal structures (cif) have been deposited at the Cambridge Crystallographic Data Centre and allocated the deposition numbers: CCDC 1517726-1517728. Data collection, structure solution and refinement details are available in each cif.

2.4   Molecular modelling

The calculations reported in this paper were obtained using the Gaussian 09 [14] suite of programs. Calculations were carried out in the singlet spin state using the hybrid functional B3LYP [15,16]. Geometries of the neutral complexes were optimized in gas phase with the triple-ζ basis set 6-311G* on all atoms except for the metal atoms. Stuttgart/Dresden (SDD) pseudopotential was used to describe the metal electronic core, while the valence electrons were described def2-TZVPP [17]. No symmetry constraints were applied and only the default convergence criteria were used during the geometric optimizations. Vibrational frequencies [18] were calculated at the optimized geometries and no imaginary frequencies were observed, to confirm true minima. Donor-acceptor interactions have been computed using

[11] APEX2 (including SAINT and SADABS); Bruker AXS Inc., Madison, WI (2012).
[12] G.M. Sheldrick, Acta Crystallogr. A64 (2008) 112.
[13] L.J.J. Farrugia, Appl. Crystallogr. 30 (1997) 565.
[14] M.J. Frisch, G.W. Trucks, H.B. Schlegel, G.E. Scuseria, M.A. Robb, J.R. Cheeseman, G. Scalmani, V. Barone, B. Mennucci, G.A. Petersson, H. Nakatsuji, M. Caricato, X. Li, H.P. Hratchian, A.F. Izmaylov, J. Bloino, G. Zheng, J.L. Sonnenberg, M. Hada, M. Ehara, K. Toyota, R. Fukuda, J. Hasegawa, M. Ishida, T. Nakajima, Y. Honda, O. Kitao, H. Nakai, T. Vreven, J.A. Montgomery (Jr), J.E. Peralta, F. Ogliaro, M. Bearpark, J.J. Heyd, E. Brothers, K.N. Kudin, V.N. Staroverov, T. Keith, R. Kobayashi, J. Normand, K. Raghavachari, A. Rendell, J.C. Burant, S.S. Iyengar, J. Tomasi, M. Cossi, N. Rega, J.M. Millam, M. Klene, J.E. Knox, J.B. Cross, V. Bakken, C. Adamo, J. Jaramillo, R. Gomperts, R.E. Stratmann, O. Yazyev, A.J. Austin, R. Cammi, C. Pomelli, J.W. Ochterski, R.L. Martin, K. Morokuma, V.G. Zakrzewski, G.A. Voth, P. Salvador, J.J. Dannenberg, S. Dapprich, A.D. Daniels, O. Farkas, J.B. Foresman, J.V. Ortiz, J. Cioslowski, D.J. Fox, Gaussian 09, Revision D.01, Gaussian Inc., Wallingford CT, 2010.
[15] A.D. Becke, J. Chem. Phys. 98 (1993) 5648.
[16] C. Lee, W. Yang, R.G. Parr, Phys. Rev. B 37 (1988) 785.
[17] F. Weigend, R. Ahlrichs, Phys. Chem. Chem. Phys. 7 (2005) 3297.
[18] J.W. McIver, A.K. Komornicki, J. Am. Chem. Soc. 94 (1972) 2625.

the natural bond order (NBO) method [19]. For the ETS-NOVC analysis, complexes **1**, **B1** and **C1** were optimized in ADF 2014.01 [20], using BP86 with a triple-ζ basis set and with up to 2*p* frozen cores on metal atoms, in the gas phase. Optimized structures were then investigated using the Extended Transition State coupled with Natural Orbitals for Chemical Valence (ETS-NOCV) [21] energy decomposition technique. Mn–L bonds were broken and the corresponding fragments were used as promolecules, without any adjustment of fragment occupations.

2.5   General procedure for the dimerization of thiols

On the basis of literature and for purposes of the comparison of computed percentage buried volume and solid angle predictions to experimental obtainable results, 3 mol% of catalyst, in the presence of the ethylthiol and cyclohexane were irradiated in an inert argon atmosphere for the duration of 2.5 hours. The resulting solution was analysed directly by GC/MS using hexadecane as internal standard upon which the dimerization yields were based. All reported yields are based on the average of three runs.

3   Results and discussion

3.1   Synthesis and characterization
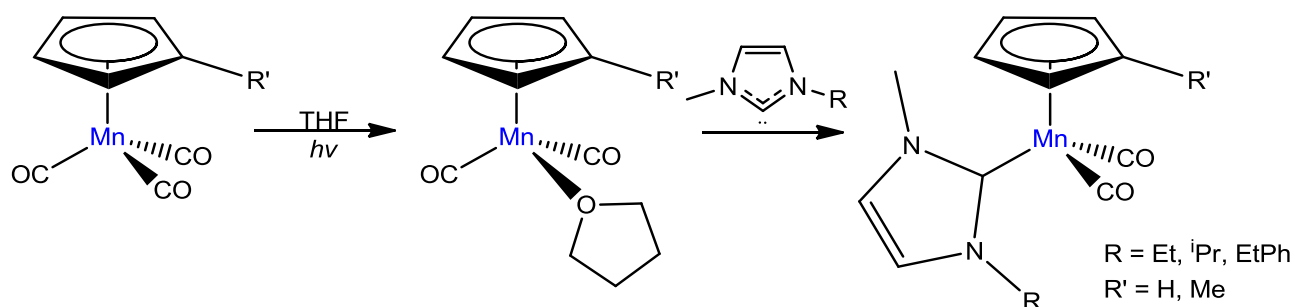
Scheme 1: Synthesis of group VII NHC complexes

[19] (a) J.P. Foster, F. Weinhold, J. Am. Chem. Soc. 102 (1980) 7211; (b) A.E. Reed, F. Weinhold, J. Chem. Phys. 83 (1985) 1736; (c) A.E. Reed, R.B. Weinstock, F. Weinhold, J. Chem. Phys. 83 (1985) 735; (d) A.E. Reed, L.A. Curtiss, F. Weinhold, Chem. Rev. 88 (1988) 899.

[20] E. J. Baerends, T. Ziegler, J. Autschbach, D. Bashford, A. Bérces, F. M. Bickelhaupt, C. Bo, P. M. Boerrigter, L. Cavallo, D. P. Chong, L. Deng, R. M. Dickson, D. E. Ellis, M. van Faassen, L. Fan, T. H. Fischer, C. Fonseca Guerra, A. Ghysels, A. Giammona, S. J. A. van Gisbergen, A. W. Götz, J. A. Groeneveld, O. V. Gritsenko, M. Grüning, S. Gusarov, F. E. Harris, P. van den Hoek, C. R. Jacob, H. Jacobsen, L. Jensen, J. W. Kaminski, G. van Kessel, F. Kootstra, A. Kovalenko, M. V. Krykunov, E. van Lenthe, D. A. McCormack, A. Michalak, M. Mitoraj, J. Neugebauer, V. P. Nicu, L. Noodleman, V. P. Osinga, S. Patchkovskii, P. H. T. Philipsen, D. Post, C. C. Pye, W. Ravenek, J. I. Rodríguez, P. Ros, P. R. T. Schipper, G. Schreckenbach, J. S. Seldenthuis, M. Seth, J. G. Snijders, M. Solà, M. Swart, D. Swerhone, G. te Velde, P. Vernooijs, L. Versluis, L. Visscher, O. Visser, F. Wang, T. A. Wesolowski, E. M. van Wezenbeek, G. Wiesenekker, S. K. Wolff, T. K. Woo, A. L. Yakovlev, ADF2012, SCM, Theoretical Chemistry, Vrije Universiteit, Amsterdam, The Netherlands, http://www.scm.com

[21] M. Mitoraj, A. Michalak, T. Ziegler, J. Chem. Theory Comput. 5 (2009) 962.

Complexes **1**-**6** were prepared in reasonable yields by photochemical substitution of a carbonyl ligand with the free NHC ligand, generated in situ from the reaction between an imidazolium salt and [t]BuOK. The imidazolium salts (**L1**-**L3**) were prepared according to literature procedures [22]. The infrared (IR) spectrum of the complexes have been recorded using hexane as the solvent, and indicated the presence of two stretching frequencies. Both stretching frequencies are attributed to the carbonyl ligands of the $Mn(CO)_2$-moeity [4,5]. The observations of these stretching frequencies are supported by literature. The structural predictions were also confirmed with X-ray diffraction studies of three complexes and will be presented in the next sections.
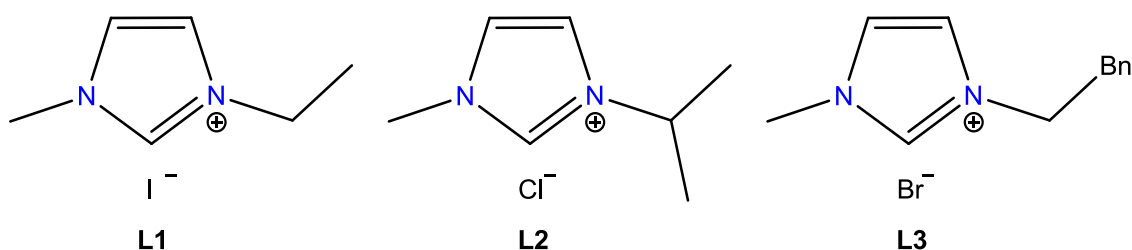
Figure 4: NHC ligands used in this study

3.2 Spectroscopic characterization

Using NMR spectroscopy, with CD_3CN as solvent, the structural aspects of the NHC complexes could be investigated. The ^{1}H NMR spectroscopic peaks for both the imidazolium salts and the complexated ligands had similarity in their spectral pattern and chemical shifts. The imidazolium ligand salts had a characteristic carbene carbon proton peak around δ = 9 ppm, which disappeared instantly upon deprotonation and coordination to the metal centres, indicating the formation of the desired carbene complexes. The protons peaks on the C4 and C5 ring positions of the imidazolylidene ligand of **1**-**6** were also clearly visible at chemical shifts between δ = 6.83 and δ = 7.46 ppm. The ^{13}C NMR of complexes **1**-**6** indicated the presence of a single distinct CO peak at *ca*. 235 ppm, a down-field shift of 10 ppm from the MMT and cymantrene starting synthons. The distinct carbene carbon peak can be witnessed at *ca.* 195 ppm. The NMR spectroscopy data is in accordance with literature [4,5]. The IR spectra of **1**-**6** were measured in hexane and indicated two stretching frequencies attributed to the cymantrenyl metal carbonyl stretching frequencies. The stretching frequencies for the two carbonyls ligands were observed at *ca*. 1850 (symmetric A') and 2020 (antisymmetric A'') cm^{-1}.

[22] F.P. Malan, E. Singleton, P.H. van Rooyen, M. Landman, J. Organomet. Chem. 813 (2016) 7.

3.3 Single crystal X-ray diffraction studies

Selected structural parameters are summarized in Table 1. The conformation of the carbene moiety, as represented by the C7-N1-C6-Mn dihedral angles, deviate from planarity by less than 1° (**3**, see Figure 5**)** and 7° (**6**, see Figure 6**)**. The carbene-metal bond lengths were determined to be 1.9904(17) Å and 1.990(3) Å respectively and seem to be insensitive to the size of the carbene substituents. The carbene-metal bond lengths are slightly shorter compared to published literature on symmetrical NHC MMT and cymantrenyl complexes [4]. The angles between the carbene plane (Mn, C6, N1 and N2) and the Cp ring were measured as 31.76° for **3** and 30.40° for **6** (Figure 7). Complex **6** crystallized with two molecular units (molecule A and molecule B) in the asymmetric unit and displays intramolecular hydrogen interactions between the carbene substituents and the carbonyl groups.
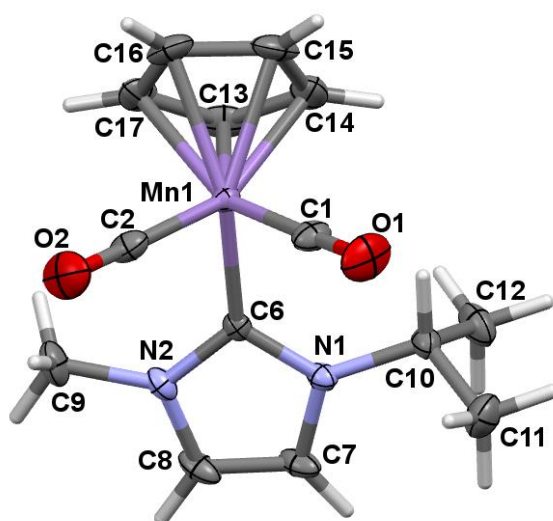
Figure 5: Perspective view of **3** with thermal ellipsoids drawn at the 50% probability level
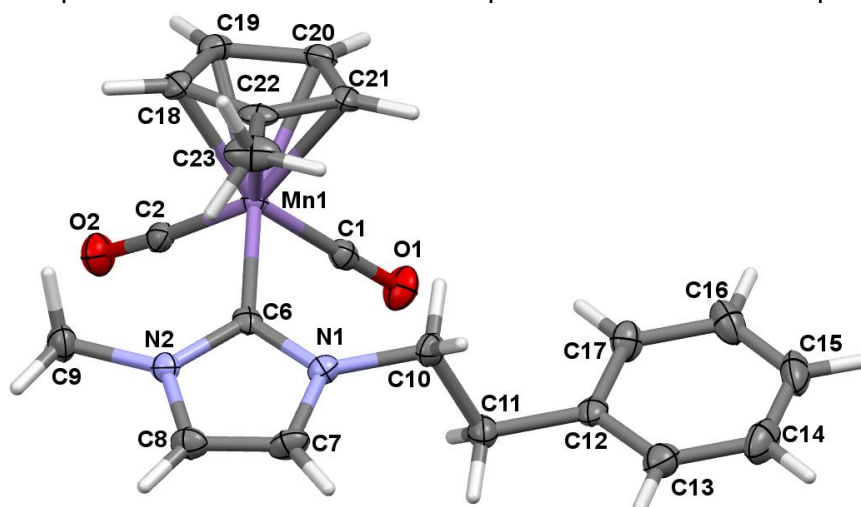
Figure 6: Perspective view of **6** (molecule A) with thermal ellipsoids drawn at the 50% probability level

121

Table 1: Selected bond lengths and angles

	3	**6[a]**
Bond length (Å)		
Mn-COx (x = 1-2)	1.7565(19)	1.761(4)
Mn-C6	1.9904(17)	1.990(3)
N1-C6	1.363(2)	1.373(4)
N2-C6	1.367(2)	1.377(5)
Bond angle (°)		
C1-Mn-C2	87.96(9)	89.44(15)
N1-C6-N2	103.08(14)	102.6(3)
N1-C6-Mn	128.79(12)	128.6(2)
N2-C6-Mn	128.12(12)	128.6(2)
Torsion angle (°)		
Mn-C6-N1-C7	-179.94(12)	-0.5(4)
Mn-C6-N2-C8	-179.97(12)	0.6(4)
Plane angle (°)		
Carbene/Cp	31.77	30.40

[a] Bond lengths and angles are average values calculated due to the presence of two units per asymmetric unit
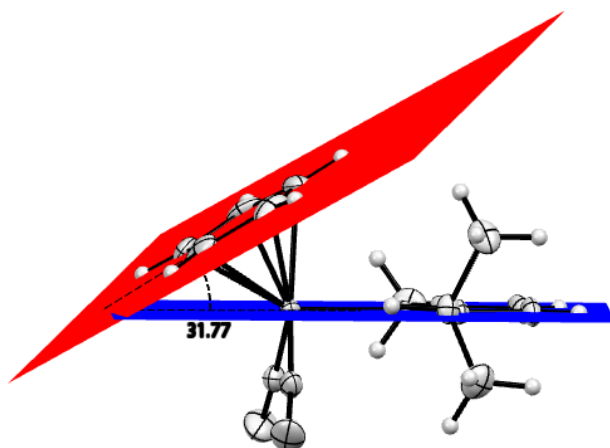
Figure 7: The angle (°) between the Cp and carbene planes of **3**

The incidence of hydrogen interactions can also be witnessed in both **3** and in **6** between the methyl group on the N substituent and the carbonyl ligands of the manganese metal atom. The presence of these hydrogen interactions will be quantified using the Extended Transition

122

State coupled with Natural Orbitals for Chemical Valence (ETS-NOCV) [21] energy decomposition technique in the DFT study section (Figure 8).
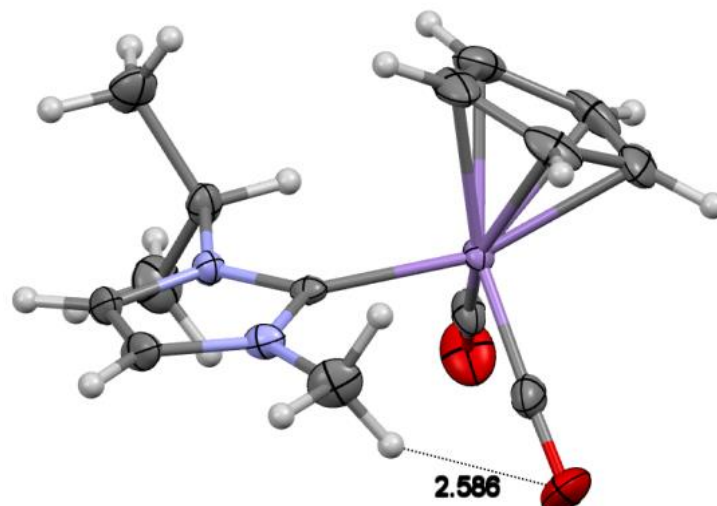
Figure 8: Hydrogen interactions (in Å) witnessed in **3**

During the synthesis of complex **C1** a single crystal, suitable for X-ray diffraction, was also obtained. **C1** crystallized in a P2₁/c space group and displays a linearly coordinated nitrile functionality (Figure 9). The Mn-N-C3 displays a bond angle of nearly 180⁰ (175.6⁰) and a C1-M-C2 bond angle of 91.37⁰ which is bigger compared to the NHC ligated complexes **3** and **6**.
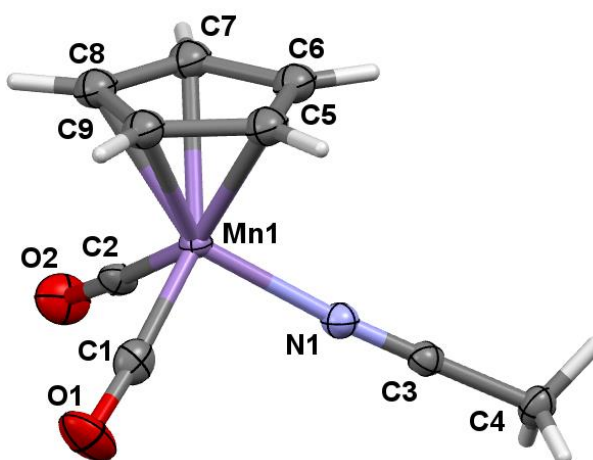
Figure 9: Perspective view of **C1** with thermal ellipsoids drawn at the 50% probability level

3.4 Theoretical study

Theoretical aspects of manganese carbene complexes are well described in literature [5,23,24]. Computational studies typically focus on the interactions of the frontier orbitals and the predictions that can be made from these interactions on the oxidation and reduction potential trends witnessed for metal centres [24]. Theoretical studies by Whittlesey [4] focused on aspects of agostic interactions witnessed in MMT NHC complexes. These studies have, however, been confined to electronic parameters and limited data have been provided on the steric aspects of NHC-substituted complexes of cymantrene and MMT. A DFT study has thus been considered to describe not only the electronic influences that the carbene moiety imparts on the coordination sphere of metal centres but also structural and steric influences by these ligands on the metal moiety. Complexes **1-6**, with increasing steric bulk on one of the nitrogen substituents of the carbene ligand, have been studied.

3.4.1 Ligand steric parameters

In this study the steric characteristics of NHC ligands have been determined using two different methods, namely the percentage buried volume ($\%V_{bur}$) and the solid angle measurement of the ligands. The $\%V_{bur}$ of a ligand is determined by defining the volume of a sphere, centred on the metallic centre, occupied only by the atoms of the NHC ligand (Figure 10) [25]. The $\%V_{bur}$ thus measures the steric space occupied by a ligand in the first coordination sphere of the metal centre [26]. Accordingly, increasing the bulkiness of the substituents on the N atoms of the ligand should result in a greater $\%V_{bur}$ in relation to the metal-ligand bond distance. We investigated the DFT-optimized geometries of a variety of NHC ligands by using the software developed and made freely available by Cavallo and co-workers [25]. The $\%V_{bur}$ was determined by taking the optimized metal-ligand bond distance, a sphere radius of 3.5 Å and a mesh spacing of $s = 0.05$ Å as advised by literature [25]. The $\%V_{bur}$ values were found to be similar irrespective of the identity or bulkiness of R-group substituents on the N atoms of the NHC ligands (26% for **L1**, 25% for **L2** and *ca.* 26% for **L3**). Due to size and rotation possibilities, steric repulsion is minimized by rotating the bulky substituents away from the coordination sphere of the manganese metal centre.

[23] N. Lugan, I. Fernández, R. Brousses, D.A. Valyaev, G. Lavigne, N.A. Ustynyuk. Dalton Trans. **42** (2013) 898.

[24] (a) B. Tumanskii, D. Sheberla, G. Molev, Y. Apeloig, Angew. Chem. Int. Ed. 46 (2007) 7408; (b) R. Fraser, P.H. van Rooyen, M. Landman, Polyhedron, 118 (2016) 133; (c) R. Fraser, P.H. van Rooyen, M. Landman, J. Coord. Chem. 69 (2016) 2972.

[25] H. Clavier, A. Correa, L. Cavallo, E.C. Escudero-Adán, J. Benet-Buchholz, A.M.Z. Slawin, S.P. Nolan, Eur. J. Inorg. Chem. (2009) 1767.

[26] A. Poater, B. Cosenza, A. Correa, S. Giudice, F. Ragone, V. Scarano, L. Cavallo, Eur. J. Inorg. Chem. (2009) 1759.
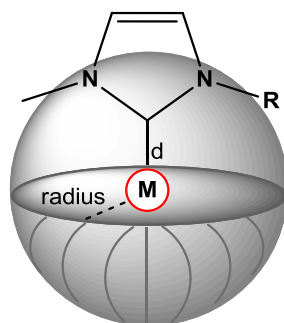
Figure 10: Graphical representation of the sphere defining the %V$_{bur}$ of metal complexes **1-6**

Although groups are increasingly bulkier, only hydrogen atoms are allowed to penetrate the coordination centre, while the alkyl and aryl groups are accommodated away from the coordination sphere, minimizing the steric requirements of the substituents. Since the %V$_{bur}$ of all the complexes are similar in value, and the NHC ligands occupy only a quarter of the total available space around the manganese atom, the deduction can be made that the steric demands of the NHC ligands have little consequence on available catalytic space.

Several other measurements of ligand steric parameters [27] have been attempted to establish a correlation between the steric bulk of a ligand and chemical and physical characteristics of inorganic and organometallic systems [28]. The use of solid angle parameters, where each ligand can be defined by the percentage of the coordination sphere of the central atom shielded by the ligand, has found application in describing the steric influences of ligands [29]. Using this approach, each ligand is expressed by a $G_M(L)$ value which is the percentage of the metal coordination sphere shielded by the particular ligand. The G_M(Complex) value defines the total shielding of the metal centre and is primarily suggestive of the total crowding and available ligation space surrounding the metal centre. The $G_{(\gamma)}$ value provides insights into the percentage of the metal sphere shielded by more than one ligand and generates overlapping regions of steric inaccessibility. Shielded regions would severely limit metal-substrate interactions and affect the catalytic potential of the pre-catalyst. The solid angle parameters are provided in Table 2.

[27]G.K. Fukin, I.A. Guzei, E.V. Baranov, J. Coord. Chem. 9 (2007) 937.
[28]I. Guzei, M.E. Sánchez-Castro, A. Ramirez-Monroy, M. Cervantes-Vásquez, I. R.A. Figueroa, M.A. Paz-Sand, Inorg. Chim. Acta. 359 (2006) 701
[29]I.A. Guzei, M. Wendt, Dalton Trans. (2006) 3991.
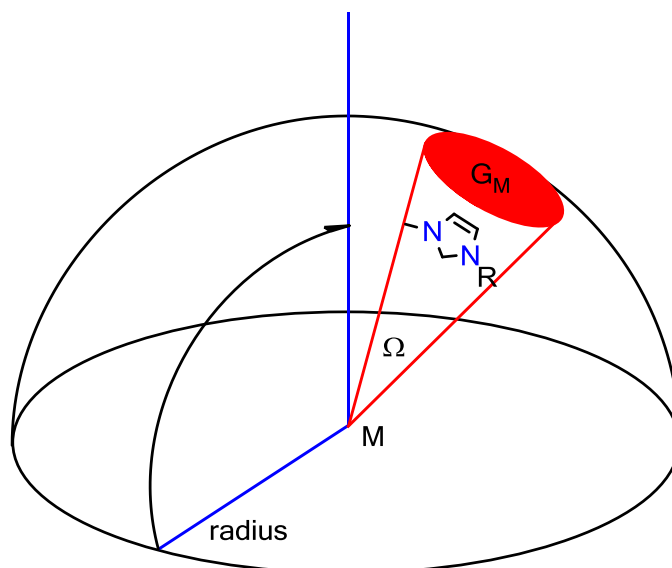
Figure 11: Representation of the solid angle and G_M of a complex

Table 2: Solid angle parameters for **1-6**

Ligand	Complex	Solid Angle Steradians[a]	G_M(Complex) %	$G_{(\gamma)}$ %
1	1	3.11	96.88	12.89
1	2	3.20	96.91	13.19
2	3	3.06	96.70	13.87
2	4	3.18	96.93	14.14
3	5	3.34	96.35	15.50
3	6	3.34	96.55	16.03
	$CpMn(CO)_3$	-	97.07	16.66
	$MeCpMn(CO)_3$	-	95.41	12.08

a: Solid angle of the NHC ligand

The G_M of **1**, **3**, **5** and the cymantrene starting synthon have been visualized and presented in Figure 12.
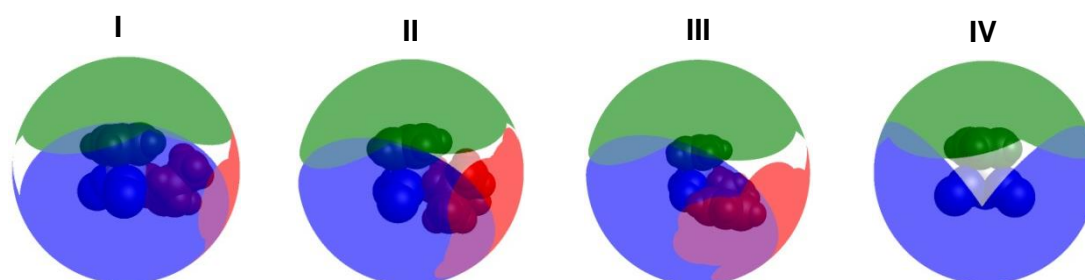
Figure 12: The G_M(Complex) of **1** (I), **3** (II) and **5** (III) and $CpMn(CO)_3$ (IV)

The solid angles of **1-6** indicate the size of the ligand increases in the order of **L1 ≈ L2 < L3**. The G_M and $G_{(Y)}$ of the cymantrenyl synthon has also been calculated and indicates a small decrease in both parameters after the coordination of the NHC moiety. As expected, the G_M and $G_{(Y)}$ increase when two ethyl groups occupy the carbene nitrogen substituents positions compared to the ethyl methyl substituted ligand Figure 13. The $G_{(M)}$ predictions for **1-6** have similar values as also seen in the %V_{bur}. Although the solid angles indicate a similar size of **L1** and **L2**, the increasing $G_{(Y)}$ values is indicative of increasing steric bulk of the ligands in the order of **L1 < L2 < L3**.

II	I	III
G_M = 98.01%	G_M = 95.41%	G_M = 96.91%
$G_{(Y)}$ = 18.94 %	$G_{(Y)}$ = 12.08 %	$G_{(Y)}$ = 13.19 %
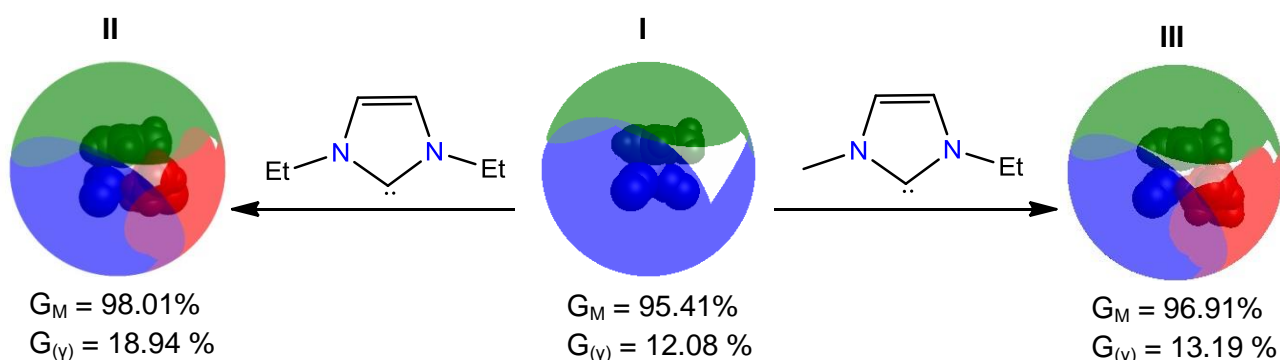
Figure 13: Solid angle parameters of the MeCpMn(CO)$_3$ (I), diethyl substituted NHC (II) and complex **2** (III)

3.4.2   Wiberg bond indices

Literature exists for the determination and applicability of Wiberg bond orders in the endeavour to study NHC ligands [30, 31] and the coordination to metal centres [32,33]. The Wiberg bond indices quantified single or double bond character and can be utilized to determine bond strength orders (BSOs). From our calculated results, the Wiberg bond indices (Table 3) indicate a relatively strong sigma-donation from the NHC ligand towards the metal centre. The indices are similar in all the NHC complexes and show no variation despite steric difference between the carbene nitrogen substituents. The bonding interaction of the NHC ligands was determined to be similar to that of phosphine ligands (M-L bond order of 0.77) and stronger in comparison to the nitrile ligand analogues such as **C1** (BO = 0.66). These values are, however, in line with reported literature values [32].

[30] D.M. Andrada, N. Holzmann, T. Hamadi, G. Frenking, Beilstein J. Org. Chem. 11 (2015) 2727.

[31] D. Setiawan, R. Kalescky, E. Kraka, D. Cremer, Inorg, Chem. 55 (2016) 2332.

[32] A. Baishya, V.R. Mundlapati, S. Nembenna, H.S. Biswal, J. Chem. Sci. 126 (2014) 1781.

[33] G. Occhipinti, H. Bjørsvik, K.W. Törnroos, A. Fürstner, V.R. Jensen, Organometallics 26 (2007) 4383.

3.4.3   Bond dissociation energies (BDEs)

Table 3: Wiberg bond indices and BDE for complexes **1-6**

Complex	M-C$_{Carb}$ BO	C$_{Carb}$-N$_1$ BO	C$_{Carb}$-N$_2$ BO	BDE kJ·mol^{-1}
1	0.73	1.03	1.03	-191.09
2	0.77	1.25	1.25	-187.65
3	0.77	1.26	1.25	-193.16
4	0.77	1.26	1.25	-189.65
5	0.78	1.25	1.25	-197.79
6	0.77	1.25	1.25	-194.87

Bond dissociation energy (BDE) is defined as the change in enthalpy at 298 K and 101.3 kPa for the gas-phase reaction as defined by A-B(g) → A•(g) + B•(g) [34]. Although DFT methods tend to systematically underestimate the absolute bond dissociations, estimations based on these models are still applicable in the comparison of molecules and ligand systems. The bond dissociation energies for **1-6** are listed in Table 3. From the data presented, NHC ligands bound more tightly towards the manganese centre bearing cyclopentadienyl ligands compared to the methylcyclopentadienyl analogues. NHC ligands with ethyl phenyl substituents had greater BDEs followed by isopropyl and finally ethyl groups respectively (Figure 14). The dissociation energies thus decreases in the following trend CpMn-**L3** > MeCpMn-**L3** > CpMn-**L2** > MeCpMn-**L2** > CpMn-**L1** > MeCpMn-**L1**.

BO: 0.76
BDE: +194.01 kJ.mol^{-1}

BO: 0.77
BDE: +139.59 kJ.mol^{-1}

BO: 0.66
BDE: +112.51 kJ.mol^{-1}
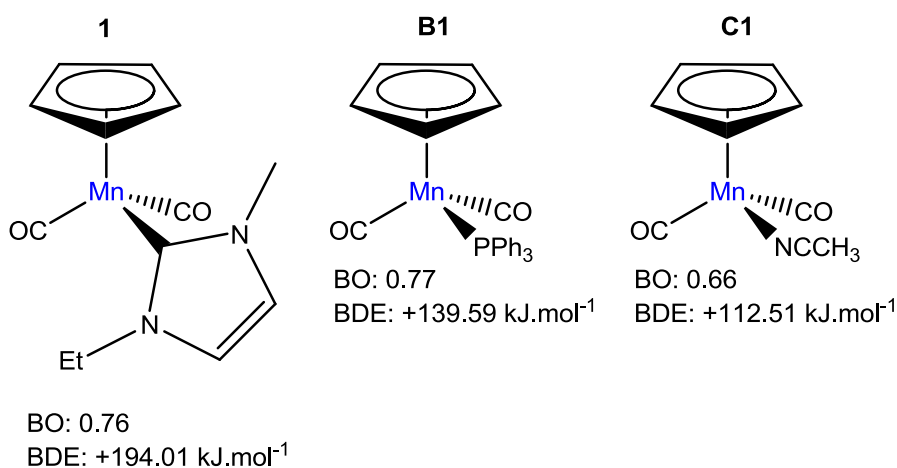
Figure 14: Wiberg bond indices and BDE of NHC complexes (**1**), phosphines (**B1**) and acetonitriles (**C1**)

[34] Qi, X., Feng, Y., Liu, L., Guo, Q., Chin. J. Chem. 23 (2005) 194.

The average bond dissociation energy for the NHC ligands were significantly greater compared to both phosphine and nitrile ligands despite the similarity in Wiberg bond orders. The heightened BDEs are ascribed to the superior coordination interactions offered by NHC ligands. The existence of a linear relationship between the molar mass of the NHC ligand and the bond dissociation enthalpy was determined in this study (Figure 15). Complexes with larger substituents on the nitrogen backbone of the ligands displayed greater BDE compared to smaller substituents. This finding is supported by literature and the steric effects of the heteroatomic substituents are well described. Increasing the bulkiness of the nitrogen substituents leads to increases in the stability of the NHC ligands and greater donation to the ligated metal centre.
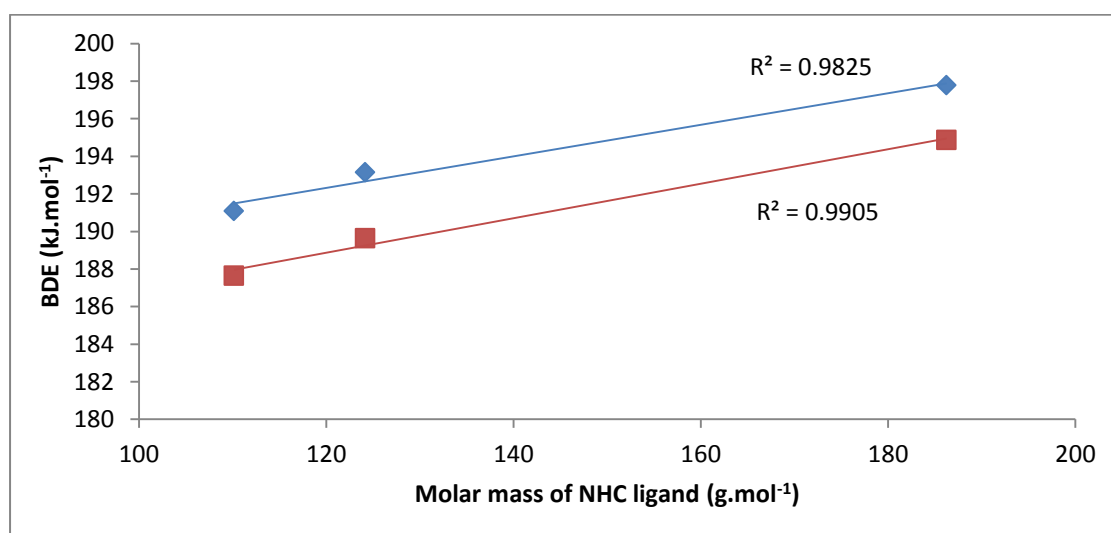
Figure 15: Correlation between the molar mass of the complexes (blue - cymantrenyl, red - MMT) and BDE

3.4.4 Extended Transition State coupled with Natural Orbitals for Chemical Valence (ETS-NOCV)

ETS-NOCV is a powerful computational tool with which the formation of an M–C bond can be investigated and analysed in terms of the absorbed or released interaction energy, ΔE_{Int}, as well as the change in electron density, commonly known as the deformation density, $\Delta\rho$, associated with bond formation [20,21]. Both ΔE_{Int} and $\Delta\rho$ can be decomposed into different components to aid interpretation of a bond formation process. The interaction energy can be decomposed into three terms,

$$\Delta E_{Int} = \Delta E_{Elstat} + \Delta E_{Pauli} + \Delta E_{Orb} + \Delta E_{Disp} \tag{1}$$

where ΔE_{Elstat} gives the change in electrostatic energy upon bringing unperturbed promolecules from an infinite separation to the final bonding distance, ΔE_{Pauli} gives the

129

change in energy required to orthogonalize (ensuring antisymmetry) the promolecular (ensuring antisymmetry) wavefunctions and is commonly known as Pauli repulsion, ΔE_{Orb} gives the change in energy related to the minimization of the energy of the final structure and is commonly known as the orbital interaction term and ΔE_{Disp} is the dispersion energy, usually calculated through empirically-derived functionals. The electrostatic and Pauli energy changes are often combined into a single value, ΔE_{Steric}, to give an indication of the steric (electrostatic + electronic) interaction between promolecules. Similarly, the deformation density can be decomposed into two terms,

$$\Delta \rho = \Delta \rho_{Pauli} + \Delta \rho_{Orb} \qquad (2)$$

where each terms gives the change in density associated with the energetic term of Eq. 1 (no density change is observed with the change in electrostatic energy) [20,21]. The various decomposition terms of Eq. 1 can be used to compare the properties associated with the formation of different M–C bonds, and the associated density changes can be used for visual inspection [20,21]. Of more interest to us, however, is the further decomposition of the ΔE_{Orb} and $\Delta \rho_{Orb}$ terms into contributions from natural orbitals, as given by the NOCV addition to ETS. Specifically, the total $\Delta \rho_{Orb}$ term can be decomposed into i natural orbitals,

$$\Delta \rho_{Orb} = \sum_{i} \Delta \rho_{i} \qquad (3)$$

and each NOCV channel is associated with a specific change in energy, ΔE^{i}_{Orb}. The highest occupied NOCV channels can usually be associated with specific components of molecular orbital interactions between promolecules, such as σ and π bonding, giving associated deformation density channels and energy changes for these components, i.e. $\Delta \rho_{\sigma}$ and ΔE^{σ}_{Orb} describing a σ-bonding component of an M–C bond [20,21]. These features of the ETS-NOCV approach allow qualitative as well as quantitative comparison of specific attributes of different M–C bonds in various systems [20,21].

The formation of various Mn–L bonds in **1**, **B1** and **C1** was investigated theoretically using ETS-NOCV. Of primary interest is the various NOCV channels of each Mn–L bond, describing the density and energy changes of specific (σ and π) attributes of each bond. The primary NOCV channels for the NHC (structure **1**) are shown in Figure 16. $\Delta \rho \sigma$ describes the clear σ-donation from the ligand to the metal with an associated energy change of –146.86 kJ·mol^{-1}, whereas $\Delta \rho \pi 1$ and $\Delta \rho \pi 2$ describe the π-back donation from metal to ligand for two different axes, with a combined energy contribution of –59.50 kJ·mol^{-1}. Finally, $\Delta \rho_{4}$ shows the formation of two hydrogen CH⋯C interactions, contributing –5.69 kJ·mol^{-1} to the total interaction energy. The NOCV channels for the remaining structures **B1** and **C1** are

qualitatively very similar, except for the lack of CH···C interactions in **C1**. The presence of hydrogen interactions was also witnessed in the solid-state crystal structures of **3** and **6**.

$$\Delta\rho_\sigma \qquad\qquad \Delta\rho_{\pi1}$$

$$\Delta E_{Orb}^{\sigma} = -146.9\,\mathrm{kJ\cdot mol^{-1}} \qquad \Delta E_{Orb}^{\pi1} = -37.4\,\mathrm{kJ\cdot mol^{-1}}$$

$$\Delta\rho_{\pi2} \qquad\qquad \Delta\rho_4$$

$$\Delta E_{Orb}^{\pi2} = -22.1\,\mathrm{kJ\cdot mol^{-1}} \qquad \Delta E_{Orb}^{4} = -5.7\,\mathrm{kJ\cdot mol^{-1}}$$
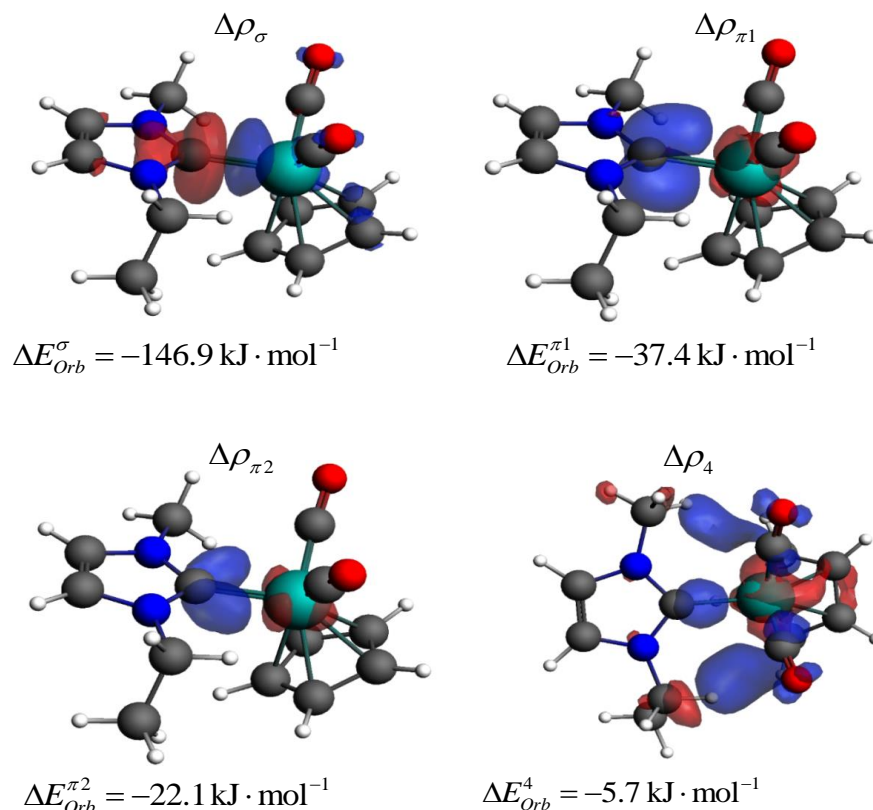
Figure 16: Primary NOCV channels and associated orbital energy changes for **1**. Blue and red regions indicate an accumulation and depletion of electron density, respectively. Isosurfaces for Δρ$_\sigma$, Δρ$_{π1}$, Δρ$_{π2}$ and Δ$_{ρ4}$ are 0.002 au, 0.001 au, 0.001 au and 0.00015 au, respectively

In Table 4, decomposition of the total interaction energy into relevant components for each structure is shown; for a complete ETS-NOCV decomposition, please see Table S1 in the Supplementary Information. Comparing first the total interaction energies, ΔE_{Int} , **1** forms the strongest M–L bond, with the phosphine **B1** and the acetonitrile **C1** weaker by +29.12 and +125.10 kJ·mol^{-1}, respectively. The biggest contribution to the strength of **1** is a very large electrostatic contribution (–485.26 kJ·mol^{-1} as opposed to –348.61 and –227.61 kJ·mol^{-1} in **B1** and **C1**, respectively, as seen in Table 4). Electronically, however, **1** and **B1** is equivalent, with a total orbital interaction of –233.47 and –237.61 kJ·mol^{-1}, respectively. Interestingly, the σ-donation of both **1** and **B1** is very similar (differing by –7.41 kJ·mol^{-1} in favour of **1**) but **1** experiences considerably weaker π-back bonding (differing by -16.78 kJ·mol^{-1} in favour of **B1**). On the other hand, **B1** and **C1** show equivalent π contributions, but **C1** forms a considerably weaker σ bond than the other structures. Therefore, the combination of large electrostatic attractions coupled with comparatively small electronic

131

steric repulsions result in **1** forming a stronger M–L bond than **B1**, despite comparative orbital and dispersion interactions.

Table 4: Selected ETS-NOCV energy contributions

	ΔE_{Int} [a]	ΔE_{Elstat} [a]	ΔE_{Pauli} [a]	ΔE_{Steric} [a]	ΔE_{Orb} [a]	ΔE_{Disp} [a]
1	–276.14	–485.26	+493.96	+8.70	–233.47	–51.35
B1	–247.02	–348.61	+405.68	+57.07	–237.61	–66.46
C1	–151.04	–227.61	+265.27	+37.66	–173.64	–15.21

[a] All values in kJ·mol^{-1}

	ΔE^{σ}_{Orb} [a]	ΔE^{π}_{Orb} [a]	σ/π [b]	%σ [c]	%π [d]
1	–35.10	–14.22	*2.47*	53%	22%
B1	–33.33	–18.23	*1.83*	56%	31%
C1	–20.40	–18.40	*1.11*	13%	12%

[a] All values in kJ·mol^{-1}
[b] Ratio of ΔE^{σ}_{Orb} over ΔE^{π}_{Orb}
[c] Percentage of σ contribution to ΔE_{Int}
[d] Percentage of π contribution to ΔE_{Int}

The ratio of the σ contributions over π contributions for each structure is shown in Table 4. This metric gives us a direct indication of the relative σ-donation over π-back bonding capability of each system. Clearly, **1** shows by far the most σ character (2.47 times more σ-bonding than π-bonding), whereas the phosphine **B1** is slightly more prevalent for σ-bonding (1.83) and the **C1** is more or less equivalent for both σ and π (1.11). However, since the total interaction energies of each system differ, the final columns of Table 4 present each attribute of bonding as a percentage of the total interaction energy, allowing direct comparison between different ligands.

Complexes **1** and **B1** are equivalent σ-donors, with 53% and 56% of the total binding energy originating from σ-donation, respectively. However, **1** shows considerably less π character than **B1**, with 22% π-back donation for **1** and 31% for **B1**. The acetonitrile **C1** shows equivalent σ and π character (13% and 12%, respectively), and overall lower contributions from electronic interactions. The remaining contributions to the total interaction energy includes energetically weaker electronic interactions (such as weak non-covalent

interactions and various polarizations), as well as stearic effects (including electrostatic interactions and Pauli repulsion). The stronger M-L bond in **1** illustrates the superior ability of the NHC ligand to stabilize the metal centres compared to phosphine and acetonitrile ligands. The ETS-NOCV results also mirror findings of the bond dissociation energies were NHC-M complexes displaying significantly stronger M-L bonds.

3.4.5   Frontier orbital analysis

The calculated energy levels and energy gaps for the frontier orbitals of the studied complexes are presented in Figure 17. The band gap between the frontier orbitals is indicative of the stability and reactivity of transition metal complexes [35]. In this study, band gaps of between 5.11 and 5.48 eV were determined for the complexes, with the greatest differences witnessed for **5** and **6**. The highest molecular orbital (HOMO) was positioned on the metal d-orbital for all the complexes and the lowest unoccupied molecular orbital (LUMO) positioned on the carbene carbon atom for complexes **1**-**4**.

Adding aromatic groups to the NHC nitrogen substituent displaces the LUMO towards the aromatic moiety. The biggest contributor to the LUMO was found to be the *ipso*-carbon atom, followed by the contribution of the *para*-carbon atom for **5** and **6**. The $4p_z$ orbital contributed significantly towards the LUMO for all the complexes. The frontier orbital band gap indicated no correlation between wave length and complex colour. According to theoretical findings, the complexes should absorb light in the UV spectrum of light and thus should present as colourless complexes. Experimental findings indicate yellow-orange coloured complexes. Band gap analysis also indicates greater stability and lower reactivity for **5** and **6** and higher reactivity of NHC complexes of MMT compared to cymantrenyl synthons. The average band gap difference between cymantrenyl and MMT complexes was found to be 0.047 eV (4.44 kJ·mol^{-1}).

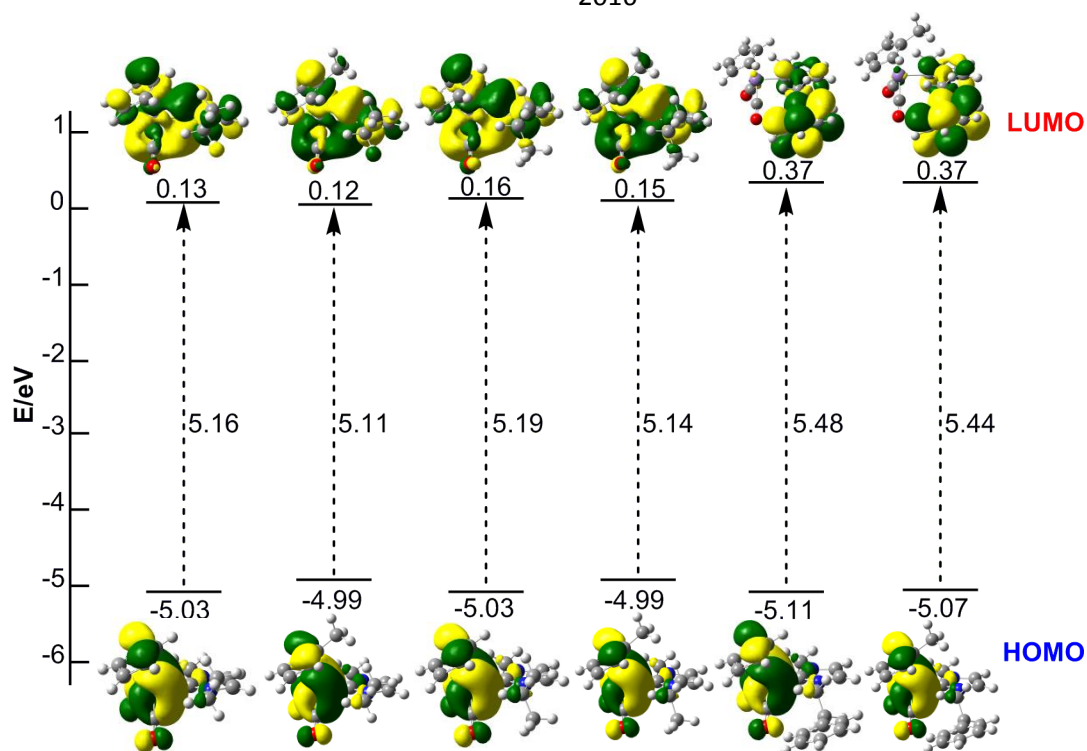[35] J.S. Griffith, L.E. Orgel, Q. Rev. Chem. Soc. 11 (1957) 381.

2016

Figure 17: Energy levels, energy gaps (in eV), and orbital composition distributions of the frontier orbitals of complexes **1-6**

3.5 Catalytic study

Organosulfur chemistry has always been of particular interest both in the field of chemistry and biology [36]. The transformation of sulfur-containing compounds has attracted much research interest and specifically the oxidation of thiols to disulfides has remained an area of importance [37]. Reactions focussing explicitly on the dimerization of sulfides into disulfides normally require a basic catalyst [38], stoichiometric amounts of oxidants [39] or toxic reagent and long reaction times. Apart from the high demand of these reaction conditions, many synthetic methodologies generate elevated levels of unwanted side-products. The side-products are commonly produced as a result from over oxidation, producing sulfoxides, sulfones, thiosulfinates and thiosulfonates [40-42]. Literature examples have been reported for the employment of rhodium(I) transition-metal complexes that illustrated the ability to selectively oxidize thiols into disulfides as an attractive alternative to the use of hazardous oxidants [43], but such processes have been fairly unexploited. The UV photolysis of

[36] R.J. Cremlyn, An Introduction to Organosulfur Chemistry, Wiley: New York, (1996).
[37] G.H. Whitham, *Organosulfur Chemistry*, Oxford University Press: Oxford (1995).
[38] A.V. Joshi, S. Bhusare, M. Baidossi, N. Qafisheh, Y. Sasson, Tetrahedron Lett. 46 (2005) 3583.
[39] A.R. Ramesha, S. Chandrasekaran, J. Org. Chem. 59 (1994) 1354.
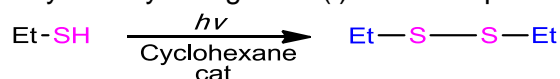[40] N. Iranpoor, D. Mohajer, A.R. Rezaeifard, Tetrahedron Lett. 19 (2004) 3811.
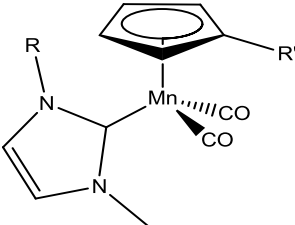[41] F. Freeman, C.N. Angeletakis, J. Am. Chem. Soc. 105 (1983) 4039.
[42] F. Lazzaro, M. Crucianelli, F.D. Angelis, V. Neri, R. Saladino, Tetrahedron Lett. 45 (2004) 9237.
[43] K.Y.D. Tan, J.W. Kee, W. Y. Fan, Organometallics 29 (2010) 4459.

cymantrene with thiols at room temperature offered a viable, greener alternative to classic published method of dimerization of thiols and produced H_2 as the only side product [43]. Although the dimerization of thiols have been investigated, the extension to the catalytic potential of functionalized cymantrene and MMT complexes towards dimerization of more complex molecules has been mostly ignored. Pre-catalysts **1**-**6** have been investigated for application in the dimerization of thiols into disulfides[39]. Based on literature [43] and for purposes of the simple comparison of %V_{bur} and solid angle predictions to experimental obtainable results, 3 mol% of catalyst, in the presence of the substrate and cyclohexane were photo-irradiated in an inert argon atmosphere for the duration of 2.5 hours to test for catalytic activity.

Table 5: Dimerization of ethylthiol by manganese(I) NHC complexes **1-6**

Catalyst[a]	Complex	R	R'	Cat. (mol%)	Conversion[b] (%)
	1	Et	H	3	28
	2	Et	Me	3	22
	3	^{i}Pr	H	3	16
	4	^{i}Pr	Me	3	6
	5	EtPh	H	3	47
	6	EtPh	Me	3	48

[a] General reaction conditions: Ethylthiol (2.0 mmole), Catalyst (0.06 mmole), Cyclohexane (10 ml), Room temperature, 150 min.
[b] Conversion based on internal standard.

All six complexes displayed catalytic activity in the dimerization of thiols into disulfides (Table 5). Although lower yields were obtained for complexes **3** and **4**, complexes **5** and **6** displayed superior activity with yields of (*ca.* 47%) and turn over frequencies (TOF) of 49 h^{-1}. The obtained yields were lower in comparison to literature [43] (*ca.* 99% for alkyl thiols) for the CpMn(CO)$_3$-photoconversion of thiols. Complexes displayed diminished activity over the 150 min reaction period, which might indicate the decomposition of the catalysis under the harsh photo-irradiation conditions. The higher catalytic activity of **5** and **6** could thus be explained by the greater stability of these complexes where decomposition is concerned, displaying higher BDE of the metal-carbene bond and slightly larger HOMO-LUMO band gaps. The dimerization occurs through the substitution of a carbonyl ligand for an ethylthiol group. The ligand exchange can occur at two different carbonyl ligand positions in reference to the

135

substituents on the NHC ligand. Bond dissociation energies of the metal-carbonyl bonds indicate similar dissociation energies for carbonyl ligands CO_a and CO_b (Figure 18). It can thus be hypothesized that ligand exchange could occur at either carbonyl ligand to initiate the catalytic cycle.
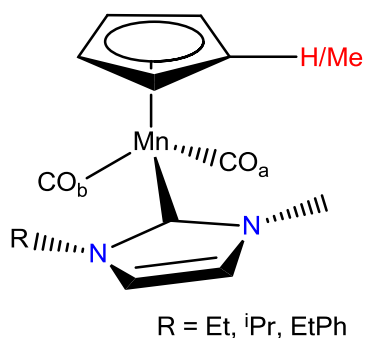

R = Et, ^{i}Pr, EtPh

Figure 18: Possible carbonyl substitution positions CO_a and CO_b available on **1-6**

The ligand steric parameter results indicate that the steric trend increases in the order **L1** < **L2** < **L3** and literature associates the steric influences of NHC substituents with the greater stability these ligands afford to the metal moiety. The solid angle and %V_{bur} parameters thus correlate with the stability associated with the pre-catalysts and therefore might suggest a probable explanation for the catalytic activity witnessed. Although the ligands increase in bulkiness, the steric groups do not directly influence the coordination space of the metal moiety (as indicated by the solid angle). The ligands thus afford greater stability while not crowding the metal atom. Complexes **5** and **6** contain the most steric ligand **L3**, according to the steric parameters, which then implies that the most stable complexes were found to have the best catalytic activity. A feasible catalytic cycle is proposed in Figure 19, describing the catalytic conversion of the thiol substrates into disulfides. The cycle is based on experimental data obtained from the similar study on the dimerization of thiols using cymantrene only as catalyst [39]. The cycle is initiated with the photo-induced substitution of a carbonyl ligand for a thiol substrate and terminates with the liberation of disulfides and the regeneration of the active catalyst species. The process is dependent on the availability and lability of carbonyl ligands of the pre-catalyst species and thus might explain the lower activity of our pre-catalysts in comparison with the cymantrene analogue.
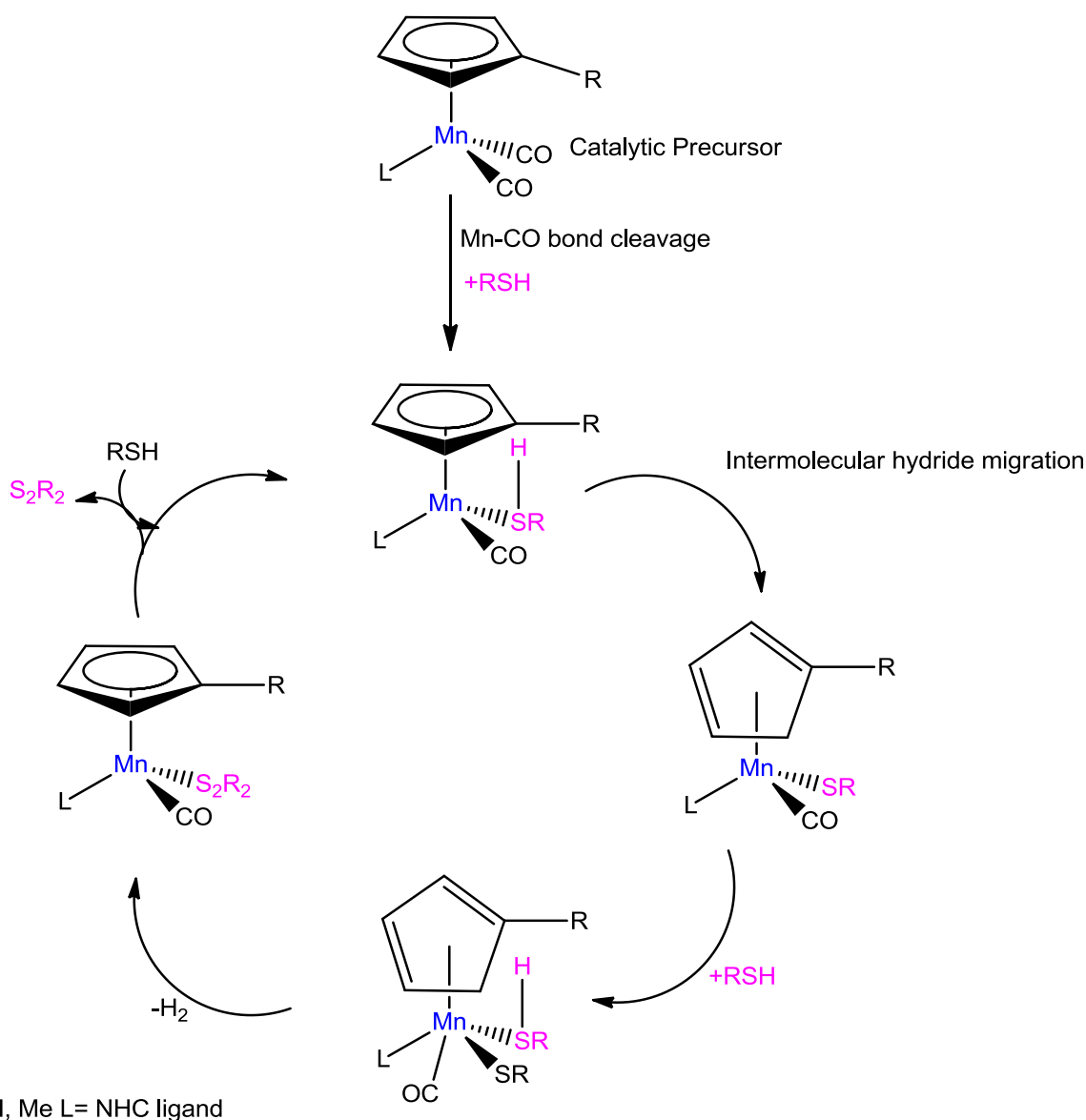
Figure 19: Catalytic cycle associated with the dimerization of thiol substrates

4   Conclusion

NHC complexes **1-6** were synthesized in satisfactory yields from MMT and cymantrenyl synthons. The molecular structures of the novel complexes were confirmed with NMR and IR spectroscopy, and single crystal X-ray diffraction studies of **3** and **6**. Through DFT calculations, it was possible to describe the steric influences the NHC ligands impose on the metal synthon. Wiberg bond indices indicated orders of *ca.* 0.7 for the NHC complexes, which is similar to bonding aspects of triphenylphosphine. Both ligands thus display negligible π-back donation from the metal centre. The frontier orbital analysis indicated increases in the band gaps upon the substitution of NHC ligands with larger molecular masses. Lower mass ligands had smaller

band gaps. The increases in the band gaps may indicate higher stability of complexes **5** and **6** or greater inertness towards decomposition pathways. Finally, BDE energies indicated a linear relationship between the associated energies and the molar mass of the NHC moiety. The BDE of the NHC-metal bonds were higher in cymantrenyl complexes compared to MMT analogues.

7 Bonding aspects of Group VII transition metal carbene complexes
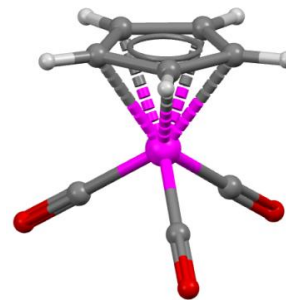
7.1 Overview:

Since the elucidation of the correct structure of King's complex by Casey [1] as that of a carbene complex, numerous new examples of group VII transition metal Fischer carbene complex have emerged in literature [2]. Structural aspects of these mono- and dinuclear carbene complexes have also been examined and a few examples of modification to the metal and ligand spheres have been reported in recent years [3]. With the isolation of the first free N-heterocyclic carbenes (NHCs) focus have, however, shifted to prospects of finding new synthetic routes to produce novel NHC complexes of group VII transition metals [4]. In comparison to group VI transition metal carbene complexes, group VII metal carbenes complexes (Fischer and N-heterocyclic carbenes) have been fairly neglected. The synthesis of di- and trinuclear Group VII transition metal Fischer-type carbene complexes have recently been reported by our research group and in correlation with literature (chapter 2), the carbene ligand is found in the axial position in dimanganese carbonyl complex and equatorial in the rhenium analogue [5]. Examples of equatorial dimanganese carbene complexes are rarely seen in literature since bulky carbene substituents and the shorter metal-metal bond cause steric interference in the equatorial positions. In contrast, dirhenium Fischer carbene complexes contain an elongated metal-metal bond and the crowded equatorial position is favoured, even with bulkier carbene substituents. Computational

[1] R.B. King, J. Am. Chem. Soc. 85 (1963) 1922.
[2] (a) E.O. Fischer, A. Maasböl, Angew. Chem. Int. Ed. Engl. 3 (1964) 580; (b) D.I. Bezuidenhout, S. Lotz, D.C. Liles, B. Van der Westhuizen, Coord. Chem. Rev. 256 (2012) 479; (c) M. Landman, R. Pretorius, R. Fraser, B.E. Buitendach, M.M. Conradie, P.H. van Rooyen, J. Conradie. Electrochim. Acta. 130 (2014) 104; (d) A. Arrieta, F.P. Cossío, I. Fernández, M. Gómez-Gallego, B. Lecea, M.J. Mancheño, M.A. Sierra, J. Am. Chem. Soc. 122 (2000) 11509; (e) M. Landman, R. Liu, R. Fraser, P.H. van Rooyen, J. Conradie. J. Organomet. Chem. 752 (2014) 171.
[3] K.H. Dötz, J. Stendel, Chem. Rev. 109 (2009) 3227.
[4] (a) O. Kaufhold, A, Stasch, T. Pape, A. Hepp, P.G. Edwards, P.D. Newman, F.E. Hahn. J. Am. Chem. Soc. 131 (2008) 306; (b) J. Ruiz, A. Berros, B.F. Perandones, M. Vivanco. Dalton Trans. (2009) 6999.
[5] R. Fraser, P.H van Rooyen, M. Landman. J. Mol. Struct. 1105 (2016) 178.

insights into the electronics and structural aspects of the metal-carbene and the carbene-substituent bonds have been presented by Frenking [6] and Chan [7] and indicated a historical misunderstanding of the bond order between the metal-carbene bonds found in Fischer carbene complexes. Theoretical calculations indicate limited back-donation from the metal centre to the empty p_z orbital of the singlet carbene centre, which is in stern contrast to the historical consideration of a formal double bond character between the two centres. Calculation indicate that the σ-donation to π-back-donation ratio of Fischer carbene complexes are significantly higher compared to NHC carbene complexes but bond order calculation of both carbene types reflect single bond rather than double bond character. Figure 1 displays the change in metal-carbene back-donation when the heteroatom substituent is varied in Fischer carbene complexes from the perspective of electron donation to the carbene carbon atom.
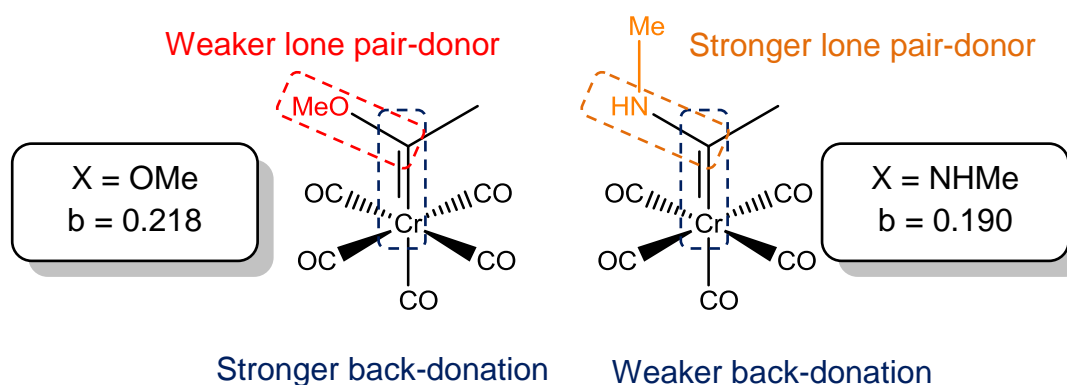

Figure 1: The change in the metal-carbene back-donation (b) witnessed for alkoxy- and aminocarbene complexes

Changes in the ratio of donation to back–donation (b) is evident in experimental results published [8], specifically when one considers the fluctuation in metal-carbene and carbene-heteroatom bond lengths of carbene complexes of group VI and VII transition metals. Experimental bond lengths of the ethoxy-carbene complexes for a specific metal tend to be longer compared to their aminocarbene analogues and display less π-donation from the heteroatom substituent to the carbene moiety [9]. Subsequently, the carbene-metal bond length shortens due to additional back-donation provided from the metal centre to the electrophillic carbene [9]. Complimentary studies by Poater [10] found the σ-donation from

---

[6] G. Frenking, M. Solà, S. F. Vyboishchikov. J. Organomet. Chem. 690 (2005) 6178.

[7] W. M Xue, M.C.W. Chan, Z.M. Su, K.K. Cheung, S.T. Liu, C.M. Che, Organometallics 17 (1998) 1622.

[8] (a) S. Thompson, H.R. Wessels, R. Fraser, P.H. van Rooyen, D.C. Liles, M. Landman. J. Mol. Struct. 1060 (2014) 111; (b) M. Landman, R. Pretorius, B.E. Buitendach, P.H. van Rooyen, J. Conradie. Organometallics 32 (2013) 5491; (c) S. Lotz, M. Landman, D.I. Bezuidenhout, A.J. Olivier, D.C. Liles, P.H. van Rooyen, J. Organomet. Chem. 690 (2005) 5929.

[9] D.I. Bezuidenhout, D.C. Liles, P.H. van Rooyen, S. Lotz, J. Organomet. Chem. 692 (2007) 774.

[10] J. Poater, M, Cases, X. Fradera, M. Duran, M. Solà, Chem. Phys. 294 (2003) 129.

the carbene ligand to be significantly stronger than the back-donation from the $M(CO)_5$ fragment in Fischer carbene complexes. In general it was found that back-donation from the metal moiety, as defined by charge decomposition analysis (CDA) [11] and energy decomposition analysis (EDA) [12] methods, is proportional to the $M\text{-}CO_{trans}$ distance and inversely proportional to the M-C(carbene) distance. In comparison, Group VI metal-NHC bond distances have been found to be mostly influenced by σ-donation of the ligand to the metal centre with only 17-18% of the overall orbital interaction attributed to M→NHC π-back-donation [13].

7.1.1 Bonding Models of Carbene complexes

Comparative studies between metal carbene complexes have mainly focused on single parameters either concentrating on the effect of changing the metallic centre or the derivatization of the carbene ligand [14]. These studies are unfortunately restricted to Fischer-type carbene complexes of group VI transition metals or NHC complexes of late transition metals, while limited mention is made of the bonding characteristics of group VII mono- and dimetallic monocarbene complexes. This lack of information in literature is surprising since Fischer-type and N-heterocyclic carbene complexes display similar bonding models. The typically accepted bonding model employs the singlet state of the ground state multiplicities of the fragments CR_2 and L_nM as building synthons for the Fischer-type and N-heterocyclic carbene complexes [15]. Donation of electron density occurs through σ-donation towards the metallic moiety and in both models the carbene carbon atom is electrophillic in nature and receives additional electron density from neighbouring heteroatoms [16]. The Dewar-Chatt-Duncanson (DCD) model defines the synergic interactions observed in the Fischer carbene bond as a primary interaction of a σ-donation from the sp^2 orbital on the carbene carbon atom to the metal σ-hybrid orbital, and π-back-donation from the metal d-orbitals to the empty unhybridized p-orbital on the carbene carbon atom. In models applied to NHC complexes, p-orbitals are available for back-donation primarily from adjacent heteroatoms towards the carbene carbon atom, defining the ligand as mostly σ-donating, as recently verified by charge-density studies [17], with negligible π-back-donation from the metal moiety (Figure 2). NHC ligands are thus four π-electron three-

[11] S. Dapprich, G. Frenking. CDA 2.1 Marburg, 1994. (b) S. Dapprich, G. Frenking. J. Phys. Chem. 99 (1995) 9352.

[12] T. Ziegler, A, Rauk. Inorg. Chem. 18 (1979) 1755; (b) F.M. Bickelhaupt, N.M.M. Nibbering, E.M. van Wezenbeek, E.J. Baerends, J. Phys. Chem. 96 (1992) 4864.

[13] R. Toner, G. Heydenrych, G. Frenking, J. Chem. Asian. 2 (2007)1555.

[14] (a) A. Krapp, K.K. Pandey, G. Frenking, J. Am. Chem. Soc. 129 (2007) 7596; (b) I. Fernández, F.P. Cossío, A. Arrieta, B. Lecea, M. J. Mancheño, M.A. Sierra, Organometallics, 23 (2004) 1065.

[15] D. Bourissou, O. Geurret, F.P. Gabbaï, G. Bertrand, Chem. Rev. 100 (2000) 39.

[16] M.L.H. Green, J. Organomet. Chem. 500 (1995) 127.

centre systems. Beilstein and co-workers [17] presented NBO data on the occupancies of the lone pair orbital $C_{carbene}(\sigma)$ and $p(\pi)$ atomic orbitals of the N-heterocyclic carbene carbon atoms and found high occupancies of between 1.84 to 1.91 and 0.49 to 0.69 for the σ and $p(\pi)$ orbitals, respectively. Wiberg bond orders of the carbene-nitrogen bonds indicated orders of between 1.22 and 1.56 and confirm the π-donation from the heteroatoms, as implied by NHC models [17].

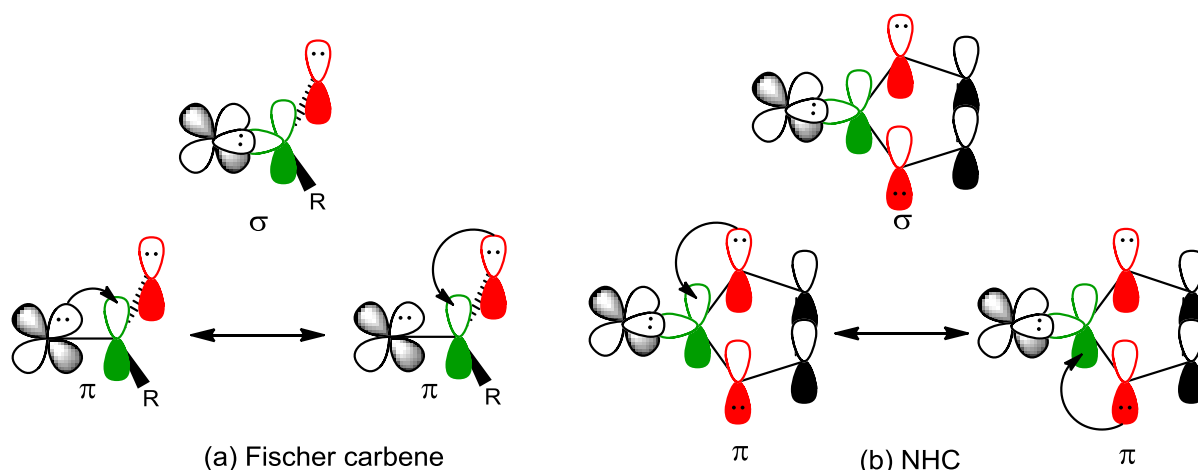

(a) Fischer carbene   (b) NHC

Figure 2: The bonding model for a (a) Fischer carbene and (b) N-heterocyclic carbene complex. Colour codes: Grey - metal, red - heteroatom and green - carbene carbon.

7.1.2 Theoretical modelling and Intent of this study

Of the most applicable electronic structure method in the field of chemistry and specifically organometallic systems is the density functional theory methods (DFT). The method has become more attractive because of the inclusion of the effects of electron correlations as well as the limited computational cost of calculations [15]. Throughout chapters 2-6, DFT calculations predicted bond orders, bond dissociation energies, natural bonding orbital interactions, the position and energies of the frontier orbital associated with molecules as well as structural parameters associated with ligands. DFT calculations have also been applied as predictive models for application in electrochemistry [18] and catalytic activity [19]. These studies suggested the existence of a linear relationship between the oxidation of the metal moiety and the HOMO (highest occupied molecular orbital) and between the reduction of the carbene carbon atom and the LUMO (lowest unoccupied molecular orbital) [18]. In catalysis the analysis of frontier orbital can prove very useful especially since the band gaps between the two frontier orbitals are indicative of the stability and reactivity of

[17] D.M. Andrada, N. Holzmann, T. Hamadi, G. Frenking, Beilstein J. Org. Chem. 11 (2015) 2727.
[18] (a) A. Jansen van Rensburg, M. Landman, D. Van der Westhuizen, M.M. Conradie, J. Conradie, Electrochim. Acta. 186 (2015) 321; (b) M. Landman, R. Liu, R. Fraser, P.H. van Rooyen, J. Conradie. J. Organomet. Chem. 752 (2014) 171.
[19] J.S. Griffith, L.E. Orgel, Q. Rev. Chem. Soc. 11 (1957) 381.

transition metal complexes. The HOMO-LUMO band gaps have also been correlated with the observed colour of complexes and provide theoretical quantification of energy absorbance [19]. Catalytic pathways were modelled with DFT calculations and energy profiles deduced from the energetic of intermediates, substrates and products. DFT calculations have been particularly important in the field of carbene chemistry especially in explaining structural futures observed in the solid state structure [20], for the determination and explanation of isomeric preferences as well as depicting high and low electron density areas. In chapters 2-6, electronic and structural calculations were performed on numerous synthesised carbene complexes. Both Fischer carbene complexes and NHCs were modelled in an attempt to gain an in-depth understanding of parameters underlying experimental observations. Energy calculations and analysis resolved questions of solid state structure observations especially when both *syn* and *trans* complexes are synthetically feasible (chapters 2 and 6) whereas electronic and steric parameters predicted stability and reactivity of complexes (chapters 3, 4 and 5). Since the afore mentioned chapters have been written as separate scientific studies and published in peer reviewed journals, this chapter will focus mainly on the comparison of electronic, structural and steric aspects of complexes between the published studies. In this study we present the synthesis and computational insights of group VI and VII transition metal Fischer carbene complexes and NHCs with focus on defining structural similarities and differences between the compared complexes. The study will compare bonding parameters of Fischer-type complexes directly to NHCs in aims to better understand the electronics that govern each type of complex. Finally, this chapter will provide a sound basis for future structural and theoretical studies on group VII transition metal carbene complexes, specifically toward ligand influences on the metal-metal bond characteristics associated with multi-metallic carbonyl complexes.

[20] R. Fraser, P.H. van Rooyen, M. Landman, Polyhedron 118 (2016) 133.

7.2 Comparative Bonding Studies

7.2.1 Study 1

7.2.1.1 Focus of study

This study will focus on the comparison of the following group VII Fischer carbene complexes:
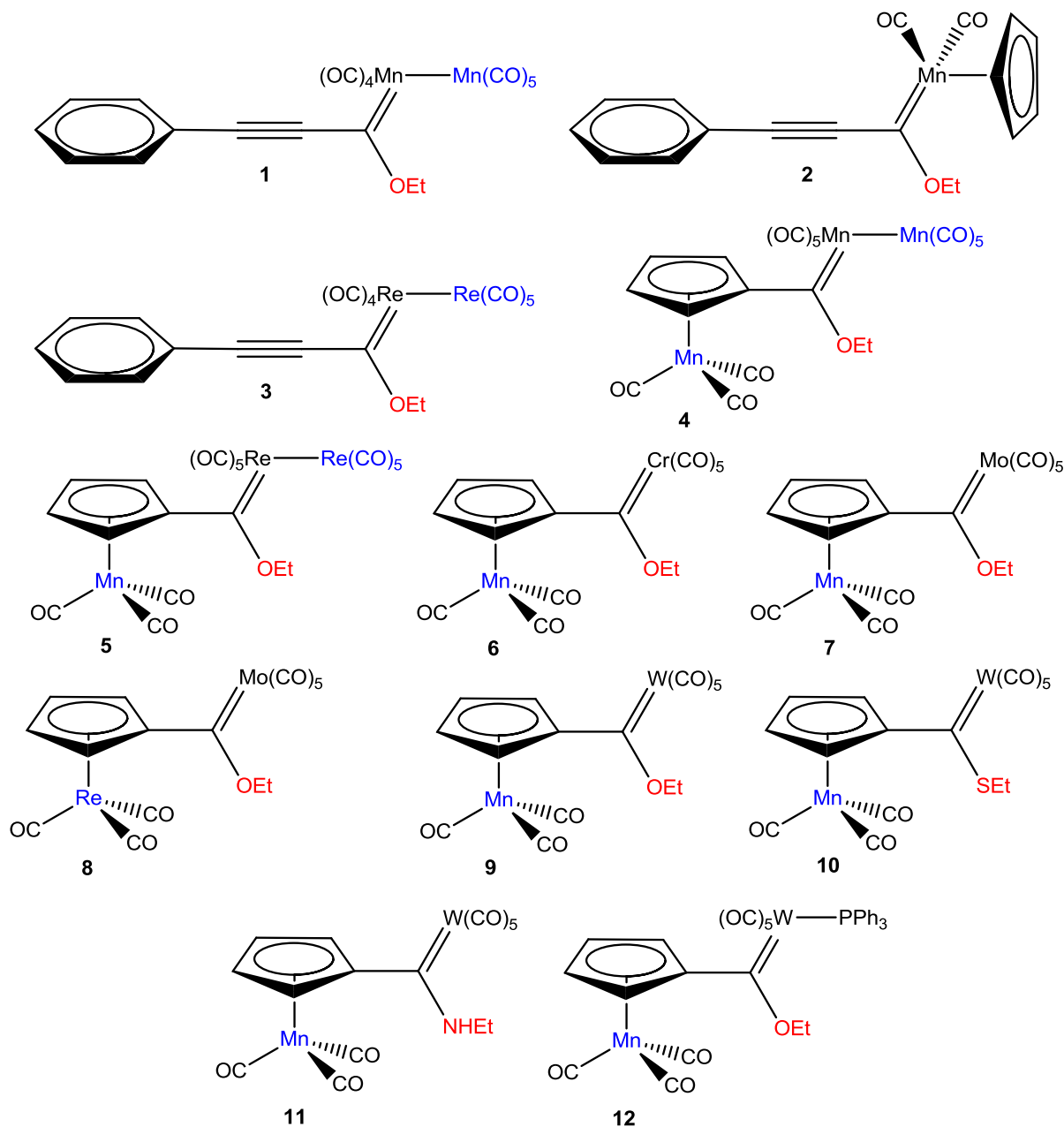

Figure 3: Complexes included in theoretical study 1

7.2.1.2   Experimental

General

All reactions, unless otherwise noted, were performed under inert nitrogen or argon atmospheres using standard Schlenk techniques [21]. All solvents were freshly distilled, dried and collected under inert conditions, with the exception of toluene. Toluene was not dried, but used after bubbling nitrogen gas through the solvent for 5 to 10 minutes. Column chromatography was carried out under inert nitrogen and argon atmospheres using silica gel (particle size 0.063-0.200 mm) as the stationary phase. Percentage yields were calculated relative to the limiting reactant. Crystallization was done using hexane:DCM or hexane:ether diffusion methods. Triethyloxonium tetrafluoroborate [22] was prepared according to a reported literature procedure. The reagents $CpMn(CO)_3$, $CpRe(CO)_3$, $Cr(CO)_6$, $Mo(CO)_6$, $W(CO)_6$, $Mn_2(CO)_{10}$, $Re_2(CO)_{10}$, n-butyl lithium (1.6 M solution in hexane) and other commercial reagents were used as purchased. Complex **3** was synthesized according to a literature method [14]. NMR spectra were recorded on a Bruker ARX-300. NMR spectra were recorded in $CDCl_3$ using the deuterated solvent peak as internal reference. ^1H and ^{13}C NMR spectra were measured at 300.1 and 75.5 MHz, respectively. IR spectra were recorded on a Perkin Elmer Spectrum RXI FT-IR spectrophotometer as KBr pellets or hexane and only the vibration bands in the carbonyl-stretching region (ca. 1500-2200 cm^{-1}) are reported.

Synthesis of complexes **1-3**

Synthesis of **1**

Phenylacetylene (0.329 ml, 3.0 mmole) was dissolved in 40 ml of dry THF. n-Butyl lithium (2.00 ml, 3.0 mmole) was added at -30 °C and stirred at this temperature for 30 min. The colour of the reaction mixture changed from a colourless to a deep brown solution. $Mn_2(CO)_{10}$ (1.170 g, 3.0 mmole) were added to the reaction mixture at -79 °C and allowed to react at this temperature for 1 hour and warmed to room temperature. After completion of the reaction, the solvent was removed in vacuo and the residue redissolved in dichloromethane. Triethyl oxonium tetrafluoroborate (0.55 g, 3.0 mmole) was dissolved in 20 ml of dichloromethane and this was added to the cooled reaction mixture (-20 °C). An immediate colour change was observed, from brown to a brown-red solution, and the reaction mixture was dry loaded onto a silica gel column for purification. The product was isolated using a 10:1 hexane: DCM eluent ratio. As a deep red-brown monocarbene complex **1** (yield: 1.233 g; 75%)**.**

[21] D.F. Schriver, M.A. Drezdzon, The manipulation of air-sensitive compounds, 2nd ed., Wiley, New York, USA, 1986.
[22] H. Meerwein, Org. Synth. 46 (1966) 113.
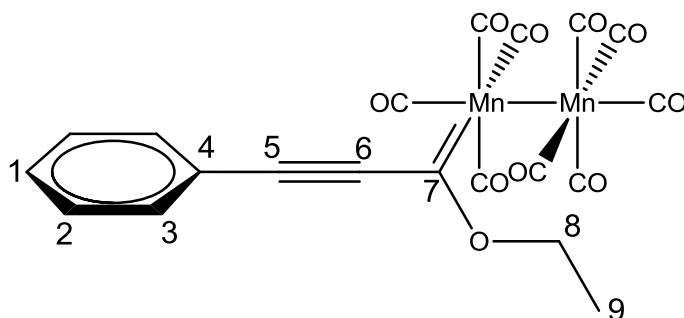
^{1}H NMR (δ(ppm)), J(Hz)): H1 7.47 (d, J = 7.3 Hz); H2 7.53 (d, J = 6.9 Hz); H3 7.60 (d, J = 7.4 Hz); H8 4.71 (q, J = 7.2 Hz); H9 1.57 (d, J = 7.1 Hz). ^{13}C{^{1}H} NMR (δ(ppm)): C1 128.9; C2 131.9; C3 132.7; C4 133.2; C5 77.2; C6 92.9; C7 302.6; C8 76.0; C9 14.5; Mn(**CO**)$_4$ 225.8; Mn(**CO**)$_5$ 221.1 and 220.8. IR (cm^{-1}): 2086 (m), 2027 (s), 1997 (s), 1975 (s), 1963 (m), 1932 (s).

Synthesis of **2**

The synthesis of **2** was done using a similar procedure as for the synthesis of **1**. Phenylacetylene (0.329 ml, 3.0 mmole) was dissolved in THF and lithiated at -30 ˚C. The lithiated moiety was then metallated with 0.612 g (3.00 mmole) of CpMn(CO)$_3$ and quenched with the oxonium salt. The monocarbene product was isolated as a light orange complex **2** (yield: 0.612 g; 60%).
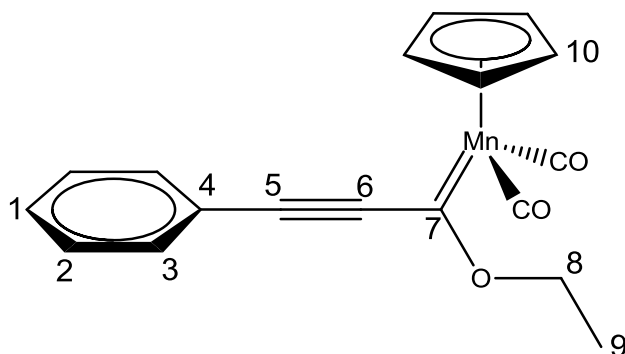
^{1}H NMR (δ(ppm)), J(Hz)): H1 7.37 (d, J = 6.3 Hz); H2 7.46 (d, J = 7.7 Hz); H3 7.53 (m); H8 4.06 (q, J = 7.2 Hz); H9 1.57 (t, J = 7.2 Hz); H10 4.78 (s). ^{13}C{^{1}H} NMR (δ(ppm)): C1 128.7; C2 131.3; C3 131.4; C4 133.6; C5 82.8; C6 95.4; C7 327.2; C8 76.6; C9 14.1; Mn(**CO**)$_2$ 231.2. IR (cm^{-1}): 2029 (s), 1947 (s).

Synthesis of **3**

The synthesis of **3** was done using a similar procedure as for the synthesis of **1**. Phenylacetylene (0.329 ml, 3.0 mmole) was dissolved in THF and lithiated at -30 ˚C. The lithiated moiety was then metallated with 1.958 g (3.00 mmole) of Re$_2$(CO)$_{10}$ and quenched

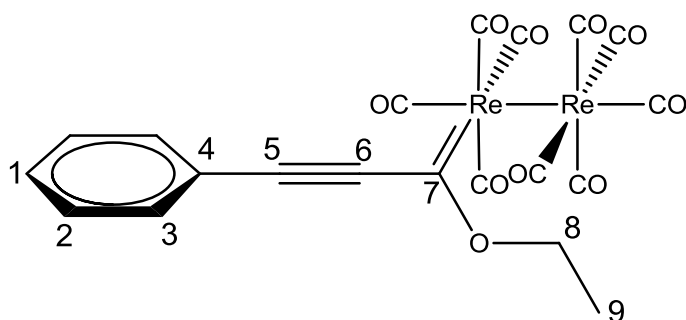with the oxonium salt. The monocarbene product was isolated as a light red complex **2** (yield: 1.751 g; 72%).

^{1}H NMR (δ(ppm)), J(Hz)): H1 7.46 (d, J = 1.7 Hz); H2 7.54 (t, J = 1.4 Hz); H3 7.62 (d, J = 1.5 Hz); H8 4.57 (q, J = 7.1 Hz); H9 1.56 (d, J = 7.1 Hz). ^{13}C{^{1}H} NMR (δ(ppm)): C1 128.2; C2 129.1; C3 131.8; C4 132.8; C5 77.2; C6 97.9; C7 278.0; C8 75.4; C9 14.3; Re(**CO**)$_4$ 194.0; Re(**CO**)$_5$ 191.2 and 186.5. IR (cm^{-1}): 2102 (m), 2049 (s), 2021 (s), 2001 (vs), 1974 (m), 1957 (vs), 1930 (w), 1920 (w).

Synthesis of **4-7, 9 and 12**

Complexes **4-7** and **9** were synthesised in chapters 2 and **12** in chapter 4.

Synthesis of **8**

CpRe(CO)$_3$ (1.006 g, 3.0 mmole) was dissolved in THF and lithiated at -30 ˚C. The lithiated Cp metal moiety was then metallated with 0.792g (3.0 mmole) of Mo(CO)$_6$ and quenched with the oxonium salt. One product was isolated: a red monocarbene complex **8** (yield: 0.791 g; 42%).
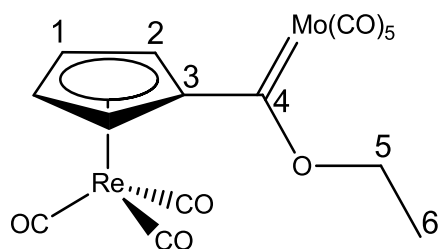
^{1}H NMR (δ(ppm)), J(Hz)): H1 5.49 (t, J = 2.4 Hz); H2 6.10 (t, J = 2.4 Hz); H5 5.00 (q, J = 7.1 Hz); H6 1.61 (t, J = 7.1 Hz). ^{13}C{^{1}H} NMR (δ(ppm)): C1 85.6; C2 89.7; C3 110.9; C4 313.5; C5 78.1; C6 14.9; Mo(**CO**)$_5$ 201.0 (trans) and 191.6 (cis). IR (cm^{-1}): 2072(w), 2032 (s), 1952 (m), 1941 (s).

Synthesis of **10**

Complex 9 (0.584 g, 1.0 mmole) was dissolved in 5 ml MeOH and ethylthiol (0.108 ml, 1.5 mmol) added (at -30 ˚C. The reaction was allowed to stir at room temperature until the majority of starting material has been converted into the brown product. The thiolated monocarbene was purified with column chromatography and isolated as a brown complex with a pungent odour (yield: 0.450 g; 75%).
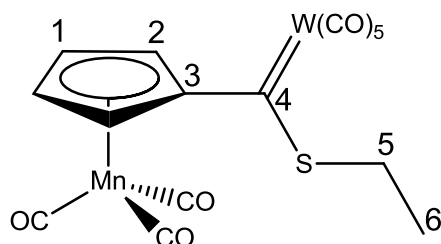
^{1}H NMR (δ(ppm)), J(Hz)): H1 5.37 (t, J = 2.3 Hz); H2 5.54 (t, J = 2.3 Hz); H5 4.94 (m); H6 1.59 (t, J = 7.7 Hz). ^{13}C{^{1}H} NMR (δ(ppm)): C1 86.5; C2 88.8; C3 108.7; C4 303.9; C5 77.2; C6 14.1; W(**CO**)$_5$ 202.0 (trans) and 197.0; Mn(**CO**)$_3$ 223.4. IR (cm^{-1}): 2067(w), 2029 (s), 1957 (m), 1946 (s).

Synthesis of **11**

Complex **9** (0.584 g, 1.0 mmole) was dissolved in 5 ml ether and ethylamine (0.098 ml, 1.5 mmol) added at room temperature. The reaction immediately turned orange-yellow and was allowed to stir at room temperature for 10 minutes. The solvent was removed and the yellow-orange solid washed with cold hexane. The aminolized monocarbene was purified via recrystilization from a hexane:DCM solution (yield: 0.571 g; 98%).
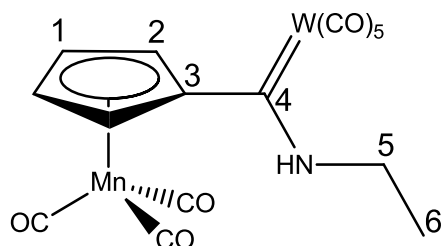
^{1}H NMR (δ(ppm)), J(Hz)): H1 4.80 (s br); H2 4.92 (s br); H5 4.01 (s br); H6 1.53 (s br); N**H** 8.72. ^{13}C{^{1}H} NMR (δ(ppm)): C1 80.6; C2 83.1; C3 119.8; C4 246.3; C5 77.2; C6 14.2; W(**CO**)$_5$ 202.9 (trans) and 197.7; Mn(**CO**)$_3$ 223.4. IR (cm^{-1}): 2066(w), 2030 (s), 1957 (m), 1943 (s).

148

X-ray crystallography

Data for complexes **1**, **3**, **8**, **10** and **11** were collected at 150 K on a Bruker D8 Venture kappa geometry diffractometer, with duo Iμs sources, a Photon 100 CMOS detector and APEX II control software using Quazar multi-layer optics, monochromated Mo-Kα radiation and by means of a combination of φ and ω scans. Data reduction was performed using SAINT+ and the intensities were corrected for absorption using SADABS [23]. The structures were solved by intrinsic phasing using SHELXTS and refined by full-matrix least squares using SHELXTL and SHELXL-2013 [24]. In the structure refinement, all hydrogen atoms were added in calculated positions and treated as riding on the atom to which they are attached. All nonhydrogen atoms were refined with anisotropic displacement parameters, all isotropic displacement parameters for hydrogen atoms were calculated as X × U_{eq} of the atom to which they are attached, X = 1.5 for the methyl hydrogens and 1.2 for all other hydrogens. Crystallographic data and refinement parameters are given in Table 1. Ortep drawings [25] of the three structures are included in Figure 5 - Figure 9. The crystal structures (cif) have been deposited at the Cambridge Crystallographic Data Centre and allocated the deposition numbers: CCDC 1417538-1417541. Data collection, structure solution and refinement details are available in each cif.

Molecular modelling

The calculations reported in this paper were obtained using the Gaussian 09 [26] suite of programs. Calculations were carried out in the singlet spin state using the hybrid functional B3LYP [27],[28]. Geometries of the neutral complexes were optimized in gas phase with the triple-ζ basis set 6-311G* on all atoms except for the metal atoms. Stuttgart/Dresden (SDD) pseudopotential was used to describe the metal electronic core, while the valence electrons were described def2-TZVPP [29]. No symmetry constraints were applied and only the default convergence criteria were used during the geometric optimizations. Vibrational frequencies [30]

[23] APEX2 (including SAINT and SADABS); Bruker AXS Inc., Madison, WI (2012).

[24] G.M. Sheldrick, Acta Crystallogr. A64 (2008) 112.

[25] L.J.J. Farrugia, Appl. Crystallogr. 30 (1997) 565.

[26] M.J. Frisch, G.W. Trucks, H.B. Schlegel, G.E. Scuseria, M.A. Robb, J.R. Cheeseman, G. Scalmani, V. Barone, B. Mennucci, G.A. Petersson, H. Nakatsuji, M. Caricato, X. Li, H.P. Hratchian, A.F. Izmaylov, J. Bloino, G. Zheng, J.L. Sonnenberg, M. Hada, M. Ehara, K. Toyota, R. Fukuda, J. Hasegawa, M. Ishida, T. Nakajima, Y. Honda, O. Kitao, H. Nakai, T. Vreven, J.A. Montgomery (Jr), J.E. Peralta, F. Ogliaro, M. Bearpark, J.J. Heyd, E. Brothers, K.N. Kudin, V.N. Staroverov, T. Keith, R. Kobayashi, J. Normand, K. Raghavachari, A. Rendell, J.C. Burant, S.S. Iyengar, J. Tomasi, M. Cossi, N. Rega, J.M. Millam, M. Klene, J.E. Knox, J.B. Cross, V. Bakken, C. Adamo, J. Jaramillo, R. Gomperts, R.E. Stratmann, O. Yazyev, A.J. Austin, R. Cammi, C. Pomelli, J.W. Ochterski, R.L. Martin, K. Morokuma, V.G. Zakrzewski, G.A. Voth, P. Salvador, J.J. Dannenberg, S. Dapprich, A.D. Daniels, O. Farkas, J.B. Foresman, J.V. Ortiz, J. Cioslowski, D.J. Fox, Gaussian 09, Revision D.01, Gaussian Inc., Wallingford CT, 2010.

[27] A.D. Becke, J. Chem. Phys. 98 (1993) 5648.

[28] C. Lee, W. Yang, R.G. Parr, Phys. Rev. B 37 (1988) 785.

[29] F. Weigend, R. Ahlrichs, Phys. Chem. Chem. Phys. 7, (2005) 3297.

[30] J.W. McIver, A.K. Komornicki, J. Am. Chem. Soc. 94 (1972) 2625.

were calculated at the optimized geometries and no imaginary frequencies were observed, to confirm true minima. Donor-acceptor interactions have been computed using the natural bond order (NBO) method [31].

7.2.1.3 Results and discussion

Synthesis and characterization
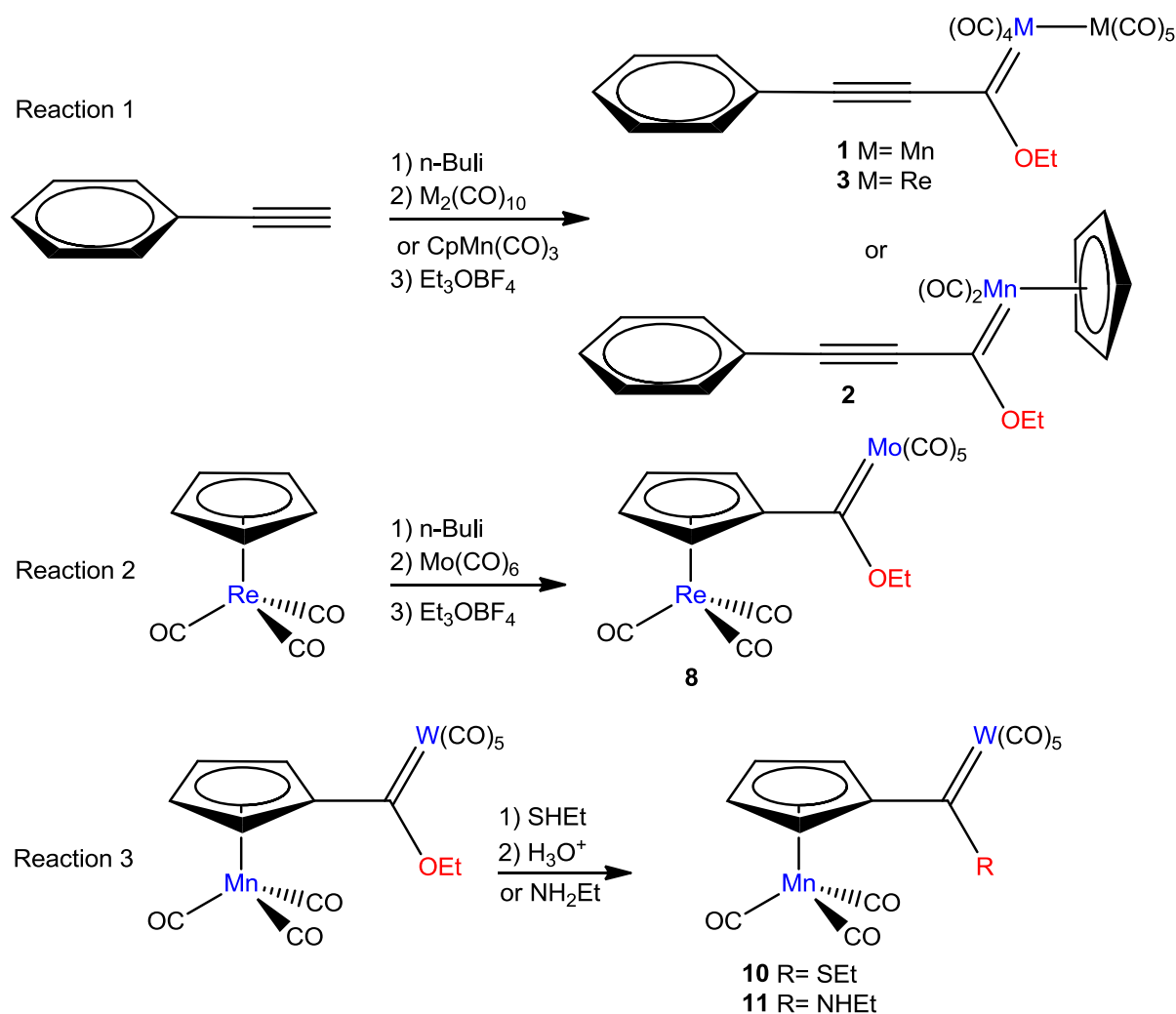
Figure 4: The synthetic procedure followed in the synthesis of **1-3, 8, 10** and **11**

The synthesis of Fischer-type carbene complexes has been well described in previous chapters. The synthetic procedures followed in the synthesis of additional complexes, not

[31] (a) J.P. Foster, F. Weinhold, J. Am. Chem. Soc. 102 (1980) 7211. (b) A.E. Reed, F. Weinhold, J. Chem. Phys. 83 (1985) 1736. (c) A.E. Reed, R.B. Weinstock, F. Weinhold, J. Chem. Phys. 83 (1985) 735. (d) A.E. Reed, L.A. Curtiss, F. Weinhold, Chem. Rev. 88 (1988) 899.

described in chapters elsewhere, have been depicted in Figure 4. The complexes were synthesised as major products in the reactions based on classic Fischer methodology [32].

Spectroscopic characterization

Using NMR spectroscopy, with $CDCl_3$ as solvent, the structural aspects of the Fischer carbene complexes could be investigated. The ^{1}H NMR spectra indicated the presence of the characteristic quartet methylene peaks (heteroatomic carbene substituent) between 4.01-5.00 ppm and the triplet methyl peaks between 1.53-1.61 ppm. The ^{13}C NMR of the complexes showed the presence of a single distinct carbene peak between 278.0-327.2 ppm for the ethoxycarbene complexes, 303.9 ppm for the thioxycarbene and 246.3 ppm for the aminocarbene complex. The IR spectra of **1**-**3**, **8**, **10** and **11** were measured in hexane and indicate two stretching frequencies attributed to the cymantrenyl and cyclopentadienyl rhenium tricarbonyl metal carbonyl stretching frequencies. The stretching frequencies for the carbene metal carbonyls were observed between 1920 and 2102 cm^{-1}.

Single crystal X-ray diffraction studies

Crystals suitable for X-ray diffraction were obtained from slow diffusion of hexane into a saturated solution of the complexes in DCM at cooled temperatures. Selected structural parameters are summarized Table 1. The conformation of the carbene moiety, as represented by the M1-C6-X-C7 dihedral angles, deviate from planarity by less than 4° (**1**, see Figure 5), 6° (**3**, see Figure 6), 11° (**10**, see Figure 8) and 6° (**11**, see Figure 9). The M-Carbene bond lengths of **1**, **3**, **10** and **11** were determined to be 1.940(3) Å, 2.077(11) Å, 2.162(4) Å and 2.230(4) Å respectively, and **1** and **3** displayed M-M bond lengths of 2.885(3) Å and 3.0395(7) Å. Complex **11** crystallized with two molecular units molecule A and molecule B) in the asymmetric unit cell while the thioxy substituent in **10** displays 45 % sulfur - and 55% oxygen characteristics. Bonding angles of 176.9(3)º and 179.1(13)º for C9-C10-C11 illustrate the linearity of the alkyne bond. No satisfactory solution for **8** (Figure 7) could be derived and the crystal has only been included to illustrate the current progress in the elucidation of the crystal structure.

[32] (a) A. Jansen van Rensburg, M. Landman, D. van der Westhuizen, M.M. Conradie, J. Conradie, Electrochim. Acta. 186 (2015) 321; (b) M. Landman, R. Liu, R. Fraser, P.H. van Rooyen, J. Conradie. J. Organomet. Chem. 752 (2014) 171.

Figure 5: Perspective view of **1** with thermal ellipsoids drawn at the 50% probability level

Figure 6: Perspective view of **3** with thermal ellipsoids drawn at the 50% probability level

University of Pretoria logo

UNIVERSITEIT VAN PRETORIA
UNIVERSITY OF PRETORIA
YUNIBESITHI YA PRETORIA

Chapter 7

2016

Figure 7: Perspective view of **8** with thermal ellipsoids drawn at the 50% probability level (preliminary study)
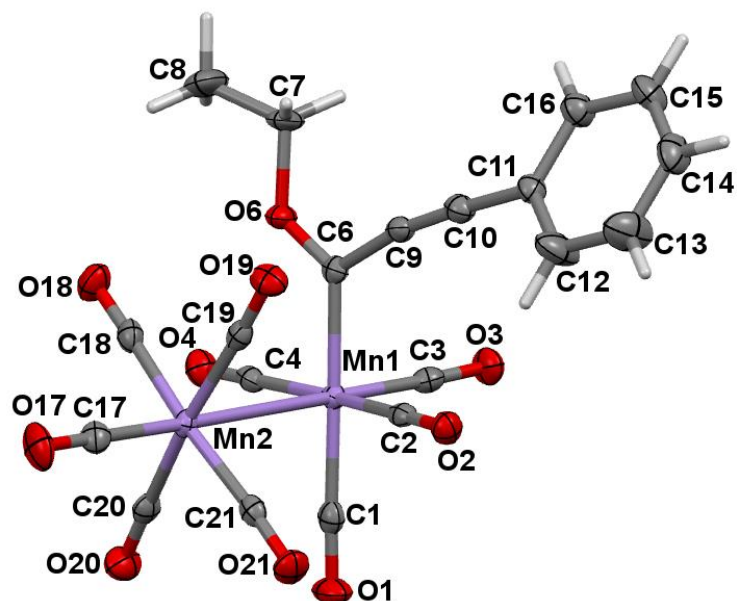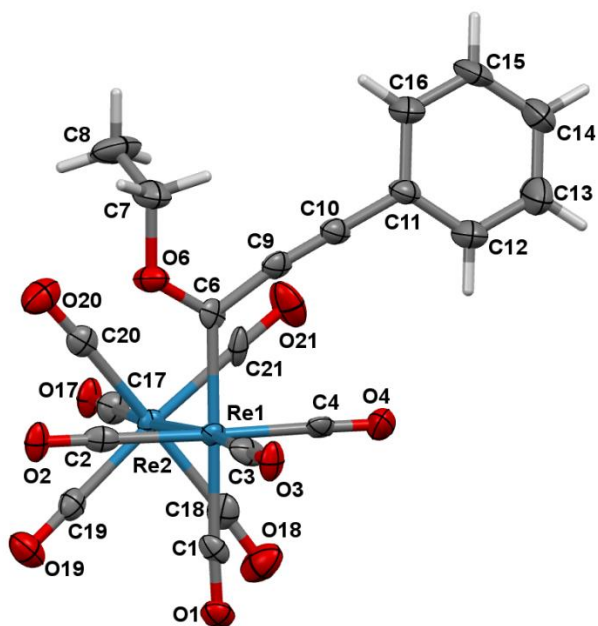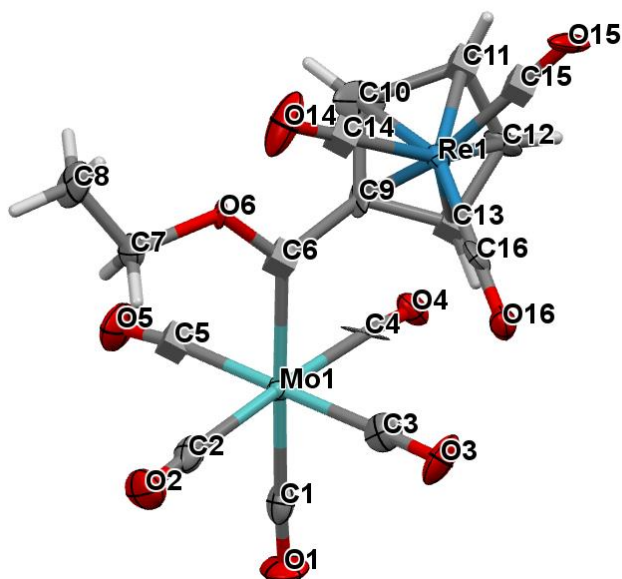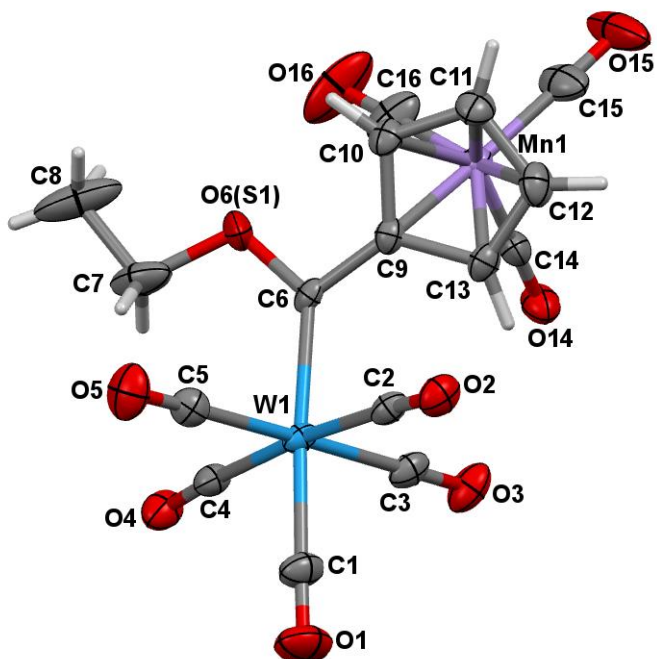

Figure 8: Perspective view of **10** with thermal ellipsoids drawn at the 50% probability level

153
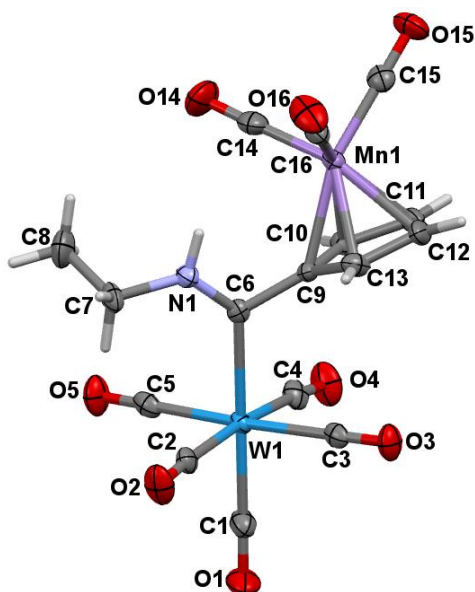
Figure 9: Perspective view of **11** with thermal ellipsoids drawn at the 50% probability level

Table 1: Selected bond lengths (Å), bond angles (⁰) and torsion angles (⁰) for **1, 3, 10** and **11**

	Complexes			
	1	**3**	**10**	**11**
Bond Length (Å)				
M1-C6	1.940(3)	2.077(11)	2.162(4)	2.230(4)
X-C6	1.468(3)	1.325(14)	1.615(4)	1.292(5)
C6-C9	1.421(4)	1.423(16)	1.478(5)	1.488(5)
M1-C1	1.850(3)	2.077(11)	2.029(5)	1.998(5)
M-CO$_x$ (X=2-4)^a	1.843(3)	1.995(12)	2.047(4)	2.047(5)
M1-M2	2.885(3)	3.0395(7)	-	-
Bond Angles (⁰)				
C1-M$_{carb}$-C6	178.79(12)	176.2(4)	175.21(16)	177.62(16)
X-C6-C9	116.6(2)	116.3(10)	106.0(3)	113.5(3)
X-C6-M1	122.01(18)	120.9(8)	131.5(2)	130.3(3)
C9-C6-M1	121.14(19)	122.7(8)	122.5(3)	116.0(3)
C6-M1-M2	92.97(7)	93.3(3)	-	-
C3-M1-M2	178.55(9)	174.0(3)	-	-
Torsion Angles (Å)				
C7-X-C6-M	-176.05(17)	174.5(9)	10.4(4)	-5.8(6)

^{a} Average distances of carbonyl groups: For **1** and **3** (x = 2 and 4), for **10** and **11** (x = 2- 4)

7.2.1.4   Theoretical study

In study 1, the theoretical aspects of VII transition metal Fischer-type carbene complexes have been investigated. Bond order values, frontier orbital energy gaps and bond dissociation energies were calculated and compared between the carbene complexes to provide both a qualitative and quantitative understanding about the similarities and differences observed when changing the carbene substituents or metal ligand sphere. Of specific focus was the source of possible influences on the metal-carbene bond as well as the electronic stability of complexes before and after carbene formation. The M-M bond character of **1**, **3**, **4** and **5** and the parameters influencing the metallic bond have also been investigated.

Bond Order and bond dissociation energy analysis

Chapters 3, 4 and 5 have provided an in-depth understanding of the theory and application of Wiberg bond indices to metal carbene complexes. In this study, focus will only be placed on the results and discussion of trends seen between different carbene complexes with the specific focus on differences and similarities that arise from the coordination modes of these complexes. Table 2 displays the Wiberg bond indices of **1**-**12** as well as the bond dissociation energies of the metal-carbene bond.

Table 2: The bond order and bond dissociation energies of the carbene-metal bond of **1-12**

Complex	Wiberg bond indices			BDE kJ·mol^{-1}
	C_{carb}-M	C_{carb}-X	C_{carb}-C_R	M-Carbene
1	0.85	1.16	1.22	238.25
2	0.99	1.15	1.19	226.18
3	0.88	1.16	1.21	300.96
4	0.95	1.18	1.12	242.57
5	0.89	1.19	1.09	266.78
6	0.87	1.21	1.12	208.05
7	0.86	1.19	1.12	228.72
8	0.87	1.22	1.11	225.00
9	0.86	1.20	1.11	241.22
10	0.85	1.38	1.13	241.22
11	0.75	1.51	1.04	236.10
12	0.96	1.14	1.08	240.31

The bond indices of **1-5** indicate higher orders between the metal-carbene bonds when cymantrene acts as carbene substituent compared to the phenylacetylene substituent. This finding is also reflected in the decrease in donation between the cymentrenyl substituent to the carbene carbon atom. The phenylacetylene, with the ability to form extensive delocalized networks, actually displays double bond characteristics between the carbene carbon atom and the alkyne functionality and thus less back-donation is required from the metal centre to stabilize the electron poor carbene moiety. In **1**-**3** the carbene-R bond order exceeds the bond order values between the carbene-ethoxy bond, the bond that typically displays higher indices values than 1. The bond dissociation energies indicates that the carbene-metal bond is considered stronger when bound to rhenium atoms compared to the manganese carbonyl analogues since the rhenium atoms are able to donate more electron density to the electrophillic carbene moiety. Complex **2** displays the highest carbene-metal bond order, since less carbonyl ligands are present, limiting back-donation possibilities to these groups and increasing donation to the carbene carbon atom. Complexes **6**, **7**, **9** display similar bond indices around the metal-carbene, carbene-substituent and carbene-heteroatom bonds, however, the bond dissociation energies differ significantly and increases in the trend Cr < Mo < W with BDEs of 208.05, 228.72 and 242.22 $kJ.mol^{-1}$ respectively. Similar to the rhenium carbene complexes, heavier atoms are able to donate more electron density to the carbene moieties, ultimately strengthening the metal-carbene bond and increasing the bond dissociation energies. Complexes **7** and **8** show no real differentiation structurally or chemically with the bond orders and BDEs essentially identical, irrespective if cymantrene or cyclopentadienyl rhenium tricarbonyl acts as synthetic starting synthon. Interestingly, the bond order changes significantly between the carbene carbon atom and the heteroatom substituent when the identity of the heteroatom changes. The indices increase in the order OEt < SEt < NHEt with orders of 1.20, 1.38 and 1.51 respectively. The bond orders suggest that the aminocarbene (**11**) displaying almost exclusively double bond character between the carbene and amino group, whilst sulfur donates more strongly to the carbene carbon atom than oxygen. Figure 10 indicates the isostructural aspects of **9** and **10**, with the exception of the lengths of the OEt and SEt bonds. Complex **9** can undergo carbonyl substitution upon thermal reaction of the carbene complex with triphenylphosphine. The substituted carbene complex (**12**) displays similar bonding characteristics compared to **9** apart from the increase in the bond order of the carbene-metal bond. The increase in the bond order can be ascribed to the increase of sigma donation from the phosphine ligand to the metal centre, increasing the electron density situated on the metal centre and ultimately donated to the carbene moiety. Phosphine ligands are weaker π-acceptors compared to carbonyl ligands.
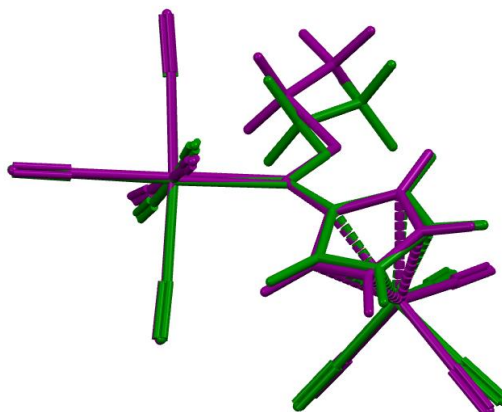
Figure 10: The structural overlay of the DFT optimized structures of **9** and **10**

Frontier orbital analysis

In previous chapters the frontier orbital energies and HOMO-LUMO band gap have been used to describe relative stabilities and reactivities of a group of carbene complexes. As noted before, frontier orbitals and the relationship between the orbitals are significant to electrochemical processed. Linear relationships exist between the oxidation of the metal sphere and the HOMO and between the reduction of the carbene carbon and the LUMO. In this study a larger group of compound has been studied and the frontier orbitals associated with each complex presented in Table 3.

Table 3: Frontier orbital energies for **1-12**

Complex	Frontier orbital energies (eV)		
	HOMO	**LUMO**	**Energy Gap**
1	-5.50	-2.96	2.54
2	-5.47	-2.36	3.11
3	-5.93	-3.04	2.89
4	-5.85	-2.67	3.18
5	-6.10	-2.42	3.68
6	-6.16	-2.41	3.75
7	-5.94	-2.48	3.46
8	-6.04	-2.64	3.40
9	-5.96	-2.64	3.32
10	-5.86	-2.93	2.93
11	-5.72	-2.04	3.68
12	-5.45	-2.22	3.23

From the data in Table 3, complexes where the phenylacetylene is incorporated as the carbene substituent have smaller HOMO-LUMO band-gaps. The average band gap of the multimetal phenylacetylene carbene complexes (**1** and **3**) was determined to be 2.72 eV compared to 3.43 eV for the average between **4** and **5**. Complex **5** were found to have the largest HOMO-LUMO band gap and thus could be speculated to be the most stable and inert to decomposition pathways (solely based on frontier orbital analysis). Rhenium carbene complexes (**3** and **5**) in general have larger band gaps (3.28 eV average) compared to 2.80 eV (average) for the manganese carbene complexes (**1** and **4**). In contract to this, the group VI carbene complexes follow the opposite periodic trend: for complexes **6**, **7** and **9**, the theoretical band gap increases in the order W < Mo < Cr. The thioxycarbene (**11**) displays the largest band gap, followed by the ethoxycarbene (**9**) and lastly the aminocarbene complex (**10**). A small decrease in the size of the band gap is seen when **9** undergoes substitution to form **12**.

7.2.2 Study 2

7.2.2.1 Focus of study

This study will focus on the comparison of the following group VII dimetallic Fischer carbene and NHC complexes:
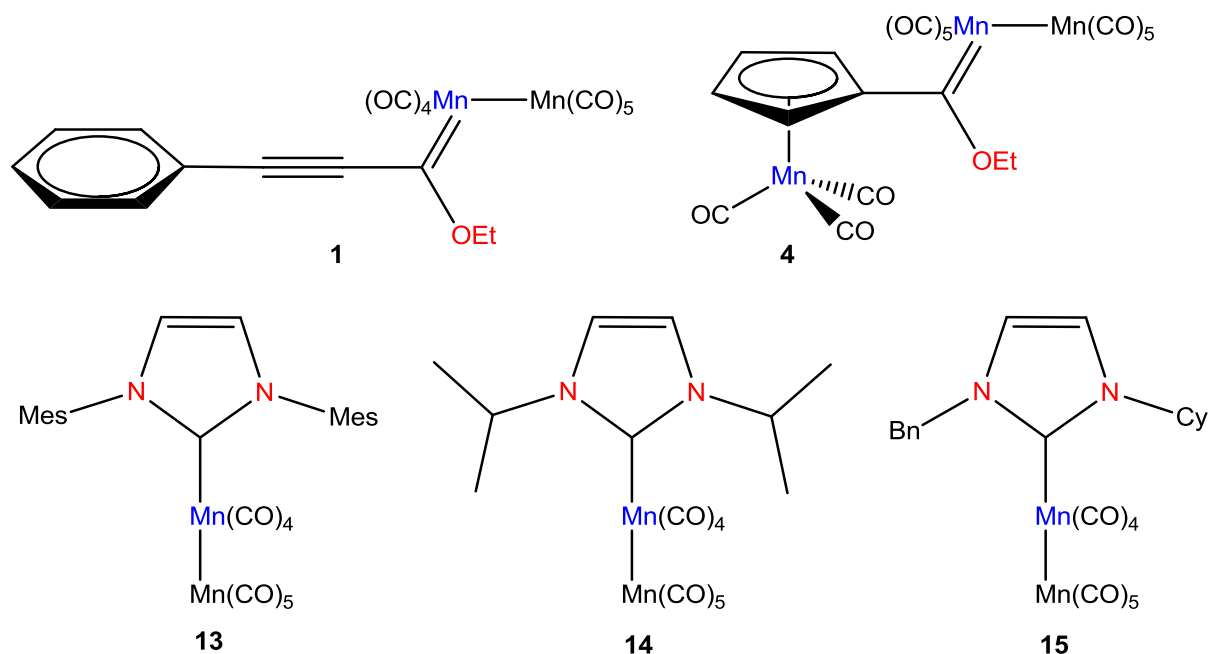

Figure 11: Complexes included in theoretical study 2

7.2.1.2 Experimental

The general comments, synthesis, x-ray crystallography and molecular modelling aspects have been described in chapters 2, 5 and 7.

7.2.1.3 Theoretical study

Although fundamental differences exist between the bonding mode of Fischer and N-heterocyclic carbene complexes, many similarities still remain. The accepted model still depicts both carbene fragments as singlet moieties with significant σ-donating abilities. The main difference between the carbene types originates from the position and amount of stabilizing back-donation received towards the electron poor carbene carbon atom. Fischer carbene complexes are stabilized from π-back-donation from both the metal- and heteroatomic moieties whereas the NHC ligand receives negligible back-donation from the metal centre and significant donation from the neighbouring heteroatomic groups. The best depiction of the internal stabilization can be seen from the resonance hybrid produced from the delocalization of π-electrons (Figure 12). NHC and Fischer carbene complexes have

thus been compared to observe electronic differences in the binding to group VII transition metals as well as the influences induced by this carbene formation towards the M-M bond character.
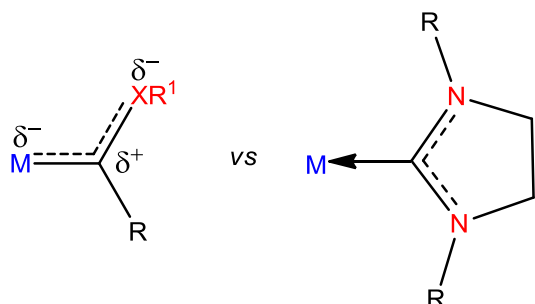

Figure 12: The difference in the resonance of the Fischer carbene (left) and NHC (right) complexes

Bond Order analysis

NHC ligands are often considered as phosphine analogues in their ability to donate electron density towards the metal centre. The ability to strongly donate allows for stabilization of formally unstable metal complexes. The use of Wiberg bond indices gave unique insight into the difference in the bonding of Fischer-type carbene and NHC complexes. From the indices in Table 4 it was deduced that the ratio of bonding to back-donation to the manganese metal atom was significantly less in the NHC complexes (**13**-**15**) compared to the Fischer carbenes. Complexes **1** and **4** have an average BO of 0.89 compared to 0.77 of the NHC complexes. The donation received by the carbene carbon atom from the heteroatom back-donation was higher in the NHC complexes compared to **1** and **4**. The evidence presented by the bond indices thus confirms the bonding modes depicted by literature and described earlier in this chapter. Fischer carbene complexes display greater back-donation from the metal centre as indicated by the higher bond orders between the carbene-metal bond compared to the NHC analogues. The N-heterocyclic carbene carbons in return received additional electronic donation from the flanking nitrogen heteroatoms. The donation from both heteroatoms is found to be higher in the NHC complexes and thus supports this deduction.

Table 4: Wiberg bond indices of **1**, **4** and **13-15**

Complex	Wiberg bond indices			
	C_{carb}-M	C_{carb}-O/N$_1$	C_{carb}-C$_R$/X$_2$	Mn-Mn
1	0.85	1.16	1.22	0.27
4	0.92	1.18	1.12	0.27
13	0.77	1.25	1.09	0.30
14	0.77	1.26	1.26	0.30
15	0.77	1.26	1.27	0.30

Frontier orbital analysis

The frontier orbital analysis indicates smaller HOMO-LUMO gaps for Fischer carbene complexes compared to the NHC analogues. In comparison to the dimanganese decacarbonyl starting material, the Fischer carbene complexes both had smaller energy differences between the frontier orbitals whilst the NHC complexes displayed similar values to the starting decacarbonyl. The NHC complexes should thus be theoretically more stable and less reactive. The HOMO of the Fischer carbene complexes had energy values close to the decarcarbonyl starting material and significantly lower in energy compared to the NHC complexes. The LUMO was also lower in energy and the resulting band gap between the HOMO-LUMO overall less significant in the Fischer complexes. The energy values associated with the frontier orbitals are displayed in Table 5 and Figure 13.

Table 5: Energy values associated with the frontier orbitals of **1, 4, 13-15**

Complex	Frontier orbitals		
	HOMO (eV)	LUMO (eV)	Energy Gap (eV)
SM[*]	-6.14	-2.26	3.88
1	-5.50	-2.96	2.53
4	-5.85	-2.67	3.18
13	-5.13	-1.37	3.76
14	-5.31	-1.41	3.90
15	-5.30	-1.41	3.89

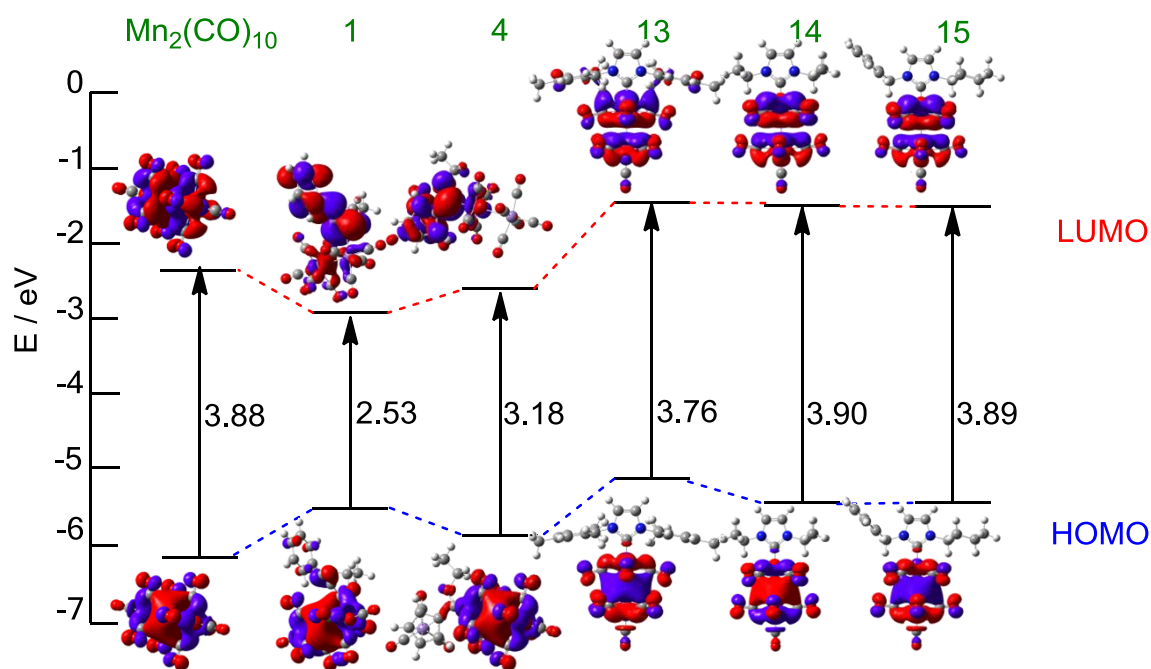* SM = $Mn_2(CO)_{10}$ starting material synthon

Figure 13: HOMO-LUMO band gaps of **1, 4, 13-15**

Bond Dissociation energy analysis

Bond dissociation energies (BDE) have been calculated in a similar fashion as for study 1 and the values presented in Figure 14. Both the BDE of the carbene-metal and the Mn-Mn have been calculated to determine any observable influence carbene formation may have on the M-M bond energy. BDE analysis indicates significantly higher energy values of the carbene-metal bond of Fischer carbene complexes compared to NHC complexes (on average 29.26 kJ·mol^{-1} greater in energy). The metal-metal bond energies in NHC complexes were the most influenced by carbene formation with average value of 115.06 kJ·mol^{-1} compared to 111.00 kJ·mol^{-1} for the Fischer carbene complexes. Both carbene types thus displayed increased bonding interaction between the metal-metal fragments upon carbene formation since the BDE of the $Mn_2(CO)_{10}$ is only 103.28 kJ·mol^{-1}. The higher BDE of the metal-carbene bond in **1** and **4** correlates with the bonding model applicable to Fischer carbene complexes where more bonding interactions are expected between the metal and the carbene carbon atom as well as the higher Wiberg bond indices described earlier.
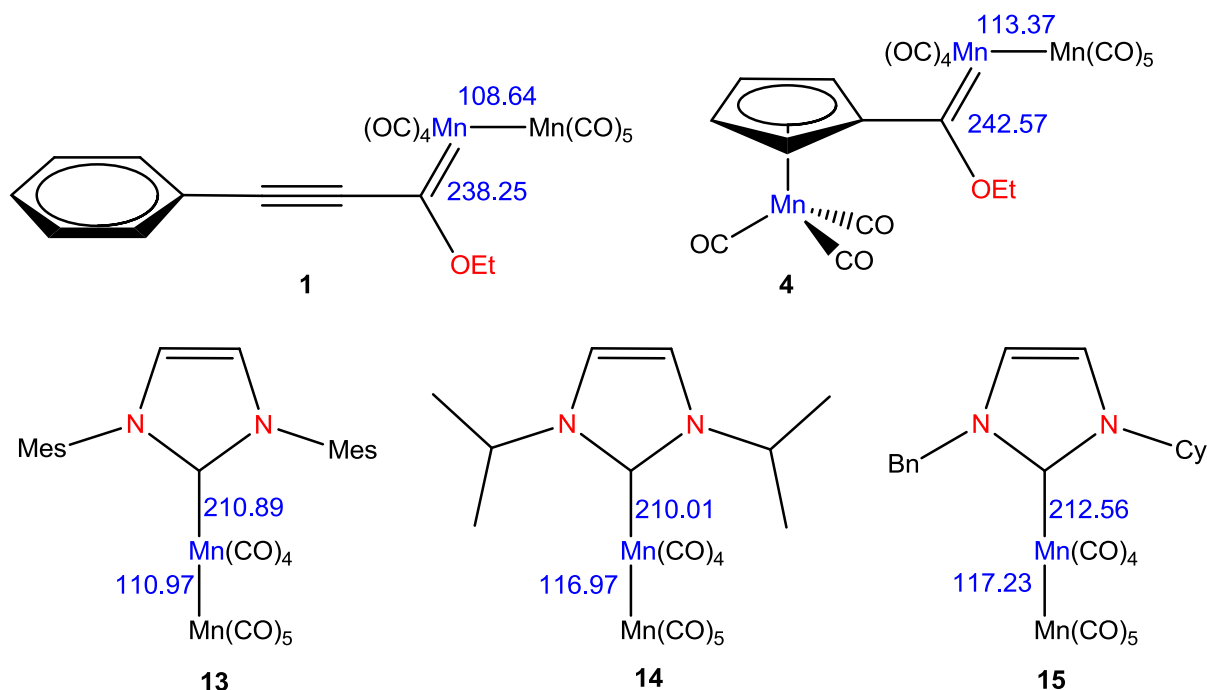
Figure 14: Bond dissociation energies of **1, 4** and **13-15** in kJ·mol^{-1}

Mulliken Charges

Mulliken charges provide a simple platform to indicate the presence of higher and lower atomic charge regions in a specific molecule. Although the Mulliken charge values are not significant when molecules are compared with one another, the model is still applicable to indicate regions of similar electron densities in the molecules. For simplicity, only **4** and **13** were compared to provide a correlation between the two carbene types and the bonding models applicable to each (Figure 15). In both carbene complex types, the carbene carbon atom is definable as electronically poor whilst the neighbouring substituent atoms attached to the carbene carbon atom electronically negative. Additional electron density is thus available from these substituents as supported by the Wiberg bond indices having values of above 1. The metal atom coordinated by the carbene ligand is also electronically poor whilst the second metal atom is seen as overall more negative (dark red). In Fischer carbene complexes the carbene-metal bond orders are higher compared to the NHC complexes and thus would explain the less positive metal centre in complex **4** (darker green) in comparison to the Mn of the NHC complex (light green).
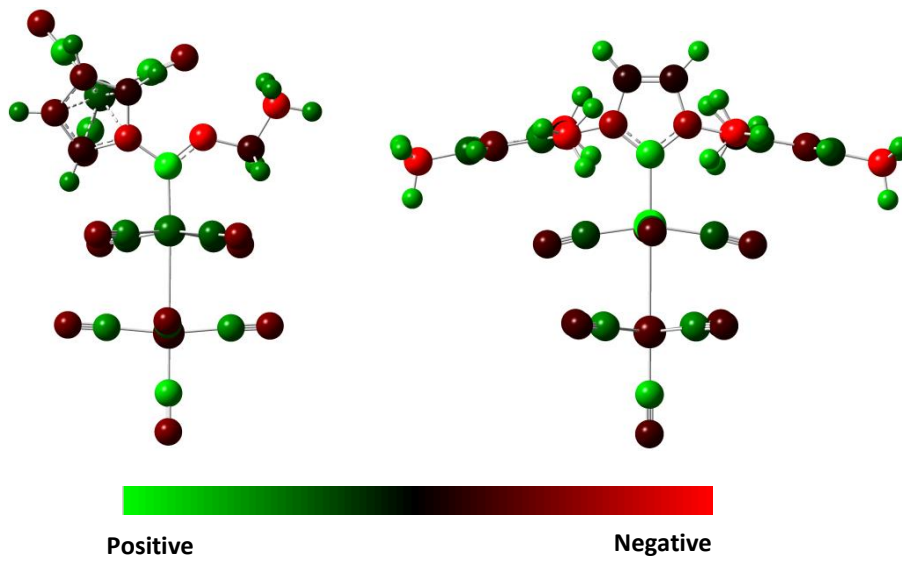
Positive   **Negative**

Figure 15: The Mulliken charge distribution of **4** and **13**

7.2.3 Study 3

7.2.3.1 Focus of study

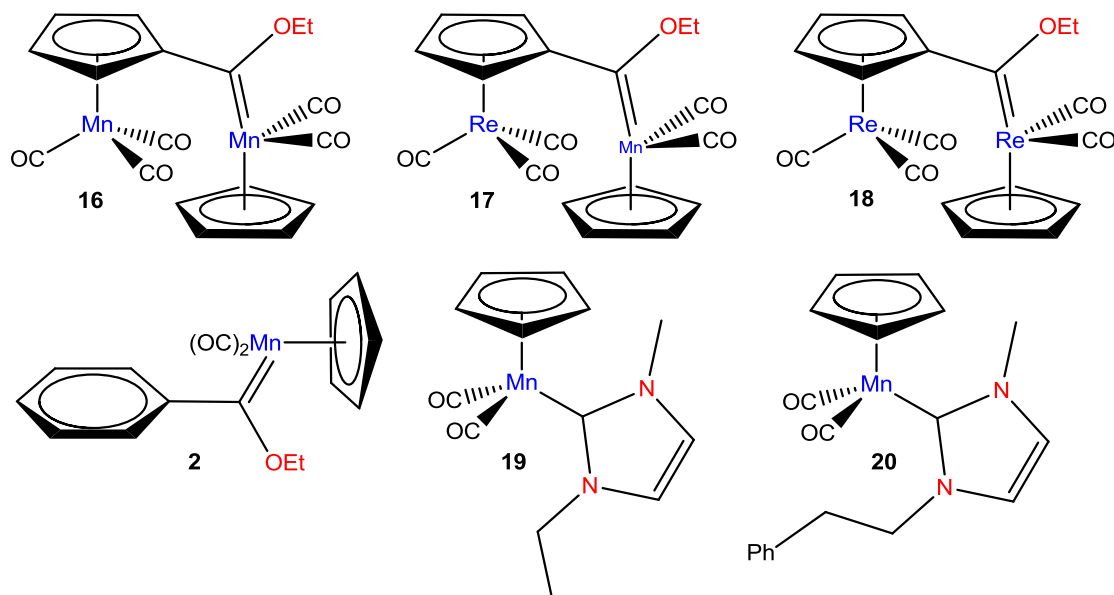This study will focus on the comparison of the following group VII Fischer carbene and NHC complexes:

Figure 16: Complexes included in theoretical study 3

7.2.1.2 Experimental

The general comments, synthesis, X-ray crystallography and molecular modelling aspects of these complexes have been described in chapters 3, 6 and 7.

7.2.1.3 Theoretical study

In studies 1 and 2 the theoretical aspects of VII transition metal Fischer- and N-heterocyclic carbene complexes have been investigated. Bond order values, frontier orbital energy gaps and bond dissociation energies were calculated and compared between the carbene types to provide both a qualitative and quantitative understanding about the influences that variation in the carbene ligand or type would have on different metal- or dimetallic carbonyl systems. In the concluding study of this chapter, the bonding of Fischer and N-heterocyclic carbene ligands to cyclopentadienyl manganese dicarbonyl moieties will be probed to indicate any similarities or differences observe in the coordination of carbenes to a specific metallic complex.

Bond Order and Bond dissociation energy analysis

Similar to study 2, the Fischer carbene complexes **2**, **16**-**18** displayed higher BDEs compared to the NHC complexes (Table 6). The increased BDEs are also supported by higher bond indices between the carbene-metal bonds. The similar indices of the carbene-nitrogen bonds in **19** and **20** supports the bonding model where the carbene atom received electron donation from both substituents, equally, forming a resonance hybrid between the three centre. The Fischer carbene complexes receives greater electronic donation from the ethoxy substituent compared to the cyclopentadienyl metal tricarbonyl group and, as described earlier, in **2** the phenylacetylene substituent donates significant electron density from the alkyne functionality to the carbene carbon atom, competing in electronic donation with the ethoxy group. The metal-carbene bond of **18** displays the greatest BDE since rhenium serves as the metallating moiety.

Table 6: Wiberg bond indices and BDE of **2, 16-20**

Complex	Wiberg bond indices			BDE kJ/mol
	C_{carb}-M	C_{carb}-O/N$_1$	C_{carb}-C$_R$/X$_2$	
2	0.99	1.15	1.19	226.18
16	0.99	1.17	1.09	218.49
17	0.98	1.18	1.09	218.49
18	1.10	1.12	1.08	326.62
19	0.73	1.03	1.03	191.09
20	0.78	1.25	1.25	194.87

The similar bond orders of complexes **17** and **18** are also depicted in the solid state structures of the complexes. The complexes are isostructural as depicted in Figure 17.
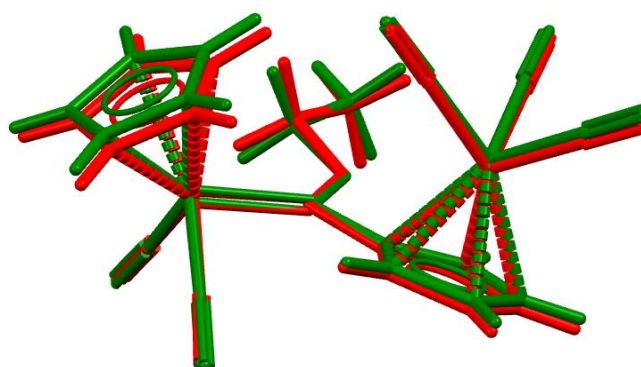

Figure 17: The structural overlay of the DFT optimized structures of **17** (red) and **18** (green)

Frontier orbital analysis

The frontier orbital analysis of the six complexes displayed larger energy gaps for the NHC complexes of cymantrene compared to the values for the Fischer carbene complexes. This correlates well with the results obtained in study 2. The carbene complexes of $CpM(CO)_3$ moieties were determined as more stable than the phenylacetylene complex **2** and complex **20** indicated the biggest HOMO-LUMO energy gap and also had a significantly band-gap compared to **19**. It could thus be suggested that bulkier NHC ligand would stabilize the $CpMn(CO)_3$ better and would result in an overall more stable complex. The energy gap also decrease with 0.05 eV in the order **16 > 17 > 18**, suggesting that the homonuclear carbene complex of cymantrene would be less reactive that the homonuclear direhenium carbene analogue, **18**. The energy values attributed to the frontier orbitals are given in Table 7.

Table 7: Energy values attributed to the frontier orbitals

Complex	Frontier orbitals		
	HOMO (eV)	LUMO (eV)	Energy Gap (eV)
2	-5.47	-2.36	3.11
16	-.5.53	-2.08	3.45
17	-5.64	-2.24	3.40
18	-5.60	-2.25	3.35
19	-5.03	-0.13	5.16
20	-5.11	-0.37	5.48

Mulliken Charges

In study 2, the Mulliken charges arising from the coordination of the carbene ligand to the metallic centre were found to similar in both the Fischer and NHC complexes. In this study, both carbene complex types displayed a carbene carbon atom which is definable as electronically deficient, especially compared to the neighbouring substituent atoms (Figure 18). Additional electron density is thus available from these substituents to stabilize the carbene moiety and bond indices of above 1 support the notion of electronic donation from both substituents. The metal atom coordinated by the carbene ligand is electronically poor whilst the cyclopentadienyl ligand displays a delocalized electronic system and thus hase a more negative Mulliken charge associated with the ring (dark red). In Fischer carbene complexes the carbene-metal bond orders are higher compared to the NHC complexes and thus would explain the less positive carbene centre in complex **16** (darker green) in comparison to the carbene carbon atom of the NHC complex (light green) **19**.
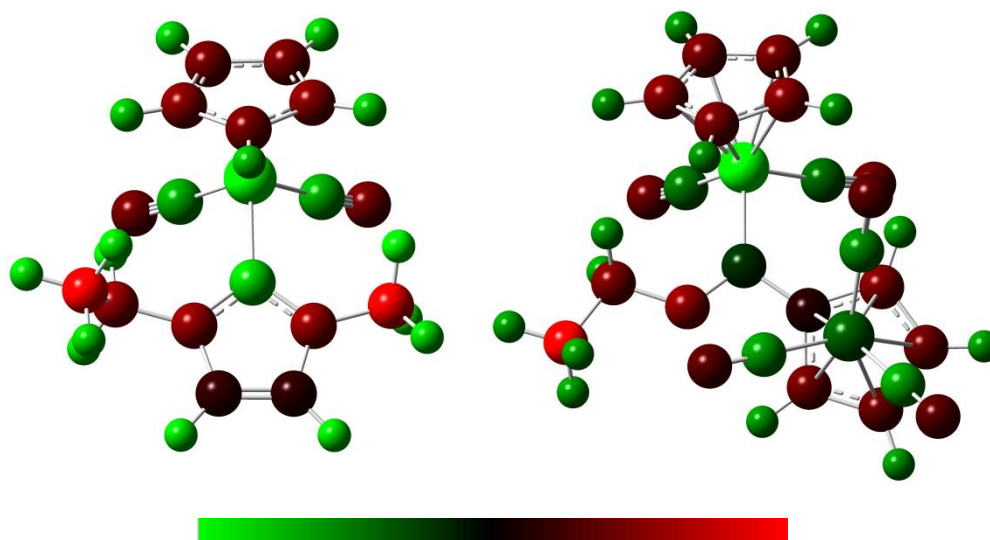
Figure 18: Mulliken charge comparison between **16** and **19**

4.3   Concluding remarks

A series of Fischer and N-heterocyclic carbene complexes of group VII transition metals was synthesized and characterized spectroscopically. Carbene complexes incorporating different metallic centres (Cr, Mo, W, Mn and Re), heteroatomic substituents (alkoxy, thioxy and amino) and aryl and aromatic R-group substituents (CpMn(CO)$_3$, CpRe(CO)$_3$ and phenylacetylene) were synthesised and studied with theoretical DFT calculations. Thermal and photochemical substitution reactions on the metal atom associated with the carbene have also been attempted and yielded phosphine-substituted carbene complexes also forming part of the theoretical studies.

DFT calculations provided insight into the electronic environments, coordination patterns and reactivity centres of the multimetallic carbene complexes. The theoretical findings also established parameter to help understand the bonding interactions witnessed in the complexes. The study determined intramolecular natural bonding orbital (NBO) interactions in cymantrenyl carbene complexes of group VI and VII transition metals as well as conformational and isomeric aspects of the polymetallic complexes. Application of the second-order perturbation theory (SOPT) of the natural bond orbital (NBO) method revealed stabilizing interactions between the methylene C-H bonds and the carbonyl ligands of the carbene metal moieties. These stabilization interactions show a linear decrease for the group VI metal carbene complexes down the group. The study also determined Wiberg bond indices, the percentage buried volume (%V$_{bur}$), solid angle and bond dissociation energies

168

(BDEs) of the complexes. The results indicate that the NHC complexes had significantly lower bond indices for the carbene-metal bonds, indicating only strong σ-donor interactions between these ligands and metal centres. Lower indices also confirm the limited back donation from the metal centres towards the carbene carbon atom. In contrast, Fischer carbene complexes display higher bond orders for the metal-carbene bond, confirming a σ and a π back-donation interaction between the carbene and metal moiety and higher bond dissociation energies. Carbene complexes of rhenium display significantly higher BDEs compared to the manganese analogues, a similar periodic trend as seen for group VI transition metal complexes.

Alterations of the heteroatomic substituents lead to changes in the colour, BDE, bond indices and HOMO-LUMO band-gap energies of the carbene complexes. The theoretical bond order indices increase in the order OEt < SEt < NHEt with orders of 1.20, 1.38 and 1.51 respectively. The bond indices imply that aminocarbenes displaying almost exclusively double bond character between the carbene and amino group, while alkoxy substituents are seen to stabilize the carbene carbon atom more that thioxy-substituents but to a lesser extent than amino-substituent. Thioxycarbene complexes display the largest band –gap energies, followed by ethoxycarbenes and lastly the aminocarbene complexes. Based on the band-gap, the ethoxycarbene starting material thus shows a red shift when aminolized and a blue shift when the thioxycarbene is formed. Phosphine-substituted Fischer carbene complexes of cymantrene have been synthesized through thermal substitution of carbonyl ligands in the presence of the triphenylphosphine ligand. Through the variation of the carbene metal group, subtle structural differences were witnessed. DFT calculations indicated that three plausible substituted structures were possible namely substitution of a carbonyl ligand on the tricarbonyl cymantrene synthon or the substitution of a *cis* or *trans* carbonyl group on the carbene metal coordination sphere. The solid state crystal structures of three of the complexes provided insight into the substitution and indicated an isomeric preference of *cis* coordination.

20 complexes were selected for inclusion in a larger overall comparative study, aiming at defining the bonding characteristics of Fischer- and N-heterocyclic carbene complexes. Complexes were compared based on structural and bonding similarities, ultimately serving as a predictive basis on defining aspects of the carbene-metal bonds. The study was able to indicate similarities and differences between the two carbene types and provided a quantitative understanding of the bonding models applicable to the complexes. The complexes were group into one of three studies, based on structural and chemical

similarities and the electronic parameters and bonding modes of the Fischer and NHC complexes compared. Wiberg bond indices indicated higher electron densities between the carbene-metal bonds of Fischer carbene complexes and supported the notion of the existence of back-donation from the metal centre towards the electron poor carbene carbon atom. Back-donation from the heteroatomic substituents plays a significant role in the bonding mode of NHC ligands and the electronic stabilization the carbene carbon atom receives from the heteroatomic substituents produces a resonance hybrid between the three centres. The unique stabilizing bonding interactions in NHC ligands limits back-donation needed from the metal centre as correlated by the lower bond indices determined for the carbene-metal bonds. The higher electron densities found in Fischer carbene complexes between the metals and carbene moieties are also supported by higher bond dissociation energies displayed in this carbene type. Although Fischer carbene complexes displayed greater BDEs and higher Wiberg indices between the metal-carbene bonds, the frontier orbital analysis indicated that NHC ligands were able to stabilize metal centres better in comparison to Fischer carbene ligands. The NHC ligands also displayed the unique ability to stabilize M-M bonds better than the Fischer complexes. Finally, Mulliken charges arising from the coordination of the carbene ligands to the metallic centre were found to be similar for both the Fischer and NHC complexes. Both types of carbene moieties displayed electronically poorer carbene carbon atoms, electron poor carbene metal centres and electron rich heteroatomic substituents. In the Fischer carbene complexes the aryl substituents were also found to be electronically richer and the bonding model applicable to Fischer carbene complexes is thus relatable to NHC complexes.

Finally, NHC complexes of cymantrene showed catalytic activity in the dimerization of thiols to disulfides. A plausible mechanism can be proposed based on similar literature reactions of the cymantrene starting materials, which also display dimerization abilities.

Future work:

- Since the NHC complexes of cymentrene displayed catalytic activity in the dimerization of simple thiols, the study should be expanded to incorporate more complex sulfur-containing molecules. The dimerization of biological thiols would also be a potential prospect as well as the possibility of dimerization studies on the cyclopentadienyl rhenium tricarbonyl NHC analogues. A literature survey indicated that no NHC of cyclopentadienyl rhenium tricarbonyl have been synthesised.
- Preliminary catalytic studies on group VI transition metal Fischer carbene complexes of cymantrene also displayed potential application of the dimerization of thiols. This study

needs to be revived and attempted on a publishable scale, The Fischer carbene complexes are significantly more synthetically viable and could thus potentially serve as a better catalyst for the dimerization reactions.

- Only three Fischer carbene complexes of cyclopentadienyl rhenium tricarbonyl have been synthesised in this study. A full sequence of carbene complexes of group VI and VII should be synthesised from the $CpRe(CO)_3$ synthon and together with the Fischer carbene complexes of $CpMn(CO)_3$ investigated for any application in electrochemical processes. Any evidence of metal-metal communication could also potentially be determined with the envisioned electrochemical studies.